PHASE RELATIONSHIPS IN Zn-Al BASED ALLOYS

YAO-HUA ZHU

Ph.D. THESIS

THE UNIVERSITY OF ASTON IN BIRMINGHAM

May 1983

THE UNIVERSITY OF ASTON IN BIRMINGHAM

TITLE: PHASE RELATIONSHIPS IN Zn-Al BASED ALLOYS

NAME: Yao-Hua Zhu

DEGREE: Doctor of Philosophy

YEAR: 1983

SUMMARY

The present investigation started with the establishment of equilibrium phase diagrams of Zn-Al-Si and Zn-Al-Cu-Si systems. Subsequently, hardness testing on alloys of the whole composition range in both systems was carried out at various temperatures to get a general survey of phase transformation in the quenched-ageing processes. Five alloys with pronounced age-hardening responses, i.e. Al-rich, monotectoid, and eutectoid alloys in the Zn-Al-Cu-Si system and Al-rich and monotectoid alloys in Zn-Al-Si systems, were studied in detail using X-ray diffraction examination. Eleven sets of X-ray diffractograms and seven fraction transformation curves revealed the distinct mechanisms of phase transformations in Zn-Al, Zn-Al-Si, Zn-Al-Cu, and Zn-Al-Cu-Si systems. Two of these five alloys were investigated in the transmission electron microscope to explain the two typical structural changes occurring as a result of quench-ageing processes in Zn-Al-Si and Zn-Al-Cu-Si systems.

Using the previously established equilibrium phase diagrams and the mechanisms of phase transformation of the four alloy systems, the phase relationships between equilibrium and non-equilibrium states in multi-component Zn-Al based alloys were obtained.

A general rule of phase transformation of supersaturated alloys was derived based on thermodynamic and kinetic considerations, which may be applicable to other alloy systems.

The effect of the phase transformations on mechanical and physical properties was studied using tensile strength, impact, dimensional stability and wear property tests. This allowed the selection of particular alloys for commercial purposes, espeically for use as plain bearings or structures which require good tribological properties.

KEY WORDS: Zn-Al ALLOY, HEAT TREATMENT, PHASE DIAGRAM, PHASE TRANSFORMATION, TRIBOLOGICAL PROPERTIES.

CONTENTS

		PAGE
List of Figures		vi
List of Tables		xx
List of Phases		xxiv
1.	INTRODUCTION	1
1.1	Solid state transformation	1
1.2	Zinc-based alloys on bearings	4
1.3	Scope of the research	5
2.	LITERATURE SURVEY	7
2.1	Phase diagram	7
2.1.1	Binary systems	7
2.1.2	Ternary Zn-Al-Cu system phase diagram	8
2.2	Phase transformations	16
2.2.1	Binary Zn-Al system	16
2.2.2	Ternary Zn-Al-Cu system	35
2.3	Effect of addition elements on phase transformations	44
2.4	Effect of some ternary additions on the mechanical properties	49
3.	EXPERIMENTAL PROCEDURE	55
3.1	Preparation of alloys	55
3.2	Heat treatment	55
3.3	Hardness testing	57

		PAGE
3.4	X-ray diffraction examination	57
3.5	Optical and Scanning Electron Microscopy	59
3.6	Electron Microprobe Analyser	60
3.7	Transmission Electron Microscopy	61
3.8	Tensile testing	62
3.9	CHARPY V-notch impact test	63
3.10	Dimensional change test	63
3.11	Wear testing	64
4.	RESULTS	67
4.1	Zn-Al-Si phase diagram	67
4.2	Zn-Al-Cu-Si phase diagram	81
4.3	Hardness testing	107
4.3.1	Zn-Al-Si system	107
4.3.2	Zn-Al-Cu-Si system	117
4.4	X-ray diffraction examination	131
4.4.1	Zn-Al-Cu-Si system	152
4.4.1.1	Alloy of monotectoid composition in Zn-Al-Cu-Si system	152
4.4.1.2	Alloy of eutectoid composition in Zn-Al-Cu-Si system	154
4.4.1.3	Al-rich alloy in Zn-Al-Cu-Si system	156
4.4.2	Zn-Al-Si system	157
4.4.2.1	Alloy of monotectoid composition in Zn-Al-Si system	157
4.4.2.2	Al-rich alloy in Zn-Al-Si system	172
4.5	TEM examination	172

		PAGE
4.5.1	Alloy AlZn30Si5	172
4.5.2	Alloy AlZn60Cu3Si2	190
4.6	Physical and mechanical properties	203
4.6.1	Dimensional stability	203
4.6.2	Impact and tensile strength	203
4.6.3	Wearing property	206
5.	DISCUSSION	208
5.1	Zn-Al-Si phase diagram	208
5.2	Zn-Al-Cu-Si phase diagram	212
5.3	Mechanism of phase transformation in Zn-Al-Si and Zn-Al-Cu-Si system	216
5.3.1	Zn-Al-Cu-Si system	216
5.3.1.1	Alloys of monotectoid and eutectoid composition in Zn-Al-Cu-Si system	216
5.3.1.2	Al-rich alloy in Zn-Al-Cu-Si system	220
5.3.2	Zn-Al-Si system	222
5.3.2.1	Alloys of monotectoid and eutectoid compositions in Zn-Al-Si system	222
5.3.2.2	Al-rich alloy in Zn-Al-Si system	223
5.3.3	Fraction transformation curves	223
5.3.3.1	The cellular reaction	224
5.3.3.2	The fraction transformation curves of α_s' and β phases	226
5.3.3.3	The activation energy of the four-phase transformation	228
5.3.4	The seqmentation of the precipitates	228

		PAGE
5.4	The General Rule of phase transformation of supersaturated solid solutions of alloys	230
5.4.1	Relationships between the equilibrium phase diagram and the phase transformation on ageing	230
5.4.2	The General Rule of phase transformation	238
5.4.3	Free energy curve and surface	242
5.4.4	Kinetic consideration	248
5.5	The response of properties to phase transformations	250
5.5.1	Hardness	250
5.5.2	Impact, tensile strength, dimensional stability and wearing property	263
6.	CONCLUSION	268
7.	FUTURE WORK	277
8.	REFERENCES	279
9.	ACKNOWLEDGEMENTS	289

After one minute, the α'_s had vanished from the X-ray diffractogram, while the intensities of η phase had greatly increased. 1 or 2 minutes later, the transition phase occurred at the high angle side of the α'_T phase peak. After 7 minutes ageing, the Al-rich matrix phase α' was observed distinctly, while the multi-peaked α''_m phase was replaced by a single peak of the α'_m phase. After 15 minutes ageing at 100°C, the α'_T phase vanished and left α' as the matrix phase in equilibrium with α'_m. On prolonged ageing, α'_m vanished and α' phase changed to the final stable phase, α_f. The intensity of the η phase increased during the whole ageing process.

On examination at 170°C, it was found that α'_T phase had formed already after 15 seconds ageing, and that the decomposition of α'_s phase to α'_T and η phases was so fast that there were only α'_T and η phases observed after this short period of ageing at 170°C. The changes in the Al-rich matrix phase and the appearance and disappearance of the transition phases α''_m and α'_m occurred in the same way as on 100°C ageing, as shown in Figure 87.

The first two stages of ageing in alloy AlZn60Si5 were essentially similar to those in alloy AlZn60Cu3Si5.

(i) the decomposition of supersaturated α'_s to α'_T and η (or α'_T, ε and η phases)

(ii) the formation of transition phases as side bands of the peak on X-ray diffractogram.

But the ageing process in AlZn60Si5 was more rapid than in AlZn60Cu3Si2.

FIGURE	TITLE	PAGE
15	Isothermal section of Zn-Al-Cu system at 250°C[23]	20
16	The shapes of the β-phase field at 350°C, 290°C, and 280°C[23]	21
17	The Al-Zn phase diagram with proposed metastable miscibility gaps for the G.P. zone and the R-phase[40]	21
18	Relationship of hardness, resistivity, dimensions and the amount of zinc with the ageing time at room temperature for different alloys[54]	28
19	X-ray diffractometer results showing the kinetics of the decomposition of Al-60%Zn alloy at 240°C and then at 95°C[54]	28
20	A scheme of transformation in Al-Zn alloys[61]	30
21	TTT diagram for zinc-aluminium eutectoid alloy[62]	31
22	Changes in the intensity and angles of diffraction of supersaturated phase α'-phase and decomposition products (η phase and α phase) for alloy AlZn74/55 quenched from 603°C and then aged at 0°C, 20°C and 40°C[66]	31
23	Change in the interdiffusion coefficient D with zinc content and temperatures used in the homogenization process[55]	36

FIGURE	TITLE	PAGE
24	Solid-state reactions in the low-copper part of the Zn-Al-Cu system[71]	36
25	Hardness/time curves of alloy AlZn20Cu aged at 100°C and 150°C[75]	38
26	Diffractograms of alloy AlZn20Cu2 aged at 100°C[75]	38
27	Hardness/time curves of alloy AlZn50Cu2 aged at 50°C and 100°C[57]	39
28	Diffractograms of alloy AlZn50Cu2 aged at 100°C[57]	40
29	Dependence of the hardness of the supercooled α'-phase of the alloys AlZn78Cu1-3 on the time of ageing at the temperature 50°C[58]	42
30	Changes in the length of the sample of supercooled α'-phase as a result of ageing at temperature 50°C.[58]	42
31	Sets of diffractograms of AlZn78Cu1-3 alloy illustrating the four-phase transformation[58]. Numbers on abscissa denote grade.	43
32	Set of diffractograms of AlZn78Cu1-3 alloy after 62 hrs of ageing at the temperature 50°C[58]	43

FIGURE	TITLE	PAGE
33	Comparison of Stage II TTT diagrams in binary and quaternary alloy[62]	47
34	Diagram of the Wear Tester[63]	66
35	Isothermal section of Zn-Al-Si system at 350°C	70
36	Isothermal section of Zn-Al-Si system at 300°C	71
37	Isothermal section of Zn-Al-Si system at 280°C	72
38	Isothermal section of Zn-Al-Si system at 272°C	73
39	Isothermal section of Zn-Al-Si system at 230°C	74
40	The $\beta/\beta+\sigma$ phase boundry in Zn-Al-Si system at 350°C	75
41	The Si-rich (σ) phase field	76
42	Scanning Electron Micrographs for alloy ZnAlSi7 at 272°C	89
43	Optical micrographs for alloy ZnAlCuSi5 at 300°C. x560	91
44	Optical micrographs for alloy ZnAlCuSi5 at 350°C. x560	91

FIGURE	TITLE	PAGE
45	Optical micrographs for alloy ZnAlCuSi5 at 300°C. x980.	92
46	Optical micrographs for alloy ZnAlCuSi5 at 350°C. x980.	93
47	Optical microgtaphs for alloy ZnAlCuSi5 at 350°C. x430.	94
48	Scanning electron micrograph for alloy ZnAlCuSi5, at 300°C	94
49	Scanning electron micrographs for alloy ZnAlCuSi4 at 285°C, showing five phases ($\alpha+\beta+\varepsilon+T'+\sigma$) coexistance.	95
50	Scanning electron micrographs for alloy ZnAlCuSi3 at 285°C showing five phases ($\alpha+\beta+\varepsilon+T'+\sigma$) coexistance	98
51	Isothermal section of Zn-Al-Cu-Si system at 350°C	101
52	Isothermal section of Zn-Al-Cu-Si system at 300°C.	102
53	Isothermal section of Zn-Al-Cu-Si system at 290°C	103
54	Isothermal section of Zn-Al-Cu-Si system at 285°C	104

FIGURE	TITLE	PAGE
55	Isothermal section of Zn-Al-Cu-Si system at 280°C	105
56	Isothermal section of Zn-Al-Cu-Si system at 275°C	106
57	Hardness curves of alloy AlZn60Si5 aged at 50°C, 70°C, 100°C, 150°C, 170°C,	111
58	Hardness curves of alloy AlZn30Si5 aged at 50°C, 70°C, 100°C, 150°C, 170°C	112
59	Hardness curves of alloy AlZn75Si2 and AlZn95Si2 aged at 50°C, 70°C, 100°C.	113
60	Hardness curves of alloy AlZn10Si5 aged at 50°C, 70°C, 100°C, 150°C, 170°C	114
61	Hardness curves of alloy AlZn60Cu3Si2 aged at 50°C, 70°C, 100°C, 150°C, 170°C	121
62	Hardness curves of alloy AlZn30Cu3Si2 aged at 100°C, 150°C, 170°C.	122
63	Hardness curves of alloy AlZn75Cu3Si2 aged at 50°C, 70°C	123
64	Hardness curves of alloy AlZn75Cu3Si2 aged at 100°C, 150°C, 170°C	124
65	Arrenhanius plot for determination of activation energies of hardening for alloy Zn-Al-Si	116

FIGURE	TITLE	PAGE
66	Activation energy plot of $\alpha_f+\varepsilon \rightarrow T'+\eta$ in alloy AlZn75Cu3 Si2	127
67	Arrenhenius plot for determination of activation energies of hardening for alloys Zn-Al-Cu-Si	128
68	Response of hardness to phase transformation deduced from X-ray diffraction for alloy alloy AlZn60Cu3Si2 aged at 100°C	129
69	Transformation curves of phases in alloy AlZn60Cu3Si2 aged at 150°C	134
70	Transformation curves of phases in alloy AlZn75Cu3Si2 aged at 100°C	135
71	Transformation curves of phases in alloy AlZn75Cu3Si2 aged at 150°C.	136
72	Transformation curves of phases in alloy AlZn75Cu3Si2 aged at 170°C	137
73	Fraction transformation of η phase in alloy AlZn60Cu3Si2 aged at 100°C deduced from η (0002) peak for $\alpha'_s \rightarrow \alpha'_T+\varepsilon+\eta$	138
74	Friction transformation of ε phase in alloy AlZn30Cu3Si2 aged at 170°C, deduced from ε (10$\bar{1}$1) peak.	139

FIGURE	TITLE	PAGE
75	Fraction transformation of ε phase in alloy AlZn75Cu3Si2 aged at 170°C, 150°C 100°C for $\alpha_f + \varepsilon \rightarrow T' + \eta$.	140
76	Set of X-ray diffractograms of alloy AlZn60Cu3Si2 aged at 100°C.	159
77	Set of X-ray diffractograms of alloy AlZn60Cu3Si2 aged at 70°C, showing the cellular reaction before G.P.zones.	161
78	Set of X-ray diffractograms of alloy AlZn60Cu3Si2 aged at 150°C.	162
79	Set of X-ray diffractograms of alloy AlZn75Cu3Si2 aged at 100°C.	163
80	Set of X-ray diffractograms of alloy AlZn75Cu3Si2 aged at 100°C, showing the cellular reaction before G.P.zones.	164
81	Optical micrograph of as-quenched alloy AlZn75Cu3Si2, showing the discontinuous precipitates along the grain boundary. x420.	165
82	Optical micrograph of alloy AlZn75Cu3Si2 showing the developed discontinuous precipitates along the boundary after 25 minutes ageing at 100°C. x420.	165

FIGURE	TITLE	PAGE
83	Set of X-ray diffractograms of alloys AlZn75Cu3Si2 aged at 150°C.	166
84	Set of X-ray diffractograms of alloys AlZn30Cu3Si2 aged at 170°C.	167
85	Set of X-ray diffractograms of alloys AlZn30Cu3Si2 aged at 100°C.	168
86	Set of X-ray diffractograms of alloys AlZn60Si5 aged at 100°C.	169
87	Set of X-ray diffractograms of alloys AlZn60Si5 aged at 170°C.	170
88	Set of X-ray diffractograms of alloys AlZn30Si5 aged at 170°C.	171
89	Transmission electron micrographs showing particles precipitation in alloy AlZn225Si7.4 after 2 months ageing at room temperature. x42.4K. a) bright field b) dark field	175
90	The electron diffraction pattern from the matrix shown in Figure 89(a).	176
91	Transmission electron micrographs showing rod shaped precipitates, parallel to a 110 direction in the (112) - oriented region. x.108K. a) bright field b) dark field	177

FIGURE	TITLE	PAGE
92	The electron diffraction pattern from the matrix shown in Figure 91 (a)	178
93	Transmission electron micrographs showing G.P. zones in alloy AlZn30Si5 aged at 100°C 8.5 minutes. x42.4K.	178
94	Transmission electron micrograph of alloy AlZn30Si5 aged at 100°C for 1.5 hrs x42.4K	179
95	The electron diffraction pattern from the matrix in Figure 94	179
96	Transmission electron micrograph of alloy AlZn30Si5 aged at 100°C for 24 hrs, showing the segmentation of the zinc-rich precipitates. x34.5K	180
97	Transmission electron micrograph of alloy AlZn30Si5 aged at 100°C for 24 hrs, showing the segmentation of the zinc-rich precipitates. x34.5K a) bright field b) dark field	181
98	Transmission electron micrograph of alloy AlZn30Si5 aged at 100°C for 24 hrs, showing the segmentation of the zinc-rich precipitates. x42.4K a) bright field b) dark field	182

FIGURE	TITLE	PAGE
99	Transmission electron micrographs of alloy AlZn30Si5 aged at 100°C for 24 hrs, showing the segmentation of the zinc-rich precipitates	183
100	Transmission electron micrographs of alloy AlZn30Si5 aged at 100°C for 24 hrs, showing the segmentation of the zinc-rich precipitates. x34.5K	183
101	Transmission electron micrograph of alloy AlZn30Si5 aged at 100°C for 24 hrs, not showing the segmentation of the zinc-rich precipitates. x130K	184
102	The electron diffraction pattern from the matrix in Figure 97	184
103	Transmission electron micrographs of alloy AlZn30Si5 aged at 100°C for 24 hrs. x86.5K a) bright field b) dark field	185
104	The electron diffraction pattern from Figure 103(a)	186
105	The index of the electron diffraction pattern in Figure 104	186
106	Transmission electron micrographs of alloy AlZn30Si5 aged at 100°C for 24 hrs a) bright field b) dark field	187

FIGURE	TITLE	PAGE
107	The dispersive X-ray energy spectrum from the matrix in Figure 106(a), obtained from the STEM.	188
108	The dispersive X-ray energy spectrum from the zinc-rich α_m' phase in Figure 106(a).	189
109	Transmission electron micrograph of alloy Al Zn60 Cu3 Si2 aged at 100°C for 2 minutes, showing a two-phase equiaxed structure. x.39K.	193
110	Transmission electron micrograph of alloy Al Zn60 Cu3 Si2 aged at 100°C for 2 minutes showing the lamellae structure. x86.5K.	193
111	Transmission electron micrograph of alloy Al Zn60 Cu3 Si2 aged at 110°C for 8.5 minutes x.130K.	194
112	The electron diffraction pattern from the matrix in Figure 111.	194
113	Transmission electron micrograph of alloy Al Zn60 Cu3 Si2 aged at 100°C for 8.5 minutes x.64.8K.	195
114	Transmission electron micrograph of alloy Al Zn60 Cu3 Si2 aged at 100°C for 8.5 minutes x.78.9K.	195

FIGURE	TITLE	PAGE
115	Transmission electron micrograph of alloy AlZn60Cu3Si2 aged at 100°C for 15 minutes. x.108K.	196
116	Transmission electron micrograph of alloy AlZn60Cu3Si2 aged at 100°C for 24 minutes. x.64.8K.	197
117	The electron diffraction pattern from the matrix in Figure 116.	197
118	Transmission electron micrographs of alloy AlZn60Cu3Si2 aged at 100°C for 18 hrs.	198
119	Transmission electron micrographs of alloy AlZn60Cu3Si2 aged at 100°C for 18 hrs, showing the ε precipitate. x.390K. a) bright field b) dark field	199
120	The electron diffraction pattern from Figure 119 (a)	200
121	The dispersive X-ray energy spectrum from ε precipitate in Figure 119(a).	201
122	Transmission electron micrograph of alloy AlZn60Cu3Si2 aged at 100°C for 48 hrs. x.42.4K.	202

FIGURE	TITLE	PAGE
123	Transmission electron micrograph of alloy AlZn60Cu3Si2 aged at 100°C for 48 hrs. x.42.4K.	202
124	Dimensional stability of alloy ZnAlSi after solution treatment, quench ageing at 150°C.	204
125	Vertical section through the Zn-Al-Si diagram at 0.21%Si.	209
126	The typical phase diagram in temperature in range 266°C - 275°C.	210
127	Free energy surfaces of phases in alloys ZnAlCu and ZnAlCuSi at various temperatures (a) and at various stages of ageing (b).	247
128	The Zn-Al binary phase diagram, showing the lever rule.	254

LIST OF TABLES

TABLE	TITLE	PAGE
1	Mechanical properties of Zn-Al based alloys.	51
2	Mechanical properties of heat-treated alloys (Zn-Al based)	51
3	Alloy Compositions used for determination of phase diagram of Zn-Al-Si system	69
4	Alloy compositions used for determination of phase idagram of Zn-Al-Cu-Si system	69
5	Alloy compositions used for ageing processes of Zn-Al-Si system	110
6	Alloy compositions used for ageing processes of Zn-Al-Cu-Si systems	110
7	The identified phases and their composition for Zn-Al-Si systems	77
8	The equilibrium temperature and time of homogenization in Zn-Al-Si systems	79
9	The lattice parameters of alloy Zn-Al-Si at 272^{o}C	80
10	The identified phases and their composition for Zn-Al-Cu-Si systems	84
11	The equilibrium temperature and time of homogenization in Zn-Al-Cu-Si systems	88

TABLE	TITLE	PAGE
12	The lattice parameters (A) of cubic phases in Zn-Al-Cu-Si systems	80
13	Data for activation energy of hardening of alloy AlZn30Si5 from the hardness curves in Figure	115
14	Data for activation energy of hardening of of alloy AlZn60Si5 from the hardness curves in Figure	115
15	Data for activation energy for four-phase transformation $\alpha_f+\varepsilon \rightarrow T'+\eta$ of alloy AlZn75Cu3 Si2 deduced from hardness testing	125
16	Data for activation energy of hardening of alloy AlZn60Cu3Si2 from the hardness curves in Figure	126
17	Data for activation energy of hardening of alloy AlZn30Cu3Si2 from the hardness curves in Figure	126
18	Hardness data of both ZnAlSi and ZnAlCuSi systems	130
19	The characteristic Bragg angle (2θ) for identification of phase transformations.	132
20	Data for transformation curves of η phase in alloy AlZn60Cu3Si2 aged at 100°C	141

TABLE	TITLE	PAGE
21	Data for transformation curves of η phase in section α'→α'+ε+η for alloy AlZn60Cu3Si2 aged at 100°C	142
22	Data for transformation curve of ε phase in alloy AlZn60Cu3Si2 aged at 100°C	142
23	Data for transformation curves of η phase in alloy AlZn30Cu3Si2 aged at 170°C	143
24	Data for transformation curve of η phase in alloy AlZn60Cu3Si2 aged at 150°C	144
25	Data for transformation curve of ε phase in alloy AlZn60Cu3Si2 aged at 150°C	144
26	Data for transformation curve of T' phase in alloy AlZn60Cu3Si2 aged at 150°C	145
27	Data for transformation curve of ε phase in alloy AlZn75Cu3Si2 aged at 150°C	146
28	Data for transformation curve of η phase in alloy AlZn75Cu3Si2 aged at 150°C	146
29	Data for transformation curve of T' phase in alloy AlZn75Cu3Si2 aged at 150°C	147
30	Data for transformation curve of phase ε in alloy AlZn75Cu3Si2 aged at 170°C	148

TABLE	TITLE	PAGE
31	Data for transformation curve of phase T' in alloy AlZn75Cu3Si2 aged at 170°C	148
32	Data for transformation curve of phase ε in alloy AlZn75Cu3Si2 aged at 170°C	149
33	Data for transformation curve of phase ε in alloy AlZn75Cu3Si2 aged at 100°C	149
34	Data for transformation curve of phase η in alloy AlZn75Cu3Si2 aged at 100°C	150
35	Data for transformation curve of phase T' in alloy AlZn75Cu3Si2 aged at 100°C	151
36	Data for activation energy for four-phase transformation $\alpha_f+\varepsilon \rightarrow T'+\eta$ of alloy AlZn75Cu3Si2 determined on X-ray diffraction examination	125
37	Mechanical properties of alloy Zn-Al-Si and Zn-Al-Cu-Si (after 100 hrs aged at 100°C)	205
38	The wear rate ($x\ w^{-8} cm^3/cm$) for Zn-Al-Cu-Si system and as-cast iron with 2kgf load and 0.84 m/s.	207
39	The wear rate ($x\ w^{-8} cm^3/cm$) for Zn-Al-Si systems systems with 2kgf load and 0.84 m/s.	207

TABLE	TITLE	PAGE
40	Heat treatment for the wear rate of alloy AlZn6OCu3Si2 with different loads	207

LIST OF PHASES

EQUILIBRIUM

α	Al-rich f.c.c. phase
β	Zn-rich f.c.c. phase
ε	$CuZn_4$ phase
η	Zinc rich h.c.p. phase
T'	Cu-rich phase
σ	Si-rich phase

NON-EQUILIBRIUM

α'_s	Supersaturated phase
β	Supersaturated phase
α'_T	Al-rich eutectoid terminal phase derived from β or α'_T going to spinodal decomposition
α''_m	The first transition phase
α''	The Al-rich matrix phase in equilibrium with α''_m
α'_m	The second transition phase
α'	The Al-rich matrix phase in equilibrium with α'_m
α_f	Al-rich final stable phase
η	Zinc-rich phase
ε	Zn-rich metastable phase
T'	Cu-rich phase
σ	Si-rich phase

1. INTRODUCTION

1.1 Solid state phase transformations

Most materials are subjected to one or more phase transformations in the course of their manufacture. The more crucial the properties of a material the more likely it is that phase transformations will be used in its preparation.

Adequate mechanical properties are primary requirements of most materials. Various methods are used to improve the properties. The most common method is alloying - the addition of other components to the base material. However, heat treatment has been found to be the appropriate way to cause alloys to undergo the phase transformation that harden and strengthen them while retaining the alloy's original shape.

During quenching, excess vacancies may be retained in solution and their movement allows easy diffusion of solute atoms which tend to cluster to form zones. The shape of these zones (spherical, disc shape etc) depends on the relative size of solute and solvent atoms. Transition phases form from the G.P. zones. Both G.P. zones and transition phases have been found to give great improvements in the mechanical properties of alloys.

The changes in structure and properties that are induced by heat treatment are of great intrinsic interest as well as of practical importance since they provide a method of obtaining high-strength alloys. The technique is to quench the alloy from a single-phase field to obtain a

supersaturated phase and then to age this at various temperatures inside the two-phase field. It is preferable to have a relatively large volume of precipitated phase and to carry out the precipitation at the lowest possible temperature to maximise the number and minimise the distance between precipitated particles. The degree of supersaturation, that is the quantity of solute which can be precipitated, and the dispersion of the phases, are sensitively involved within the technique.

However, the phase relationship is the most fundamental factor which determines the changes occurring in heat treatment of multi-component alloys. From the point of view of thermodynamics, phases of different structures give rise to different properties. Different relationships of these phases lead to different phase transformations in an equilibrium or non-equilibrium state. Based on the knowledge of phase relationships and phase transformations, various combinations of alloying and heat treament may be employed to avoid unwanted phases and to create some appropriate phases with special properties for practical purposes.

In order to produce some alloys with special properties, a basic thermodynamic investigation, including the determination of the equilibrium phase diagram and phase transformations is of paramount importance.

With the help of modern X-ray diffraction techniques, it has been possible to determine metallurgical equilibrium diagrams and furthermore to trace each step of the phase transformations

and the structural changes. By correlating X-ray diffraction results with optical metallography, the phases in an alloy and its crystal structures could be determined, and metastable and transitional states to be detected. This technique is of value where solid solubility is restricted with falling temperature and very fine precipitated particles, which may escape detection under microscopy, are formed during phase transformation, especially in the ageing processes.

Instead of regular chemical analysis, electron probe microanalysis can be used for accurate determination of chemical composition of each phase in the alloy, and hence the boundaries of a three-phase field can be determined with only a single specimen at one time.

The Scanning Electron Microscope gives high resolution images for both electrons and X-rays of each phase in the alloy. By identifying the characteristic energies and measuring the rate of emission of these X-ray photons, chemical analysis can be obtained from small selected areas, provided these are larger than about 10μm across. With flat polished samples, quantitative analyses are possible. In the case of rough surfaces such as inclusions on fracture surfaces, the chemcial analysis is normally only qualitative.

The thin foil technique is required to trace structural changes in alloys by transmission electron microscopy. It is available for any alloy system and will allow the detailed morphology of the ageing reaction to be determined, while selected area diffraction of the specimen in the electron microscope enables the structure of the precipitated

phases to be obtained. In conjunction with kinetic studies, this technique enables an almost complete account to be given of the structural changes occurring during the ageing of alloys.

Hardness testing provides another method of tracing the phase transformation during ageing processes. Combined with the X-ray examination results more detailed information about the phase transformations can be obtained.

Various methods of measurement of mechanical and physical properties are used for showing the influence of phase transformation on properties of alloys, such as hardness, tensile strength, impact properties, dimensional stability and wear resistance properties, etc.

1.2 Zinc-based alloys as bearings

Plain bearing alloys usually are characterised by a two-phase structure where one of these phases, the harder one, plays the role of a load-bearing component and the other, being softer, gives the essential properties of conformability and embeddability.

Zn-Al alloys have been considered for use as bearing materials for many years (Köster, 1941)[1]. The decomposition of the supersaturated phase in the alloy gives a uniform distribution of two phases, α and η, with low melting points, which given natural oxidation of the surface, produces surface oxide films with excellant bearing behaviour

When a small amount of a third element is present, the phase relationships are changed. Based on the broad single solid phase field, Zn-Al binary alloys with a small amount of some third element provide the possibility to develop quite different properties in alloys by heat treatment. The phase relationship also implies that a variety of hardening mechanisms will be operative, depending on the position of the alloy in the phase diagram and on the cooling rate upon casting or after heat treatment.

Several Zn-Al alloys with small amounts of copper and silicon have been found to have excellent tribological properties[2-8]. The softer matrix phase of α and η of low melting points are used to confirm to the loading, while a dispersion of hard particles of T' phase and Si-rich phase, (σ) bear the loads in the softer matrix phases.

1.3 Scope of the Research

However there is little inforamtion on Zn-Al based multi-component alloys available in the literature, and such information as is knwon can not be interpreted until the phase diagram and metastable phase transformations which occur on heat treatment have been established. It was the object of this work, to determine the Zn-Al-Si ternary phase diagram and the Zn-Al-Cu-Si quartenary phase diagram for temperatures below the solidus in each case, and compare these with the established Zn-Al and Zn-Al-Cu diagrams.

Following this several alloys could be chosen which might ultimately form the basis of commercially useful alloys,

and the details of the phase transformations and their dependence on composition and heat treatment were to be established. This was considered to be essential as the metastable phase transformations in alloys containing silicon and/or copper were either unknown or only partially understood.

Finally, the properties of selected alloys were to be determined so that an assessment could be made of the commercial advantages or disadvantages of these alloys as structural materials (for gravity or sand castings) or as stock for use as plain bearings.

2. LITERATURE SURVEY

2.1 The Equilibrium Phase Diagrams

2.1.1 Binary Systems

Al-Zn : The most important recent work on the zinc-aluminium system is that of Ellwood[9,10], the Russian group Presnyakov, Goban and Chervyakova[11] and Goldak and Parr[12]. All of them used high temperature X-ray cameras to measure lattice parameters for determining the limits of solubility in solid solutions.

The phase diagram of Presnyakov et al, modified by Goldak and Parr has been adopted for representation of the Zn-Al binary diagram, shown in Figure 1. The aluminium-rich terminal solid solution is called α. That part of it which lies on the zinc-rich side of the monotectoid is α' and f.c.c. zinc-rich eutectoid phase is called β. η is the zinc-rich terminal solid solution. The lattice parameter/temperature curves and the lattice-parameter isotherms of Al-rich phase are given in Figures 2, 3[12] and show the presence of a narrow $\alpha' + \beta$ two-phase field. This is interpreted as proof of the peritectic and eutectoid features shown in the above binary diagrams.

The Zn-Al system is characterised by the wide range of aluminium content in the solid solution with f.c.c. crystal structure, from about 19% Al to 100% Al at 350°C to 400°C, and a large two phase field, $\alpha + \eta$, below the horizontal eutectoid (275°C).

Al-Si and Zn-Si : The two binary phase diagrams[15]

are shown in Figures 5,6. According to lattice-parameter measurements, it was concluded that zinc and silicon are insoluble in each other. Silicon dissolves very slightly in aluminium but aluminium is insoluble in silicon.

Al-Cu and Zn-Cu : The phase diagrams of these two systems are shown in Figures 7,8[16][17]. The Zn-Cu system phase diagram shows five peritectics. Four intermediate phases exist, β, γ, δ and ε which with the exception of the δ phase, have broad range of solid solubility.

The phase diagram of the Al-Cu system consists of two parts, eutectoids at both Cu- and Al-rich ends and several peritectics between these two eutectics. Al-,Zn-rich solid solutions are especially investigated in the Al-Cu and Zn-Cu binary systems for further understanding of the ternary and quaternary system.

From the phase diagrams the solubilities of copper in aluminium or zinc are of the order of 1 to 4% at 300°C-400°C.

2.1.2 The Ternary Zn-Al-Cu Alloy Phase Diagram

With the help of microscopic and X-ray analysis, Köster and Moeller[1] established the isothermal section of the Zn-Al-Cu system at 350° initially. It is shown in Figure 9. One narrow single-phase field between 56% and 58% Cu and 10% to 30% Zn was formed and named the ternary phase T. It was isomorphous with Cu_3NiAl_6 and had an ordered

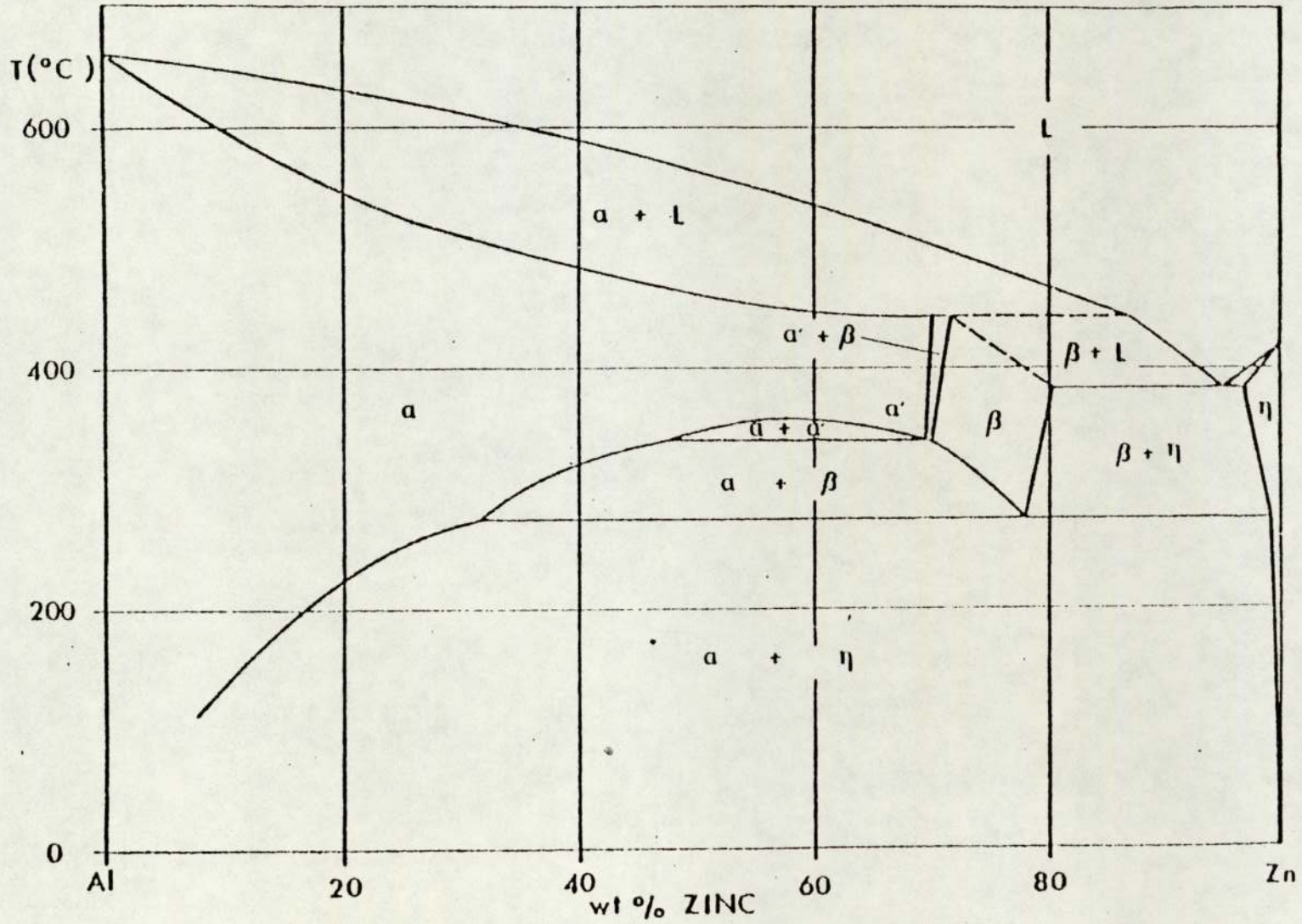

Fig.1 phase diagram of Al-Zn system.

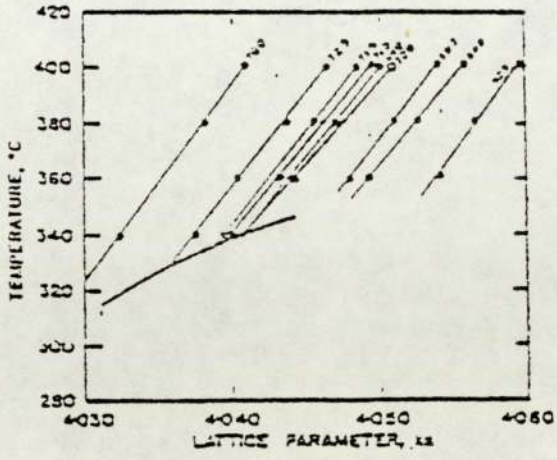

Fig. 2 Lattice-parameter/temperature curves

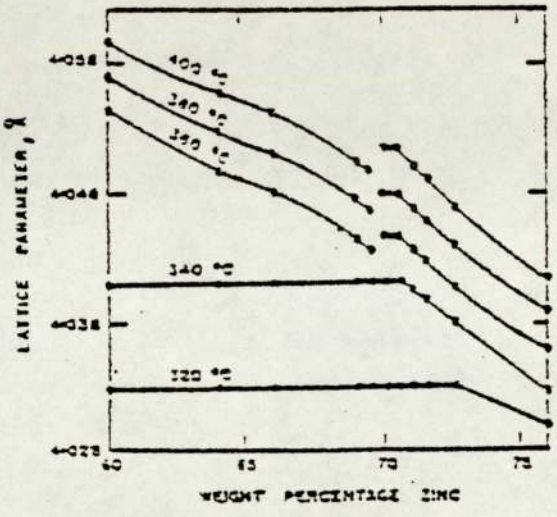

Fig. 3 Lattice-parameter isotherms

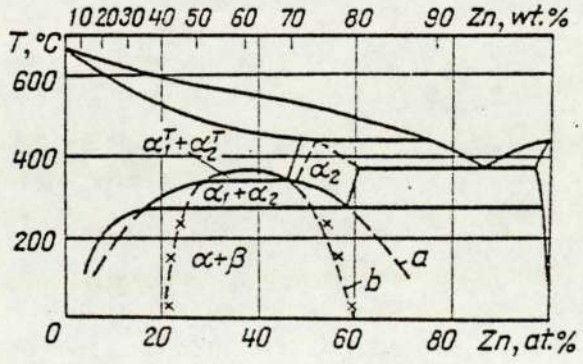

FIG. 4. Phase diagram of system Al–Zn: *a*, *b* — metastable diagrams according to [68]

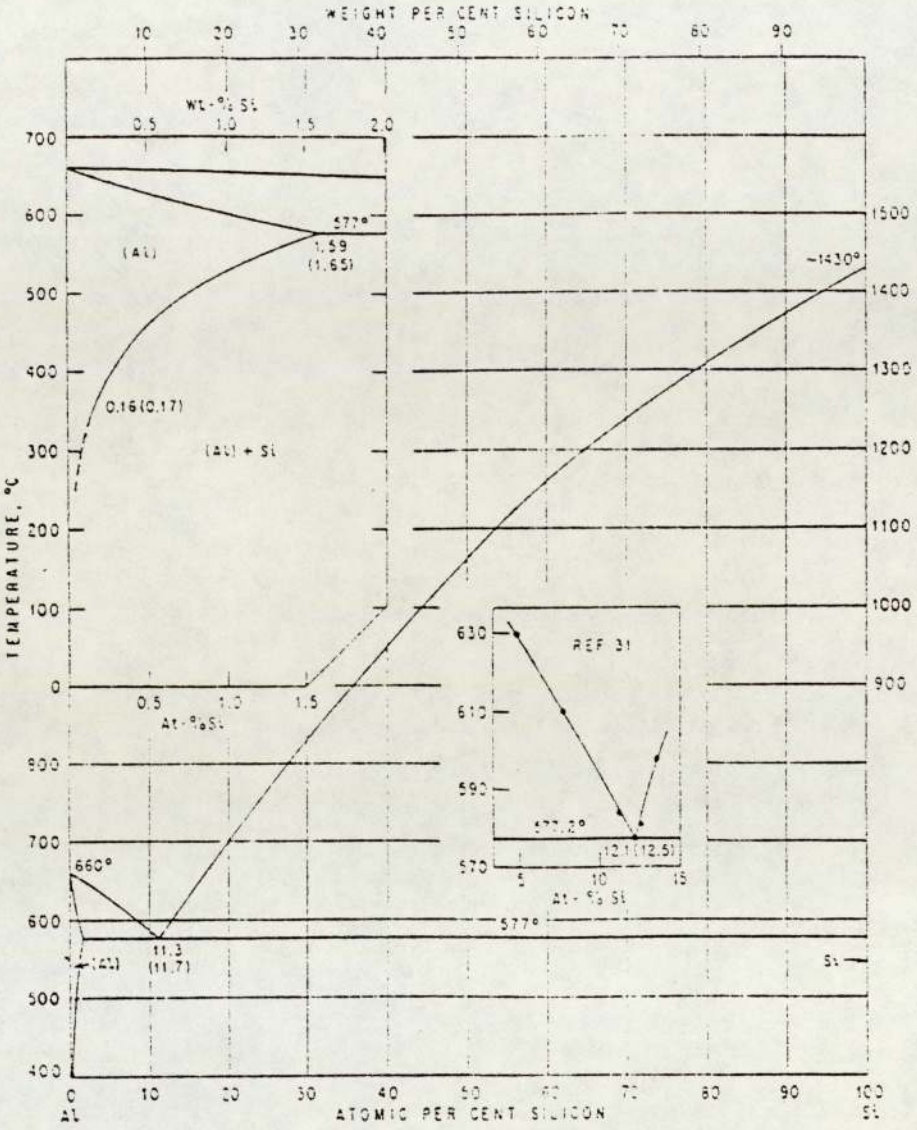

Fig.5

Phase Diagram of Al-Si System

Si-Zn Silicon-Zinc

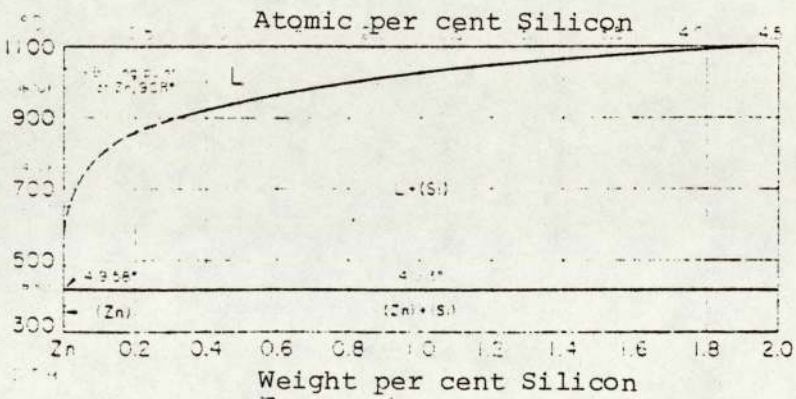

Fig. (6)

Phase Diagram of Si-Zn System

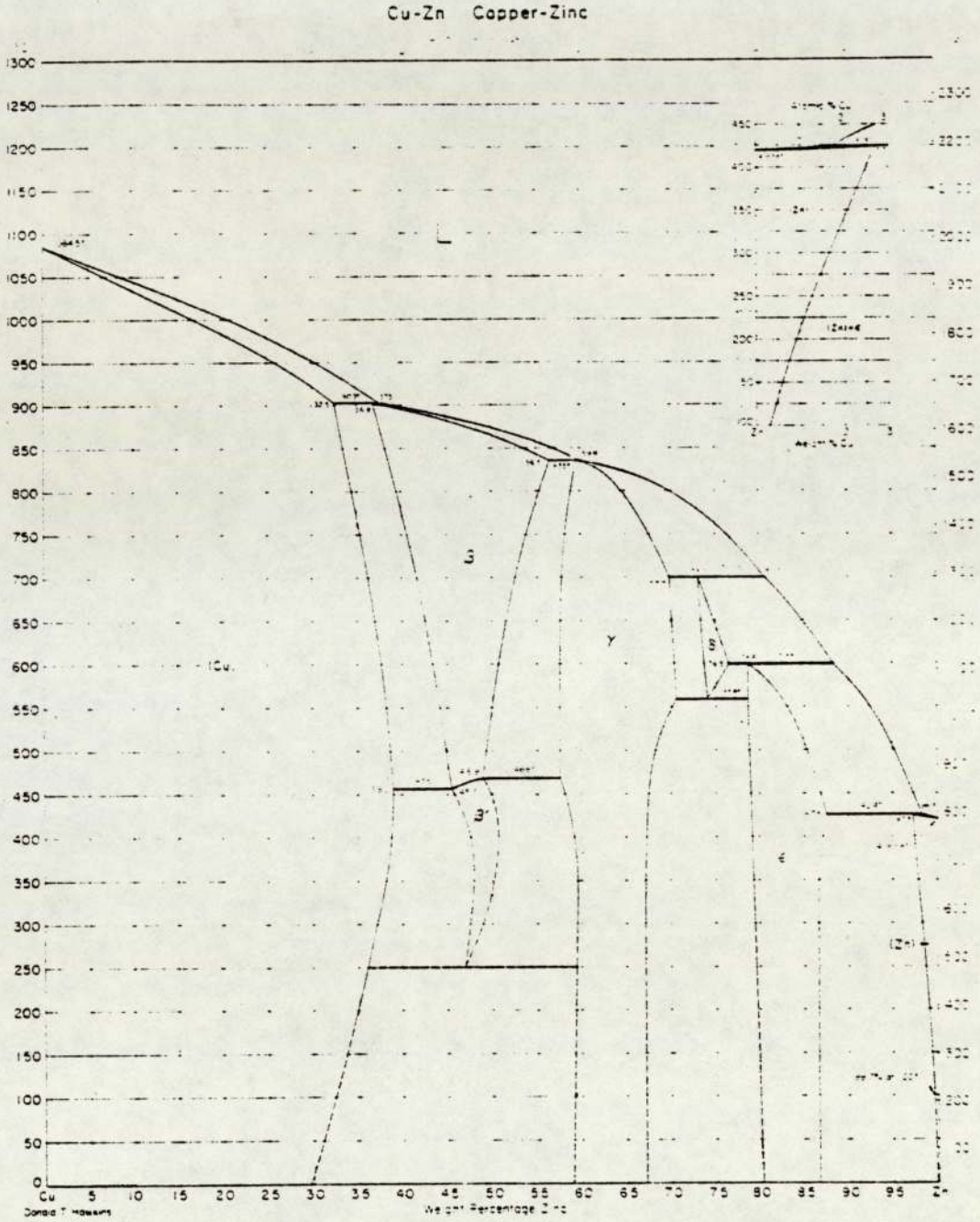

Copper-zinc phase diagram showing five peritectics.

Fig. 8

CsCl-type structure at high temperature.

In their later papers, Köster and Moeller[18][19] extended the work to several other temperatures, i.e. 400°C, 500°C, 600°C and 700°C and determined the shape of the liquidus surface, Figure 10. The principle feature of this is a eutectoid through which extends from the Al-Cu binary edge at 67% Al across to a point near 90% Zn where it meets a peritectic through from the Cu-Zn edge and a eutectic trough from the Al-Zn edge to form a ternary eutectic point. The peritectic reaction in the Al-Zn systems was not established when this work was carried out and does not appear in this diagram.

From their extended work it was found that the Al-rich end of the single-phase field T (at approximately Al_5Cu_4Zn) had a lower symmetry at temperatures below 450°C. The other end of the phase field corresponding to approximately $Al_{3.5}Cu_5Zn_2$ retained the CsCl structure. Köster denoted the ordered CsCl type structure as T phase and called the low symmetry structure T'[18][19].

The structure of T phase was also investigated by Bradley and Lipson[20]. It was found to be a structure based on a deformed b.c.c. cell.

Recently Murphy[23] established the structure of this T' phase. This was found to be similar to T phases in other systems[21][22] (with a rhombohedral structure with $a = 8.676$ Å and $\alpha = 27.41°$). The structure was a super-lattice based on an assemblage of five small CsCl-type

cells, joined corner to corner along the [111] direction. The phase was found to consist of alternate planes of Al and Cu atoms arranged perpendicular to the triad axis, with the central atom site in the cell vacant. This ordered vacancy was responsible for the superlattice lines in the diffraction patterns.

It was suggested that the zinc replaced a small proportion of the aluminium than the T lattice in order to reduce the electron/atom site ratio.

Conflicting results were obtained as a result of work on the solid-state phase reactions in the low-copper part of the phase diagram[12,18,23]. Murphy[23] resolved these by using electron probe microanalysis to determine the isothermal sections at 350°C, 290°C, 280°C, 270°C and 250°C as shown in Figures 11-15.

The shape and extent of the β phase field was considered to be important by Murphy as it determined the phase structure of some commercially important bearing alloys[23]. The β phase field was large at 350°C, but changed shape quite considerably on cooling. The copper-rich β in equilibrium with ε and η reduced rapidly in zinc content on cooling. The shapes of the β phase fields at 350°C, 290°C and 280°C are shown in Figure 16. The strong change in zinc content of β phase with copper content at the 0 to 2% level significantly altered the relative proportions of β and η phases.

Murphy[23] investigated the low-copper part of the Zn-Al-Cu phase diagram. As a result of this work, the

Zn-Al-Cu system was firmly established and more detailed information on the solid state phase reactions was obtained. It was found that the series of solid state phase reactions was obtained. It was found that the series of solid-state phase changes which occurred on cooling was similar to that proposed by Gebhadt and Köster[1][18][19][72-74].

The 350°C isothermal section was characterised by broad two-phase fields although the exact extent of the $\beta+T'$ field could not be ascertained due to the difficulty of differentiating α,α' and β from each other when the compositions were similar.

At 290°C the phase relationships were similar to those at 350°C. However the T phase in the phase-field $(\alpha+\beta+T')$ was found to be too small to determine its composition in these alloys. The $(\beta+T')$ two-phase field in particular was extremely narrow. Apparently, a phase reaction was about to occur :

$$\beta + T' \rightleftharpoons \alpha + \varepsilon$$

A two-phase field $(\alpha+\varepsilon)$ appeared instead of the two-phase field $(\beta+T')$ after a Class II four-phase transformation. Two three-phase fields $(\alpha+\varepsilon+T')$ and $(\alpha+\beta+\varepsilon)$ were found to be separated by a narrow two-phase field $(\alpha+\varepsilon)$ at 280°C. The β phase still existed at this temperature. The three-phase field $(\beta+\varepsilon+\eta)$ was separated from the $(\alpha+\beta+\varepsilon)$ phase field by the two-phase field $(\beta+\varepsilon)$.

Two important changes had occurred by 270°C. The two phase field (β+ε) disappeared and the (α+ε) phase field had contracted extremely. That meant that another Class II four phase transformation was going to occur just below 270°C :

$$\alpha + \varepsilon \rightleftharpoons T' + \eta$$

This transformation lead to the vanishing of ε phase in the low-copper alloys and left three stable phases, α, T' and η, as the final products of low-temperature equilibration.

Two steps of composition modulation of the metastable α phase occurred between the two four-phase transformations :

$$\beta + \varepsilon \rightleftharpoons \alpha + \eta$$

and

$$\alpha + \varepsilon \rightleftharpoons T' + \eta$$

and after the final Class II four-phase transformation.

The three four-phase transformations which occurred under equilibrium conditions were summarised as follows :

$\beta + T' \rightleftharpoons \alpha + \varepsilon$	at 288°C
$\beta + \varepsilon \rightleftharpoons \alpha + \eta$	at 280-275°C
$\alpha + \varepsilon \rightleftharpoons T' + \eta$	at 268°C

According to Gebhardt's investigations, the solid-state reactions in the low-copper part of the Zn-Al-Cu system is shown in Figure 24.

2.2 Phase Transformations

2.2.1 Binary Zn-Al Alloys

Structural changes in the Zn-Al alloys during ageing of the supersaturated solid solution have been a subject

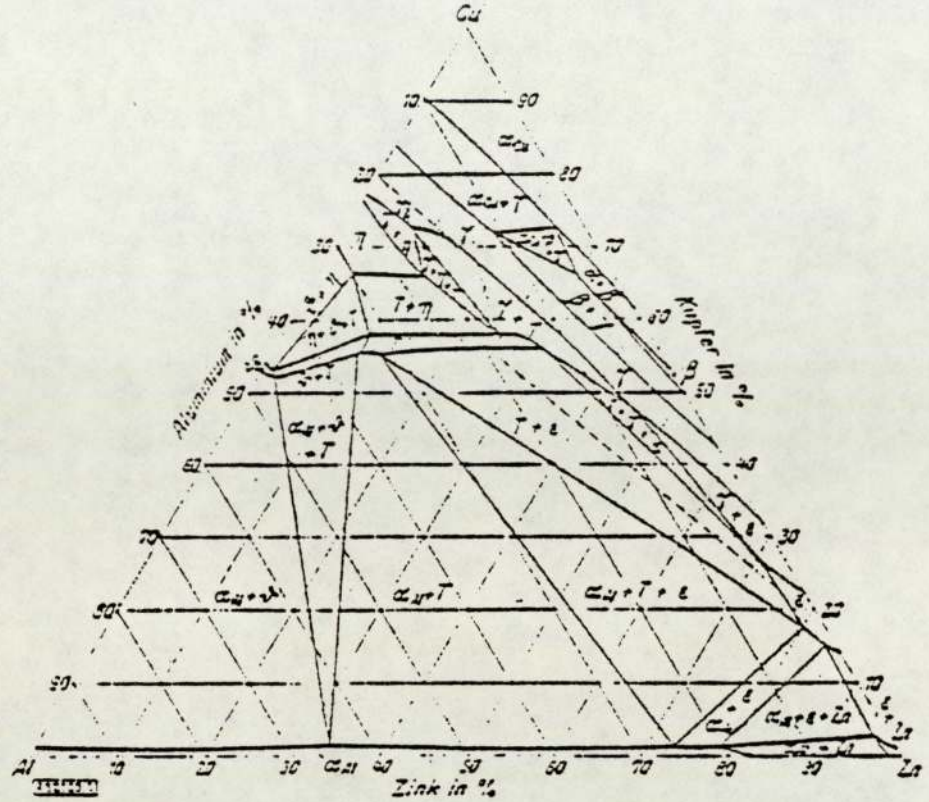

Fig. 9 Isothermal section of Zn-Al-Cu ternary system at 350°C

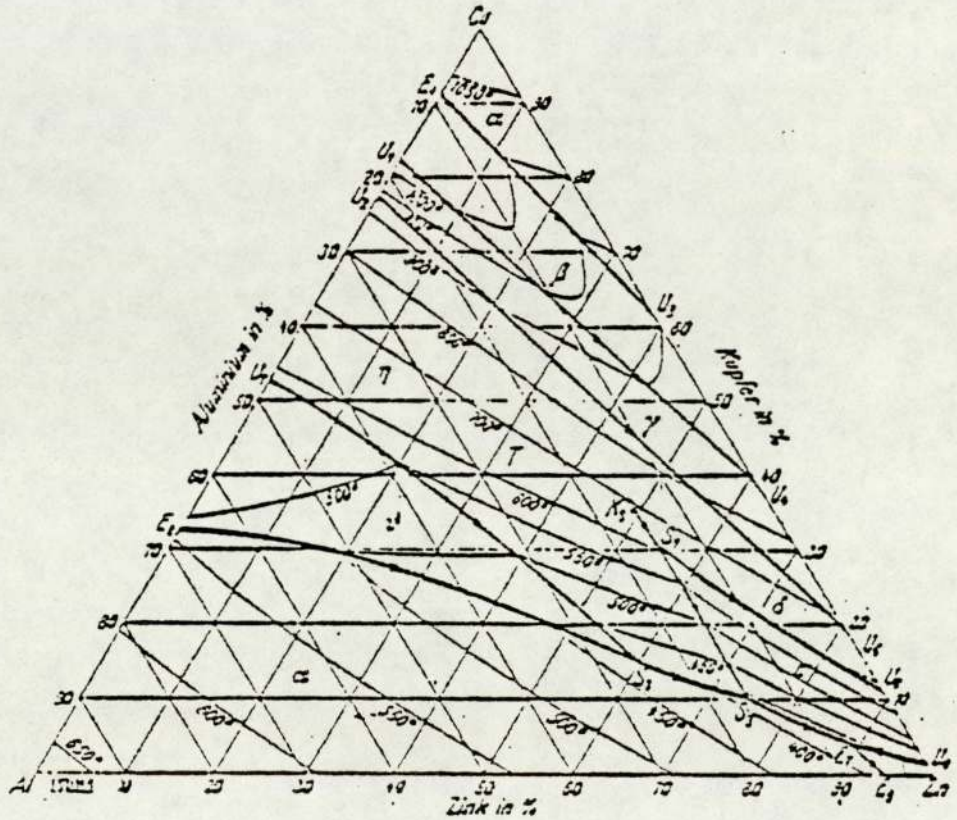

Fig. 10 Liquidus surface of the Zn-Al-Cu system

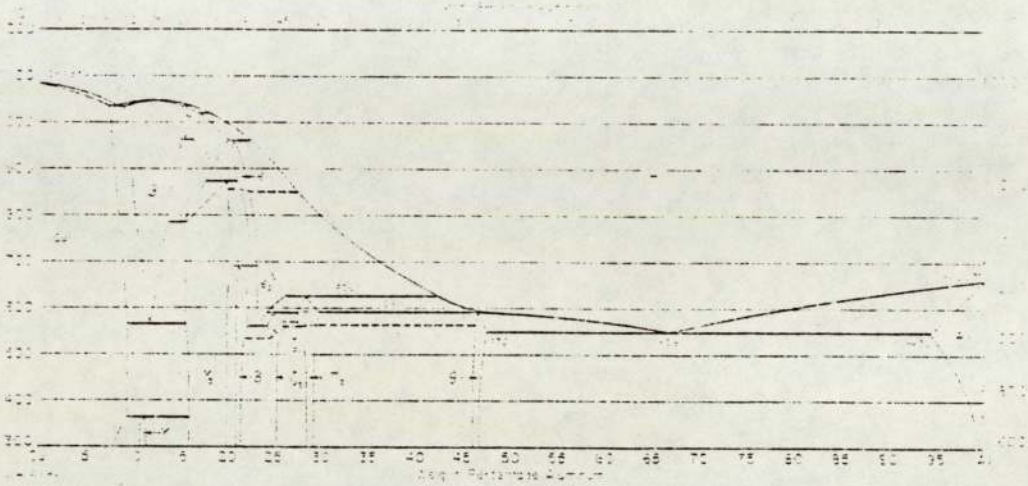

Fig.7
Phase Diagram of Al-Cu System

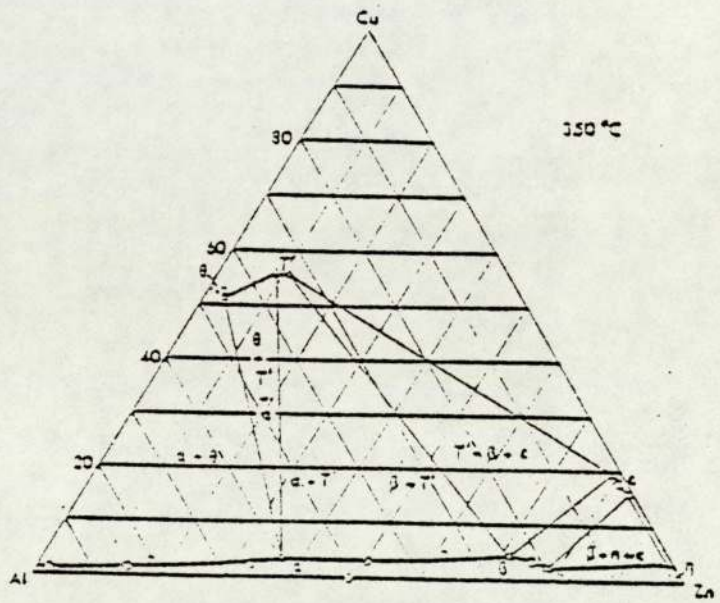

Fig. 11 Isothermal section of Zn-Al-Cu system at 350°C

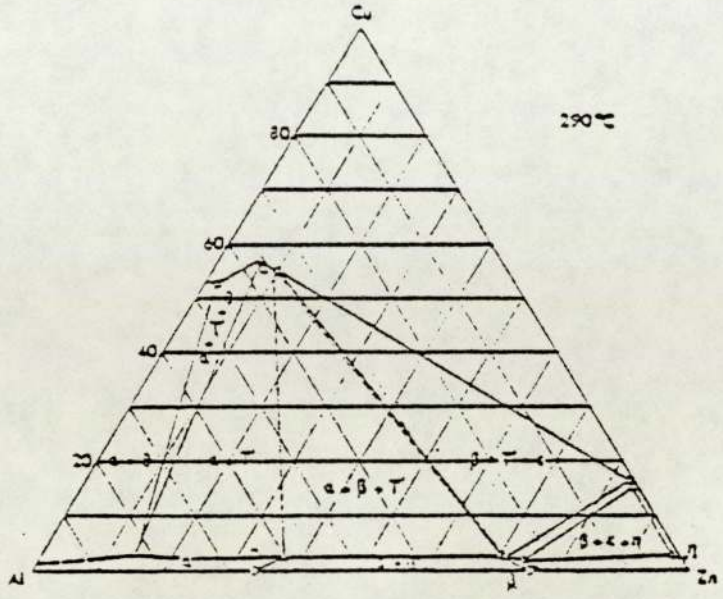

Fig. 12 Isothermal section at 290°C

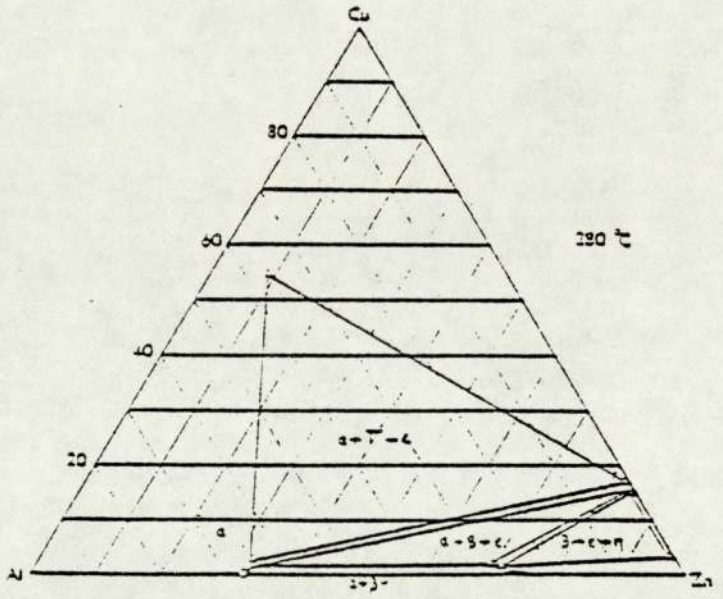

Fig.13 Isothermal section at 280°C

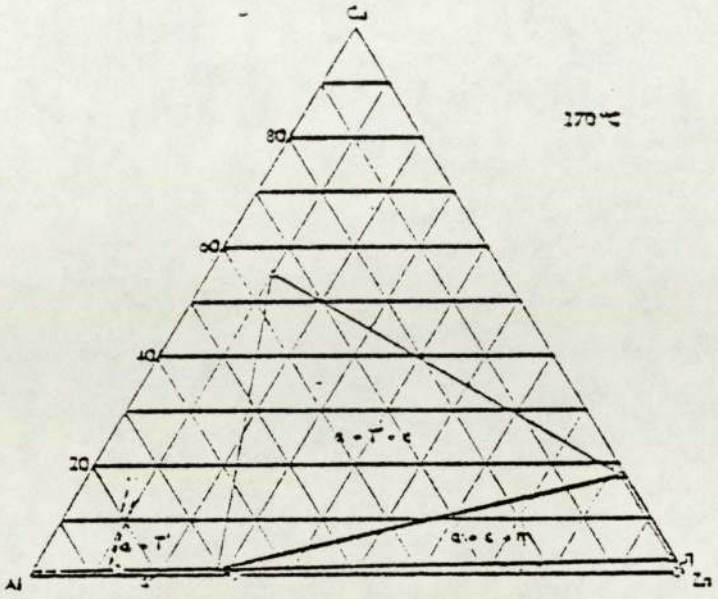

Fig. 14 Isothermal section at 270°C

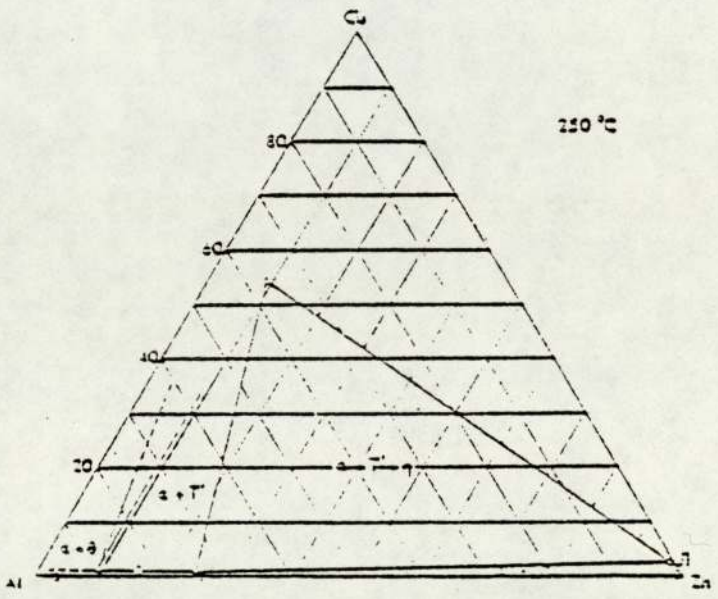

Fig.15 Isothermal section at 250°C

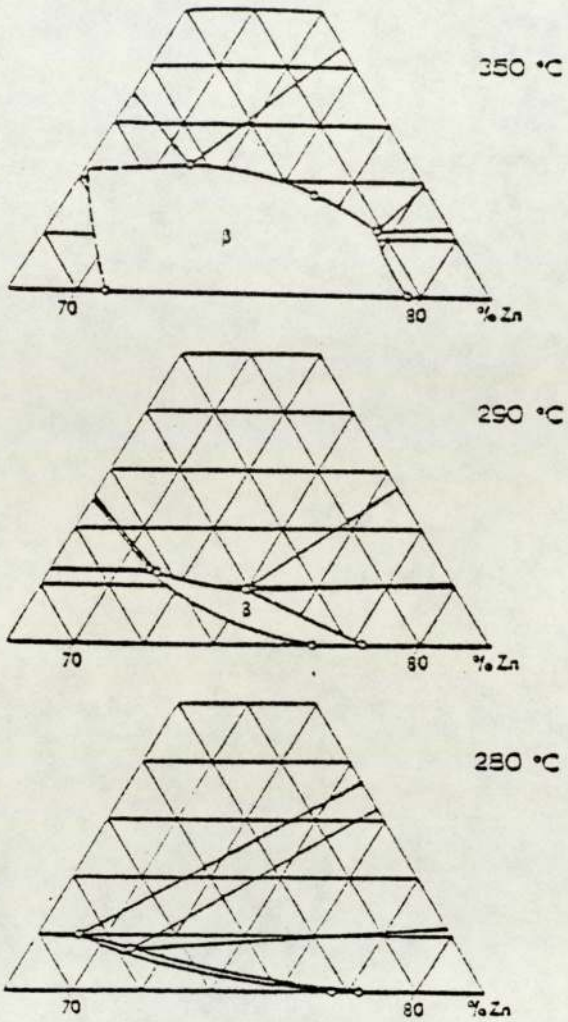

Fig. 16 The shapes of the β-phase field at 350, 290 and 280°C

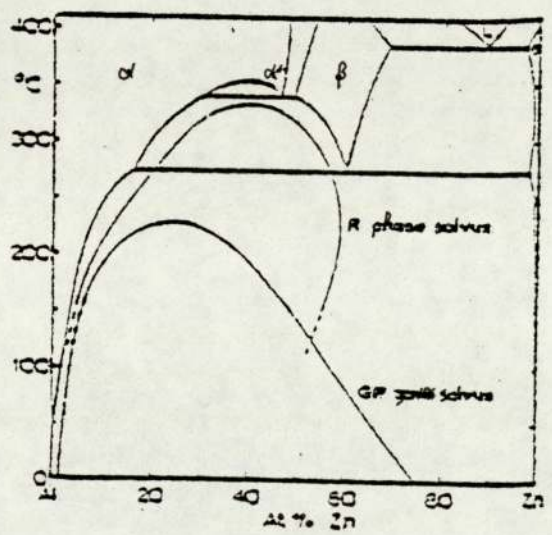

Fig. 17 The aluminium-zinc phase diagram with proposed metastable miscibility gaps for the G.P. zones and the R-phase

of discussion for many years. Based on the phase diagram of the Al-Zn system, four ranges of composition, i.e. Al-rich α phase, monotectoid α/α' phase, eutectoid β phase and a region in the $(\beta+\eta)$ composition range have been investigated. The zinc-rich phase has not been studied. The various stages of precipitation during ageing have received particular attention.

In their early work, Guinier[24] and Borellinus[25] found that small spherical aggregates rich in solute atoms (i.e. G.P.zones) were responsible for the rapid hardening at room temperature. These G.P.zones were the first decomposition product after quenching from the f.c.c. single phase field, and ageing at room or sub-zero temperature.

Studies to investigate the structure changes through the property changes have been made, e.g. by hardness measurements, electrical resistivity, calorimetry, X-ray diffraction and small angle X-ray scattering (SAXA) aided by transmission electron microscopy (TEM).

With Zn-Al alloys containing 48 to 80wt% Zn, Hari and Hirans [26] carried out precise resistivity measurements and thermal analysis. They pointed out that the G.P.zones were coherent precipitates with a limited particle size. However, nothing was said about the structure changes and only a simple miscibility gap was assumed.

A number of investigations have further shown that the zones continue to grow, and after attaining a certain

size (30-35 Å) the spherical zones became ellipsoidal. Such a change in zone shape brought about changes in both physical and mechanical properties of the alloy that occur during the early stages of ageing in this system [27]-[32].

These ellipsoidal zones further transform into a rhombohedral transition phase, R, which is precipitated in the form of plates, partially coherent with the matrix but with a zinc content less than that of zones [30-39].

Recently, there has been direct evidence [36] for the transition of G.P.zones to another phase, α''_m which is formed at high temperature either on direct quenching or by zone reversion. The kinetics of its formation were appreciably faster on reversion than on quenching. A single miscibility gap was assumed [40] for both the G.P.zones and the transition phase, shown as Figure 17, which was then confirmed experimentally through TEM studies [36].

On prolonged ageing at a certain composition the α''_m phase was found to grow to such an extent that coherency was completely lost in the {111} habit planes. Since the elastic strain due to coherency was responsible for the rhombohedral distortion, the structure became f.c.c. This new cubic phase was named the α'_m phase [41].

The rhombohedral α''_m phase (2.832 Å, = 61.3°) [42] differed only slightly from the cubic α'_m phase.

From TEM work this cubic phase was found to be lenticular in shape, about 2000 Å in diameter and about 200 Å in thickness[43]. Also the phase formed after an incubation period following the initial stage of decomposition and was supposed to contribute to hardness due to its fine plate-like or spherical structure[42].

It was found that this phase finally transformed into stable zinc-rich precipitates, with the lattice parameter of a = 2.859 Å , c = 4.947 Å , η phase[44], by continuous precipitation. Substantial discontinuous precipitation of zinc on grain boundaries during the whole process was found on ageing of polycrystalline sample[2,30]. Continuous precipitation of zinc has also been reported through heterogenerous nucleation on structural defects which were observed in quenched Al-Zn alloys[30,41,42,45,46].

The orientation relationship between zinc precipitates and the aluminium matrix was determined[47] as :

$$(111)_{Al} // (0001)_{Zn} \quad [1\bar{1}0]_{Al} // [10\cdot0]_{Zn}$$

Recently the observed growth rates for the cellular precipitation in the alloy (Al-48.5wt% Zn) were rationalised by using the G.P.zones solvus below 125°C and the α''_m phase solvus above. This interpretation led to a significantly better agreement with the theoretically predicted growth rates based on a modified Turnbull theory of decomposition[48].

The whole ageing sequence in the Al-Zn system up to a certain composition would seem to be as follows :

Supersaturated solid solutions α'_s → Spherical G.P.zones → Ellipsoidal G.P.zones → Rhombohedral transition α''_m phase → f.c.c. transition phase α'_m → Zinc-rich stable η phase.

A new phase (designed as the γ phase) has been reported[49] in the alloys rapidly quenched and aged with a narrow temperature range on either side of the limiting temperature for G.P.zone's formation. These particles were octahedral in shape with an f.c.c. structure. On isothermal ageing, these transformed into the η phase through epitaxial growth.

In order to present a proper explanation of the facts in the light of two metastable solvus curves, Setyanarayan and Hirano[50] have carried out a series of experiments on some Al-Zn (4 to 35wt% Zn) alloys using several techniques, such as electrical resistivity, X-ray diffraction and TEM.

It was found that in alloys containing up to 20wt% Zn, G.P.zones with a size characteristic of the temperature to which the alloys were quenched were formed. On further ageing at these temperatures, formation of transition phase would be followed by precipitation of the equilibrium phase. When alloys containing 85wt% Zn were reheated at or below the G.P.zone solvus peak ($225^{o}C$), competitive growth of the zones took place, with smaller zones dissolving. When partial coherency was attained, α''_m phase platelets appeared, these then transformed into the α'_m phase and finally to the equilibrium η phase.

When these and 25-35wt% Zn alloys were reheated above the zones solvus, the zones were completely redissolved, but transition phases started appearing.

In alloys having higher zinc contents (25-35wt%), on direct quenching to temperatures above the solvus, the initial product was the α''_m phase and/or the α'_m phase, the stability of which depends on the concentration of the alloy as well as the temperature of ageing.

It was evidence[39] that the precipitation and reversion behaviour of Al-Zn alloy was quite complex in the region of 160°C-230°C due to overlapping of the two metastable solvus curves, shown in Figure 17[36][51].

From their transmission electron microscope investigation, Ciach and et al[55] also concluded that the decomposition sequence in low zinc alloys (up to 30wt% Zn) was as follows :

$$\alpha'_s \rightarrow \text{G.P.zones} \rightarrow \alpha''_m \rightarrow \alpha'_m$$

Krishna[56] investigated the kinetics of the decomposition of a quenched aluminium-25wt% zinc alloy, and found that the sequence of precipitation products was dependent upon heat treatment and temperature of ageing.

A different mechanism was observed during the ageing of an alloy containing 40-70wt% Zn[54,57]. A modulated structure characteristic of the spinodal decomposition was found. Its appearance was connected with an initial growth of hardness. A lamellar structure characteristic of the discontinuous precipitation of α''_m and α'_m phases appeared after further ageing.

In the 50wt% alloy, another mechanisms of decomposition was observed on high temperature ageing, (i.e. at temperatures just below the solvus curve)[54]. The decomposed structure consisted of small η precipitates and the alloys became brittle. An increase in the wavelength of the spinodal modulations at high ageing temperatures was supposed to cause a nucleation of α_m'' and η phase which was impossible at low temperatures due to the modulation wavelength being too small. The relationship between physical or mechanical properties and ageing time at room temperature for three different alloys is shown in Figure 18.

More detailed X-ray diffractometer results showing the kinetics of decomposition of Al-60% Zn alloy at 240°C and then at 95°C were reported in his paper, as shown in Figure 19.

Many investigations on the decomposition of the eutectoid alloy during quench-ageing isothermal transformation and slow cooling to the transformation temperature have been carried out[51,59,60]. Depending on the transformation temperature, more than one type of decomposition product was found on ageing alloys with a composition corresponding to the eutectoid β phase[51,52,53].

Decomposition of the eutectoid alloy during slow cooling or isothermally transforming at high temperature produced a lamellar structure. However decomposition at room temperature after a rapid quench produced a fine (1μm) mixture of equiaxed zinc-rich α_m'' and aluminium-rich grains.

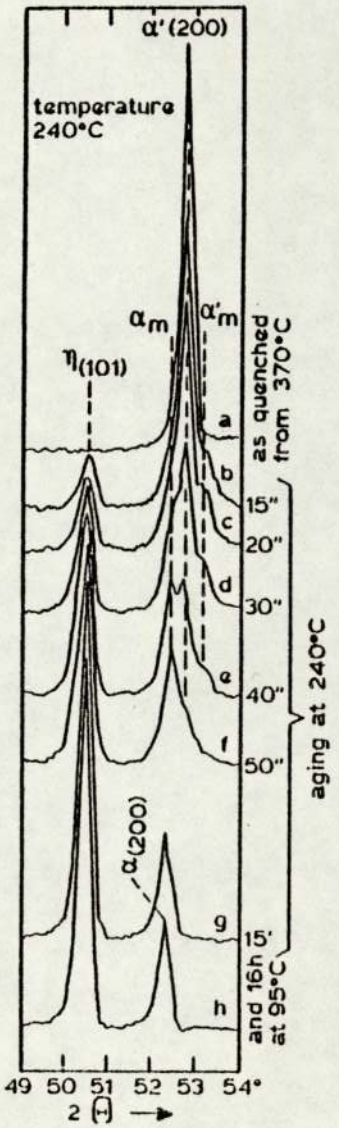

X-ray diffractometer results showing the kinetics of the decomposition of Al–60%Zn alloy at 240 C and then at 95 C

Fig.19

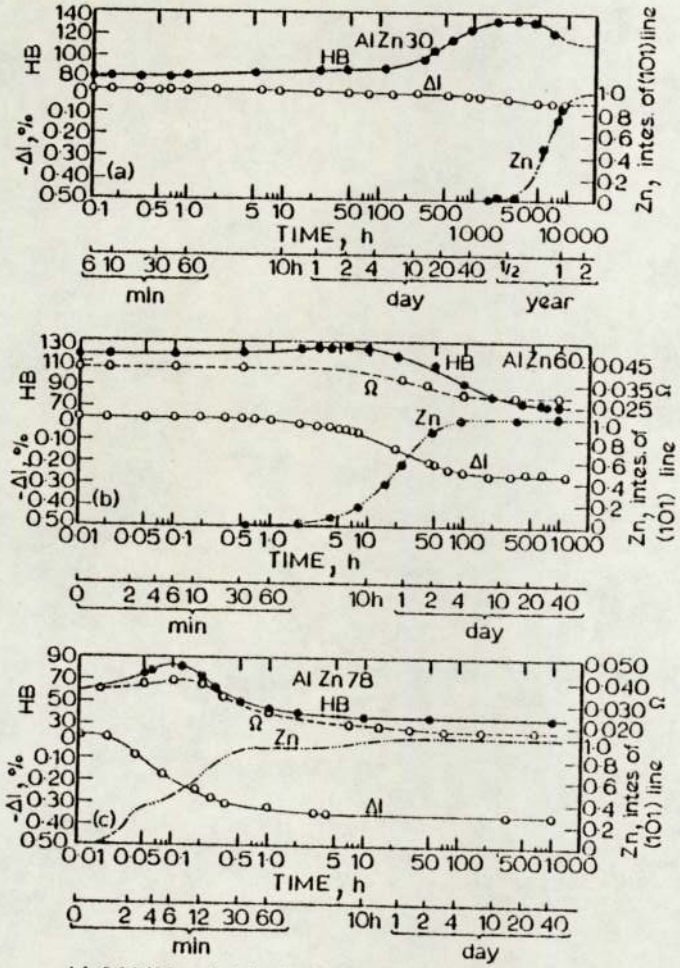

a Al–30%Zn; *b* Al–60%Zn; *c* Al–78%Zn
Relationship of hardness, resistivity, dimensions, and the amount of zinc with the aging time at room temperature for different alloys

Fig.18

These changes could be interpreted as resulting from a spinodal decomposition which took place at about room temperature[59,60].

Toldin et al[61] investigated the processes of decomposition of supersaturated solid solutions in Al-Zn alloys with 40, 50, and 60 wt% (AlZnII) and in an alloy containing 73wt% Zn (AlZnIII). Summarising these results, Toldin pointed out that there were eleven sequences of phase transformation, which depended on composition, cooling rate and heat treatment temperature. These are shown diagrammatically in Figure 20.

Each one of them may begin from one of the metastable phases R (α_m''), α_m' or from G.P.zones. A group of sequences (position 6-9 in Figure 20) was found to begin with the formation of G.P.zones after the alloy had been quenched in iced water.

The formation and development of G.P.zones is largely influenced by the process involved in the decomposition of the supersaturated solid solution; the α_m'' phase is formed preferentially by the mechanism of spinodal decomposition, and the metastable phase, α_m' by nucelation.

Recently Smith and Hare [62] investigated the isothermal transformation of the eutectoid alloy in some detail and obtained a fuller TTT diagram Figure 21, incorporated the results of Garwood and Hopkins[65].

As shown in the fuller diagram four stages of transformation of Zn-Al eutectoid alloy were studied.

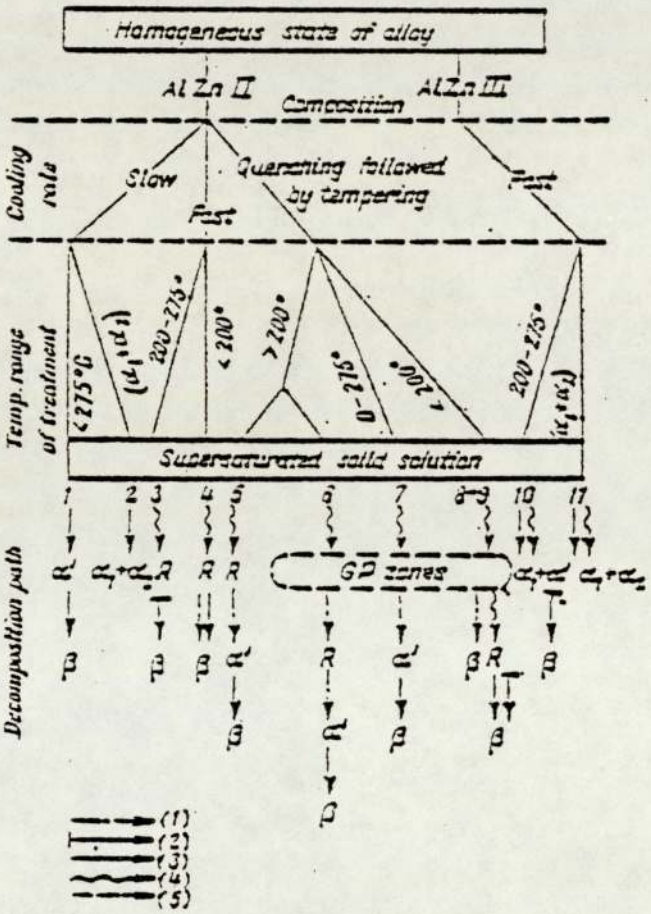

Fig. 20 R - intermediate rhombohedral phase; α' - supercooled high temperature α_2 phase (f.c.c. lattice); α_1 and α_2 - nigh temperature equilibrium phases (f.c.c. lattice); β - final equilibrium phase (h.c.p. lattice);; 1 - homogeneous rearrangement, 2 - cellular decomposition, 3 - nucleation, 4 - spiñodal decomposition, 5 - nucleation at critical defects.

A scheme of transformation in Al-Zn alloys

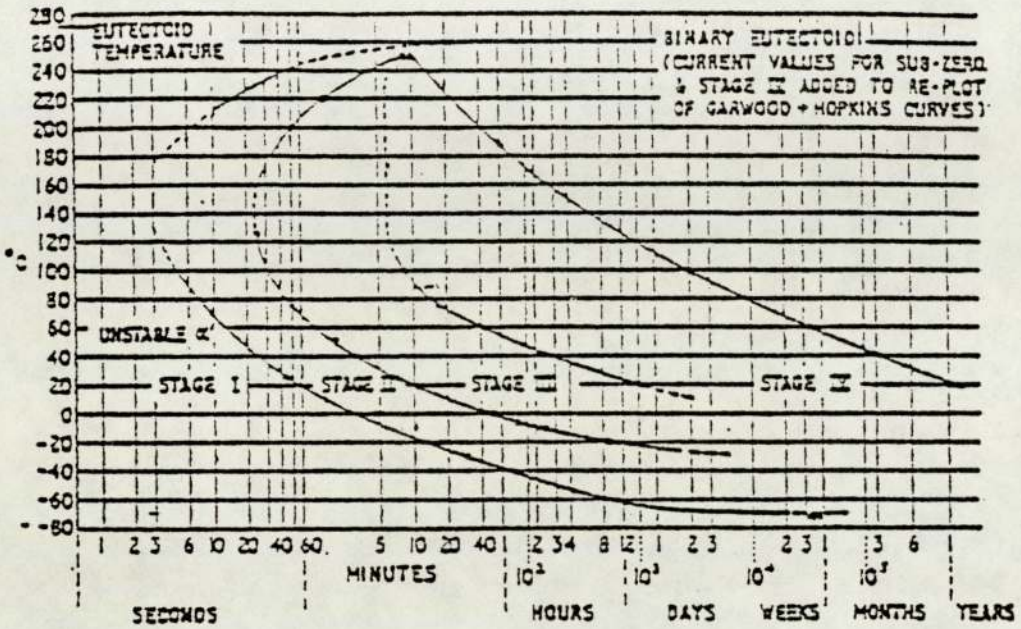

Fig. 21 TTT diagram for zinc-aluminium eutectoid alloy

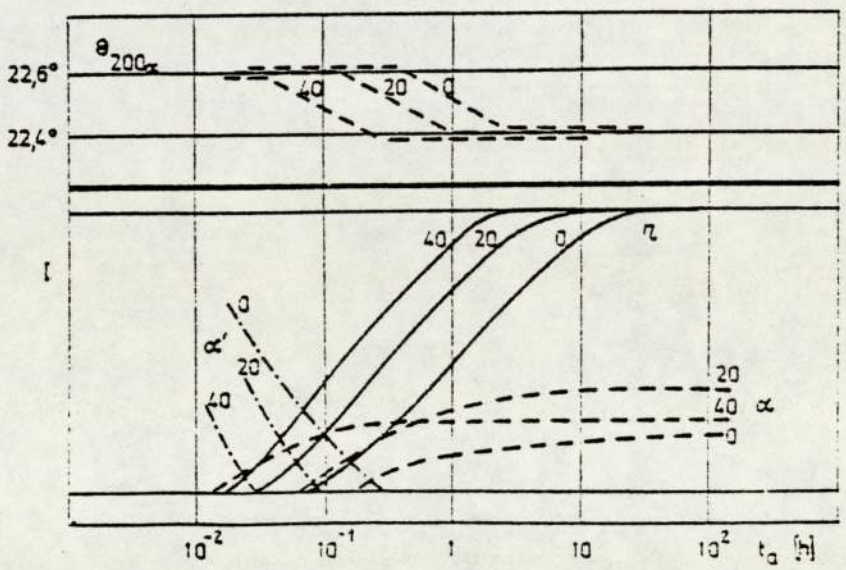

Fig.22 Changes in the intensity and angles of diffraction of supersaturated phase α' phase and decomposition products (η and α phase) for alloy AlZn74/55 quenched from 603°C and then aged at 0°C, 20°C and 40°C.

They are :

(1) The quenched condition,

(2) Breakdown of β phase to products of intermediate composition,

(3) Adjustment of these products to α and η of equilibrium chemical composition,

(4) Adjustment of structure to virtual physical stability.

It is noted that breakdown of supersaturated α_s' phase to produce intermediate products was reported to give rise to the major contribution to heat evolution, increase in hardness to a peak, and continuous rise in conductivity. This 1973 report was the first which implied the supersaturated solid phase itself undergoing some phase transformation.

Later on, in 1978, Ciach et al[66] used broken lines to describe the fractional transformation of supersaturated α_s' phase in alloys of composition A174wt% Zn, A140wt% Zn and A160wt% Zn on X-ray diffraction testing, as shown in Figure 22. The α_s' phase was dealt with as one phase changing in the processes of decomposition. It was found that the precipitation of zinc, for alloy A160wt% quenched from the two-phase field (α+β), consisted of two stages. The first stage was the decomposition of zinc-rich supersaturated α_s' phase, but the diffraction line of the α_s' phase disappeared without any apparent change in the diffraction angle. Because in this stage the influence of the precipitation of zinc on Al-rich phases and on the diffraction intensities was very small, dashed lines were

used to describe the intensity change of Al-rich phase, considering the limited experimental accuracy. In the second stage the precipitation of zinc was found to be associated with both a change of Bragg angle and intensity of Al-rich phase. However, for lower zinc alloys quenched from the two phase field ($\alpha+\beta$), the first stage of zinc precipitation was faster and the second was slower than that for the alloy quenched from the single phase field.

In 1981, more details on the stages of decomposition of the supersaturated solid solution were reported by Toldin[67]. Two types of metastable state might be realized in the low-temperature ($\alpha+\beta$) region, one being defined by the solubility limits of the ($\alpha_1 + \alpha_2$) region, which continue to the low-temperature ($\alpha+\beta$) region, and the other bounded in the same way by the boundaries of the ($\alpha_1{}^T+\alpha_2{}^T$) region continued to the low-temperature ($\alpha+\beta$) region, and the other bounded in the same way by the boundaries of the ($\alpha_1{}^T+\alpha_2{}^T$) region continued to the low-temperature range, shown in Figure 4[13,14]. It was pointed out that the decomposition of the supersaturated solid solution in pure Al60% Zn and Al73% Zn alloys involved two stages, both in natural ageing and treatment at higher temperatures (150°C and 240°C). In the first stage, metastable zinc-rich α_1' phase (f.c.c. lattice, a = 4.028 Å) was formed by a cellular reaction. The metastable phase α'_1 then decomposed in the second stage with the formation of the equilibrium η and α_1 phases, the latter almost pure aluminium with a = 4.046 Å.

The decomposition process did not follow the traditional scheme of nucleation of a precipitate phase and draining of the matrix of the excess component, but was rather of the eutectoid type with the formation of two phases at the same time. A very distinct feature of the decomposition of the supersaturated solid solution was found, i.e. both metastable phases formed from the initial decomposition were supersaturated solid solutions and subject to after-decomposition i.e. :

Supersaturated solid solutions → G.P.zones → $\alpha' \rightarrow \alpha_1+\eta$

Supersaturated solid solutions → G.P.zones → $\alpha'_1 \rightarrow \alpha_1+\eta$

where α'_1 is a low zinc metastable phase, and α' is high zinc metastable phase. α' grows in competition with the equilibrium η phase during higher temperature ageing (150°C Tnd 240°C). Low temperature ageing produces η phase with $\alpha_1^!$ and the α' phase is not formed. α_1 and η are the final equilibrium phase.

The formation of the G.P.zones was not discussed.

According to the information obtained on the initial composition of the $\alpha_1^!$ phase (44wt% Zn) Toldin pointed out that decomposition of the supersaturated solid solution in alloys Al+60 Zn and Al+73 Zn was in accordance with the extrapolated phase boundary line of $\alpha_1{}^T$ and $\alpha_2{}^T$ (at 340°C) of Figure 4,[68,70] so the $\alpha_1^!$ phase is the analog, not of the α_1 as assumed in (69), but of the $\alpha_1{}^T$ phase, which explained the considerable excess of zinc.

Ciach investigated the kinetics of solution treatment of Al-Zn alloys. To explain the phenomenon of high durability of the dendritic structure of the Al60% Zn alloy, the interdiffusion coefficient $\tilde{D}$ with zinc, was calculated[54,55] using the Darken equation :

$$\tilde{D} = D^{*}_{Zn} \cdot f \cdot N_{Al} \quad ; \quad f = 1 + \frac{d\ell n\gamma_{Zn}}{d\ell nN_{Zn}}$$

where D_{Zn} - the self-diffusion coefficient of Zn,
f - the thermodynamic factor,
γ_{Zn} - the activity coefficient of zinc,
N_{Zn}, N_{Al} - the mole fractions of Zn and Al.

The value of the self-diffusion coefficient of zinc D^{*}_{Zn} was from the work of Hillard et al, while f was calculated in (71). The change in the interdiffusion coefficient $\tilde{D}$ with zinc and temperature used in the homogenization process is shown in Figure 23[55]. It was found that the interdiffusion coefficient D decreased within the range of 20-50wt% Zn, approaching a minimum value between 0.31 and 0.40 N_{Zn}.

2.2.2 Ternary Zn-Al-Cu alloys

In recent years, the technical literature shows much attention to investigations of phase transformation in Zn-Al based alloys containing several additional elements, especially in the Zn-Al-Cu and Zn-Al-Cu-Mg systems.

Truszkowski and Dutkiewicz, established the effect of copper on the mechanism of phase transformation in AlZn20Cu2 alloys by using X-ray diffraction, thin-foil

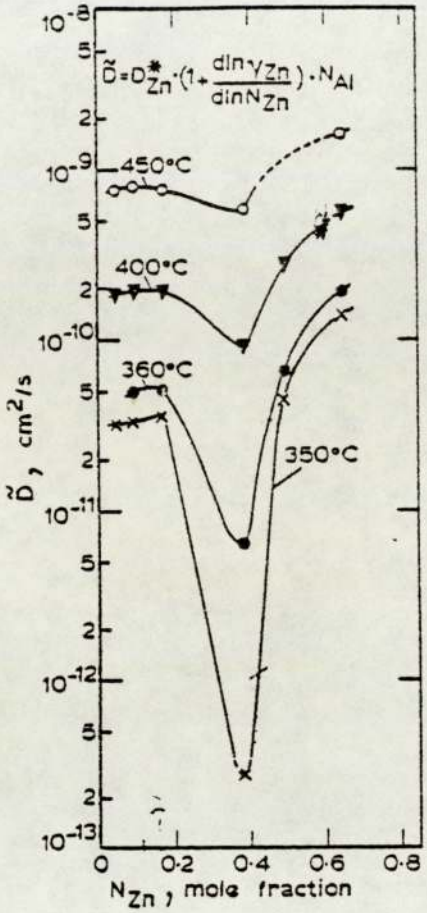

Change in the interdiffusion coefficient $\tilde{D}$ with zinc content and temperatures used in the homogenization process

Fig. 23

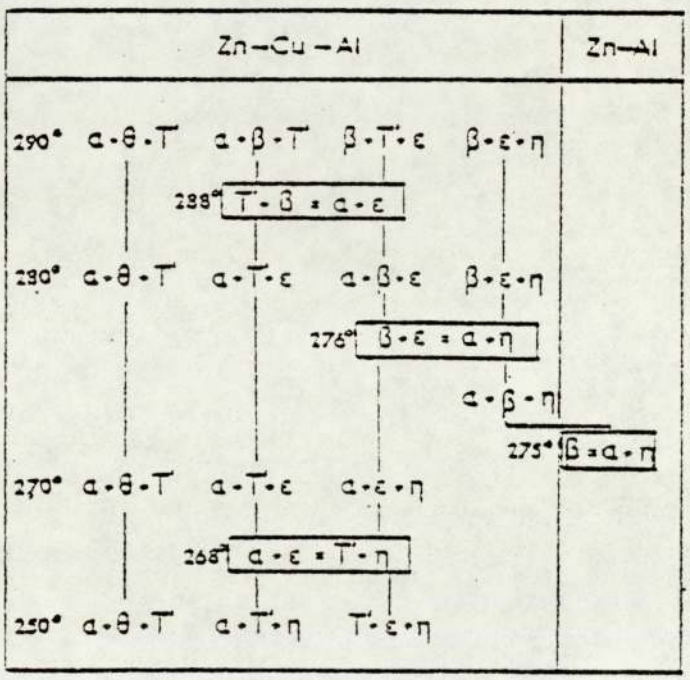

Fig. 24 Solid-state reactions in the low-copper part of the Zn-Al-Cu system

electron microscopy and hardness testing. The decomposition of the supersaturated phase was found and a tetragonal deformation inside the G.P.zones was observed in the first stage of ageing. Further ageing caused the separation of precipitates rich in copper which afterwards pass through intermediate phases into ε phase.

But no more investigations were carried out.

The TEM work shows that a shift of atoms in <110> direction caused the transition from the tetragonal to cubic symmetry inside the G.P.zones and lead to the formation of the α'm f.c.c. cubic phase. This process was not accompanied by the formation of the transitional rhombohedral phase. In the last stage of ageing the η phase formed directly from the α'm f.c.c. precipitates.

The hardness curves and X-ray diffractogram for quench-aged A1Zn20Cu2 are shown in Figures 25 and 26.

Investigations on an alloy of composition A1Zn50Cu2 aged at 50°C and 100°C were reported in Dutkiewicz's work[57]. It was found that small amounts of copper significantly influenced the mechanism of phase transformations in Al-Zn alloys, especially on the spinodal decomposition, kinetics of precipitation and mechanical properties.

The X-ray diffractogram and hardness curves are shown in Figures 27,28. On ageing at 100°C, it was found that supersaturated phase α'_s simply decomposed into α and η phases after 20 minutes, with the beginning of the formation of ε phase. The final stage shown in

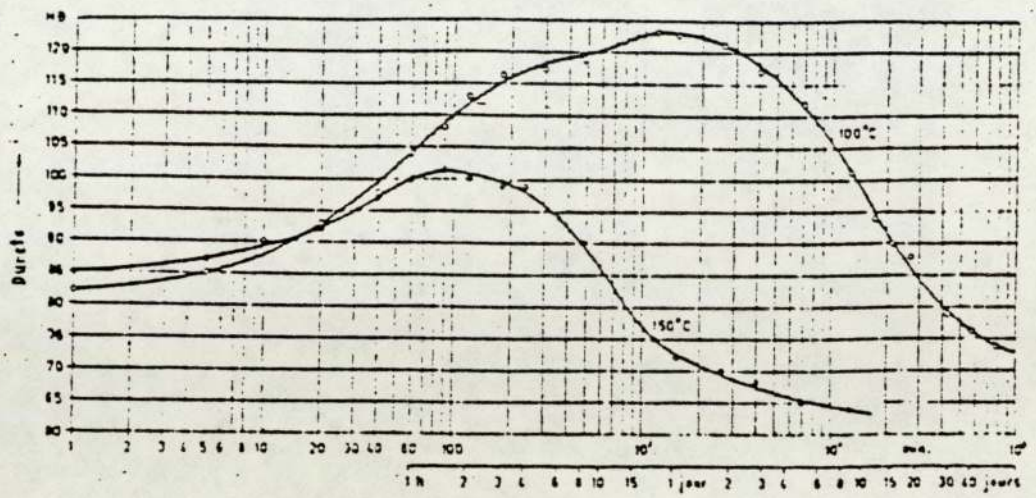

Fig. 25 Hardness/time curves of alloy A1Zn2OCu2 aged at 100°C and 150°C

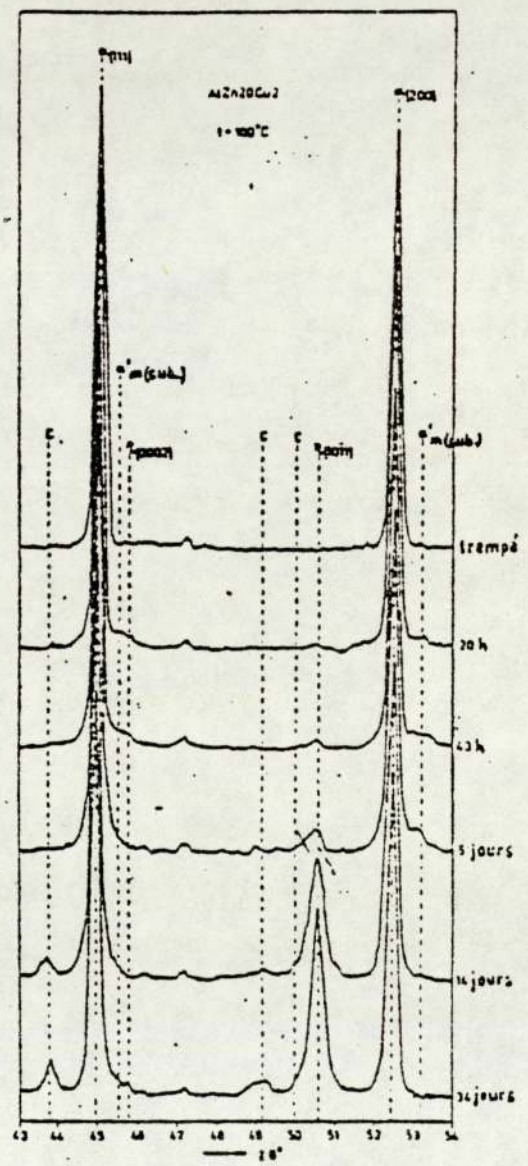

Fig. 26 Diffractograms of alloy A1Zn2OCu2 aged at 100°C

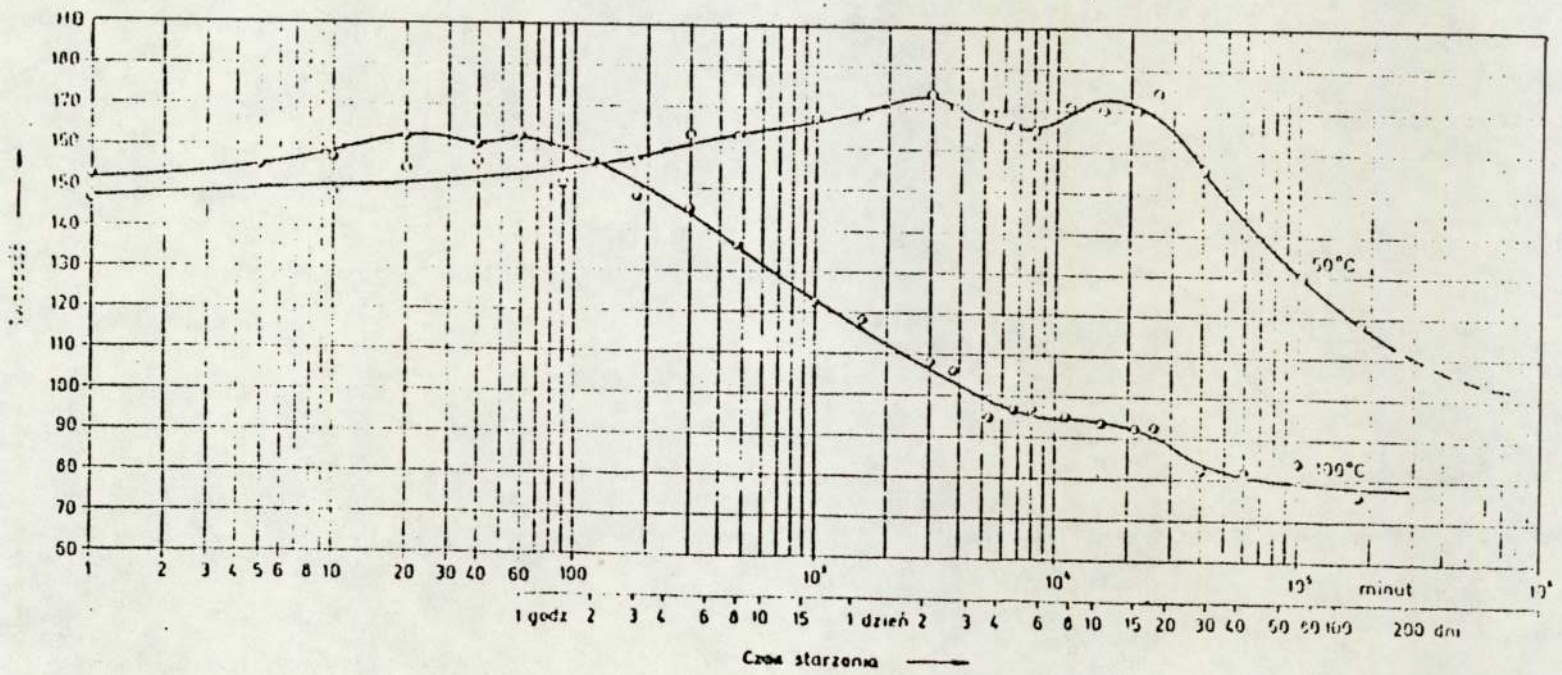

Fig.27 Hardness/time curbes of alloy AlZn5OCu2 aged at 50°C and 100°C

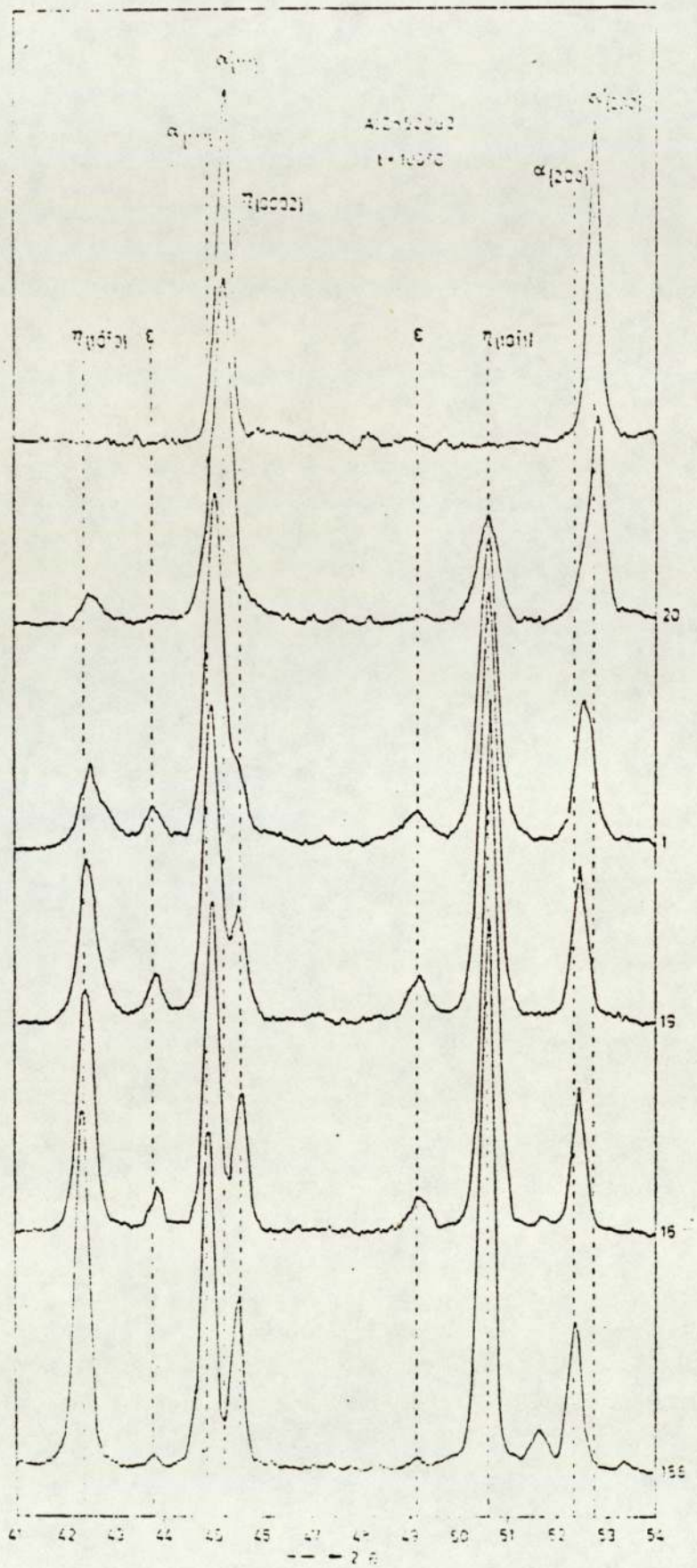

Fig.28 Diffractograms of alloy AlZn5OCu2 aged at 100°C

this work was the metastable co-existence of these phases α, ε and η.

The hardness curve of the alloy aged at 100°C show three peaks but no explanation of this was given.

More work has been carried out on alloys containing Al-73-78wt% Zn with Cu-1-10%[58,76].

Ciach[58] found that there was a four-phase transformation following the decomposition of the supersaturated β phase in alloys with 78wt% Zn and 1 to 3 wt% Cu aged at 50°C. It was found that this small amount of copper retarded the decomposition of the supersaturated phase. A period of months or years was needed to get the material stable at ambient temperature. Increases in dimensions and hardness of the samples were observed, as shown in Figures 29,30. Based on X-ray and microscopic investigations, shown in Figure 31, the pattern of the four-phase transformation was established as follows :

$$\alpha_f' + \varepsilon = T' + \eta$$

This addition of 1-3% of copper augmented the effects of dimensional and hardness changes and, at the same time, prolonged the time interval of transformation between the phases α', ε, T' and η, as shown in Figure 32.

The decomposition of β phase occurred by the phase reaction :

$$\beta \rightarrow \alpha + \varepsilon + \eta$$

More detailed X-ray diffraction and dimensional change investigations on monotectoid and eutectoid Al-Zn alloys with copper contents from 1 to 10% were done by Kröl et al[76].

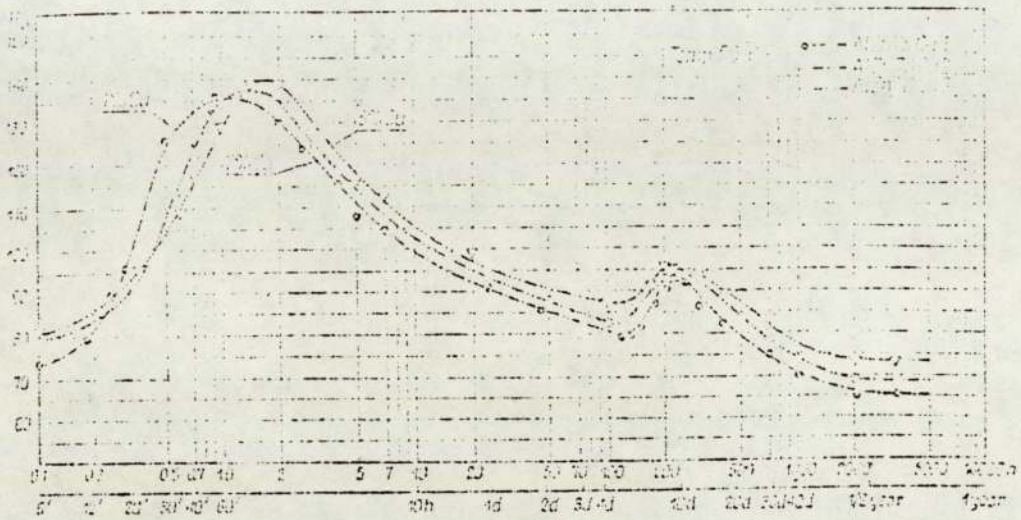

Fig. Dependence of the hardness of the supercooled α'-phase of the alloys AlZn78Cu1 –3 on the time of ageing at the temperature 50 °C

Fig. 29

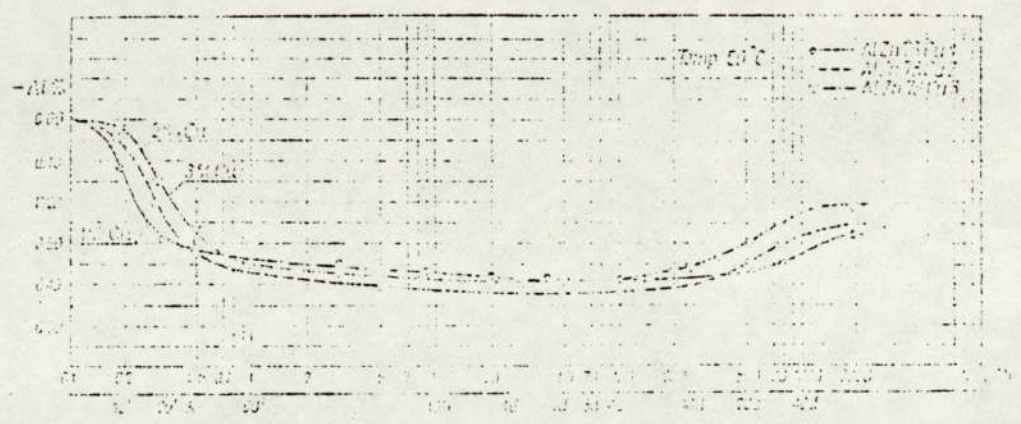

Fig.30 Changes in the length of the sample of supercooled α' phase as a result of ageing at temperature 50°C

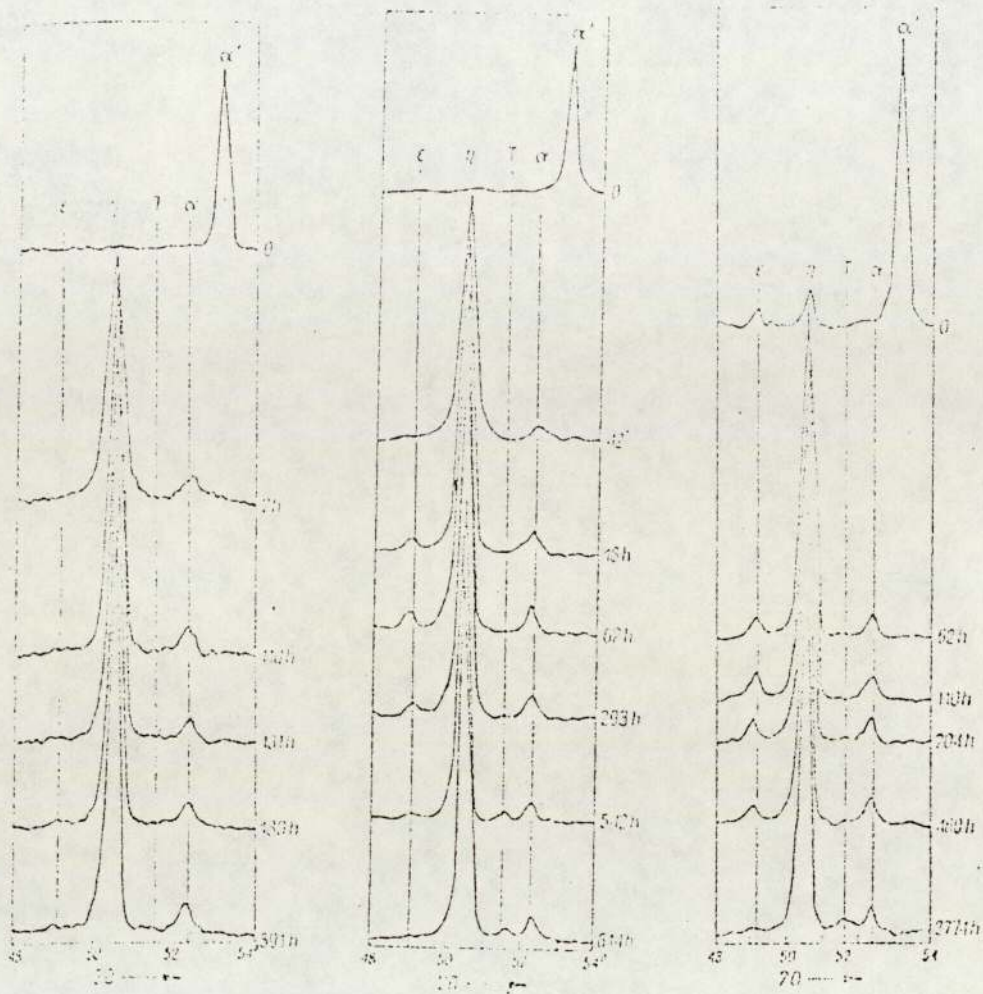

Fig 31 Sets of diffractograms of AlZn78Cu1 -3 alloys illustrating the four phases transformation
Numbers on abscissa denote grades

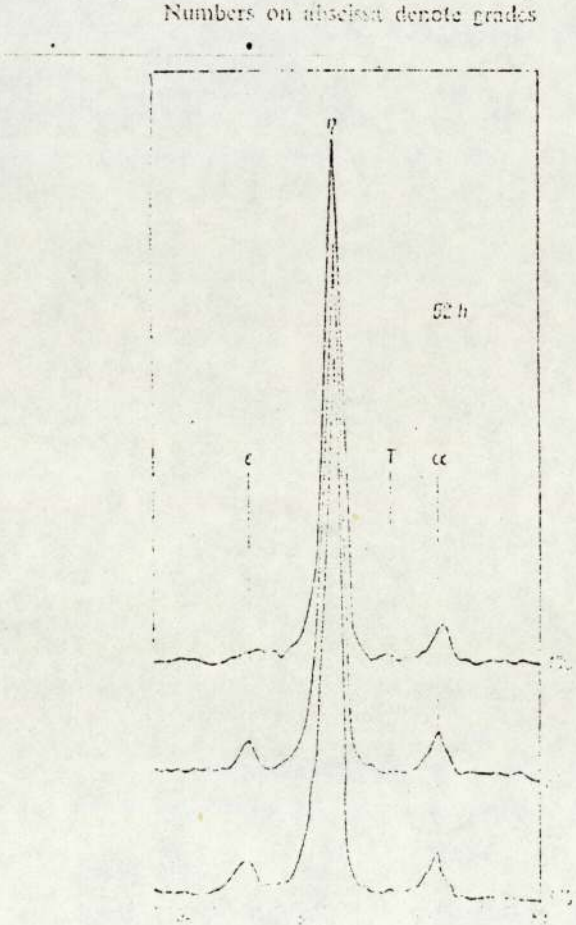

Fig. 32 Sets of diffractograms of AlZn78Cu1-3 alloy after 62 hrs of ageing at the temperature 50°C

The phase transformations in Al-Zn-Cu alloys were ascertained as :

$$\alpha' \rightarrow \alpha + \eta + \varepsilon$$

and

$$\alpha + \varepsilon \rightarrow T' + \eta$$

On the basis of these investigations, the phase quantities at different stages of ageing, and the times of starting and ending of both transformations were determined. The response on dimensional changes to phase transformations, was in good agreement with Ciach's results (shown in Figures 29,30).

In all the published papers on this topic, it is assumed that the α_s' decomposes in a single stage to the equilibrium or near equilibrium aluminium-rich solid solution α. Fraction transformation curves are represented by a single, solid line.

2.3 Effect of addition elements on phase transformations. Individual cases were known of the retardation of the zinc-aluminium eutectoid transformation by an alloy element.

It has been found that the additions most likely to be useful would be Mg, Cu, Ag, Si, Fe, Mn, Ni and Li[62]. Initial melts with each of these ingredients confirmed that all had some retarding effect on the phase transformation[62,63], but magnesium was outstanding quantitively.

By the addition of magnesium the ageing process in binary aluminium-zinc appeared to be greatly modified. Atomic-size effects and thermodynamic relationships suggested that these modifications might have their origin in the

clustering of zinc and magnesium atoms during solution treatment. At least two stages of ageing processes of most ternary systems were clearly shown in the ageing curves. It was supposed that the first stage in the ageing processes was associated with G.P.zones formation and the second stage occurs at high ageing temperature, which involved an intermediate precipitate[80]. In a subsequent report[81] the ageing sequences were represented as :

G.P.zones → M' (intermediate precipitate)

→ M(MgZn)

The lack of a systematic X-ray analysis of ageing in this ternary system made the interpretation of the ageing curves in terms of the various decomposition products a difficult matter.

Further X-ray diffraction and electron microscopic experimental evidence was given in support of suggestions above-mentioned[81].

According to Toldin and Kleshchev's recent investigation[67,82], the addition of 1% magnesium to alloy AlZn60 and AlZn73 considerably delayed the precipitation of the equilibrium η phase in the matrix; cells with η phase precipitates were only found after three days natural ageing, while the pure alloy without magnesium had a lamellar structure by that time.

In alloys AlZn60Mg1 and AlZn73Mg1, the rate at which the equilibrium η phase was precipitated during ageing at 150°C and 240°C was less than in pure Al-Zn alloys,

with the marked development of the zinc-rich metastable α' phase[67].

It was found that additions of magnesium to Al-Zn alloys reduced the rate of precipitation of the equilibrium η phase by two orders of magnitude. The intermediate R(α"m) phase developed preferentially during natural ageing, thereby retarding the cellular reaction. During ageing at 150°C and 240°C, the first stage of the decomposition of the supersaturated phase in which an equilibrium η phase was formed was considerably suppressed in alloys with magnesium, and the metastable α' phase was developed instead. However, the α' phase rapidly decomposed with precipitation of η phase in the pure alloys, because of the high rate of cellular decomposition[67].

Smith and Hare's work[62] showed that of all the elements tested none stabilised the high temperature β phase completely but many retarded the transformation, magnesium having by far the greatest effect. The retardation produced by copper was smaller than magnesium.

The TTT diagram for a eutectoid-based alloy containing nominally 0.5wt% Cu and 0.15wt% Mg is shown in Fugure 33. Transformations, instead of starting after one minute at room temperature, started after one week. Their TTT diagrams for the binary and higher systems were used to show the suitable heat treatments to produce various microstructures.

The effect of copper content in most monotectoidal and eutectoidal alloys was clearly visible on the retardation

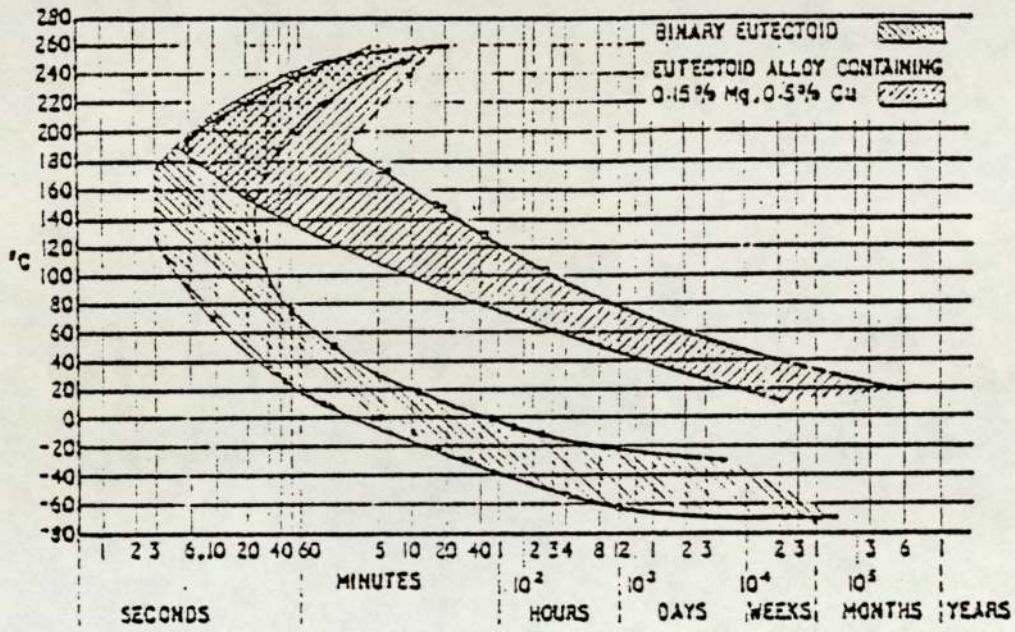

Fig. 33 Comparison of stage II TTT diagrams in binary and quaternary alloy

of the ageing processes in Ciach's work[58]. As an example, the diffractometer traces for AlZn78Cu1 to 3 alloys after 62 hours of ageing at 50°C are shown in Figure 32.

In AlZn78Cu2 alloy it was observed that the beginnings of the four-phase transformation were evidenced by the appearance of the peak of the T' phase. The figure 31 showed the completion of the four-phase transformation, i.e. the disappearance of the ε phase with a simultaneous appearance of the line of the T' phase, after 614 hours.

In AlZn78Cu2 alloy, the process of four-phase transformation was well advanced after 62 hours, as might be inferred from the occurrence of both ε and T' phases. As regards the AlZn78Cu3 alloy after the same time of ageing, only the beginning of the four phase transformation might be ascertained, this was manifested by the occurrence of a distinct line from the ε phase.

Murphy[83] determined in detail the structure and properties of two Zn-Al-Cu alloys of monotectoid and eutectoid composition, produced by rheocasting. The dimensional stability of the alloys was measured and it was found that the expansions were caused by conversion of the ε to T' by the four-phase reaction and by changes in the lattice parameters of η due to rejection of copper from supersaturated solid phase.

Unfortunately, there are few references which have been found dealing with Zn-Al-Si system. Nuttall[84] tried to study the effect of Si additions on the mechanical

properties of the Zn-Al eutectoid alloy, but he failed to prepare the specimens properly. The silicon-containing alloy cracked on hot rolling or swaging and little further work was carried out on this material.

Two other papers were published in 1978[85,86]. Alloys of Al-43.5wt% Zn-1.5wt% Si and Al-39wt% Si were used only as the metal coating of steel. No further details were given.

2.4 Effect of some ternary additions on the mechanical properties

It was reported[62] that in binary Zn-Al alloys of eutectoidal composition, as-quenched hardness was about H.V., rising to a peak of 120 H.V. during decomposition of the supersaturated β phase and falling quickly at first during attainment of chemical equilibrium and slowly thereafter and becoming almost stable with 1 day at about 60 H.V. The fine structure at this stage was readily coarsened and softened. Tensile properties were similarly dependent on structure as derived from thermal history, and on the rate of testing. Low yield strength and high elongation were found at room temperature, but below zero, as expected, the yield point rose and ductility fell.

With a third alloy addition present the mechanical properties are much superior to those of the binary materials.

The mechanical properties have been established for several eutectoid based alloys. The results for four systems :
Zn-Al-Cu, Zn-Al-Mn, Zn-Al-Cu-Mg, Zn-Al-Cu-Mn, are shown in Tables (1) [84] (2) [62].

A marked variation in hardness accompanied the room temperature ageing of the manganese-containing alloy after quenching from 375°C, which probably explained some of the variation in tensile properties observed in the first day after quenching[84]. The hardness eventually appeared to level off at a value of about 120 H.V. and little further change was observed after several weeks at room temperature. A very marked effect of small quantities of magnesium on the response of aluminium-zinc alloys to age hardening has been clearly shown in Polmer's investigation[80].

The most significant factor in the development of high strength properties in alloys based on the Al-Zn-Mg system appeared to be the pronounced effect that small quantities of magnesium have on the age hardening capacity of Al-Zn alloys.

Copper was mainly used to increase the general level of mechanical properties for any equivalent structure, retaining impact strength to lower temperatures and raising creep-resistance[62]. The peak hardness during transformation was raised, e.g. in an alloy with 0.15% Mg + 0.5% Cu it would be higher than 220 H/V. for a binary alloy. The reduced ductility was accompanied by a

Table 1 : Mechanical Properties of Zn-Al Based Alloys

Alloy	Condition	0·2% Proof Stress, N/mm²	UTS, N/mm²	Elongation, % on 25 mm	Strain-Rate Exponent, *m*	Hardness, HV
Zn-Al	As-quenched	158	186	90	0·18	64
Zn-Al-4 Cu	As-rolled	167	191	105	0·12	73
Zn-Al-0·2 Mn	As-rolled	282	335	60	0·11	100
Zn-Al-4 Cu	As-quenched	172	201	78	0·14	84
Zn-Al-0·2 Mn	As-quenched	305	361	28	0·1	108
Zn-Al-4 Cu	As-quenched† aged at 250 C (523 K) for 20 min	203	242	88	0·13	90
Zn-Al-0·2 Mn	As-quenched† aged at 250 C (523 K) for 20 min	377	410	25	0·1	115
Zn-Al-0·2 Mn	As-quenched† aged at 22 C (295 K) for 100 h	392	462	21	0·1	127
Zam[7]	—*	354–420	384–680	4–17	—	~115
Prestal[8†]	—*	232–310	310–386	—	—	—

* Depending on composition and thermomechanical history.
† Strain rate unknown.

TABLE 2

Mechanical Properties of Heat-Treated Alloys

Alloy Composition, wt.-% 78 Zn: 22 Al Base	Quenched from 360° C, Re-Heated for 2 h at 260° C, and Water-Cooled					
	Hardness, HV	Tensile Strength,* N/mm² (tonf/in²)			Impact Value,† Nm (ftlb)	
		YP	UTS	El., %		
0·15% Mg	118–122	350 (22·6)	405 (26·2)	16·7	20° C − 28° C	92 (68) 43 (32)
0·15% Mg + 1·0% Cu	119–128	392 (25·4)	437 (28·3)	15·5	20° C − 28° C − 60° C	129 (96) 121 (90) 140 (104)
0·10% Mg + 0·5% Cu	118	364 (23·6)	425 (27·5)	19·8	− 60° C	142 (105)
0·20% Mg + 0·5% Cu	117–121	374 (24·2)	442 (28·6)	17·9	− 60° C	81 (60)
	Furnace-Cooled from 360° C at 30 degC/h					
0·15% Mg	91–92	312 (20·2)	350 (22·6)	8·7	20° C − 28° C	58 (43) 57 (41)
0·15% Mg + 1·0% Cu	98–99	324 (21)	362 (23·5)	14·2	20° C − 28° C − 60° C	65 (48) 74 (55) 73 (54)
0·10% Mg − 0·5% Cu	96·5	309 (20)	350 (22·6)	14·2	− 60° C	54 (40)
0·20% Mg − 0·5% Cu	94–100	301 (19·5)	354 (22·9)	11·7	20° C − 28° C	71 (53) 64 (47)

* No. 12 testpiece: Hounsfield Tensometer, handwound.
† Un-notched Charpy specimens.

relatively high hardness. All the alloys made with and without copper, machined excellently.

The effect on mechanical properties of the addition of 0.5% Cu and 0.1% Mg to the super-plastic Zn-22% Al alloy was investigated[87]. It was found that the temperature of minimum transformation time of the TTT diagram of the modified alloy (SPZ-CM) was 50°C higher than that of the binary eutectoid alloy (SPZ), but the starting times of transformation were nearly equal. The dissolution into two phases at room temperature started 20 minutes after solution treatment and water quenching, and lasted about 2 hours. This alloy was hardened and strengthened with ageing time at room temperature and did not soften as SPZ did.

An elongation of more than 200% for SPZ-CM was obtained above 200°C, but such large elongation was not observed at room temperature[87].

Copper and magnesium were mainly dissolved in the η phase which was strengthened. The η phase was precipitated continuously at the boundary of the parent phase α'. The α'— boundary was destroyed instantaneously by cold-rolling after solution treatment. The precipitation of the η phase was made discontinuous so that the flow stress was reduced and the ductility was improved[87].

In 1973, Ananin and Efremov[88] studied the effect of silicon on the properties of aluminium-rich (Al-Zn-Mg-Cu) alloys. They found that mechanical properties were lowered by silicon for alloys in the quench-aged and

artificially aged condition, but the properties could be improved by raising the solution treatment temperature from 470°C to 500°C. This increase in temperature had no adverse effect on the corrosion properties, which, in general, were raised by silicon additions in the quenched and naturally-aged alloys.

Suzuki[89] found the hardness of the aged ternary alloy AlCu2Mg 0.9 was increased by adding Si, probably due to the change in aged structures. The silicon addition was effective only when the specimen was water-quenched and not directly quenched into the ageing bath. On the other hand, silicon additions to a ternary alloy having a high solute content, i.e. AlCu4Mg 1.8 alloy, tended to lower the hardness after ageing.

However, the influence of silicon on the instability and properties of Zn-Al alloy and Zn-Al based alloys with small amounts of copper has apparently not been investigated.

Recently Savaskan[4] has extensively studied the structure and properties of Zn-Al based bearing alloys. Five ternary alloys were involved in his work. An alloy of AlZn55Si1O was prepared successfully. He pointed out that additions of copper increased the mechanical properties (hardness, creep resistance and hot tensile strength) of the zinc-aluminium alloys, but the improvement in creep resistance was greater than that obtained in the hot tensile strength.

It was also shown that the zinc-aluminium-copper alloy had poor impact strength, but this is not a great disadvantage for bearing applications where impact loading is not a significant service factor. It was found that the monotectoid zinc-aluminium based ternary alloys had higher strength and wear resistance than the eutectoid based alloys.

Comparing the wear behaviour of these alloys with that of phosphor-bronze, he pointed out that the eutectoid copper-containing alloy A1Zn62Cu3 was inferior while the monotectoid alloy A1Zn55SiO was superior to that alloy.

In order to select the most suitable alloy composition and heat treatment condition for adequate physical and mechanical properties, it is necessary to further investigate in more detail the phase relationships and the phase transformations of these alloys, especially the monotectoid A1Zn55 to 60 based alloy, containing copper or silicon, or a combination of both.

3. EXPERIMENTAL PROCEDURE

3.1 Preparation of alloys

Alloys for the investigation were made of commercial grade zinc (99.99%Zn), high purity aluminium (99.99%Al), copper (99.99%Cu) and commercial grade silicon (99.99%Si).

The melts of Al and Si were first prepared in an induction furnace using a graphite crucible and a charcoal cover, with a shield of argon during the whole melting process.

To avoid evaporation at high temperature, zinc was added to the melt after the Al and Si were melted.

The resultant melts at 700°C-800°C were stirred mechanically and then poured into mild steel mould at room temperature to give ingots 16mm diameter and 160mm long.

In an attempt to homogenise the structure, the ingots were hot rolled to strip 1.5 to 2mm thick at 400°C. Small sections were cut from each of the rolled samples for heat treatment and chemical analysis.

Compositions of the alloys for determining phase diagrams and ageing are given in Tables 3-6. To avoid evaporation of zinc at high temperature, the four alloys with high zinc content, alloys ZAS7, ZACS26 for determination of phase diagrams and alloys AlZn95Si2, AlZn90Cu3Si2 for ageing, were made from a prepared master alloy of Al20% Si.

3.2 Heat Treatment

Pieces cut from the rolled strip were sealed in glass capsules filled with argon. Solution treatment and

homogenisation were carried out by heating in a large copper heat-sink inside a muffle furnace designed to give a temperature variation of $\pm$ 1^{o} over long periods of time.

After solution treatment, the alloys were quickly quenched in iced water, the glass capsule being broken simultaneously with the quench.

Disc-shaped specimens, 15mm diameter by approximately 10mm thick, were ground and polished to 6µm finish. The specimens for the determination of phase diagrams, were then homogenized at 400^{o}C for 2 days for alloys ZAS1.2.3. and ZACS1.2.3. or 350^{o}C for 1 day for the other alloys of Zn-Al-Si system in an air circulation furnace, while those for ageing were homogenized at 400^{o}C for alloys AlZn75Si2, AlZn95Si2 and AlZn75Cu3Si2, AlZn90Cu3Si2, AlZn30Cu3Si2, AlZn60Cu3Si2 for the same periods of time as those for determination of phase diagrams.

All these homogenized specimens for ageing were quenched in a standard way into iced water and placed in the furnaces and ovens for ageing immediately after measuring their as-quenched hardness.

Ageing processes were carried out at 21.1^{o}C in a room of constant temperature, at 50^{o}C in an oil bath, at 70^{o}C or 150^{o}C in an air-circulation oven, or at 100^{o}C and 170^{o}C in muffle furnaces. The early stage of ageing at 100^{o}C was done in boiling water. The nominal temperatures of 21.1^{o}C, 50^{o}C, 70^{o}C, 100^{o}C, 150^{o}C, 170^{o}C were maintained

with less than $\pm$ 1°C variation over the ageing period.

The times required for specimens to reach ageing temperature were 30 seconds for 50°C, 70°C, 100°C ageing and 1 minute for 150°C and 170°C ageing. The ageing times were counted from when the sample reached its proper temperature.

Special care was taken in the early stage of ageing at 100°C, where boiling water was used for the constant temperature bath. Specimens were put into boiling water with their marked surface lying on the bottom of the container. As soon as bubbles escaped from the gap between the marked surface and the container bottom, time counting was started.

3.3 Hardness testing

The aged specimens were quickly cooled in ice water for hardness testing. Hardness tests were made with a Vickers Pyramid Diamond Indentor, using 5kg load. Three to five hardness impressions were taken on each specimen, and in most cases duplicate specimens were used. After hardness testing, specimens were immediately moved back to furnaces for further ageing. The ageing time was accumulated by summing the interval ageing times.

3.4 X-ray diffraction examination

Immediately after the heat treatment, the specimens of size 15mm x 8mm x 2mm were quickly repolished on water-flooded 600 mesh silicon carbide paper to obtain a plane and clean surface.

X-ray diffraction was carried out on the plate specimens

using nickel-filtered CuK_α radiation from a Philips X-ray diffractometer at 40kV and 20mA. The specimens were slowly scanned at a speed of $1^\circ 2\theta$ /min from 25° to 100° 2θ. With integrated X-ray intensity data printing out at 6 second intervals, the diffraction peaks of the alloys were recorded on a chart simultaneously.

The Bragg angle 2θ and Miller indices (h k ℓ) of each diffraction peak in the specified range of 2θ were measured. Using standard methods, the structure cells and lattice parameters were determined for phase identification.

A quantitative X-ray diffraction technique was used to trace the phase transformation of alloys aged at $70^\circ C$, $100^\circ C$, $150^\circ C$, $170^\circ C$. The specimens for X-ray diffraction were aged at constant temperatures, then quickly transferred into iced water. X-ray diffraction was immediately carried out and followed by the next period of ageing as quickly as possible to minimise the influence of room-temperature ageing. Scanning in an angular range of 35°-48° 2θ was chosen to show the largest change of diffraction peaks in response to the phase transformation, with the shortest time of measurement.

The integrated intensities of diffraction peaks were calculated from the data print-out and the change in the intensities during transformation were determined.

Lattice parameters were calculated by using the data obtained from each peak. The method of least squares and Cohn's method were both used to determine the lattice

parameters with high accuracy ($\pm$0.001 Å). A computer program was used to ensure accuracy in these calculations.

3.5 Optical and scanning electron microscopy

In order to study the structure and the effect of heat treatment standard metallographic procedures were carried out on all specimens, taking care to avoid distortion of the soft alloys.

The heat treated specimens were cut in pieces of size 10mm x 10mm. The pieces of specimens were mounted in groups in conductive bakelite at 170°C for 4 minutes, and quickly followed by water cooling. A longer period of pressure mounting at 170°C was avoided because it would cause significant further heat treatment. The specimens were then mechanically polished to 1µm finish.

For optical microscope examination, all specimens of both the ternary Zn-Al-Si system and the quarternary Zn-Al-Cu-Si system were etched in 2% Nital for about 8-10 seconds, depending on the composition of the alloys. The optical microscopy examination was performed on a Reichart-Jung Polyvar metallurgical microscope. Both colour and black and white photographs were taken at several magnifications.

A Cambridge Instruments SEM 150, operated at an accelerating voltage of 20kV, was used to obtain high resolution images of the fine structure. All specimens from both the systems were lightly etched in 2% Nital before examining on the SEM. The characteristic X-ray and electron images were both used to identify the phases. The X-ray energy-dispersive analyser gave semi-quantitative analysis.

3.6 Electron-probe microanalysis

Determinations of phase fields in alloys of both systems were made on a Cambridge Instruments Microscan Five microanalyser, operated at 15kV at a beam current 70 to 120μA using the Kα peaks for each element in these alloys. The specimens examined on the Polyvar microscope were used for further determination of phase compositions. Fresh polished, pure elemental standards were used. The intensity ratios were corrected to true concentrations using the computer program of Duncumb and Jones[90].

It has been found that the operating voltage of the analyser and size of the phase to be analysed influenced the accuracy of composition determination. This is because over-lapping of phases by the electron beam may be caused if the operating voltage is too high, e.g. 20kV, or the particle too small. With alloys located in the α+Si-richσ phase field, some particles of Si-rich phase (σ) were very small. As a result, it was not possible to determine the exact composition of the Si-rich phase σ for several specimens despite numerous attempts. Ideally, particles should be small enough to homogenise quickly but large enough to avoid overlapping. The right size would be 50μm in diameter.

The same problem arose in determining the phase diagram of the Zn-Al-Cu-Si system. Some particles of T' phase were too small to determine the exact composition.

The great advantage of using EPMA is that usually a single specimen can be used to determine the boundary of a three or four-phase field and analyse the phases present, thus covering large areas of ternary phase diagrams quickly.

3.7 Transmission Electron Microscopy

Discs of 3mm diameter were produced in a Servomet spark erosion machine, then wet-ground on both sides by hand on 600 mesh paper to 0.5mm thickness using a small jig.

A disc-jet polishing machine was used to electro-polish the centre part of these discs using about 15V in a solution of 20% perchloric acid 80% ethanol. The electrolyte used was kept below -20°C, to avoid the formation of an oxide layer on the surface of the disc which sharply reduced the efficiency of electro-polishing. Once the discs were penetrated at the centre, the process was stopped automatically. The penetrated discs were then quickly washed in low temperature methanol solution.

Hot-rolled and homogenised strip specimens of 0.5-0.8mm thickness were solution treated and aged at various temperatures in the same way as that for X-ray diffraction testing.

Following the process of thin foil preparation, specimens of alloys AlZn60Cu3Si2 and AlZn30Si5 etc., were particularly investigated on a JEOL TEM at 100kv. Various periods of ageing were selected according to the phase transformation information given by the hardness and X-ray diffraction results. For alloy AlZn60Cu3Si2, TEM examinations were carried out in the as-quenched state,

and after 0.5 minutes, 1 minute, 2 minutes, 5 minutes, 8.5 minutes, 15 minutes, 24 minutes, 1.5 hours, 18 hours and 48 hours ageing at 100°C. The alloy AlZn30Si5 TEM examinations were carried out immediately after quenching, 8 minutes 1.5 hours, 18 hours and 24 hours ageing at 100°C.

To show the crystallographic and metallographic features of ageing processes of both the alloys, photographs of bright and dark field images were taken together with the corresponding diffraction patterns.

The tilting technique was used to distinguish the diffraction pattern of precipitates from that of the matrix phase. By using one of the precipitate diffraction pattern spots, the locations of many of the corresponding precipitates were shown up. The use of dark field illumination was often valuable when carrying out observations on foils containing more than one phase, and the formation and development of precipitates were detected clearly by the dark field images at various stages of ageing.

A limited amount of work was carried out using a Philips EM400 TEM, equipped with STEM and a quantitative EDS system. By this means the zinc contents of some phases were determined which provided further information on the understanding of certain phase reactions.

3.8 Tensile testing

The specimens for tensile testing were the standard size of Hounsfield No 12. The tests were carried out on a

5000 kgf Instron testing machine with a crosshead speed of 0.5mm/min at room temperature. Two different load cells, 500 kgf and 1000 kgf, were chosen for different alloys. The specimens aged at 100°C for 100 hours were cooled in ice water. The initial diameters and lengths of the specimens were measured before the tensile test. The load-extension curves were recorded on Farnell Model W211 X-Y Plotter. The lengths of broken specimens were measured for calculation of elongation after the test.

3.9 CHARPY V-notch impact test

To determine the impact strength, the notched bar impact tests were carried out using a Charpy machine with a striker energy of 300 Joules and a linear striking velocity of 5m/sec. Standard test pieces were used.

The homogenised specimens were solution-treated and quenched in iced water. To stop further phase transformation, specimens were plunged into ice water after ageing at 100°C for 100 hours. Two heat-treated specimens were tested for each alloy composition.

3.10 Dimensional change test

The as-cast silicon-containing alloys of compositions in various ranges were tested periodically for dimensional change during the 150°C ageing process. Ingots of 25mm diameter and 60mm long were cut longitudinally along 2 diameters at right angles to give 4 pieces with polished end faces. A Universal Measurement Machine MU-2.413 was used for length measurements. The precision of the measurement results was about $\pm$ 0.5μm.

Quench-aged alloys AlZn10Si5, AlZn30Si5 and AlZn60Si5 were homogenised at 400°C for 20 hours, and alloys AlZn75Si2 and AlZn95Si2 at 350°C for the same time, then quenched in iced water.

Ageing of these alloys was carried out in an air circulation oven at 100°C and then these alloys were cooled to carefully controlled room temperature of 21.1°C before each measurement. The dimensional changes were measured using the same procedure as for the as-cast alloys.

3.11 Wear testing

The Pin-on-Disc dry wear method was used[91]. Ten as-cast alloys of compositions in various ranges of both Zn-Al-Si and Zn-Al-Cu-Si systems were machined into pairs 6mm diameter and 50mm long, and ground flat and perpendicular to the axis on each end. The disc is made of En31, a bearing steel heat treated to 61-63Rc, machined, and then ground flat on each face. Before testing the discs were de-magnetised in order to minimise the effect of ferritic debris adhering to the surface.

Both pins and discs were thoroughly degreased and then located on to the Kupp Wear Tester, the diagram of which is shown in Figure 34. The pin was held by a 6mm collet. An accurately machined iron block was placed between the end of the loading arm and the platform for stopping the screw to ensure that the arm and the disc were parallel. Therefore the pin was secured onto the arm to touch the surface of the disc perpendicularly.

The length loss of the pin was measured by the wear transducer. The torque transducer was fixed to the machine. A stable torque was obtained during the wear testing. The linar speed of the disc relative to the pin was chosen as 0.84m/s and the speed of the chart recorder was 120mm/hr. The load was 2 kgf. The wear rate was defined as cm^3/cm, i.e. the volume of material lost from the pin due to wear, per unit distance travelled by the disc.

Heat treated alloys of composition in various ranges of both systems were carried out in the same way as for the as-cast alloys. For an alloy AlZn60Cu3Si2, wear rates were measured with three different loads : 1 kgf, 2 kgf, and 3 kgf. The conditions of heat treatment were as follows :

1. 400°C for 3 days, quenched into cold water, 150°C ageing for 3 days for alloys of AlZn10Cu3Si2, AlZn30Cu3Si2 and AlZn60Cu3Si2.

2. 350°C for 2.5 days, quenched into cold water, 150°C ageing for 2 days for alloys of AlZn75Cu3Si2 and AlZn95Cu3Si2.

As-cast iron pins were tested by the same procedure for comparison.

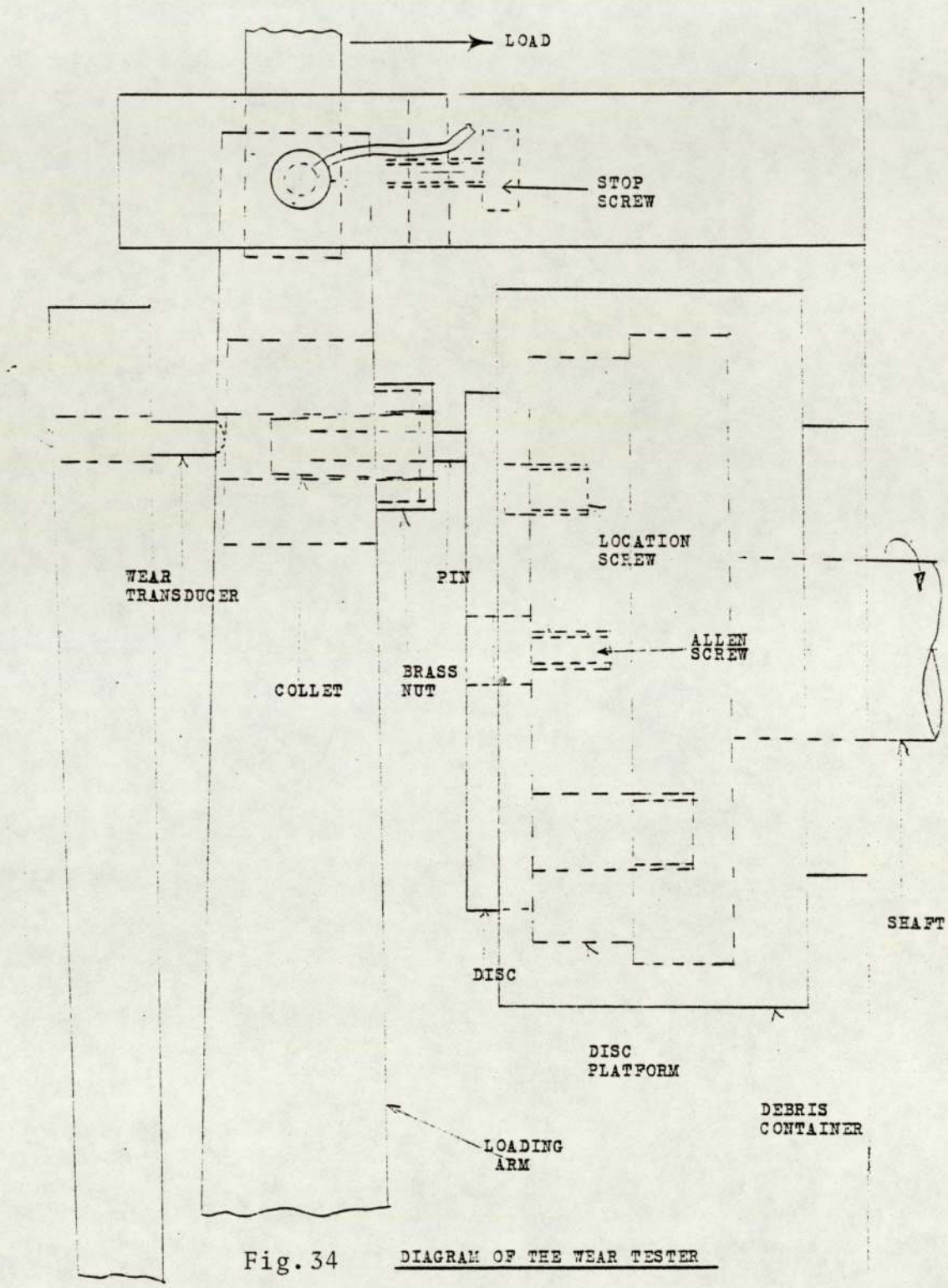

Fig. 34 DIAGRAM OF THE WEAR TESTER

4. RESULTS

4.1 Phase diagram of Zn-Al-Si ternary system

The chemical compositions of the alloys ZAS 1-8 are given in Table 3.

The phases identified by combined SEM, EPMA and X-ray diffraction and their compositions are listed in Table 7, together with alloy number and heat treatment condition, as shown in Table 8. The microanalysis results in these tables were normalised to 100% after computer correction. Results summing to <95% or >105% were discarded.

Using the data in Table 7, isothermal section of the Zn-Al-Si system at 350°C, 300°C, 280°C, 272°C, and 230°C were constructed as in Figures 35-39.

The β phase decomposed into α phase and η phase during or immediately after quenching. When specimens of compositions located in the α+β+σ, β+σ and β+η+σ phase fields were slow-scanned on an X-ray diffractometer, no matter which field the composition lay within, three sets of peaks were shown as f.c.c. (Al-rich solid solution), diamond cubic (Si-rich σ phase),and c.p.h. structure (Zn rich solid solution) η phase.

However, the heights of the peaks were different in different compositions. From the optical microscopy and EPMA, one of these phases which occurred in all specimens, was found to be a mixture of α and η phases from the decomposed β phase. Because these two phases were derived from β phase by short-range diffusion at

room temperature, a clear phase boundary between the prior β phase and the neighbouring phase could be found as shown in Figure 41. The composition of this phase could still be determined by EPMA, since even a focussed beam covered a sufficiently large volume of material to allow the mean composition to be found.

Even after prolonged annealing, sometimes there were concentration gradients shown in the analytical results from decomposed β phase. In such cases, the β phase in the three phase field α+β+σ or β+η+σ should be in equilibrium with Si-rich phase σ and α phase or η phases at the point of contact, so the composition could be determined by performing analysis close to the boundary between the two phases.

The phase boundary between the β single phase field and the two phase field β+σ was determined with particular care at 350°C, as it is of importance to the heat treatments of some commercial bearing alloys. This is shown in Figure 40.

In all the isothermal sections of the Zn-Al-Si phase diagrams investigated, a terminal solid solution of Al and Zn in Si was found, which is represented by the symbol σ. The boundaries of the σ phase field were determined by detailed examination of the compositions of the Si-rich phases in the α+σ, α+β+σ, β+σ and β+η+σ phase fields, shown in Figure 41. The saturated solubility of Al in Si at 350°C was measured as 2.4% Al in an Al*S*i20 binary alloy.

Table 3

Alloy Compositions used for Determination of Phase Diagram of Zn-Al-Si Systems

Alloy Number	Composition (wt.%)		
	Zn	Al	Si
1	10.7	80.6	8.7
2	43.9	50.8	5.3
3	69.7	27.3	3.4
4	22.5	70.1	7.4
5	60.7	29.3	10.0
6	29.8	56.6	13.6
7	81.0	14.9	4.1
8	74.0	19.6	6.4

Table 4

Alloy Compositions used for Determination of Phase Diagram of Zn-Al-Cu-Si Systems

Alloy Number	Composition (wt.%)			
	Zn	Al	Cu	Si
1	17.3	58.2	4.5	10.0
2	32.6	52.4	5.1	10.9
3	42.8	42.2	5.5	9.3
4	63.7	21.3	4.6	10.4
5	72.2	12.7	5.5	10.5
6	8.7	4.3	5.4	10.6

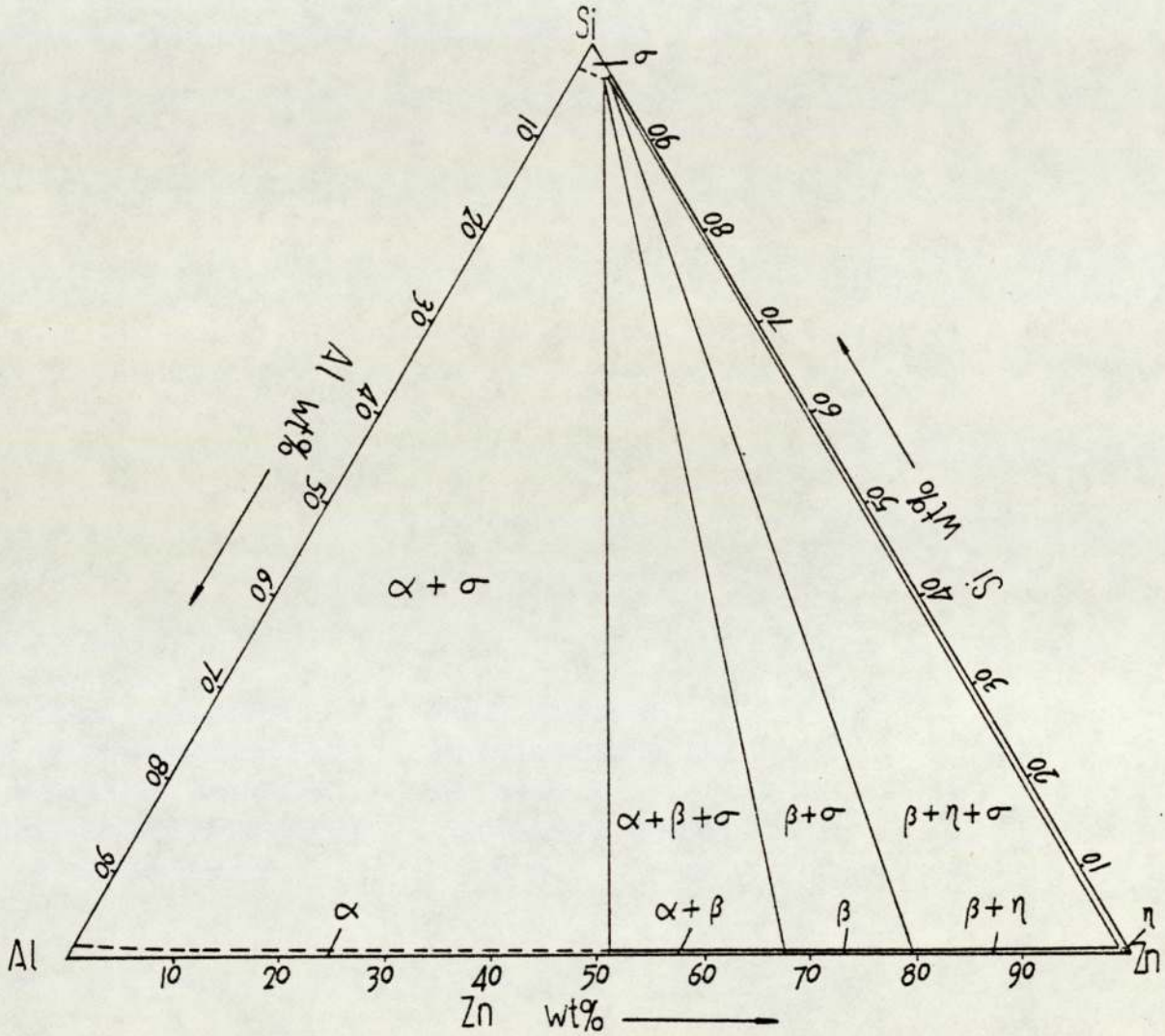

Fig.35 Isothermal section of Zn-Al-Si system at 350°C

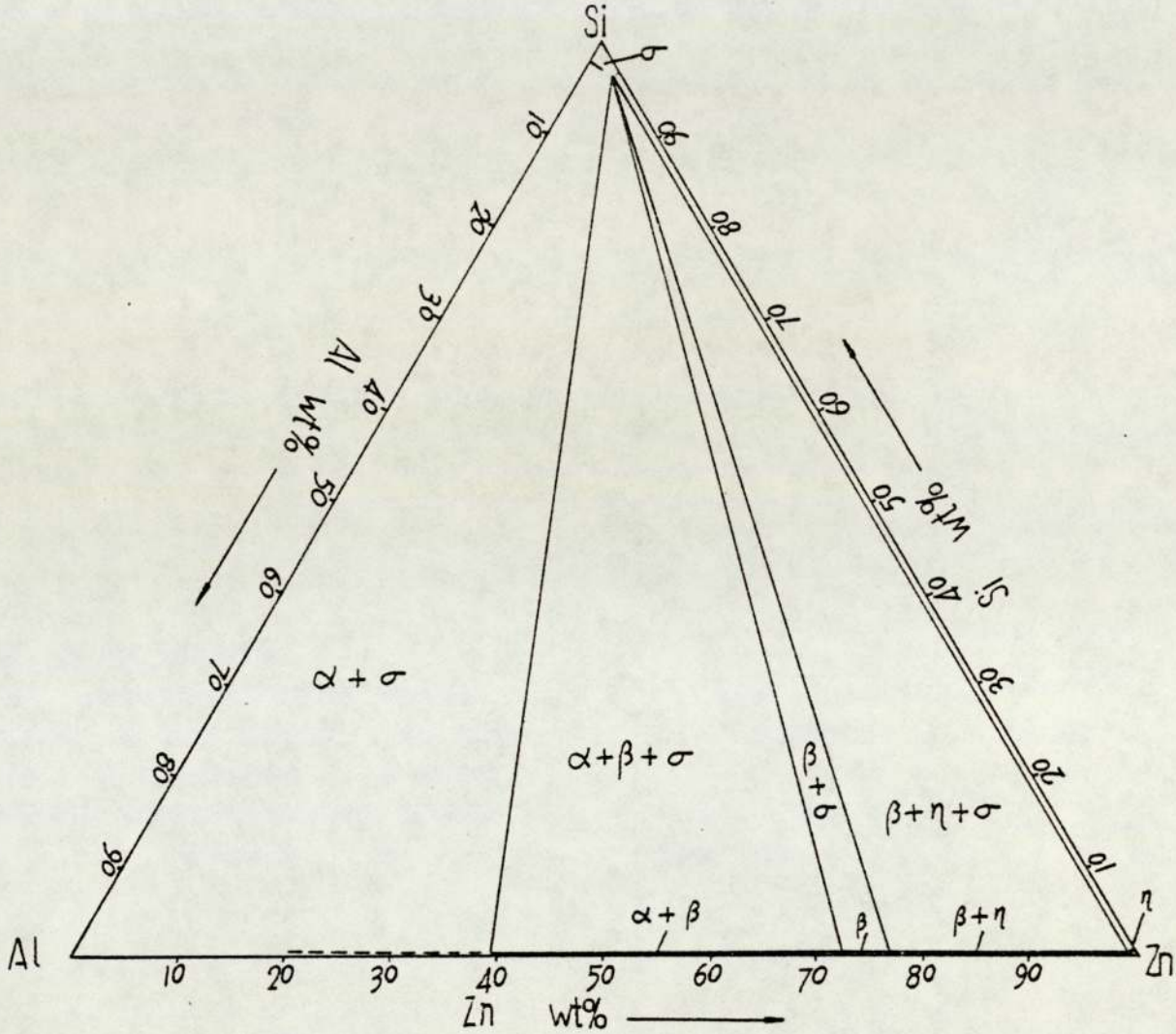

Fig. 36 Isothermal section of Zn-Al-Si systems at 300°C

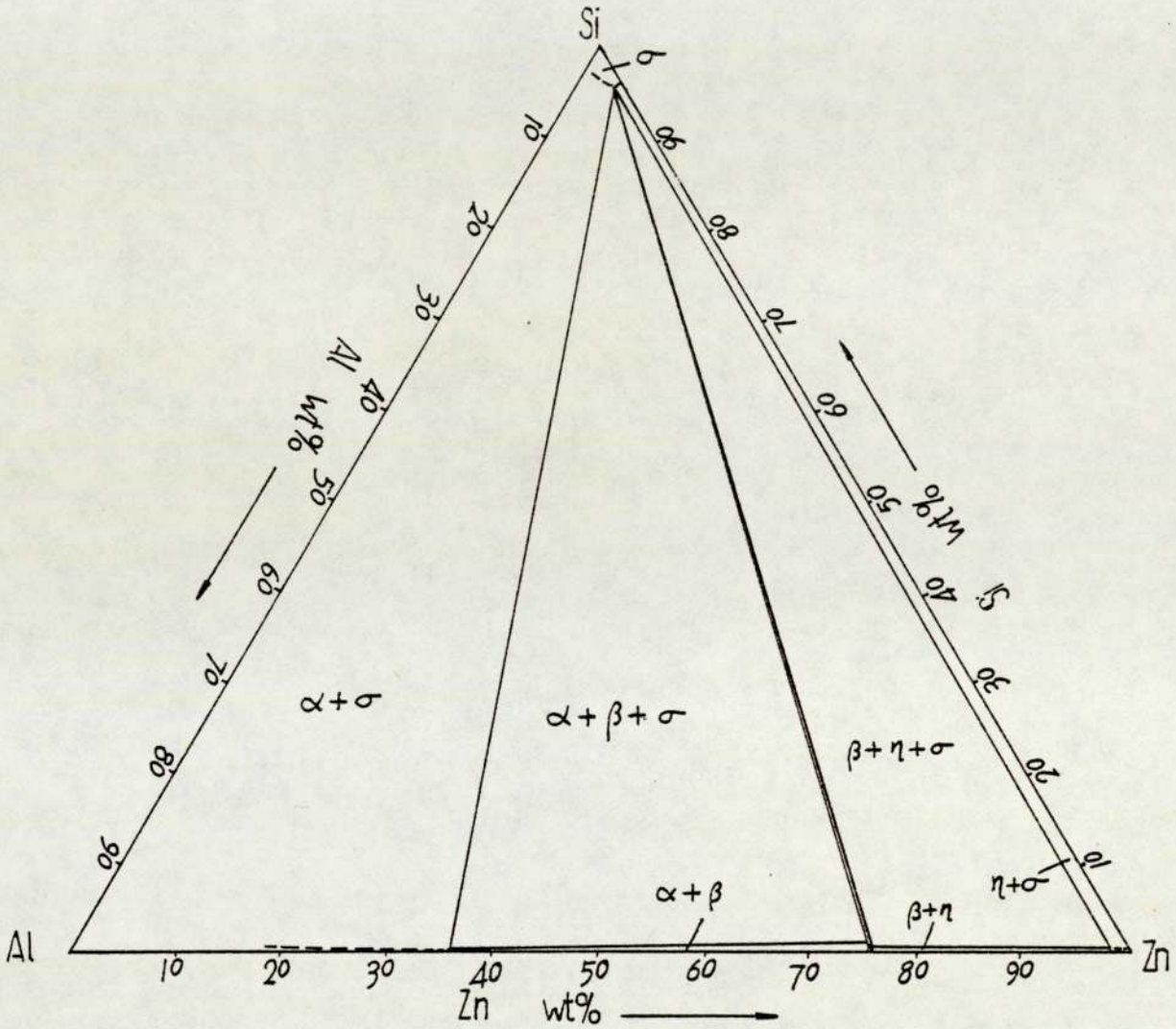

Fig. 37 Isothermal section of Zn-Al-Si system at 280°C

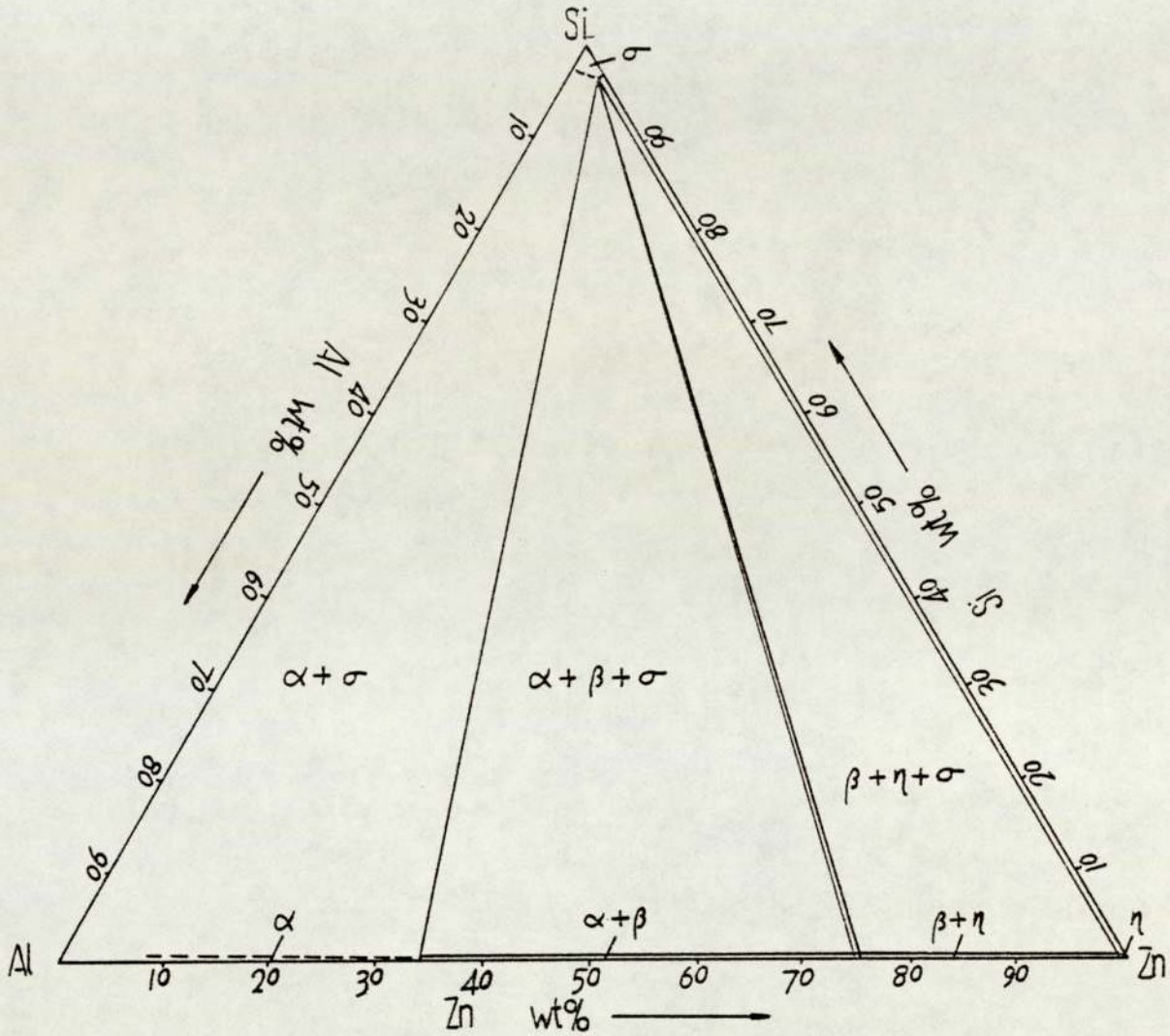

Fig.38 Isothermal section of Zn-Al-Si system at 272°C

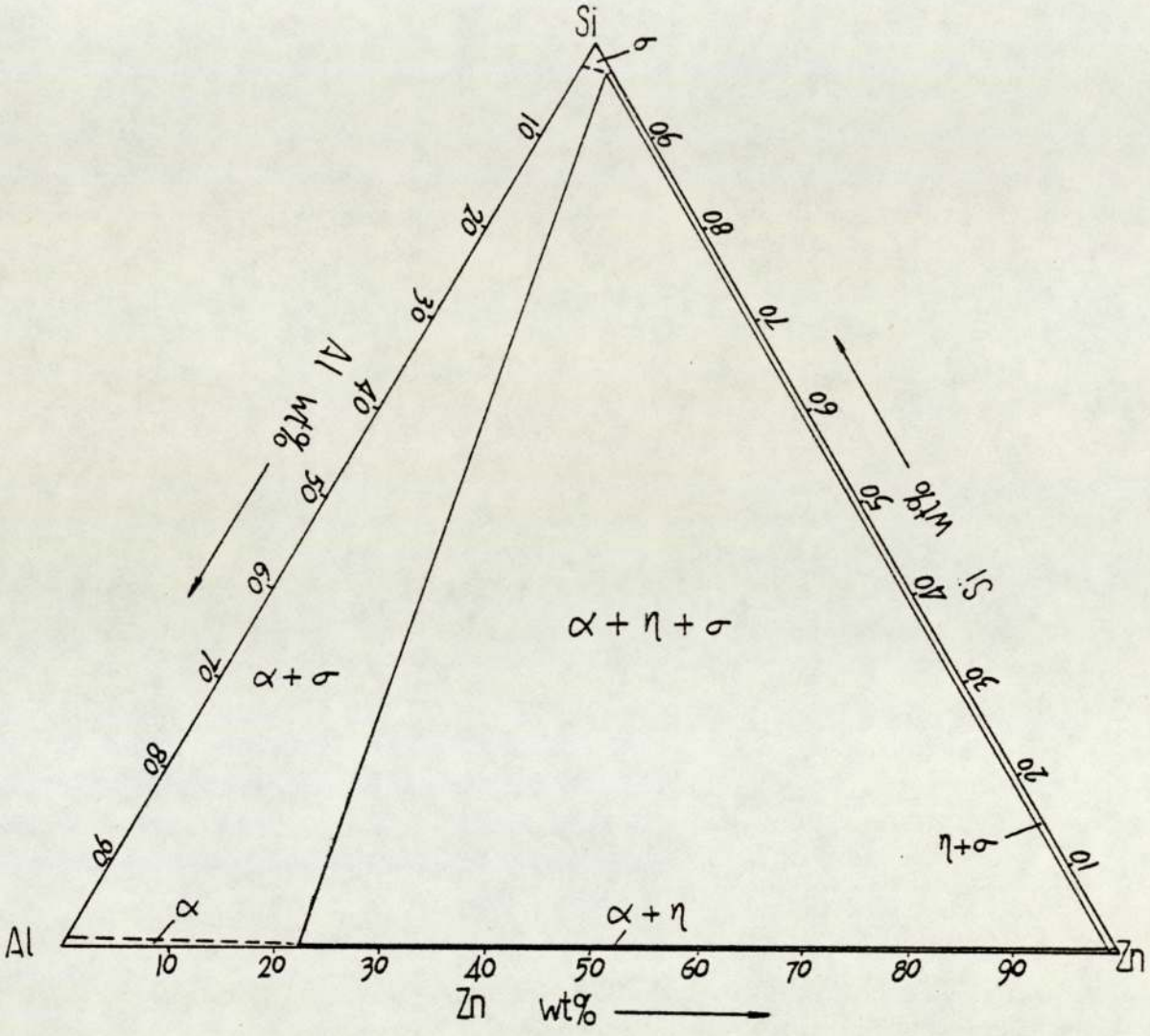

Fig. 39 Isothermal section of Zn-Al-Si system at 230°C

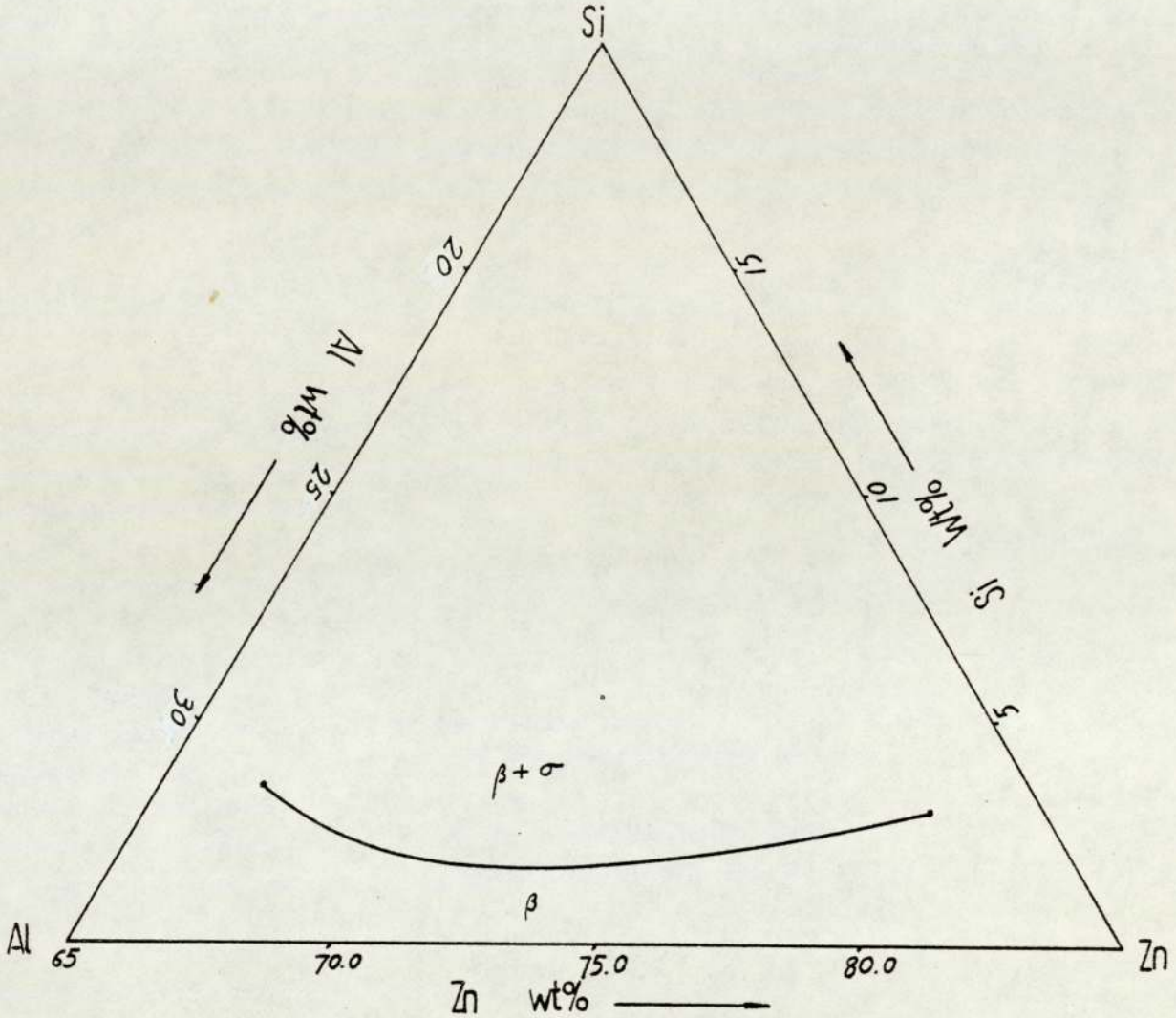

Fig. 40 The β/β+α phase boundary in Zn-Al-Si system at 350°C

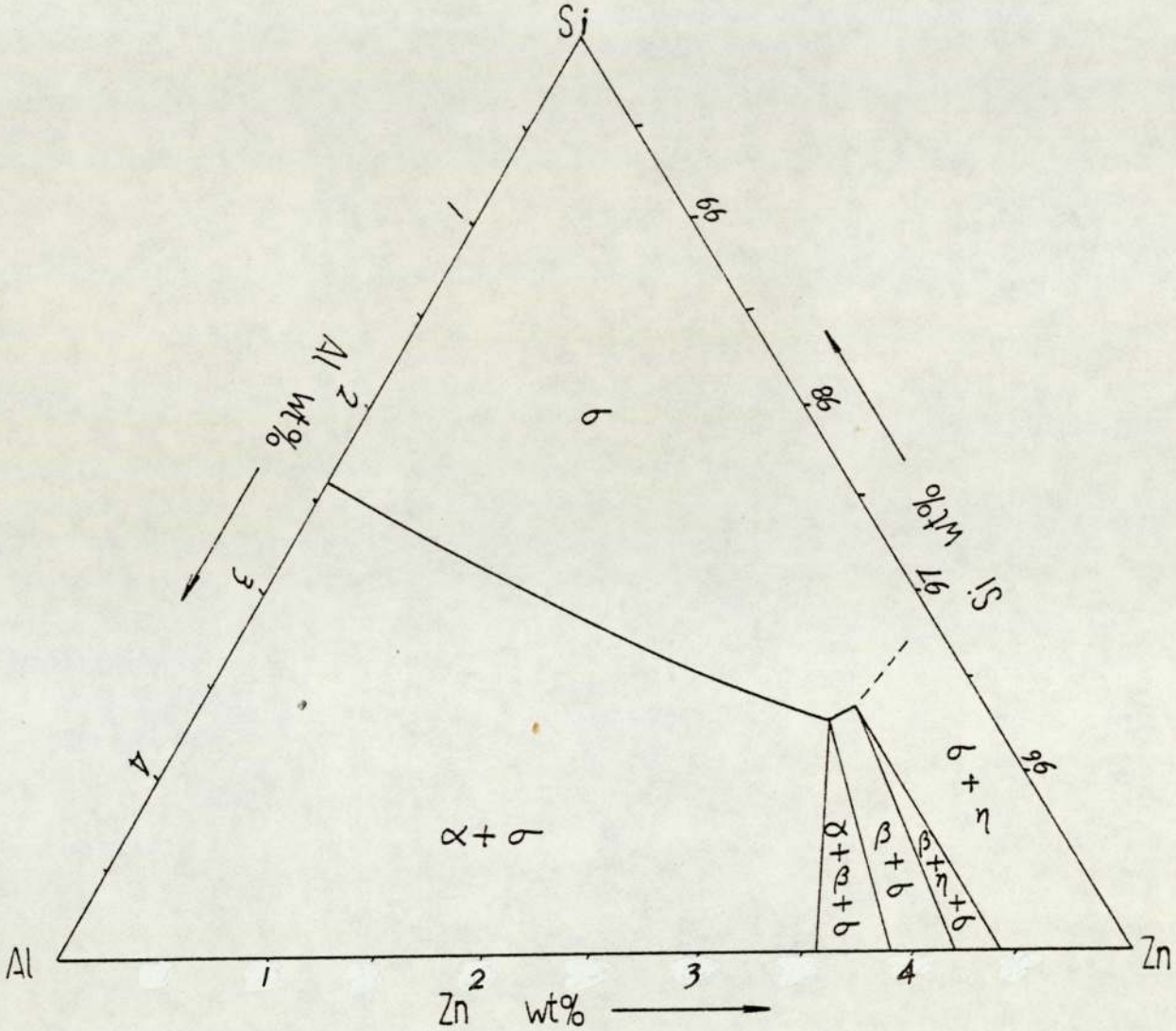

Fig. 41 The Si-rich (σ) phase figure.

Table 7

THE IDENTIFIED PHASES AND THEIR COMPOSITIONS FOR Zn-Al-Si SYSTEM

Temp(°C)	Phase Fields	Phase	Zn	Al	Si
350	α+β+Si rich	α	50.95	48.86	0.20
		β	67.06	32.59	0.35
		Si rich	2.96	0.75	96.29
	β+η+Si rich	β	79.76	19.96	0.28
		η	98.67	0.98	0.35
		Si rich	3.05	0.59	96.36
300	α+β+Si rich	α	39.11	60.68	0.21
		β	72.06	27.74	0.19
		Si rich	2.84	0.80	96.36
	β+η+Si rich	β	76.73	23.06	0.22
		η	98.92	0.73	0.35
		Si rich	2.74	1.03	96.33
280	α+β+Si rich	α	35.5	64.37	0.13
		β	74.87	24.93	1.29
		Si rich	3.59	0.77	95.63
	β+η+Si rich	β	75.23	24.56	0.21
		η	97.87	1.87	0.26
		Si rich	3.13	1.16	95.71
272	α+β+Si rich	α	33.62	66.13	0.24
		β	74.04	25.72	0.24
		Si rich	2.99	0.54	96.47
	β+η+Si rich	β	74.68	24.82	0.66
		η	98.83	0.88	0.30
		Si rich	3.17	0.75	96.18

Table 7 (contd.)

THE IDENTIFIED PHASES AND THEIR COMPOSITIONS FOR Zn-Al-Si SYSTEM

Temp(^{o}C)	Phase Fields	Phase	Zn	Al	Si
230	α+β+Si rich	α	22.47	77.49	0.04
		η	98.46	1.13	0.41
		Si rich	2.81	0.84	96.35
250	α+η+Si rich	α	33.35	66.27	0.38
		η			
		Si rich			

Table 8

THE EQUILIBRIUM TEMPERATURE AND TIME OF HOMOGENIZATION IN Zn-Al-Si SYSTEM

Heat Treatment	Alloy Number	Phase Field
350°C 216 hrs	1,2,4,6	α+Si rich
	5	α+β+Si rich
	3,8	β+Si rich
	7	β+η+Si rich
300°C 384 hrs	1,2,6	α+Si rich
	2,3,5	α+β+Si rich
	-	β+Si rich
	7,8	β+η+Si rich
280°C 840 hrs	1,4,6	α+Si rich
	2,3,5	α+β+Si rich
	-	β+Si rich
	7,8	β+η+Si rich
272°C 960 hrs	1,4	α+Si rich
	2,3,5,6	α+β+Si rich
	-	β+Si rich
	7,8	β+η+Si rich
230°C 672 hrs	1	α+Si rich
	2,3,4,5,6,7,8	α+η+Si rich
	-	η+Si rich

Table 9

LATTICE PARAMETER (Å) IN Zn-Al-Si at 272°C

Specimen	a.(f.c.c.)	a.(Diamond Cubic)	a.	c.	c/a
ZAS1	4.044	5.401			
ZAS4	4.034	5.420	2.675	4.691	1. 5
ZAS6	4.021	5.436			
ZAS2	4.024				
ZAS3	4.024	5.437			
Al	4.049				
Zn			2.665	4.947	1.856
Si		5.430			

*Specimen ZAS6, 2 and 3 were in the same phase field ($\alpha+\beta+\sigma$).

Table 12

LATTICE PARAMETERS (Å) OF CUBIC PHASES IN Zn-Al-Cu-Si SYSTEM

Alloy	Phase	Temperature		
		290°C	300°C	350°C
ZACS2	α	4.033	4.037	
ZACS3	α	3.989	4.079	
ZACS	β	3.988	4.002	
ZACS5	β	3.971	3.985	4.078
ZACS6	β	3.961	3.732	3.987

The room-temperature lattice parameters of the phases in alloys of the Zn-Al-Si system equilibrated at 272°C were measured. The data are shown in Table 9 with values for pure zinc, aluminium and silicon for comparison.

The metallographic work was performed in the SEM and the optical microscope. Figure 42 shows the X-ray and electron images for ZAS7 at 272°C. The dark field is the Si-rich σ phase. The grey field is η phase and the β phase was found decomposed in the light area.

4.2 Phase diagram of Zn-Al-Cu-Si quaternary system

The chemical compositions of six Zn-Al-Cu-Si quaternary alloys are shown in Table 4.

The phases identified by combined STEM, EPMA and X-ray diffraction and their compositions are listed in Table 10. The equilibrium temperatures and times used for different alloys are listed in Table 11.

Optical metallography showed that η phase etched in 2% Nital solution more quickly than other phases and varied in colour from various shades of brown to green or blue, as shown in Figure 43. The same figure showed that the grey Si-rich σ phase was typically angular in shape, the ε phase appeared white and was more rounded than σ . Both these phases were dispersed in a matrix consisting of β and η phases. The β phase was found to be decomposed after the quench, and was seen as an easily identified mixture of light α phase with very fine grey η precipitates, as shown also in Figures 44-48.

Identification of phases was performed semi-quantitatively using EDS on the SEM. Two sets of X-ray and electron images of specimens of Zn-Al-Cu-Si alloys quenched from 285°C show the coexistence of five phases $\alpha+\beta+\varepsilon+T'+\sigma$ as shown in Figures 49,50. The β phase was easily identified from its speckled appearance which occurs on decomposition as observed in the optical examination. ε phase occurred as a deeper etched dark area. In the X-ray image of Al, the α phase appears brighter than the β phase. Only T' phase seems not to be etched by 2% Nital solution and has a flat polished surface.

The isothermal sections of the Zn-Al-Cu-Si systems at 350°C, 300°C, 290°C, 285°C, 280°C and 275°C were constructed as in Figures 51-56 using the data in Table 10. Since the solubility of Si in all of the phases except σ was very low, these can be regarded as sections through a quaternary isothermal body at a nominal 0.1% Si. The σ phase is present in all the phase fields, but is ignored for the sake of clarity.

The compositions of phases in these isothermal sections were determined from a single specimen and are shown in Figure 42. In ZACS1, it was not possible to determine the compositions of θ phase and σ phase as the particles of these two phases were too small for analysis. Dashed lines represent boundaries which were estimated from a vertical section of the Zn-Al-Si ternary phase diagram at 0.2% Si and were incompletely measured.

In the 300°C isothermal section, the two-phase field $\beta+\varepsilon$ had narrowed and the solubility of copper in β phase in alloys ZACS4 and ZACS5 decreased from 5.5 to 3.5%. The $\beta+T'+\varepsilon$ phase field limits were determined from alloy ZACS4 and ZACS5, as shown in Figure 50.

The $T'+\beta$ phase field was constructed at 290°C and disappeared at 285°C as shown in Figures 53,54. At 285°C the coexistence of four phases $\alpha+\beta+\varepsilon+T'$ plus σ was detected in alloys ZACS3, 4 and 5 from X-ray diffraction and SEM examination. The electron-probe microanalyser gave very close agreement in the compositions of $\alpha,\beta,T',\varepsilon$ and σ phases in these three alloys. The X-ray and electron images of ZACS4, 5 are shown in Figures 49,50.

The four-phase coexistence was destroyed by the appearance of an $\alpha+\varepsilon$ two-phase field at 280°C. The composition of the phase in coexistence with T' phase shifted towards the Al corner, from 40% Zn to 31% Zn, with decreasing temperature from 300°C to 275°C. As the equilibrium temperature was reduced from 350°C, the maximum solubility of copper in α phase decreased. Between 280°C and 275°C the β phase disappeared.

The lattice parameters of α and β phases at various temperatures were measured, as shown in Table 12 and those of η and ε phases were found to change little with annealing temperature. They were as follows :

ε phase : $a_o = 2.767$ Å $c_o = 4.289$ Å $c_o/a_o = 1.550$

η phase : $a_o = 2.671$ Å $c_o = 4.946$ Å $c_o/a_o = 1.852$

Table 10

THE IDENTIFIED PHASES AND THEIR COMPOSITIONS FOR Zn-Al-Cu-Si SYSTEM

Temp(°C)	Phase Fields	Phase	Zn	Al	Cu	Si
	α+θ+Si rich	α	18.11	81.56	0.01	0.2-
		θ	-	-	-	-
		Si rich	-	-	-	-
350	α+θ+T'+Si rich	α	37.46	59.18	3.25	0.11
		θ	5.05	44.75	49.99	0.21
		T'	9.91	35.52	54.48	0.08
		Si rich	2.94	1.86	0.77	84.43
	α+T'+Si rich	α	46.78	48.59	4.54	0.10
		T'	11.20	34.41	54.25	0.09
		Si rich	2.40	1.09	0.74	96.45
	β+ε+T'+Si rich	β	67.36	27.11	5.46	0.07
		ε	77.75	2.13	20.43	0.08
		T'	11.67	33.55	54.73	0.06
		Si rich	2.65	0.49	0.46	96.39
	β+ε+η+Si rich	β	75.59	22.20	2.08	0.14
		ε	83.04	0.96	15.85	0.15
		η	93.35	2.04	4.43	0.18
		Si rich	3.19	0.26	0.46	96.08
300	α+T'+Si rich	α	18.76	80.92	0.02	0.29
		T'	-	-	-	-
		Si rich				
	α+β+T'+Si rich	α	39.79	57.74	2.31	0.15
		β	68.56	29.77	1.51	0.17
		T'	11.32	35.12	53.45	0.11
		Si rich	2.07	0.96	0.61	96.36

Table 10 (contd.)

THE IDENTIFIED PHASES AND THEIR COMPOSITIONS FOR Zn-Al-Cu-Si SYSTEM

Temp(^{o}C)	Phase Fields	Phase	Zn	Al	Cu	Si
300	β+ε+T'+Si rich	β	72.10	24.28	3.51	0.10
		ε	80.76	2.78	16.33	0.13
		T'				
		Si rich	3.76	0.80	0.64	94.8
	β+ε+η+Si rich	β	72.14	25.45	2.34	0.09
		ε	83.09	0.69	16.14	0.06
		η	97.63	1.03	0.40	0.93
		Si rich	4.77	0.57	0.52	94.14
290	α+T'+Si rich	α	36.88	60.78	2.24	0.10
		T'	9.68	35.88	54.36	0.07
		Si rich	2.44	0.55	0.42	96.59
	α+β+T'+Si rich	α	39.29	59.27	2.19	0.32
		β	70.98	26.17	2.77	0.09
		T'	9.93	35.21	54.86	0.06
		Si rich	2.28	0.57	0.59	96.45
	β+ε+T'+Si rich	β	72.10	25.19	2.36	0.08
		ε	82.14	1.21	16.56	0.09
		T'	10.05	35.36	54.57	0.04
		Si rich	2.43	0.51	0.45	96.61
	β+ε+η+Si rich	β	74.69	23.03	2.16	0.08
		ε	83.59	0.73	15.60	0.09
		η	95.46	1.06	3.37	0.10
		Si rich	2.86	0.42	0.43	96.30

Table 10 (contd.)

THE IDENTIFIED PHASES AND THEIR COMPOSITIONS FOR Zn-Al-Cu-Si SYSTEM

Temp(^{o}C)	Phase Fields	Phase	Zn	Al	Cu	Si
285	$\alpha+\beta+\varepsilon+T'+$Si rich	α	35.33	62.82	1.78	0.07
		β	71.45	26.00	2.48	0.07
		ε	83.14	0.97	15.81	0.09
		T'	10.24	34.73	54.98	0.05
		Si rich	2.79	0.47	0.49	96.26
	$\beta+\varepsilon+\eta+$Si rich	β	73.53	24.63	1.77	0.07
		ε	83.90	0.71	15.32	0.07
		ν	95.61	1.31	2.97	0.10
		Si rich	3.23	0.38	0.31	96.08
280	$\alpha+\varepsilon+T'+$Si rich	α	32.04	65.75	2.02	0.19
		ε	82.78	1.35	15.71	0.17
		T'	10.37	35.94	53.63	0.08
		Si rich	1.83	0.79	0.52	96.86
	$\alpha+\beta+\varepsilon+$Si rich	β	71.43	26.37	2.10	0.09
		α	34.08	64.08	1.76	0.07
		ε	83.70	0.79	15.40	0.10
		Si rich	2.67	0.87	0.60	95.87
	$\beta+\varepsilon+\eta+$Si rich	β	73.44	24.70	1.79	0.07
		ε	83.88	0.74	15.31	0.07
		η	95.79	1.31	2.83	0.06
		Si rich				

Table 10 (contd.)

THE IDENTIFIED PHASES AND THEIR COMPOSITIONS

FOR Zn-Al-Cu-Si SYSTEM

Temp(^{o}C)	Phase Fields	Phase	Zn	Al	Cu	Si
275	$\alpha+\varepsilon+T'+$Si rich	α	31.32	66.97	1.63	0.08
		ε	82.55	1.71	15.67	0.07
		T'	10.58	36.90	52.42	0.10
		Si rich	1.99	0.84	0.54	96.64
	$\alpha+\varepsilon+\eta+$Si rich	α	32.61	66.34	1.25	0.06
		ε	84.14	0.74	15.00	0.09
		η	95.24	1.37	3.28	0.11
		Si rich				

Table 11

THE EQUILIBRIUM TEMPERATURE AND TIME OF HOMOGENIZATION IN Zn-Al-Cu-Si SYSTEM

Heat Treatment	Alloy Number	Phase Field
350°C 336 hrs	1	α+θ+Si rich
	2	α+θ+T'+Si rich
	3	α+T'+Si rich
	4	β+ε+T'+Si rich
	5	β+ε+Si rich
	6	β+ε+η+Si rich
300°C 720 hrs	1,2	α+T'+Si rich
	3	α+β+T'+Si rich
	4,5	β+ε+T'+Si rich
	6	β+ε+η+Si rich
290°C 1080hrs	1,2	α+T'+Si rich
	3	α+β+T'+Si rich
	4,5	β+ε+T'+Si rich
	6	β+ε+η+Si rich
285°C 1440hrs	2,3,4,5	α+β+ε+T'+Si rich
	6	β+ε+η+Si rich
280°C 1440hrs	2,3	α+ε+T'+Si rich
	4,5	α+β+ε+Si rich
	6	β+ε+η+Si rich
275°C 2400hrs	2,3,4	α+ε+T'+Si rich
	5,6	α+ε+η+Si rich

Fig. 42 Scanning Electron Micrographs for alloy ZnAlSi7 at 272°C

Electron Image

Dark field - σ

Grey field - η

Matrix - β

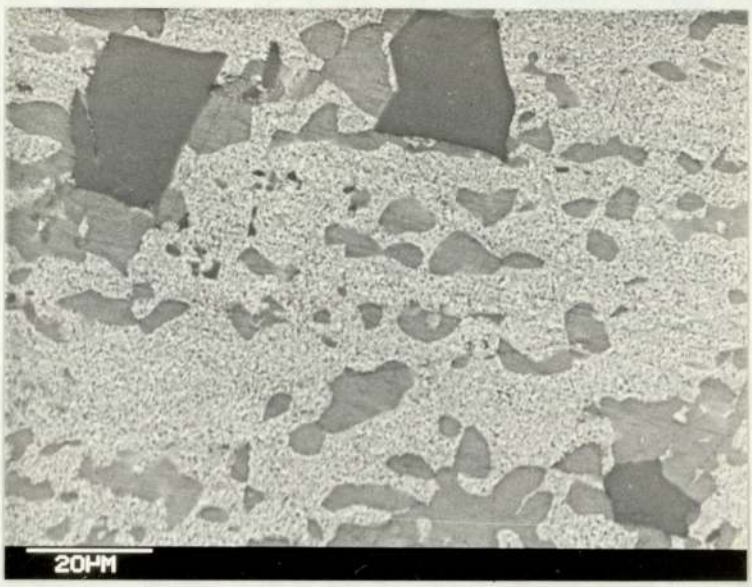

Zn X-rays image

Fig. 42 continued

Si X-rays image

Al X-rays image

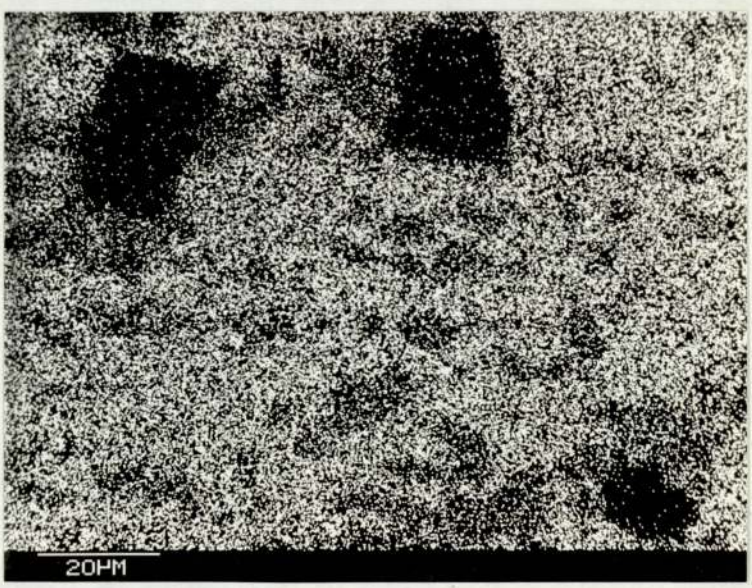

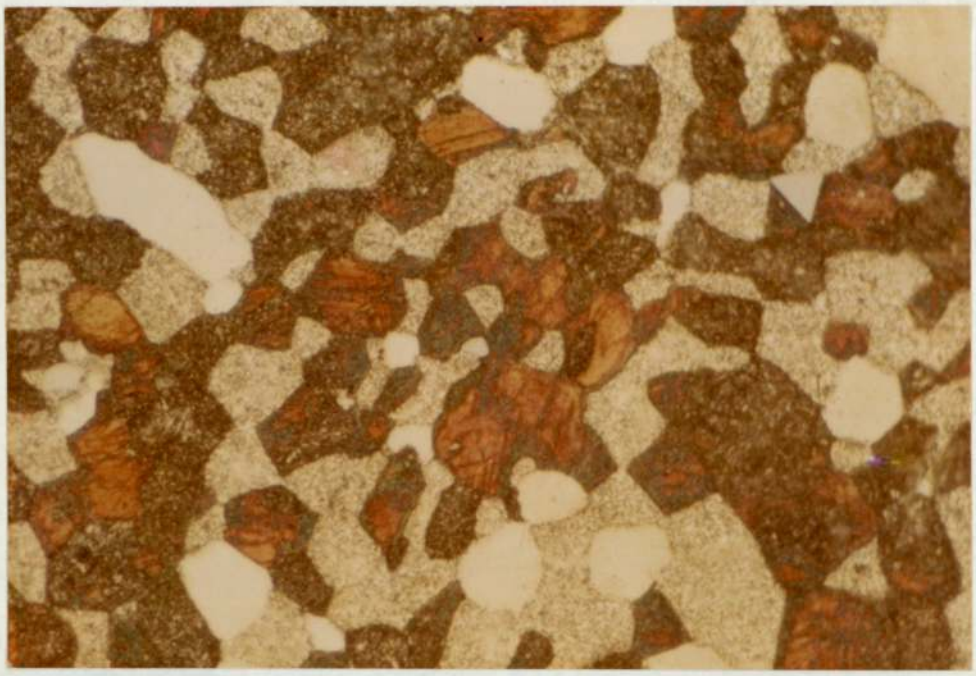

Fig.43 Optical micrographs for alloy ZnAlCuSi5 at 300°C. x560.

Fig. 44 Optical micrographs for alloy ZnAlCuSi5 at 350°C. x560.

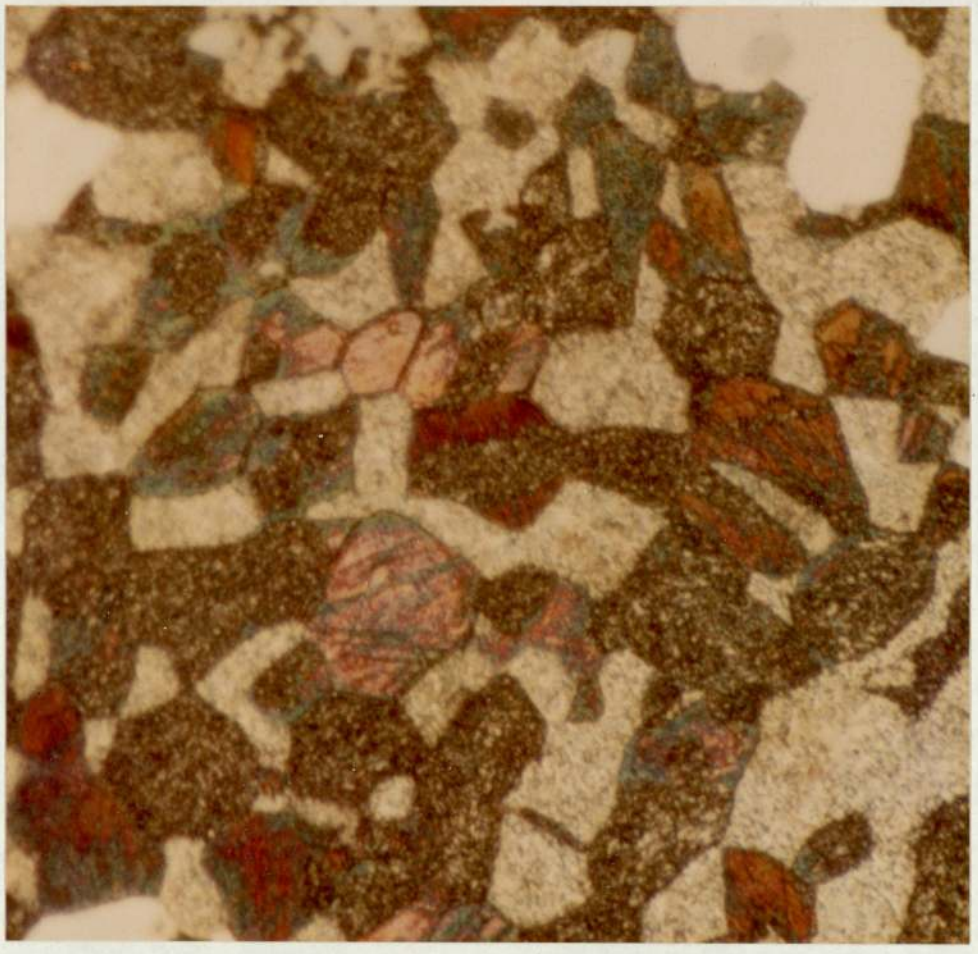

Fig.45 Optical micrographs for alloy ZnAlCuSi5 at 300°C. x980

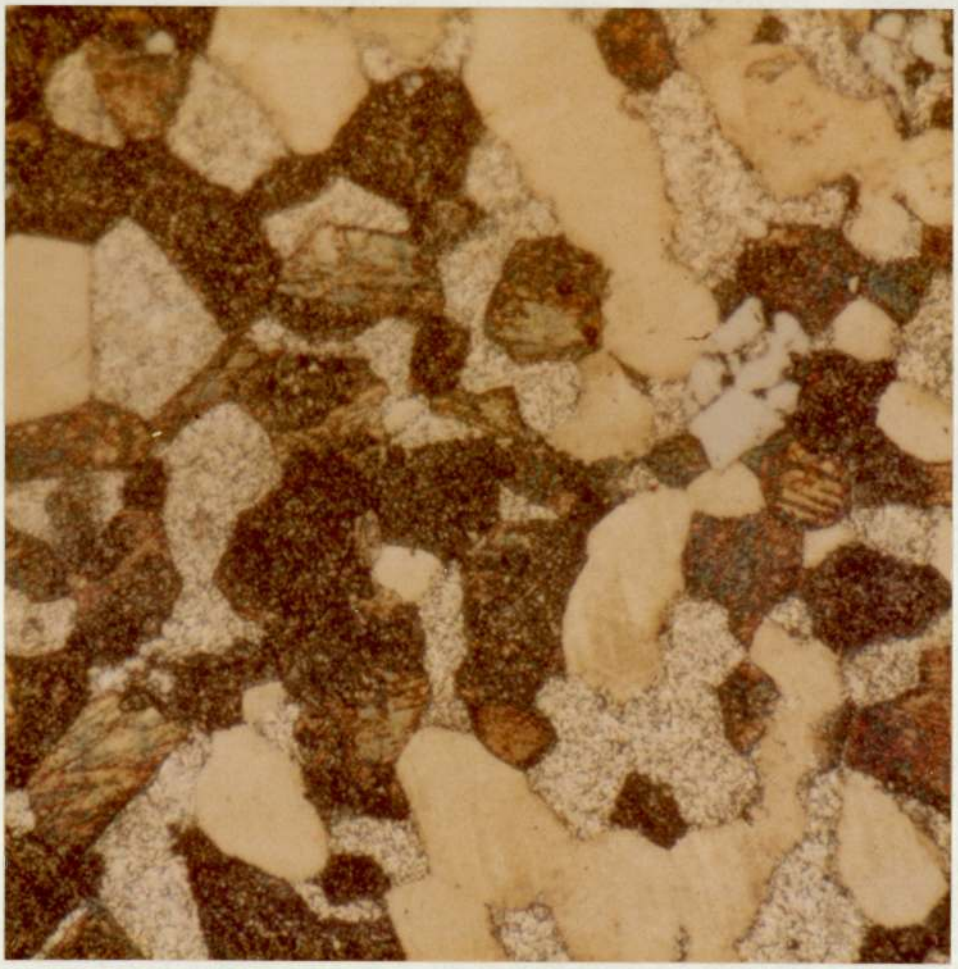

Fig. 46 Optical micrographs for alloy ZnAlCuSi5 at 350°C. x980

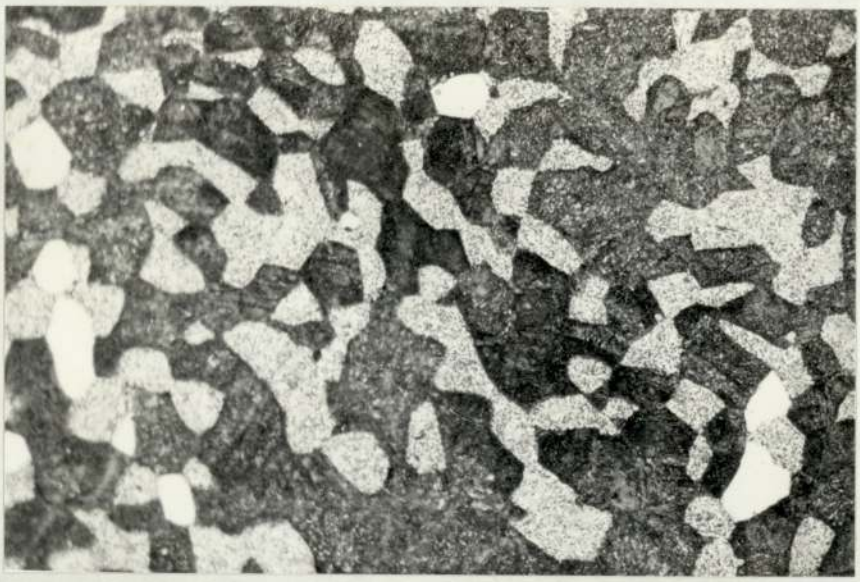

Fig.47 Optical micrographs for alloy ZnAlCuSi5 at 350°C. x430.

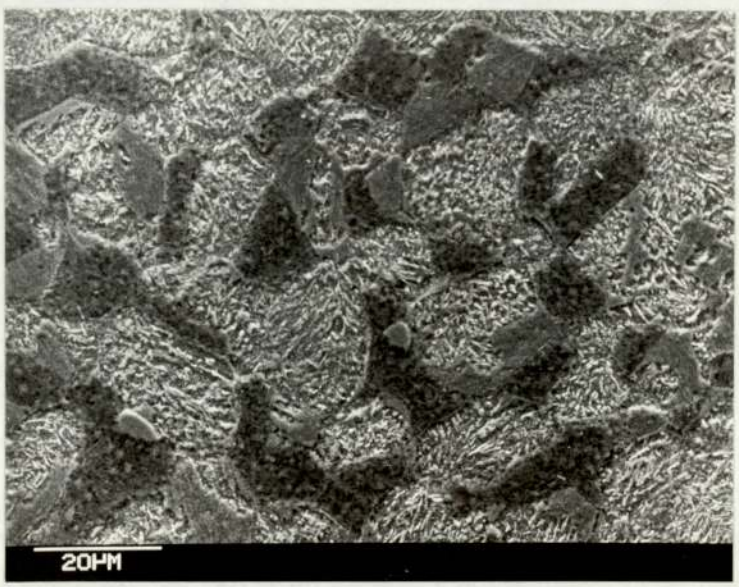

Fig.48 Scanning electron micrograph for alloy ZnAlCuSi, ZnAlCuSi5 at 300°C.

Fig. 49 Scanning Electron Micrographs for alloy ZnAlCuSi4 at 285°C, showing five phases (α + β + ε + T' + σ) coexistance

Electron image

Dark field - σ

Grey field - ε

Light grey - α

Grey flat - T'

Matrix - β

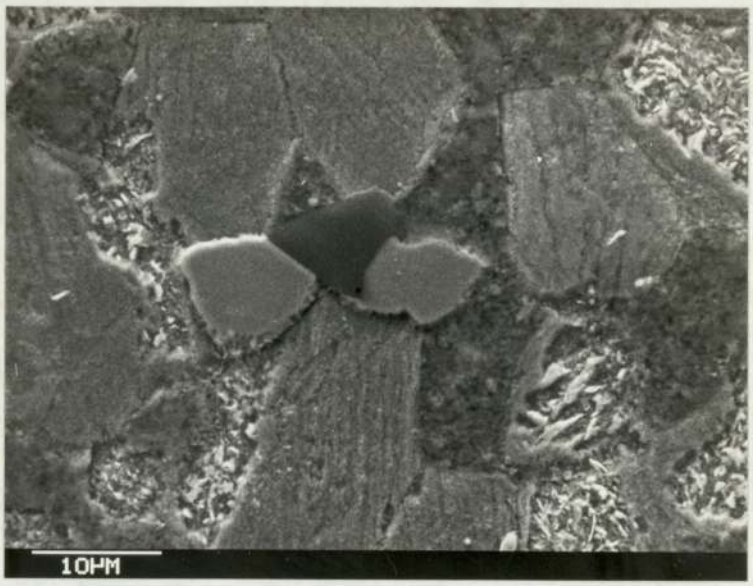

Zn X-rays image

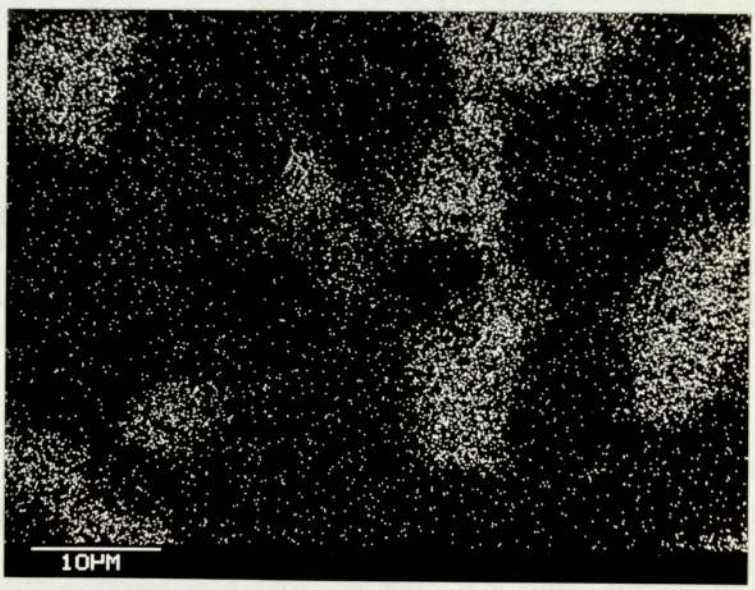

Fig. 49 continued

Cu X-rays image

Al X-rays image

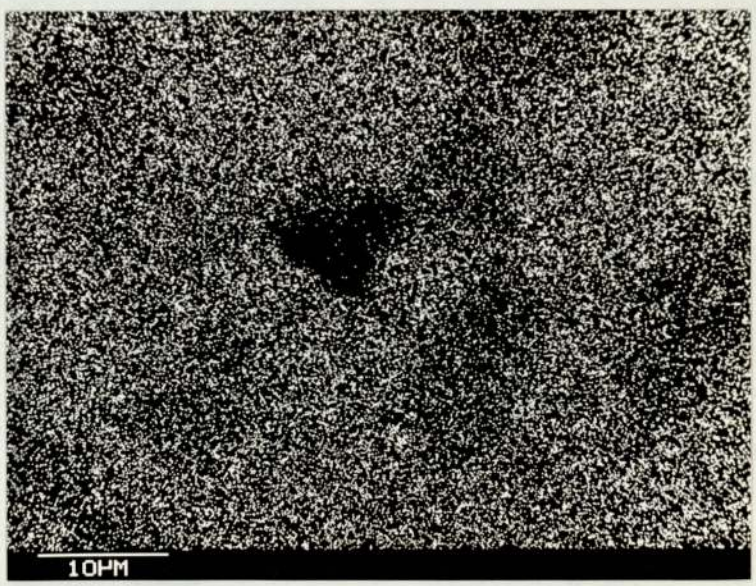

Fig. 49 continued

Si X-rays image

Fig. 50 Scanning Electron Micrographs for alloy ZnAlCuSi3 at 285°C, showing five phases ($\alpha + \beta + \varepsilon + T' + \sigma$) coexistance

Electron image

Dark field - σ

Grey field - ε

Light grey - α

Grey flat - T'

Matrix - β

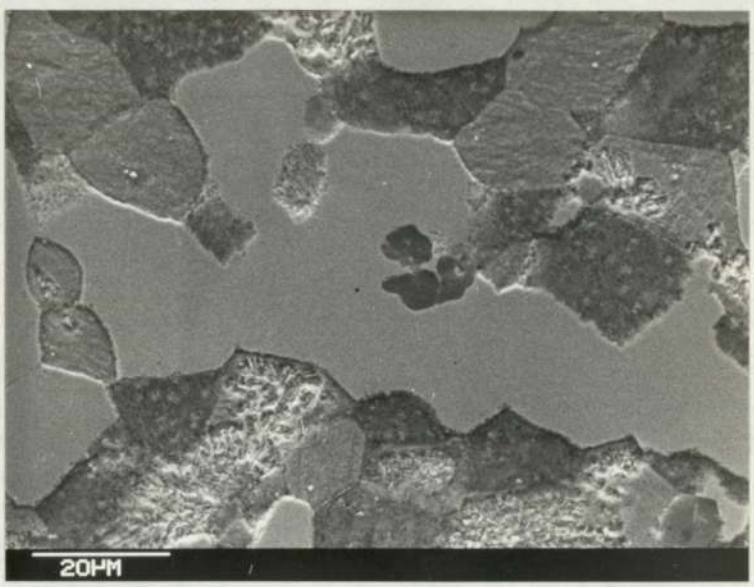

Zn X-rays image

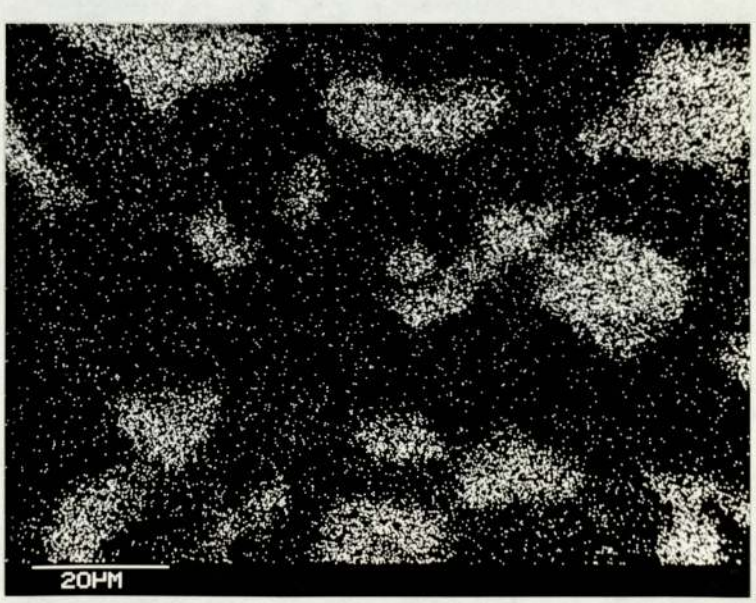

Figure 50 continued

Cu X-rays image

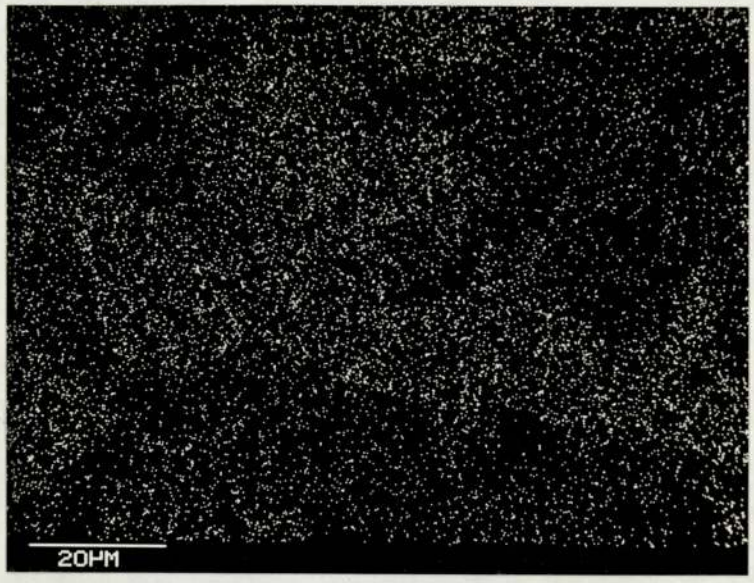

Al X-rays image

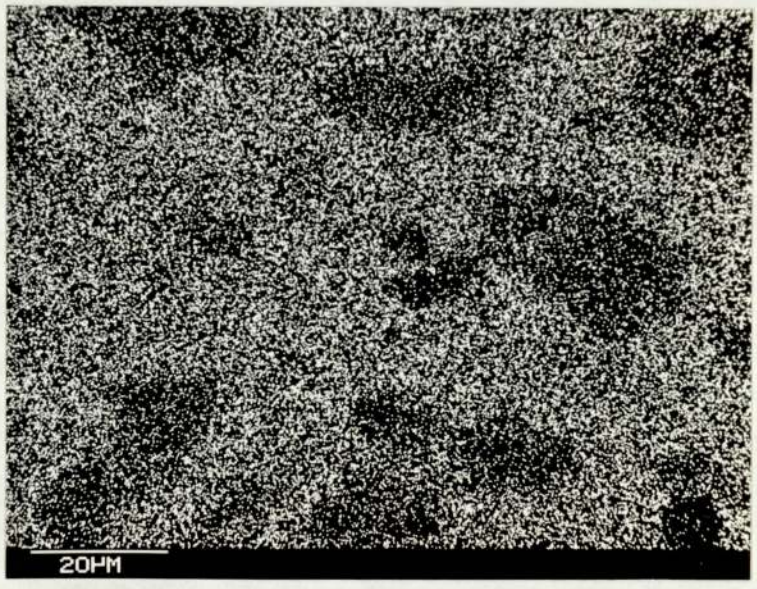

Figure 50 continued

Si X-rays image

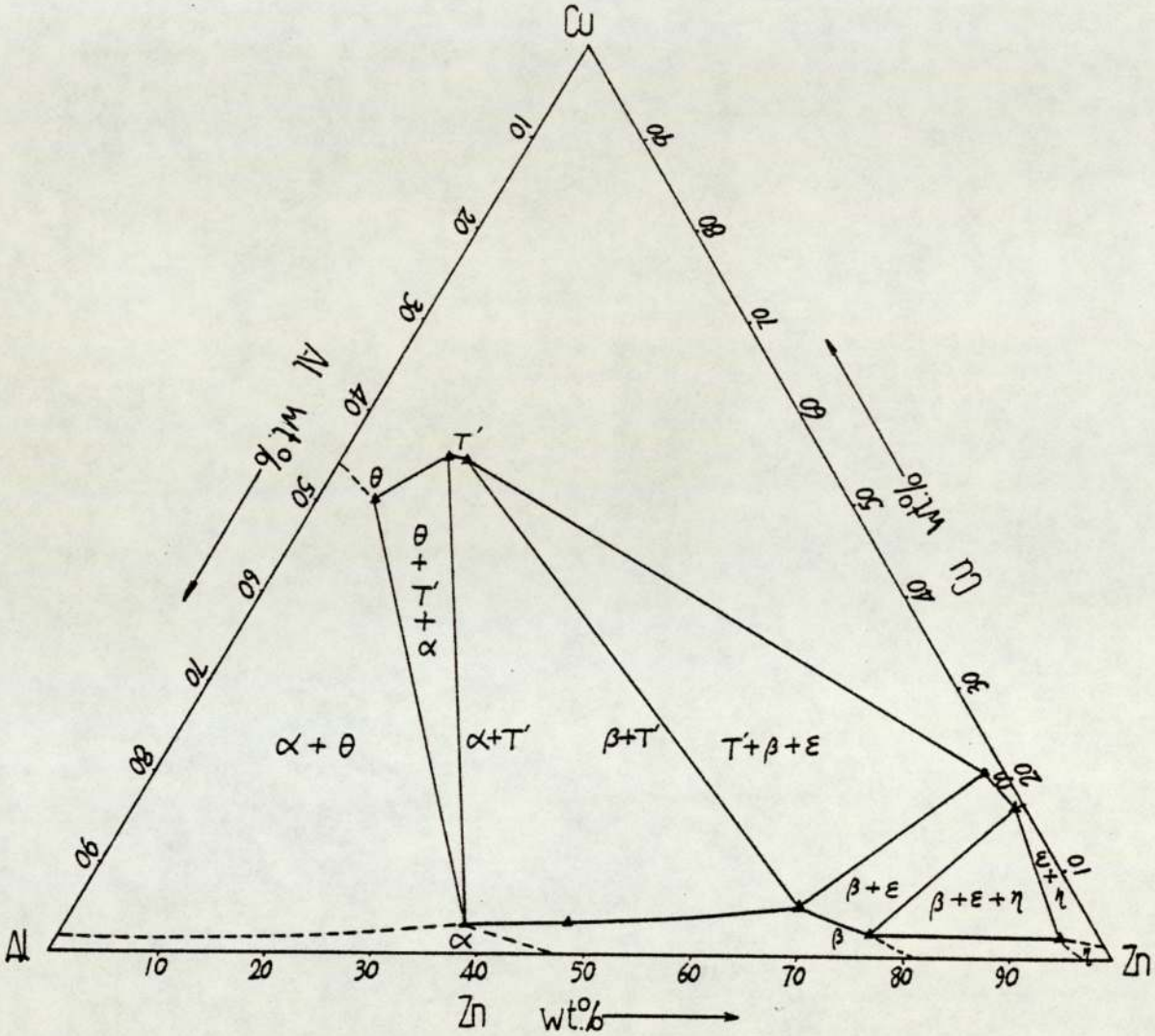

Fig. 51 Isothermal section of Zn-Al-Cu-Si system at 350°C

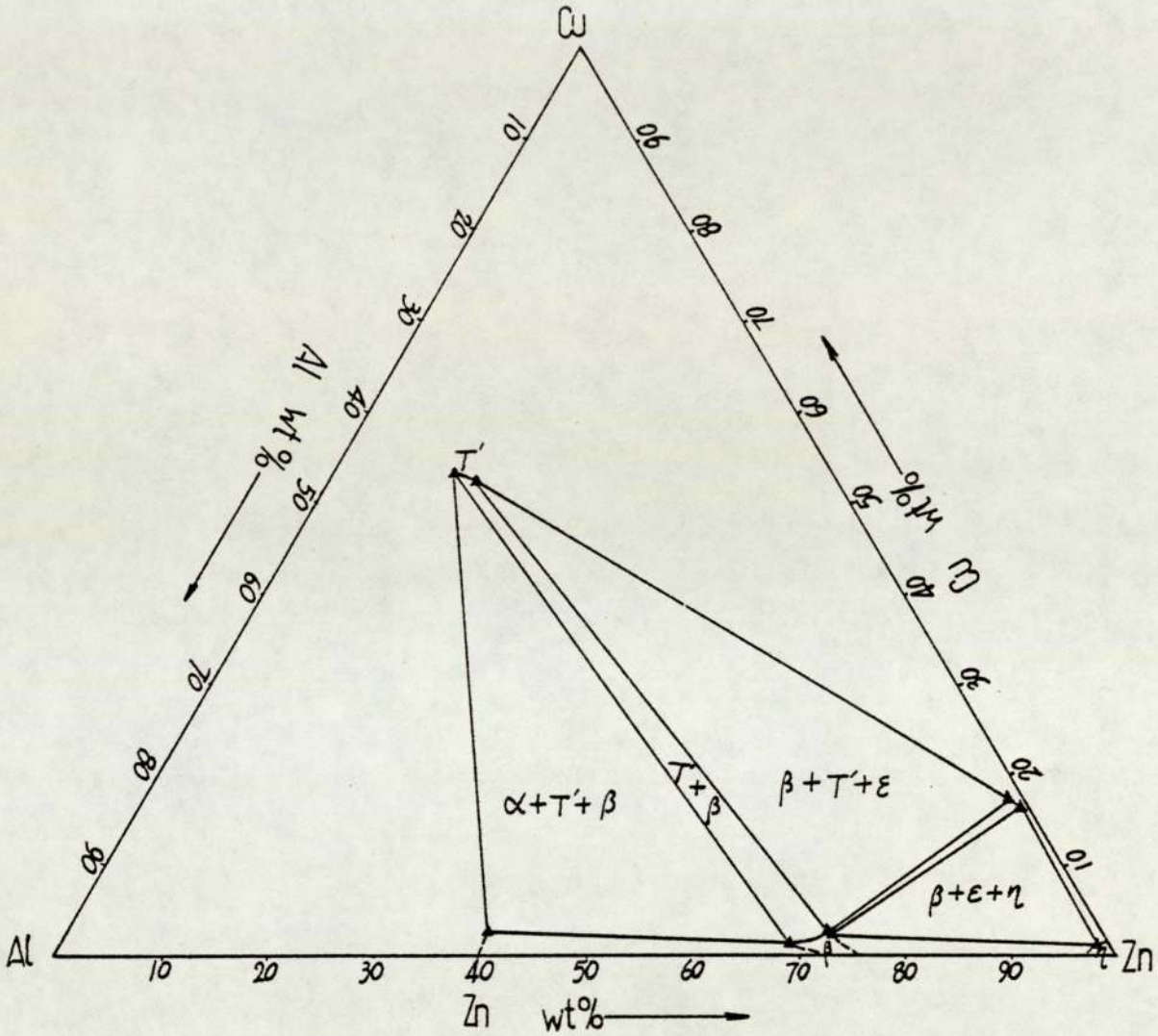

Fig. 52 Isothermal section of Zn-Al-Cu-Si system at 300°C

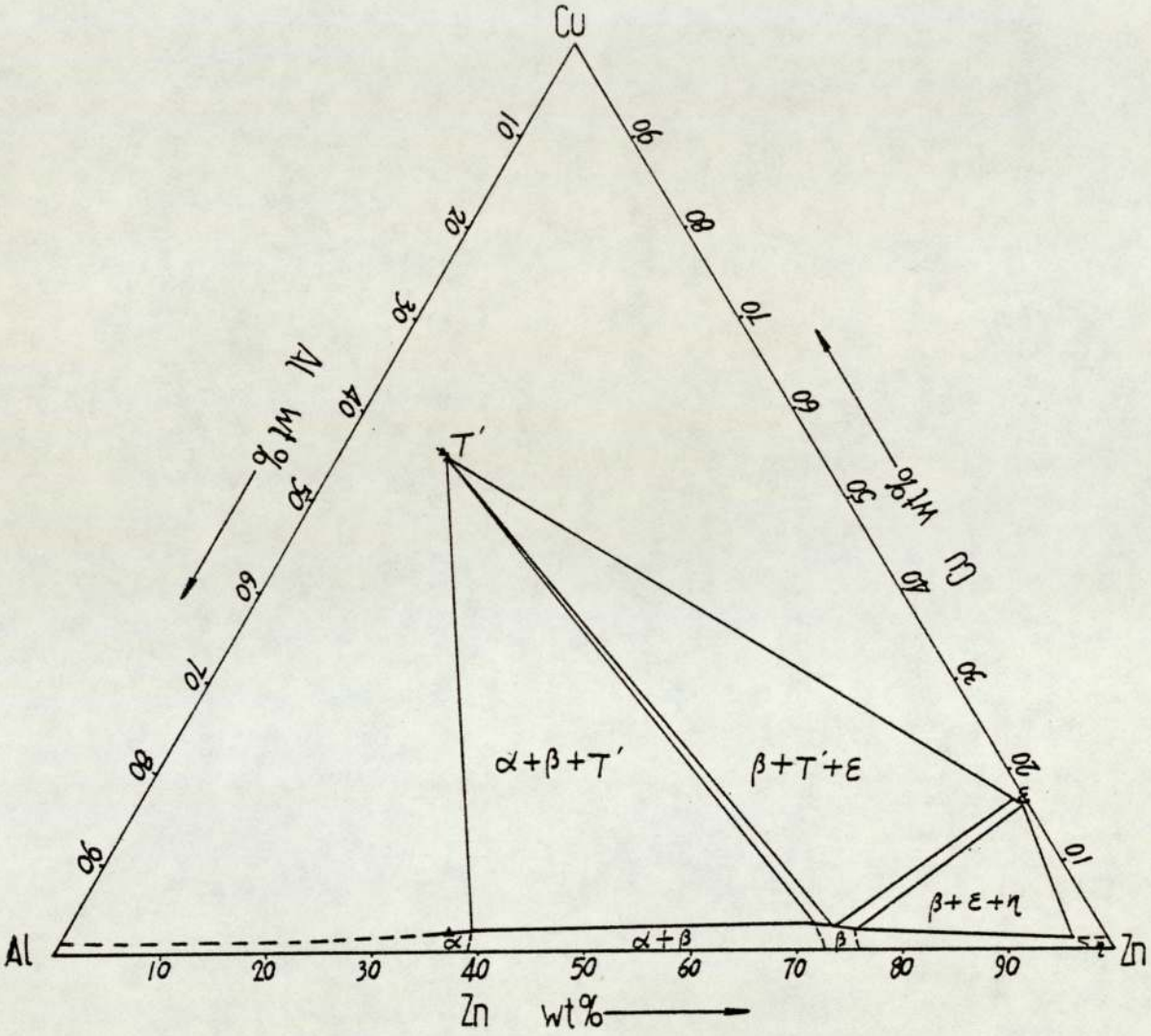

Fig. 53 Isothermal section of Zn-Al-Cu-Si system at 290°C

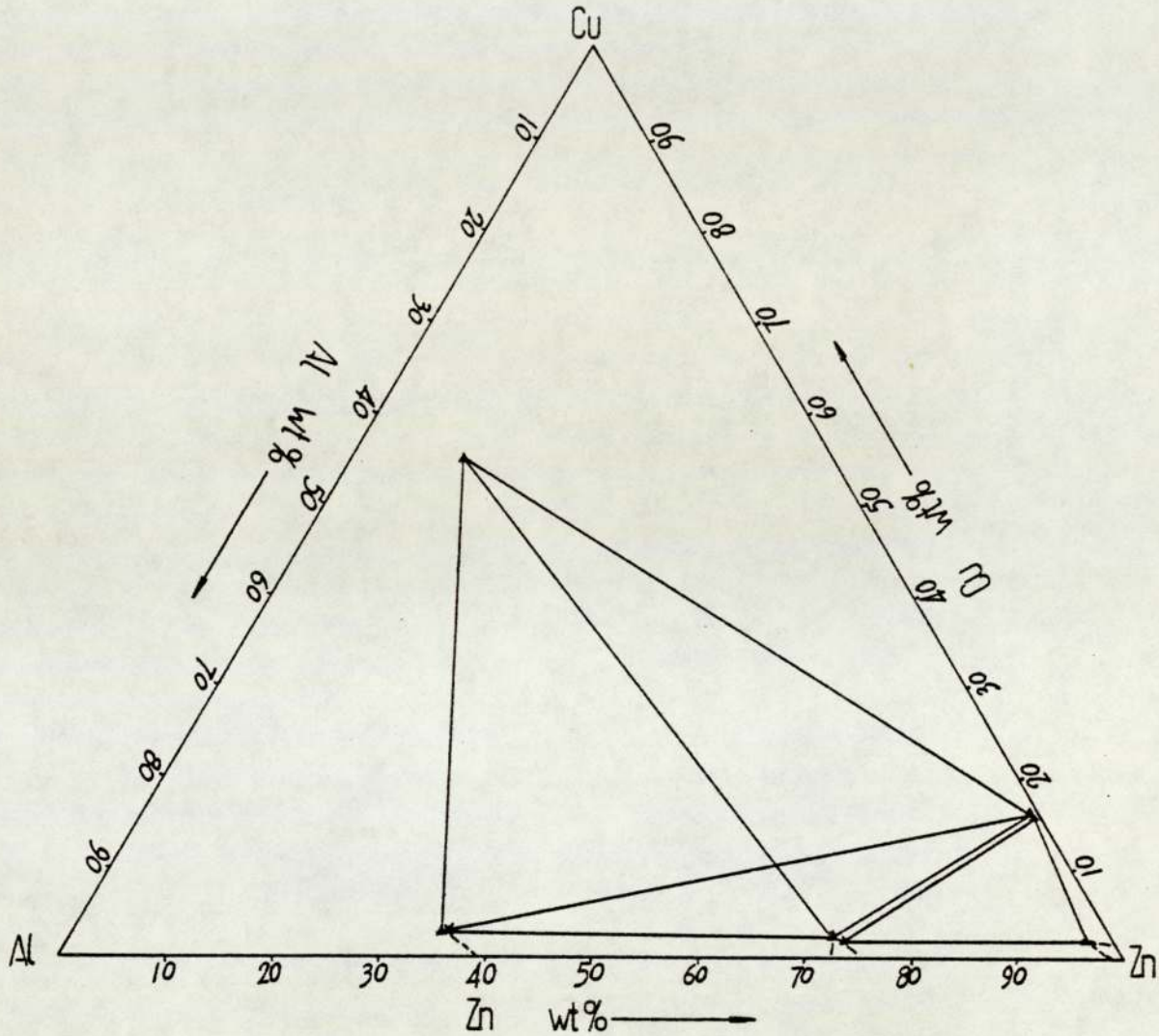

Fig. 54 Isothermal section of Zn-Al-Cu Si system at 285°C

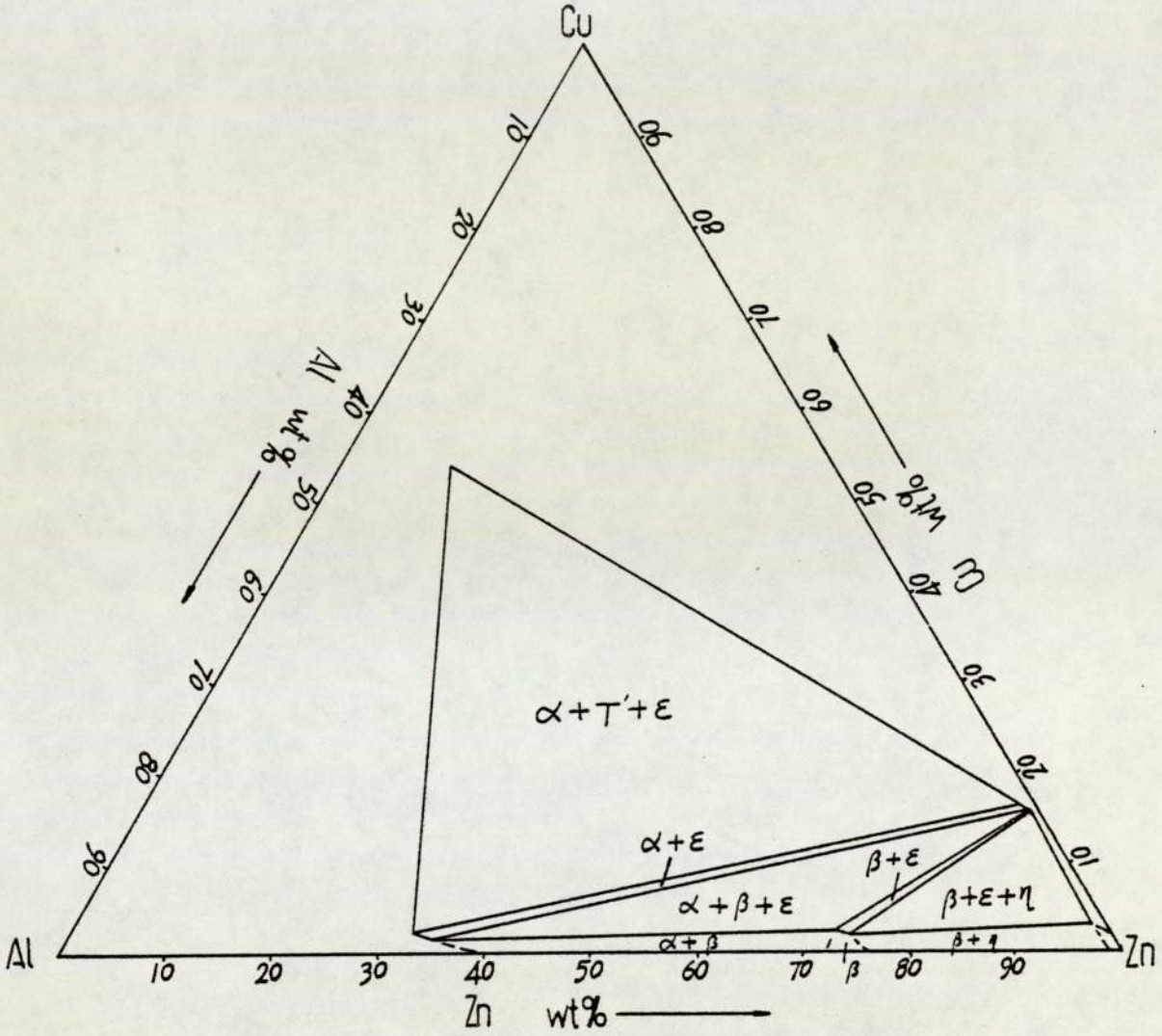

Fig. 55 Isothermal section of Zn-Al-Cu-Si system at 280°C

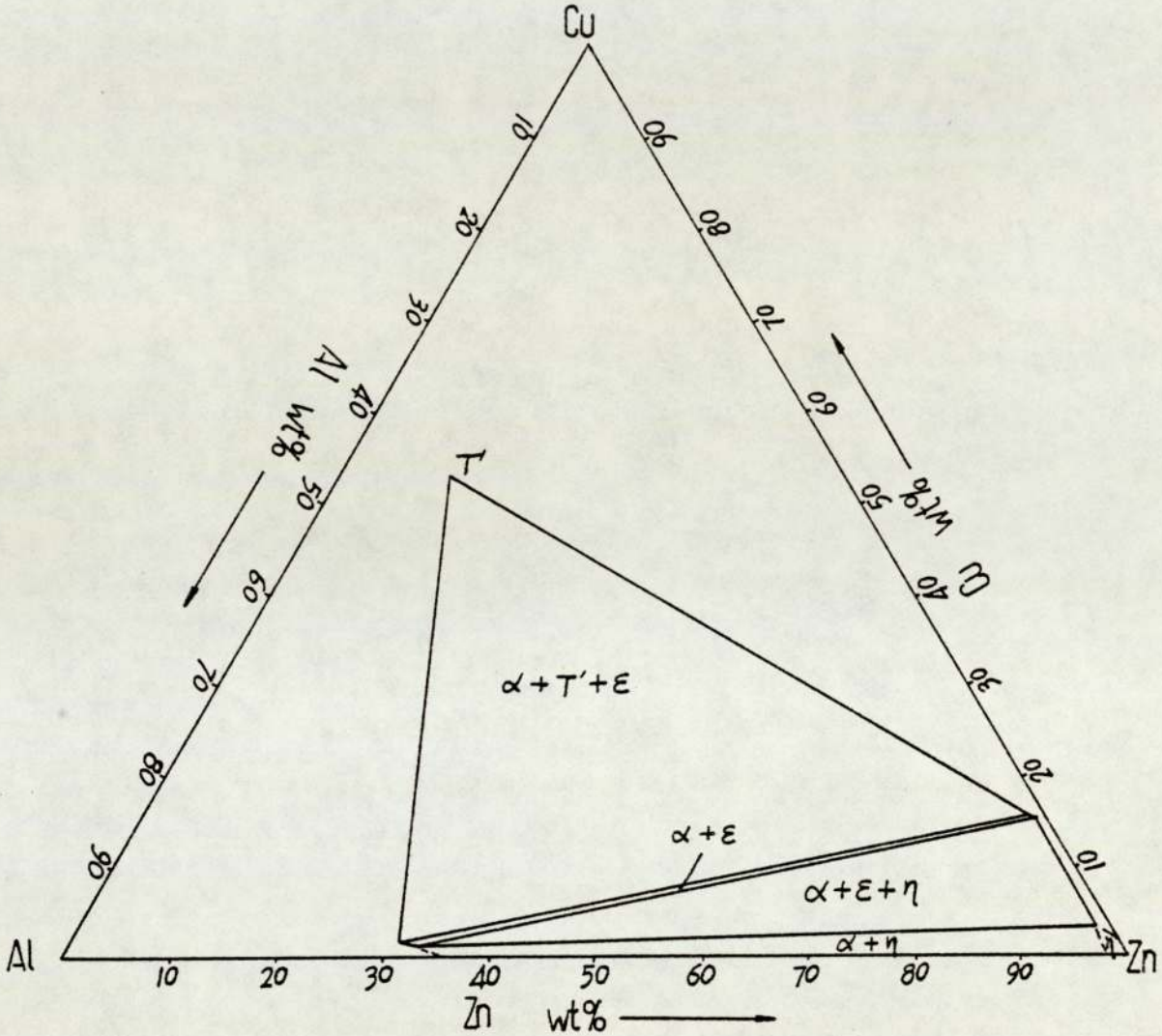

Fig. 56 Isothermal section of Zn-Al-Cu-Si system at 275°C

The copper content in η phase increased as the temperature decreased from 290°C to 275°C, while the zinc content in η phase kept at nearly the same value, about 96%.

4.3 Hardness testing

Although it is recognised that hardness is not a fundamental property, this hardness testing has proved simple and satisfactory to get a general idea about phase transformations during the ageing processes, especially when a large number of specimens has to be examined.

Ageing curves of alloys from the Zn-Al-Si system and Zn-Al-Cu-Si system have been determined from variation in hardness with ageing time over a wide temperature range. Alloy compositions used for ageing as shown in Tables 5 and 6.

Figures 57 - 64 show the hardness versus time curves for several Zn-Al-Si and Zn-Al-Cu-Si alloys aged at room temperature, 50°C, 70°C, 100°C, 150°C and 170°C. In all cases the time scale is plotted logarithmically, in order that the hardness changes occurring at short ageing times can be conveniently shown.

4.3.1 Zn-Al-Si system

Age-hardening occurred in AlZn30Si5 and AlZn60Si5 when ageing in the range from room temperature to 170°C and multi-stage ageing curves were obtained, as shown in Figures 57,58. Well defined hardness peaks were determined with alloy AlZn30Si5 aged at 70°C, 100°C, 150°C and 170°C and with AlZn60Si5 aged at 50°C, 70°C and 100°C. For example, with AlZn30Si5 three hardness peaks were

observed during ageing at 100°C. The first hardness peak came after 9 minutes ageing, the second peak, i.e. the maximum hardness peak, was observed after 250 hours, as shown in Figure 50,58.

However, for alloy A1Zn60Si2, Figure 57, the hardness increments at very short ageing times <1 hour at 50°C, <24 minutes at 70°C, <3minutes at 100°C, <1minute at 150°C and 170°C were quite large. The rapid hardness increase is interpreted as indicating a distinct stage(s) in the particular ageing processes of this alloy. Careful tests carried out at very short times showed that some small hardness peaks occurred before the maximum hardness peak. At 150°C and 170°C, even the maximum hardness peak itself was barely determined.

For alloys A1Zn10Si5, A1Zn75Si2 and A1Zn95Si2, as shown in Figures 59,60, there was no marked hardness change during the ageing processes. The over-aged hardness of alloys A1Zn75Si2 and A1Zn95Si2 were about 60 VPN and 70 VPN respectively, at 50°C, 70°C and 100°C. The ageing curves of alloy A1Zn10Si5 at all the ageing temperatures appeared to flatten out, particularly at the lower temperatures 50°C and 70°C, and there was little change in hardness over periods of dozens of days. An incubation period of 100 hours was found during the ageing at 100°C, 150°C and 170°C.

The marked effect of content of zinc on the extent of hardening in the Zn-Al-Si alloys was clearly demonstrated at various ageing temperatures. For example, after 100 hours at 70°C, the hardness of A1Zn30Si5 had increased

by 70 VPN from a quenched value of 95 VPN, as shown in Figure 58. The corresponding increase in A1Zn60Si5 was only 20 VPN while alloy A1Zn75Si2 and A1Zn95Si2 showed only 15 VPN and 10 VPN increase in hardness from as-quenched conditions respectively, as shown in Figures 57,59.

As expected, it was found that the maximum hardness peaks decreased and were recorded at short times as the ageing temperature increased.

Four peaks were found in the hardness/time curve of alloy A1Zn60Si5 aged at 100°C, Figure 57. The first peak came after 1.5 minutes ageing at 100°C accompanied by a change in the height and position of the supersaturated phase (α'_s) peak following the development of a little peak (α''_m) beside the α'_T phase peak (the shifted α'_s phase peak) on the X-ray diffraction, shown in Figure 69. Here α''_m was forming as a transitional phase.

The maximum hardness peak occurred after 2.5 minutes on ageing at 100°C with growing the peak of α''_m phase and shifting the Al-rich matrix phase (α'_T) peak. The third hardness peak occurred after 12 minutes ageing at 100°C with a further shifting of the α'_T matrix phase peak to α' peak (i.e. shifted α'_T peak). The fourth hardness peak came after 60 hours ageing at 100°C. The α''_m phase was found to be vanishing with further shifting of the matrix phase α' (the shifted α'_T) to the right at the same time.

Table 6

Alloy Compositions used for Ageing Processes of Zn-Al-Cu-Si Systems

Alloy	Composition (wt.%)			
	Zn	Al	Cu	Si
AlZn10Cu3Si2	9.14	84.13	3.82	2.91
AlZn30Cu3Si2	29.44	66.01	3.14	1.41
AlZn60Cu3Si2	61.11	32.96	3.36	2.57
AlZn75Cu3Si2	75.02	19.44	3.14	1.40
AlZn90Cu3Si2	89.53	4.21	4.01	2.25

Table 5

Alloy Compositions used for Ageing Processes of Zn-Al-Si Systems

Alloy	Composition (wt.%)		
	Zn	Al	Si
AlZn10Si5	10.85	83.73	5.42
AlZn30Si5	28.87	67.42	3.71
AlZn60Si5	61.43	33.76	4.81
AlZn75Si2	76.01	21.86	2.13
AlZn95Si2	94.56	3.10	2.34

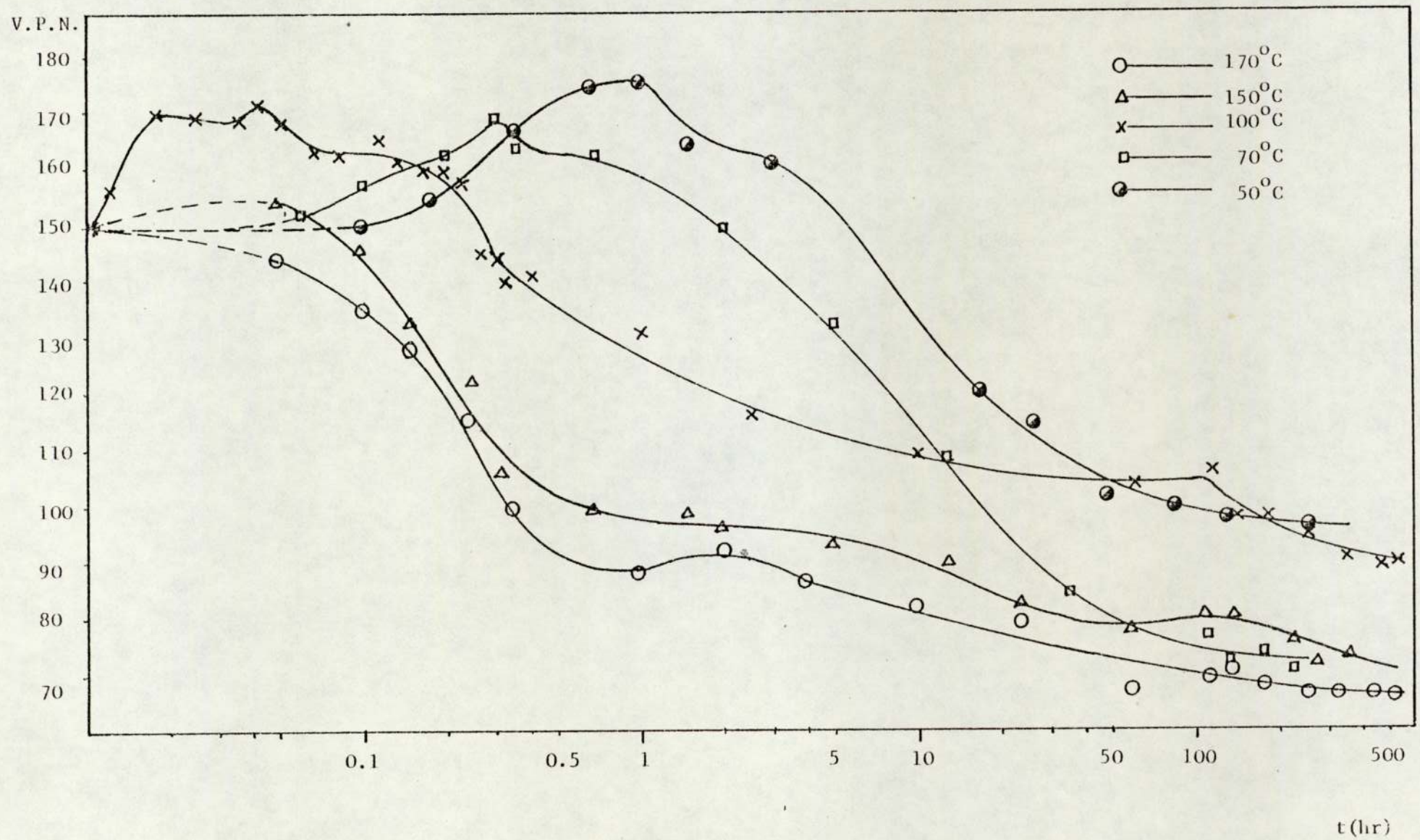

Fig.57 Hardness curves of alloy AlZn60Si5 aged at 50°C, 70°C, 100°C, 150°C, 170°C

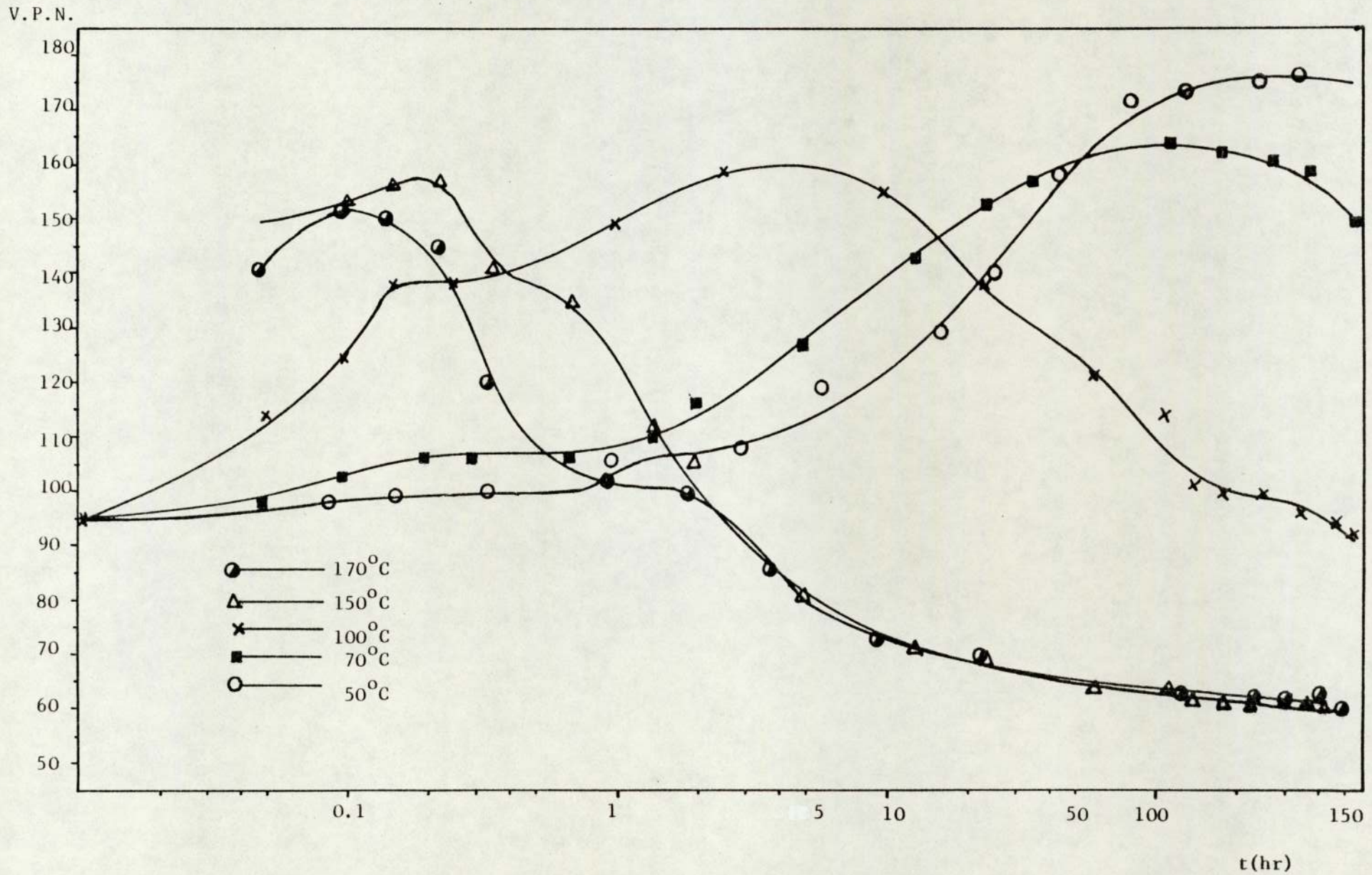

Fig.58 Hardness curves of alloy AlZn30Si5 aged at 50°C, 70°C, 100°C, 150°C, 170°C

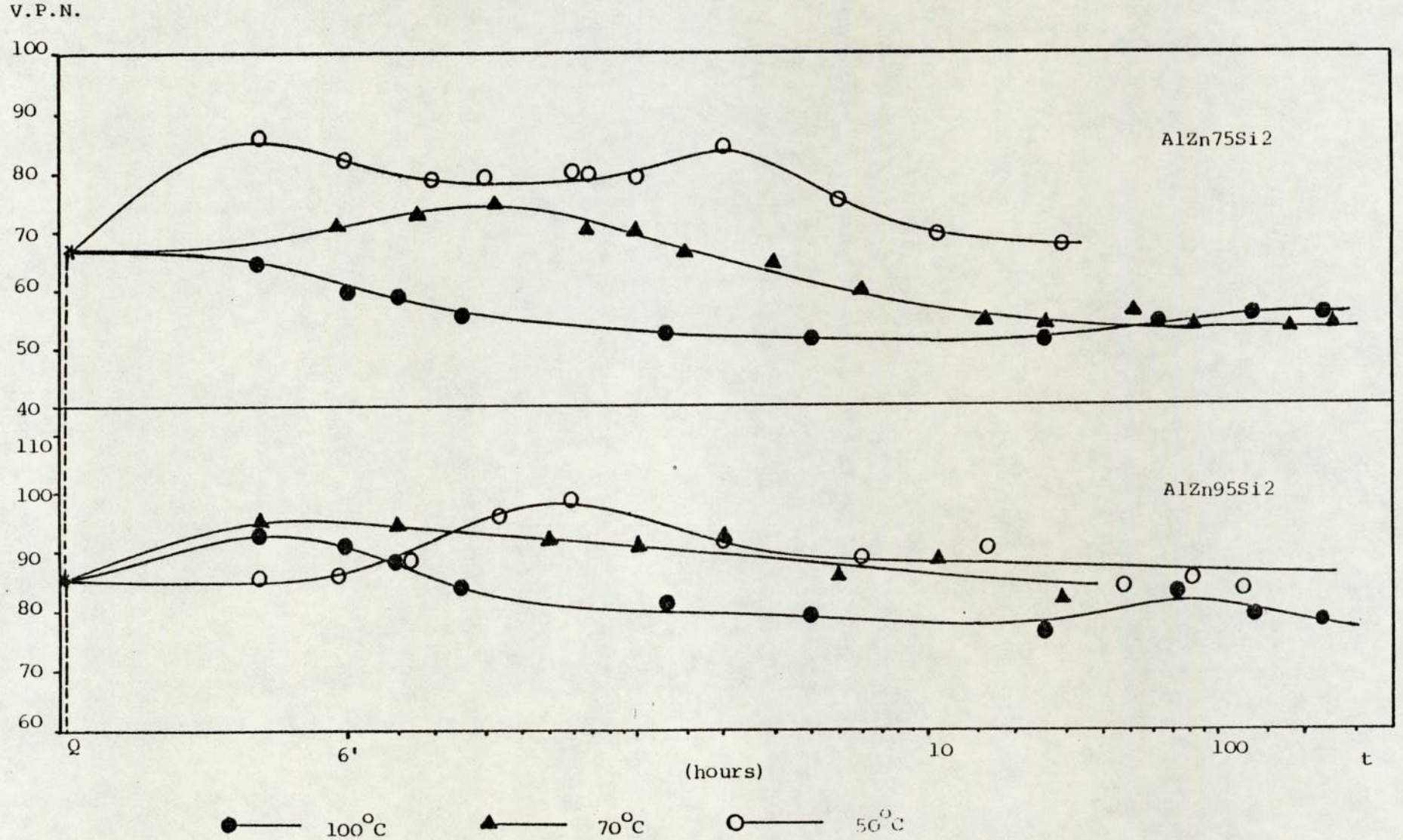

Fig. 59

Hardness curves of alloys AlZn75Si2 and AlZn95Si2 aged at 50°C, 70°C, 100°C

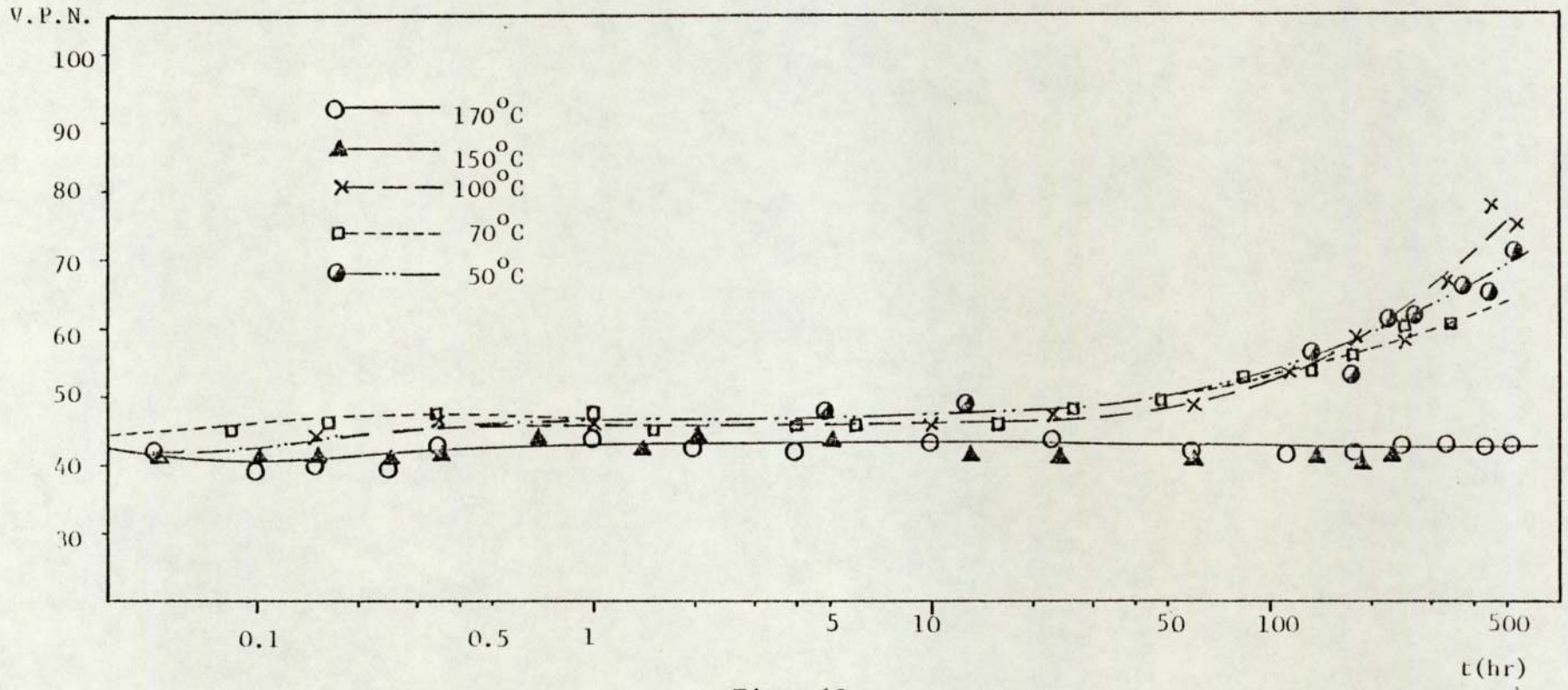

Fig. 60

Hardness curves of alloy AlZn10Si5 aged at 50°C, 70°C, 100°C, 150°C, 170°C.

Table 13

DATA FOR ACTIVATION ENERGY OF HARDENING OF ALLOY A1Zn3OSi5 FROM THE HARDNESS CURVES IN FIGURE

T^oC	T^oK	$(T^oK)^{-1} \times 10^{-3}$	t(s)	ℓnt
50	323	3.09	1260000	14.04
70	343	2.91	360000	12.79
100	373	2.68	14400	9.57
150	423	2.36	720	6.58
170	443	2.26	360	5.89

Table 14

DATA FOR ACTIVATION ENERGY OF HARDENING OF ALLOY A1Zn6OSi5 FROM THE HARDNESS CURVES IN FIGURE

T^oC	T^oK	$(T^oK)^{-1} \times 10^{-3}$	t(s)	ℓnt
50	323	3.09	3600	8.19
70	343	2.91	1080	6.98
100	373	2.68	147.6	5.00

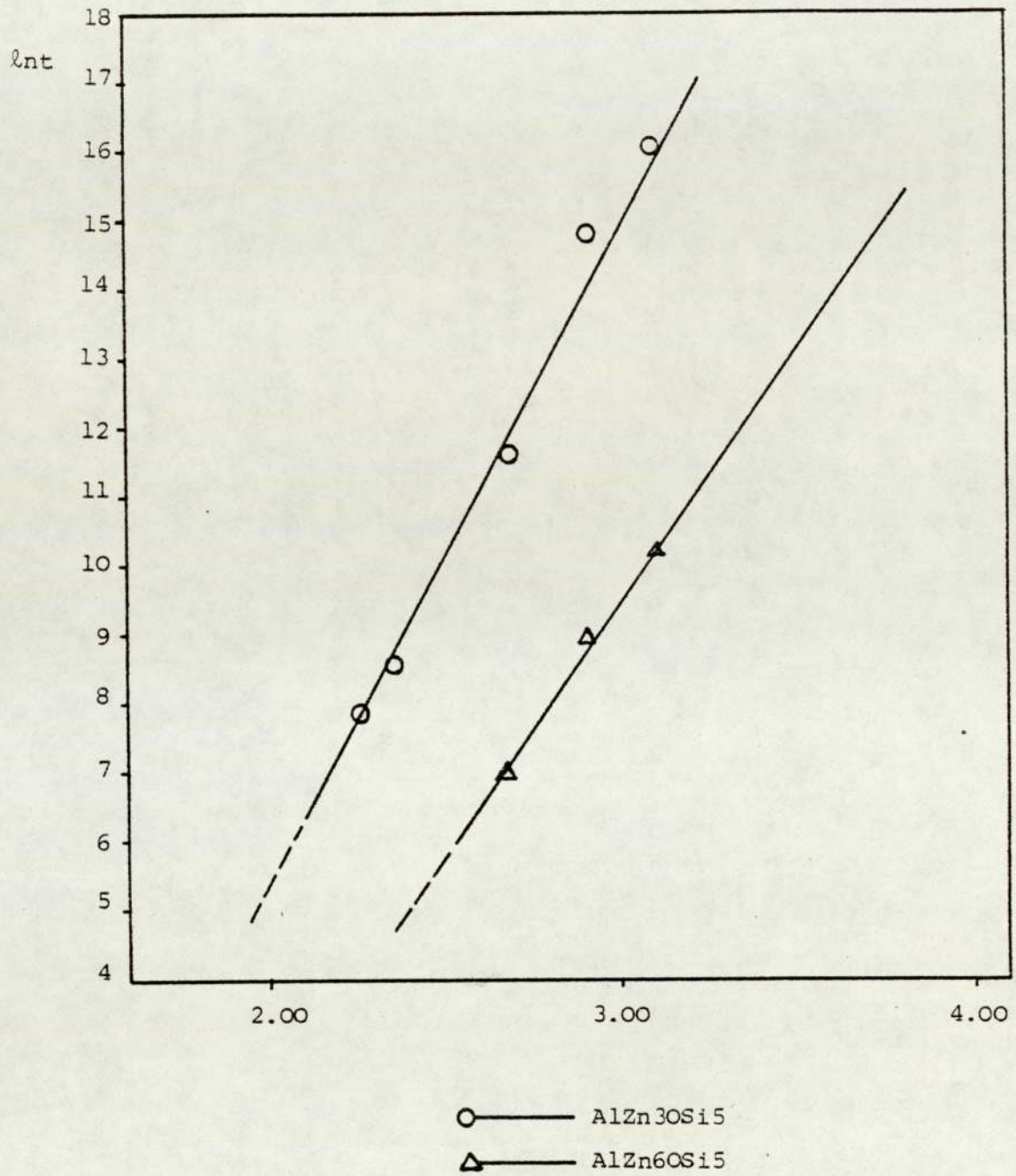

Fig.65

Arrhenius plot for determination of activation energies of hardening for alloy Zn-Al-Si

The Arrhenius plot, (time to maximum peak hardness) versus the reciprocal of absolute temperature of ageing, is shown in Figure 58, using the data in Tables 13 and 14. A good straight-line fit was obtained for AlZn30Si5 and AiZn60Si5 and the calculated activation energies were 79 and 61 KJ/mol, respectively.

4.3.2. Zn-Al-Cu-Si system

The same technique was used for hardness testing as that used for ternary Zn-Al-Si system.

Distinct age-hardening was observed not only in alloy AlZn30Cu3Si2 and AlZn60Cu3Si2, but also in AlZn75Cu3Si2 when aged in the range from room temperature to 170°C. Well determined multi-stage ageing curves were obtained with alloy AlZn30Cu3Si2 aged at 100°C, 150°C and 170°C, and with alloys AlZn60Cu3Si2 and AlZn75Cu3Si2 aged at 50°C, 70°C, 100°C 150°C and 170°C in the present work, as shown in Figures 61-64.

Five hardness peaks were found in the whole process of ageing at 100°C of alloy AlZn60Cu3Si2, and are shown in Figure 61. The first peak was observed after about 5 minutes. Ten minutes later another increment in hardness occurred. The hardness increased to the maximum after 1 hour ageing at 100°C. Two small hardness peaks were detected on prolonged ageing. One was after 2 hours ageing, which was close to the maximum hardness peak, the other was at a well over-aged stage after 150 hours at 100°C.

In order to check that the peaks were real, for the 100°C points the standard deviations were calculated using the following formula :

$$\sigma_{n-1} = \sqrt{\frac{\Sigma x^2 - \frac{(\Sigma x)^2}{n}}{n - 1}}$$

where Σx^2 - the sum of each hardness measurement squared for one ageing time,

$(\Sigma x)^2$ - the square of the sum of all the hardness measurements for one ageing time,

n - the number of measurements at the ageing time.

The error bars for the points were drawn on the 100°C ageing curve in Figure 61, and it is plain that the peaks are indeed real. Further confirmation was provided by the fact that the peaks were reproduced in repeated experiments and in curves for different temperatures.

The three lower temperature ageing treatments at room temperature, 50°C and 70°C show the first three hardness peaks too. The fourth hardness peak was also observed after 250 hours, 40 hours, 30 minutes and 18 minutes aged at 50°C, 70°C, 150°C and 170°C respectively. The fifth peak came earlier at higher temperatures 150°C and 170°C.

More complicated hardness/time curves occurred during the ageing processes of the higher aluminium alloy A1Zn30Cu3Si2, as shown in Figure 62. There were two peaks occurring both before and after maximum hardness peak during the 100°C ageing process. The first hardness peak occurred after 18 minutes ageing, and was followed by a sudden hardness change 4 minutes later, i.e. the second hardness peak observed. The maximum hardness peak developed strongly after 45 hours ageing at 100°C. After 10 hours the rate of decreasing hardness of the alloy slightly slowed down, and suddenly became faster after 80 hours.

The hardness curves for 150°C and 170°C ageing show 2 peaks after the maximum hardness peak, such as occurred during 100°C ageing, but none before.

The as-quenched zinc-rich alloy A1Zn75Cu3Si2 was quickly overaged at various temperatures, as shown in Figures 63 and 64. Maximum peak hardnesses of about 170 VPN occurred on 50°C, 70°C and 100°C ageing. The last small hardness peaks occurred during 150°C and 170°C ageing. By using the data listed in Table 15 the Arrhenius plots were constructed and are shown in Figure 66. The activation energy of the formation of the last small hardness peak (which corresponds to the fifth hardness peak in alloy A1Zn60Cu3Si2) was calculated as 33.7 KJ/mol using the same method as used for the Al-Zn-Si alloys.

Both alloys A1Zn30Cu3Si2 and A1Zn60Cu3Si2 show a great extension of hardening at various temperatures. The effect of zinc content change on the hardening in the quaternary system Zn-Al-Cu-Si was found to be not as marked as that in the ternary system Zn-Al-Si. Aged at 100°C, about 50 VPN increase in hardness from the as-quenched state was measured at the maximum peak in alloy A1Zn30Cu3Si2, while the corresponding hardness increase in alloy A1Zn60Cu3Si2 was 45 VPN. That means that the addition of small quantities of copper to Zn-Al-Si alloys counteracts the decrease in the response to age-hardening of the higher zinc alloys.

The maximum peak hardnesses of A1Zn30Cu3Si2 and A1Zn60Cu3Si2 at various temperatures are listed in Table 16 and 17. The activation energy of hardening of alloys Zn-Al-Cu-Si were calculated as 69 KJ/mol for alloy A1Zn30Cu3Si2, and 51 KJ/mol for alloy A1Zn60Cu3Si2, using the same method as that for alloy Zn-Al-Si. The Arrhenius plot is shown in Figure 67.

The pronounced response to age-hardening on adding small quantities of copper to the ternary Zn-Al-Si alloys was evident, the maximum hardness peak increased about 50 VPN. For example, the maximum peak hardness increased from 170 VPN for alloy A1Zn60Si5 to 220 VPN for alloy A1Zn60Cu3Si2, both aged at 100°C.

A great change in maximum peak hardness with zinc content was found. For example, the maximum peak hardness of alloy A1Zn30Cu3Si2 was 160 VPN while that of alloy A1Zn60Cu3Si2 was 220 VPN.

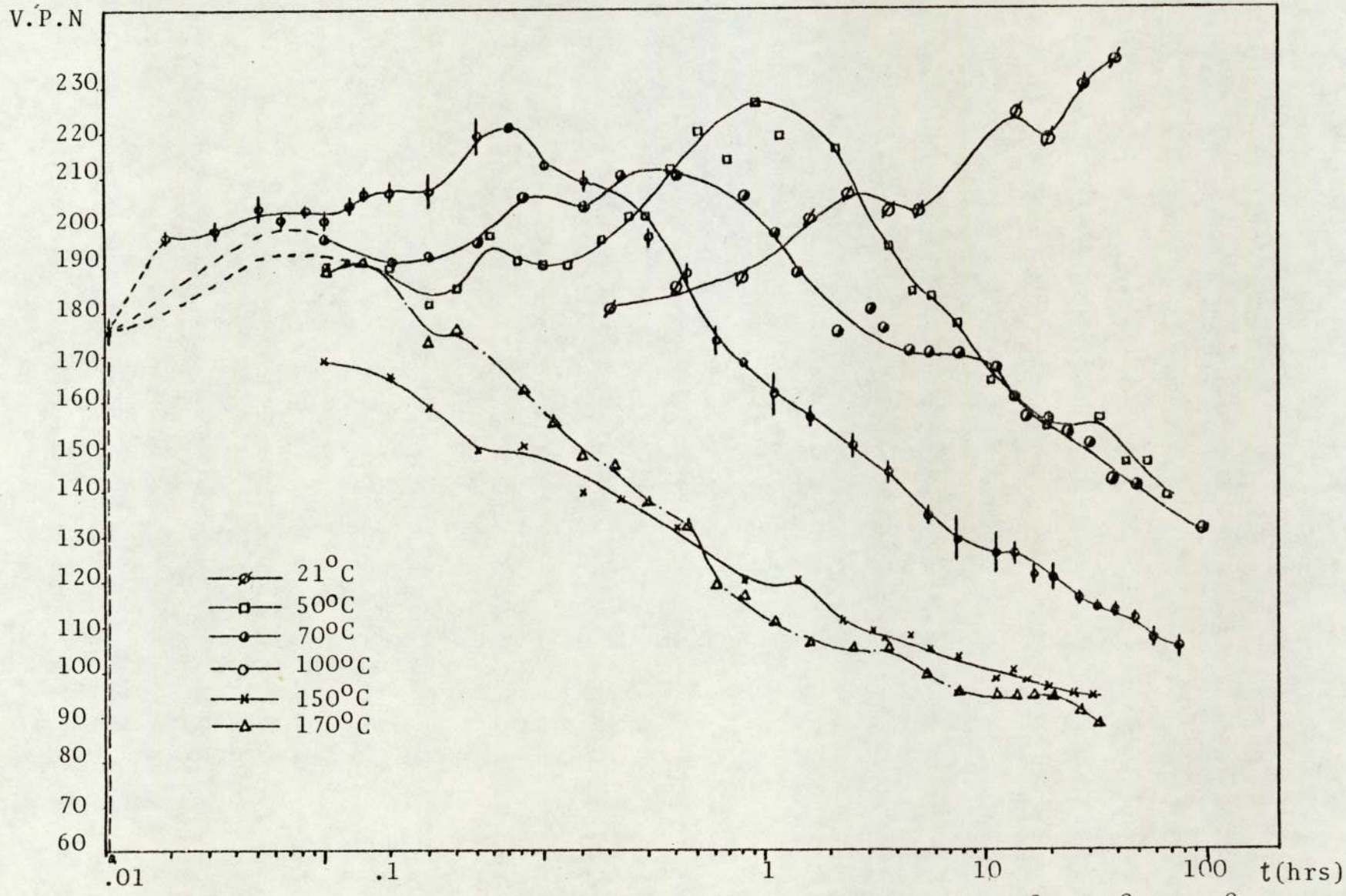

Fig. 61 Hardness curves of alloy AlZn6OCu3Si2 aged at 50°C, 70°C, 100°C, 150°C 170°C

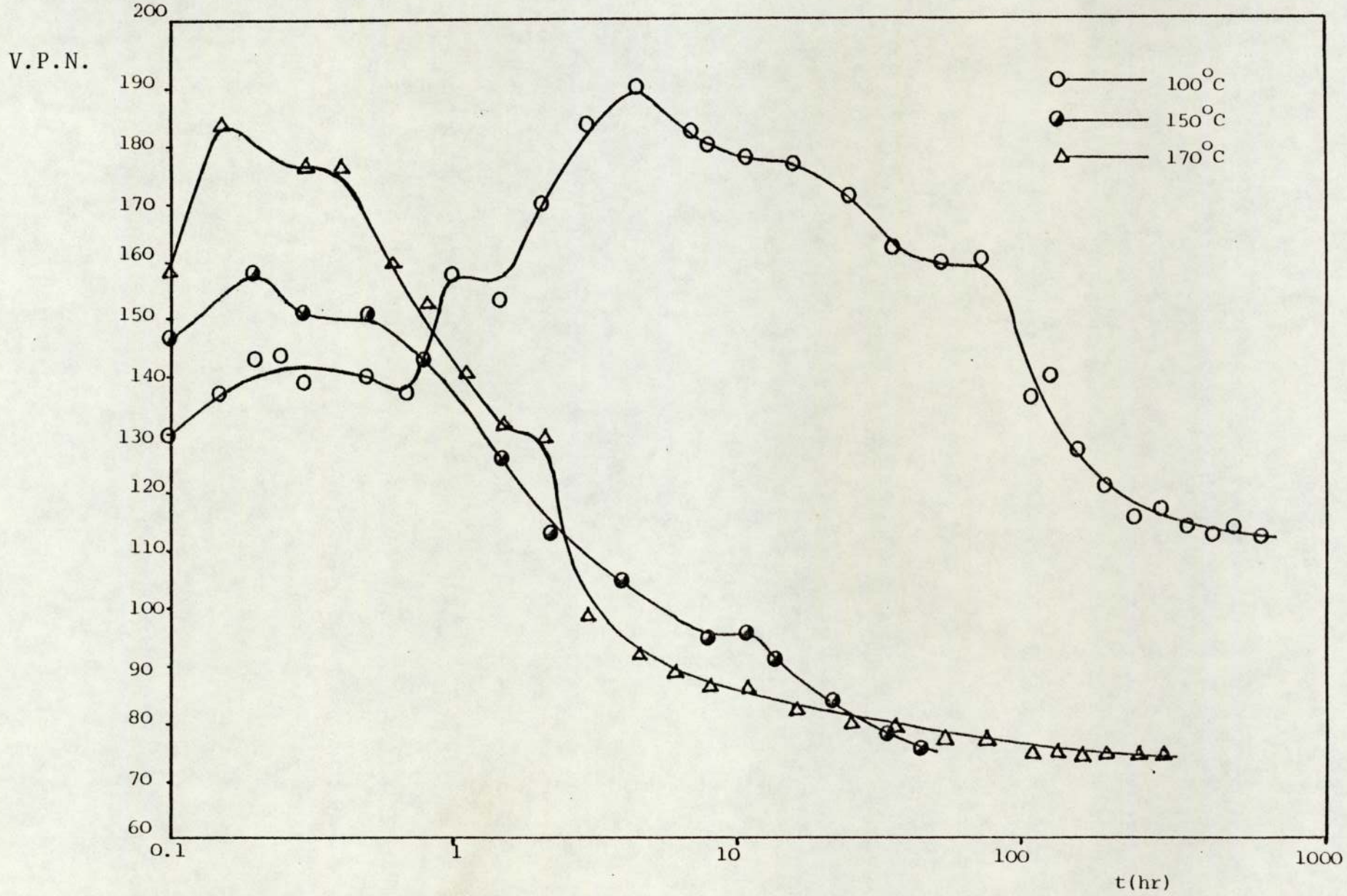

Fig.62 Hardness curves of alloy AlZn30Cu3Si2 aged at 100°C,150°C,170°C

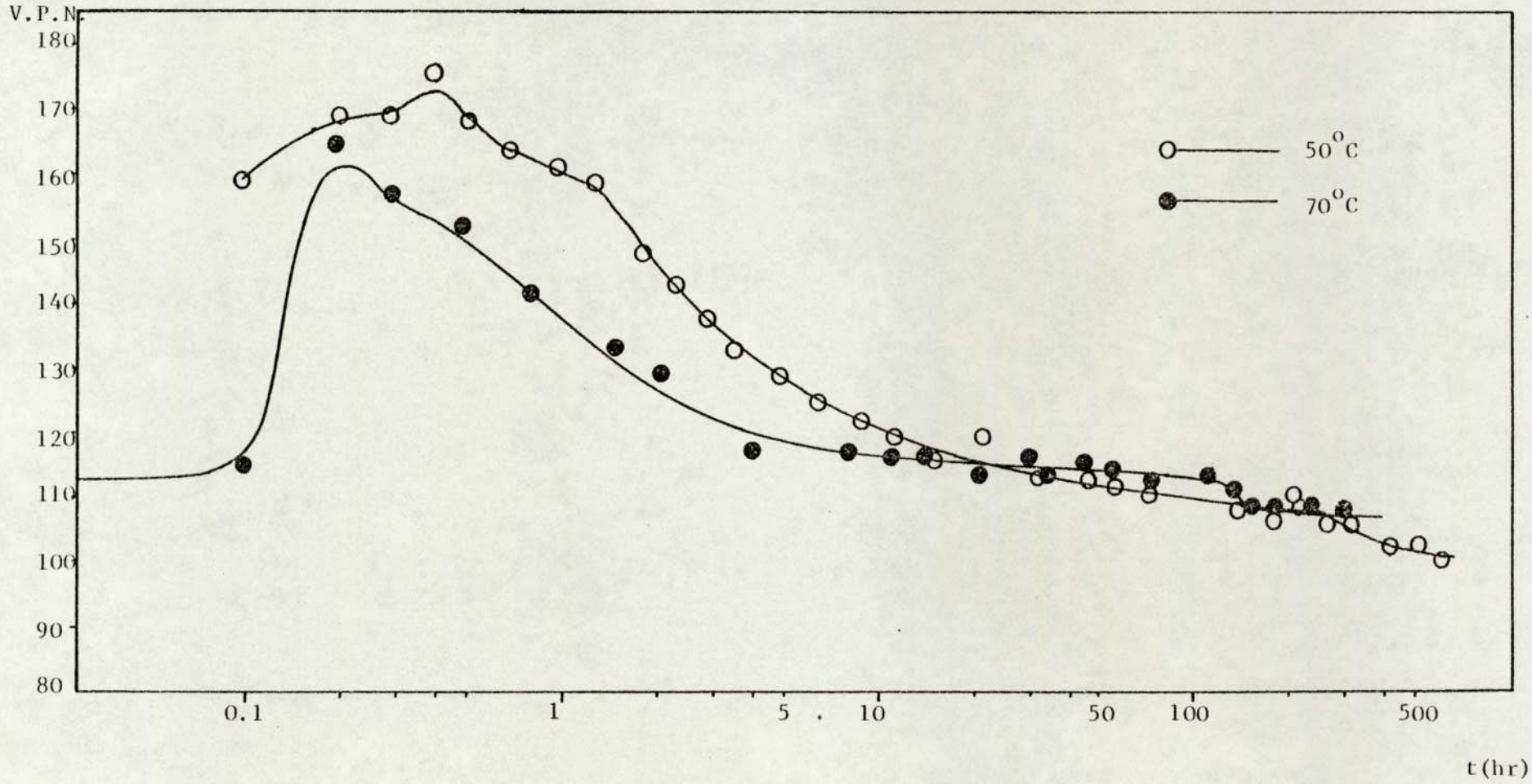

Fig.63 Hardness curves of alloy AlZn75Cu3Si2 aged at 70°C and 50°C

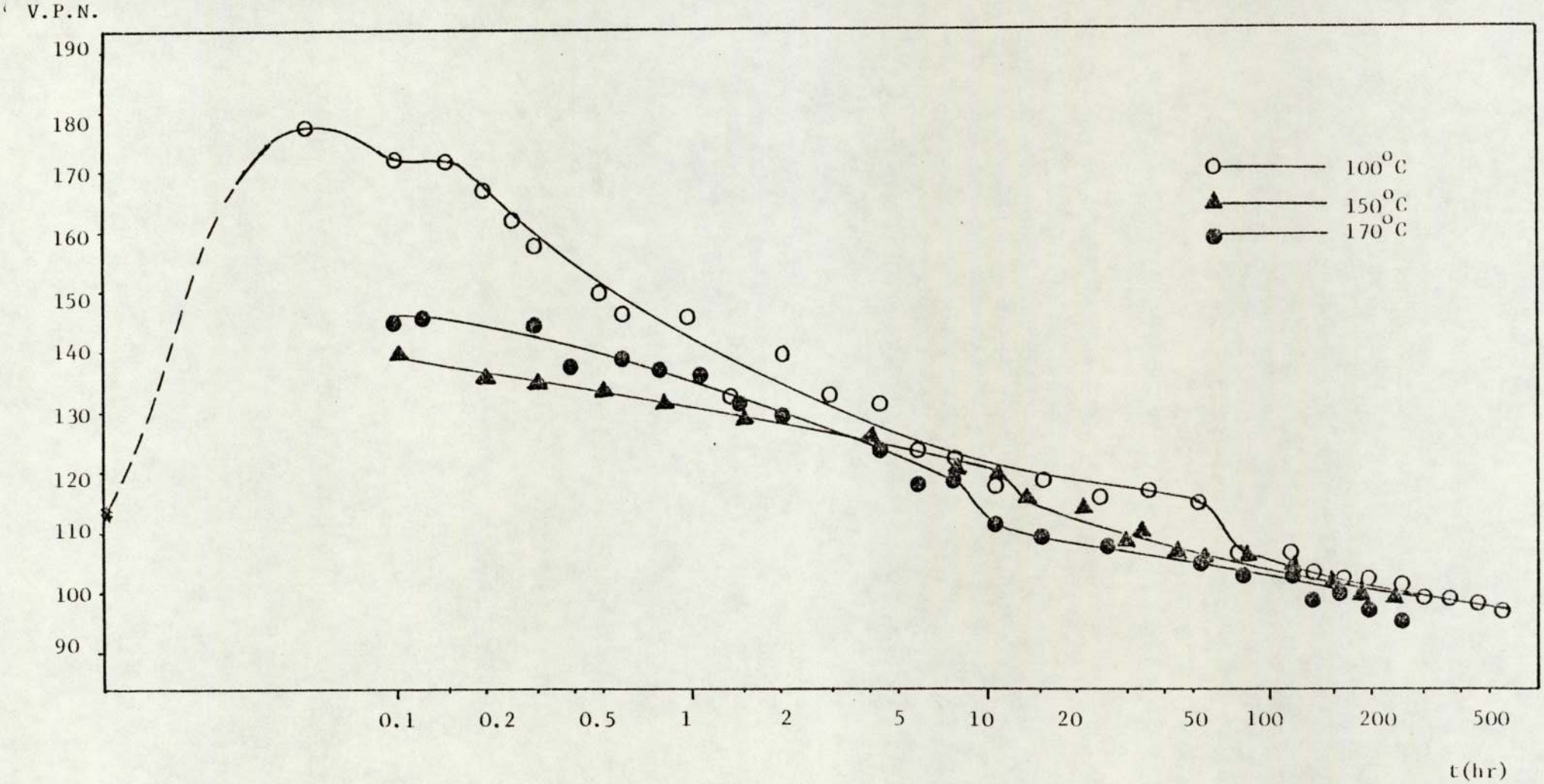

Fig 64 Hardness curves of alloy AlZn75Cu3Si2 aged at 100°C, 150°C, 170°C

Table 15

DATA FOR ACTIVATION ENERGY FOR FOUR-PHASE TRANSFORMATION $\alpha_f + \varepsilon \rightarrow T' + \eta$ OF ALLOY AlZn75Cu3Si2 DEDUCED FROM HARDNESS TESTING

T^oC	T^oK	$(T^oK)^{-1} \times 10^{-3}$	t(s)	ℓnt
50	323	3.09	736747	13.51
70	343	2.91	396329	12.89
100	373	2.68	144350	11.88
150	423	2.36	39735	10.59
170	443	2.26	28853	10.27

Table 36

DATA FOR ACTIVATION ENERGY FOR FOUR-PHASE TRANSFORMATION $\alpha_f + \varepsilon \rightarrow T' + \eta$ OF ALLOY AlZn75Cu3Si2 DETERMINED ON X-RAY DIFFRACTION EXAMINATION

T^oC	T^oK	$(T^oK)^{-1} \times 10^{-3}$	t(s)	ℓnt
100^oC	373	2.68	162754	12.0
150^oC	423	2.36	38177	10.55
170^oC	443	2.26	24343	10.10

Table 16

DATA FOR ACTIVATION ENERGY OF HARDENING OF ALLOY A1Zn60Cu3Si2 FROM THE HARDNESS CURVE IN FIGURE

T^oC	T^oK	$(T^oK)^{-1} \times 10^{-3}$	t(s)	ℓnt
50	323	3.09	32400	10.38
70	343	2.91	10800	9.28
100	373	2.68	2420	7.83

Table 17

DATA FOR ACTIVATION ENERGY OF HARDENING OF ALLOY A1Zn30Cu3Si2 FROM THE HARDNESS CURVE IN FIGURE

T^oC	T^oK	$(T^oK)^{-1} \times 10^{-3}$	t(s)	ℓnt
100	373	2.68	16200	9.69
150	423	2.36	720	6.58
170	447	2.26	540	6.29

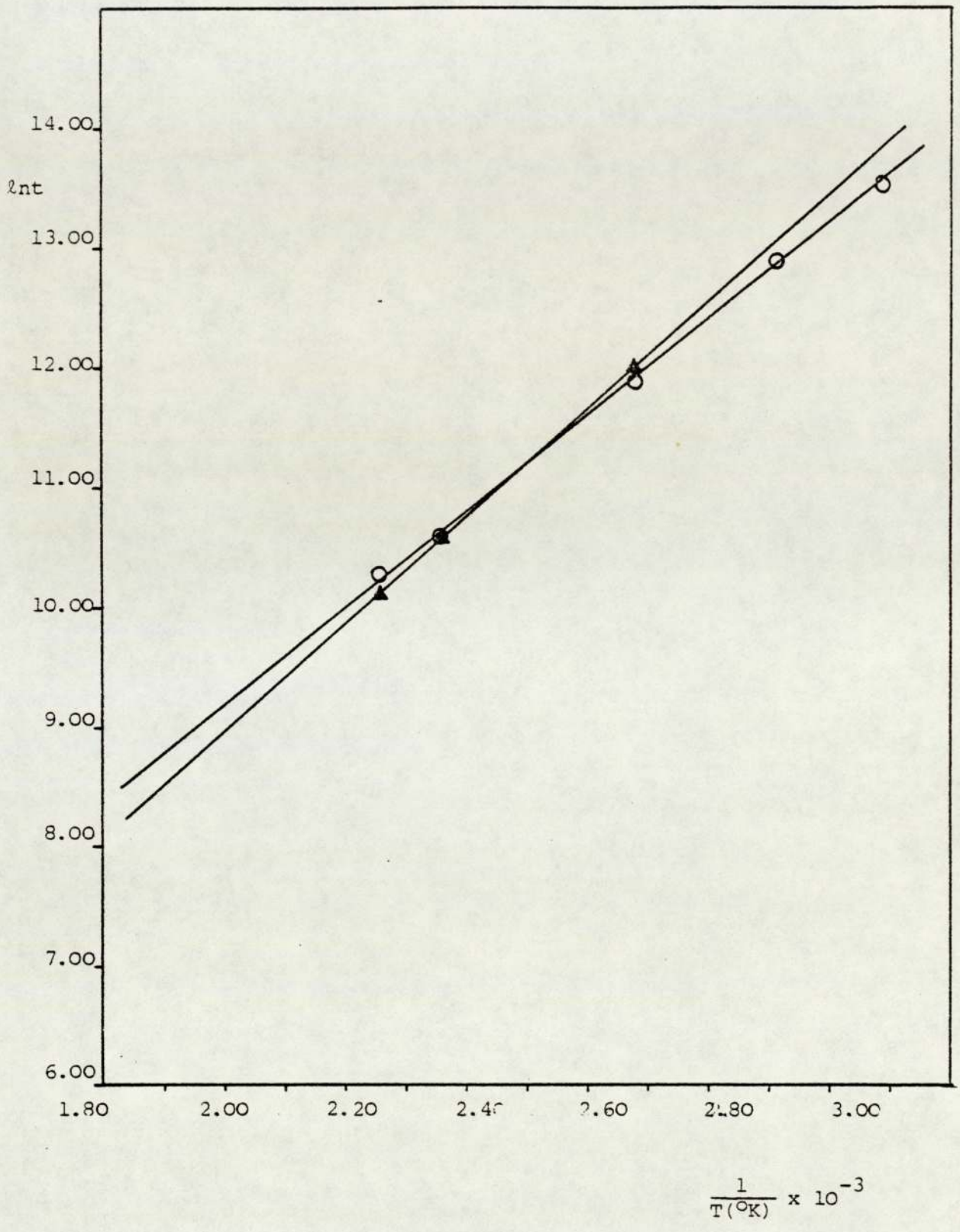

Fig.66

Activation energy plot of $\alpha_f + \varepsilon \rightarrow T' + \eta$ in alloy AlZn75Cu3Si2

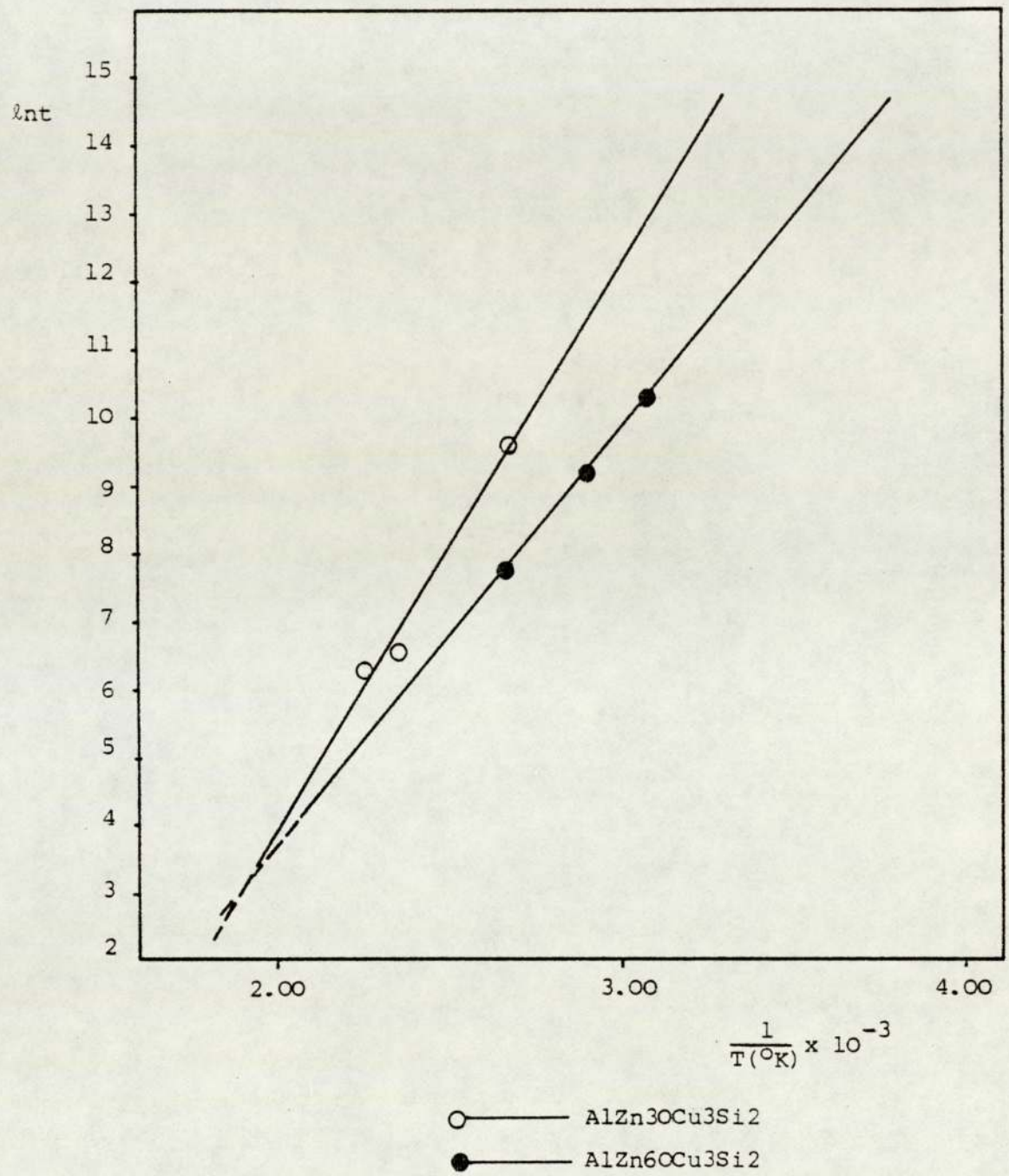

Fig.67

Arrhenius plot for determination of activation energies of hardening for alloys

Zn-Al-Cu-Si

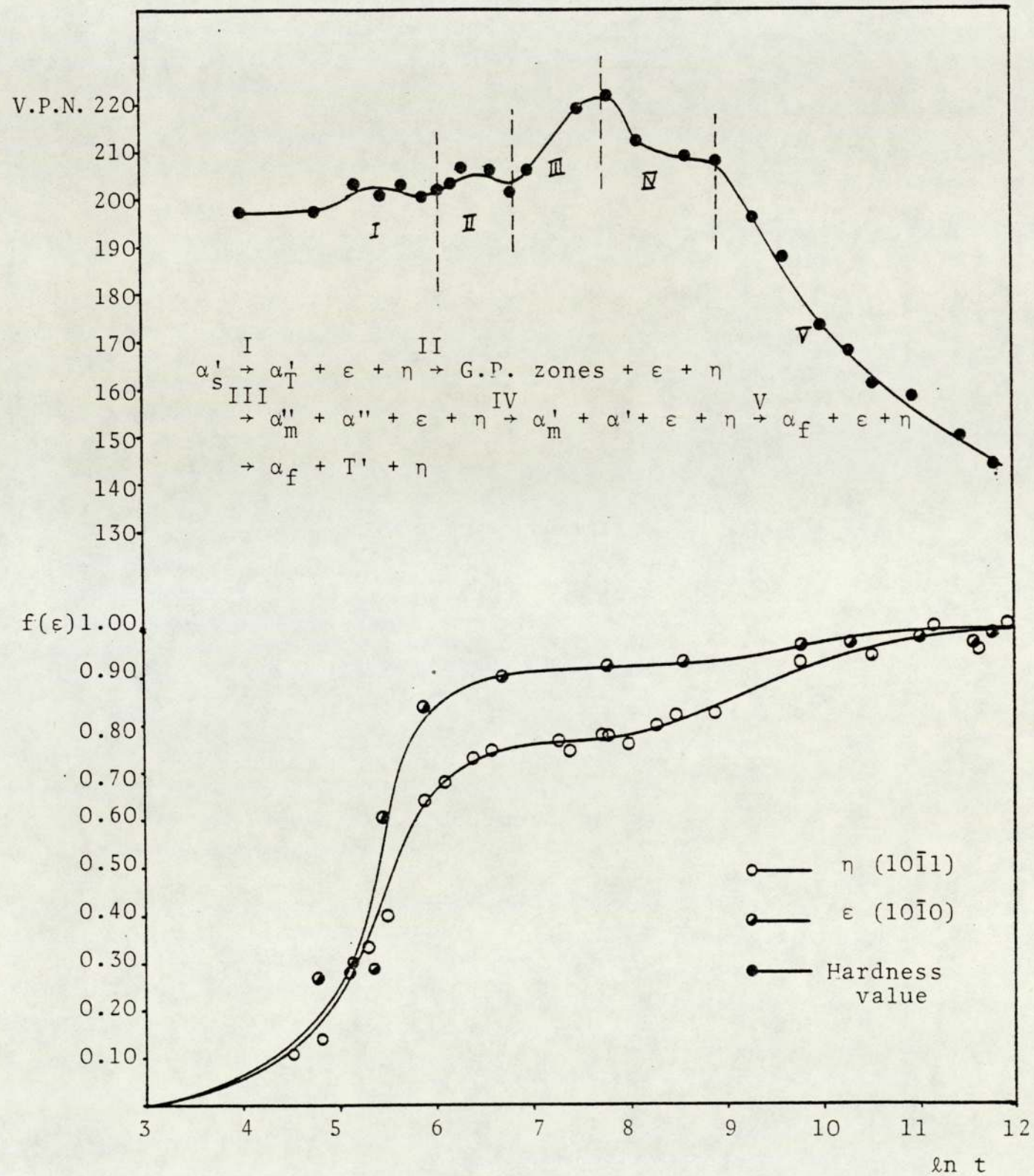

Fig. 68 Response of hardness to phase transformation deduced from X-ray diffraction for alloy A1Zn60Cu3Si2 aged at 100°C

Table 18

HARDNESS DATA

Alloy	Hardness V.P.N.			
	As Cast	After Quench	Top Peak H.V. aged at 100°C	Over Aged at 100°C
A1Zn10Si5	61.6	45.3	75*	-
A1Zn30Si5	139.3	95.4	160	85
A1Zn60Si5	119.1	149.7	171	90
A1Zn75Si2	105.8	65.6	65	50
A1Zn95Si2	85.8	86.4	93	78
A1Zn10Cu3Si2	69.1	65.8	-	60
A1Zn30Cu3Si2	142.7	137	190	110
A1Zn60Cu3Si2	150.7	176	220	110
A1Zn75Cu3Si2	145.7	113.6	-	91
A1Zn90Cu3Si2	129	113.6	-	100

* on the way to increase to top peak hardness

For both A1Zn10Cu3Si2 and A1Zn90Cu3Si2, no marked age-hardening was observed during ageing processes, and the over-aged hardnesses were about 60 VPN and 100 VPN respectively.

In both the Zn-Al-Si, and Zn-Al-Cu-Si systems, it was found that the positions of peak hardness moved to shorter times with increase in zinc in the higher-aluminium alloys, i.e. alloys A1Zn10Cu3Si2, A1Zn10Si5, A1Zn30Cu3Si2, A1Zn30Si5, A1Zn60Cu3Si2, A1Zn60Si5. The maximum hardness was decreased and shifted to shorter times by increasing the temperature of ageing.

For both alloy systems, the as-quenched hardness, maximum hardness on 100°C ageing and overaged hardness at 100°C were tabulated and are shown in Table 18.

4.4 X-ray diffraction examination

The X-ray diffraction examination was based on the hardness results obtained during the ageing process.

The various phases involved in the phase transformations, and their characteristic Bragg angles (2θ) measured at room temperature, using Cuk$_\alpha$ X-rays, are listed in Table 19.

It is possible to find the effect of zinc content and small additions of copper on the lattice parameters of the Al-rich phase, by comparing the 2θ value in Table 19.

Table 19

THE CHARACTERISTIC BRAGG ANGLES (2θ) FOR IDENTIFICATION OF PHASE TRANSFORMATIONS

Phases / 2θ° / Alloy	η (10$\bar{1}$1)	β (or α_s') (200)	α_T' (200)	α' (200)	α_m''	α_f (200)	T' (110)	ε (0002)
AlZn75Cu3Si2	43.3	45.5	45.2	45.1	45.4	44.9	44.4	42.2
AlZn60Cu3Si2	43.3	45.2	44.9	44.8	45.5	44.9	44.4	42.1
AlZn30Cu3Si2	43.3	45.0	45.0	44.8	45.6	44.8	44.4	42.1
AlZn60Si5	43.2	45.1	44.9	44.8	45.3	44.8	-	-
AlZn30 Si5	45.2	44.8	44.8	44.6	45.3	44.7	-	-

η ——— Zn-rich phase

β (or α_s')— Supersaturated phase

α_T' ——— Al-rich eutectoid terminal alloy derived from β or α' going to spinodal decomposition

α' ——— Al-rich matrix phase in equilibrium with the second transition phase

α_m'' —— the first transition phase

T' —— Cu-rich phase

ε —— Zn-rich metastable phase CuZn4

α_f —— Al-rich final stable phase

For comparison, two lists of 2θ values are derived from Table 19 :

	Al$_{Zn30}$Si$_5$	Al$_{Zn60}$Si$_5$	Al$_{Zn30}$Cu$_3$Si$_2$	Al$_{Zn60}$Cu$_3$Si$_2$	Al$_{Zn75}$Cu$_3$Si$_2$
α'_s or β	44.8	45.1	45.0	45.2	45.5
α_f	44.7	44.9	44.8	44.9	44.9

	Al$_{65}$Zn$_{30}$	Al$_{Zn60}$
Cu 3%	45.0	45.2
Cu 0%	44.8	45.1

From Braggs law, the diffraction condition is :

$$\frac{n\lambda}{2d} = \text{Sin } \theta$$

Thus an increase in 2 θ is due to a reduction in d-spacing. For f.c.c. structures the formula for interplanar spacing, (d), is :

$$d = \frac{a}{\sqrt{h^2+k^2+\ell^2}}$$

where a is the lattice parameter and h,k,ℓ are the Miller indices of the plane. Decrease in d-spacing indicates a decrease of a. So from the data listed above, it is clear that both Zn and Cu control the lattice parameter of the Al-rich phase. For the same reason, 2 θ values

of the Zn-rich transition phases α''_m and α'_m were always found to be bigger than that of α'_T , α' and α'' phases, and smaller than that of phases which contained more zinc.

During the ageing process, zinc atoms were progressively removed from the Al-rich phases, so it is found that the changes in 2 Θ are as follows :

$$2\,\Theta(\beta) > 2\,\Theta(\alpha'_T) > 2\,\Theta(\alpha_f)$$

Based on the 2 Θ changes during the ageing processes, the structural changes were determined. Different ways of changing of the diffraction peaks implied different modes of phase transformations. Two modes of precipitation were found in the decomposition of the supersaturated phases β and α'_s. Because the diffraction lines of α', β or α'_s phases were close to each other for a copper tube on the X-ray diffractometer, it was impossible to follow these transformations quantitatively.

The areas covered by the diffraction peak were a quantitative measure of the relative quantity of phases. The fractional transformation of phases in some Zn-Al-Si and Zn-Al-Cu-Si alloys aged at 100°C, 150°C and 170°C were calculated using print-out data measuring the integrated area covered by selected diffraction peaks. Figures 69-75 show fractional transformation versus ℓnt, ageing time. The values of fraction transformation were calculated by using the equations $f = \frac{I}{I_{max}}$ for the $\{10\bar{1}1\}$ or $\{0002\}$ diffraction peaks of η phase and ε phase and $\{433\}$ diffraction peak of T' phase. I is the integrated intensity of the characteristic diffraction peak at any given moment and I_{max} is the maximum intensity recorded. The data are listed in Tables 20-35.

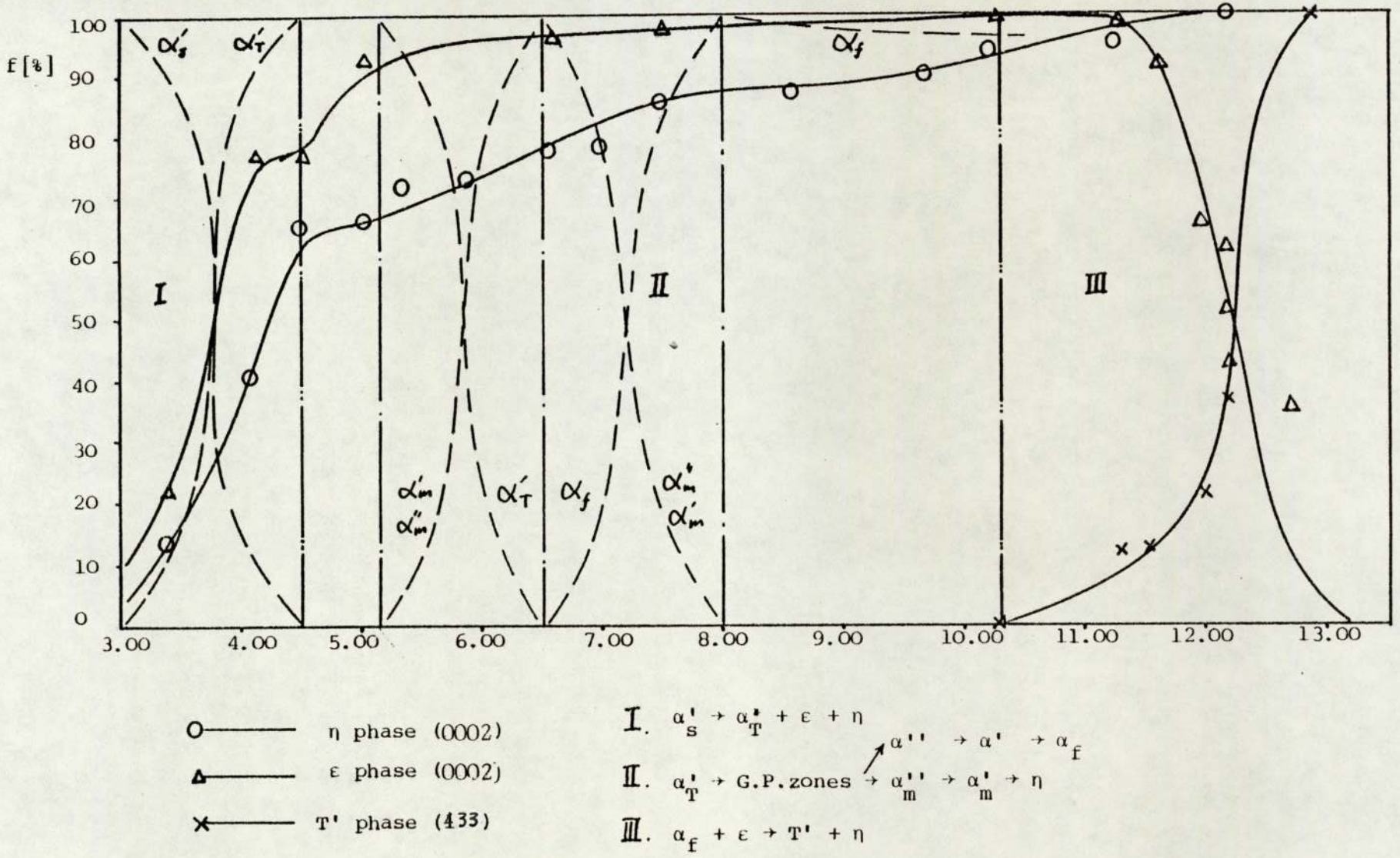

Fig.69 Transformation curves of phases in alloy AlZn60Cu3Si2 aged at 150°C

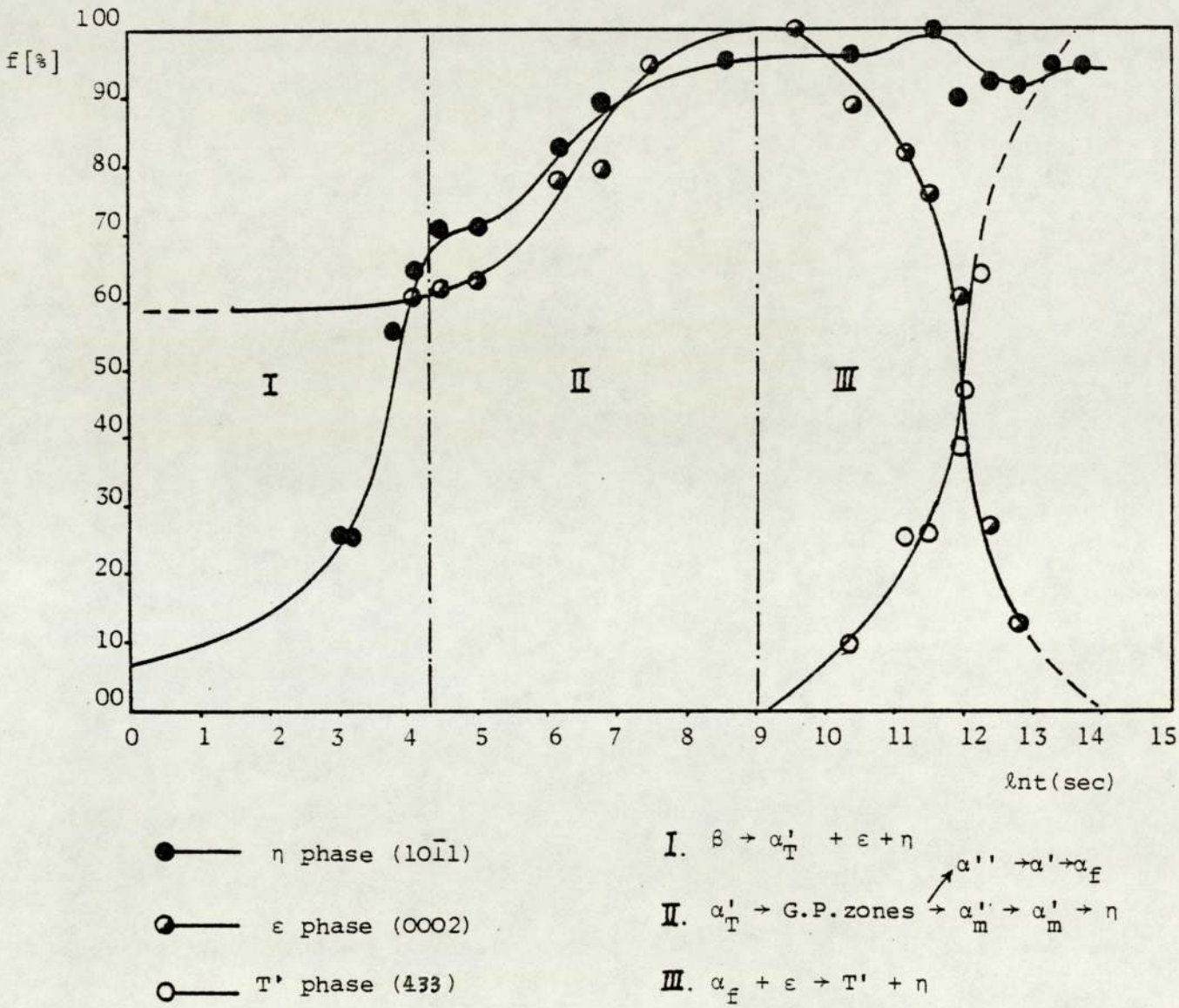

Fig. 70

Transformation curves of phases in alloy AlZn75Cu3Si2 aged at 100°C

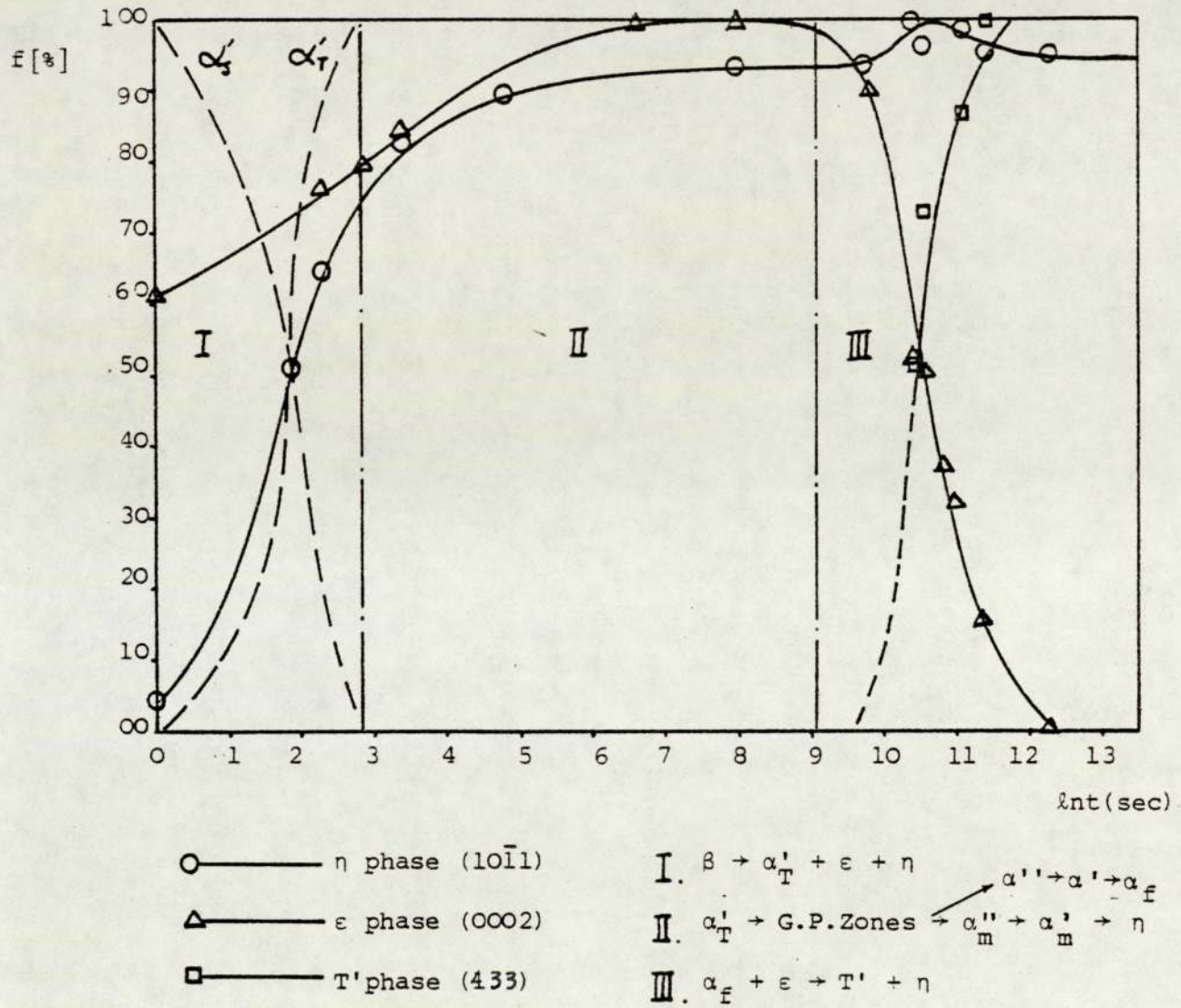

Fig. 71

Transformation curves of phases in alloy AlZn75Cu3Si2 aged at 150°C

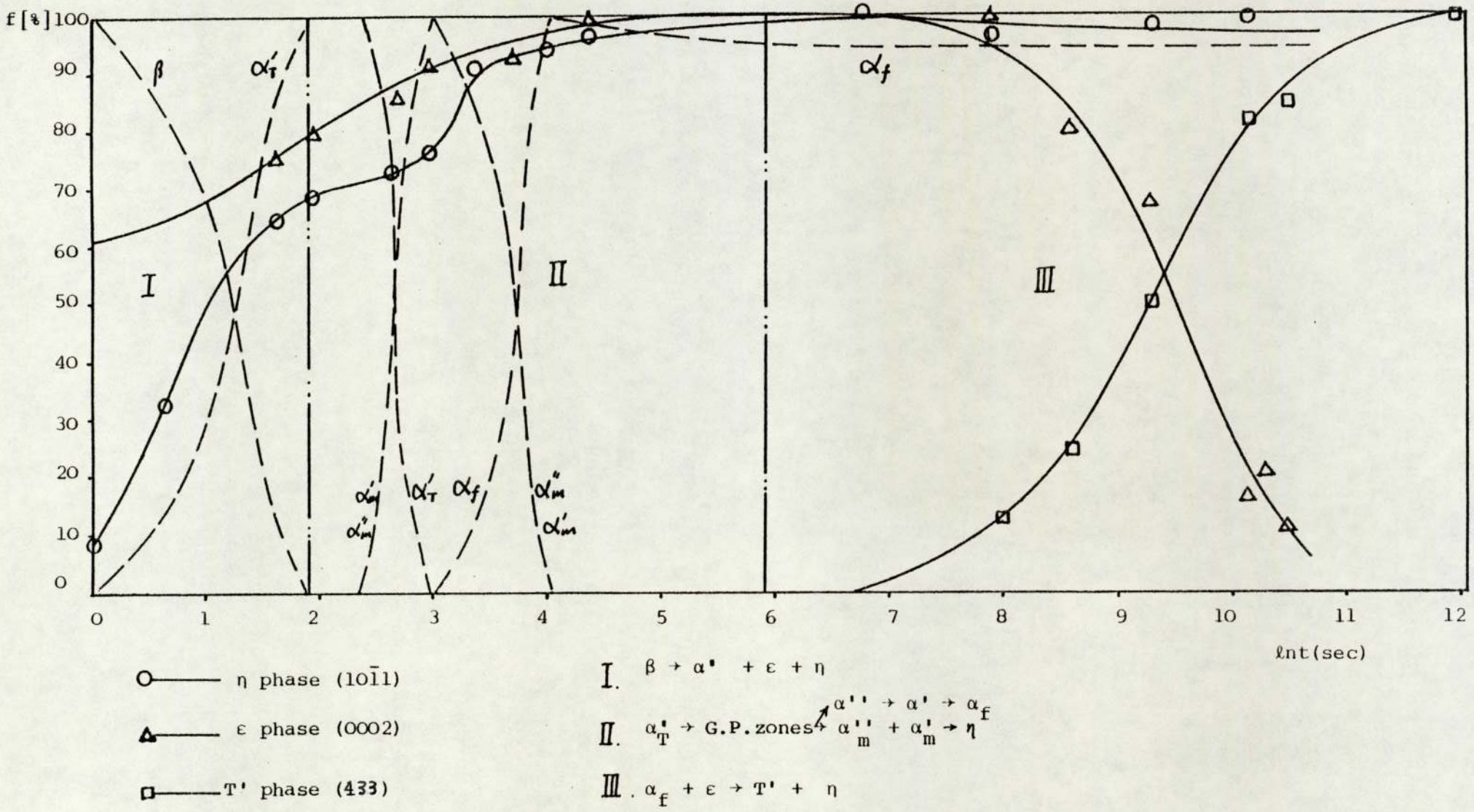

Fig.72 Transformation curves of phases in alloy AlZn75Cu3Si2 aged at 170°C

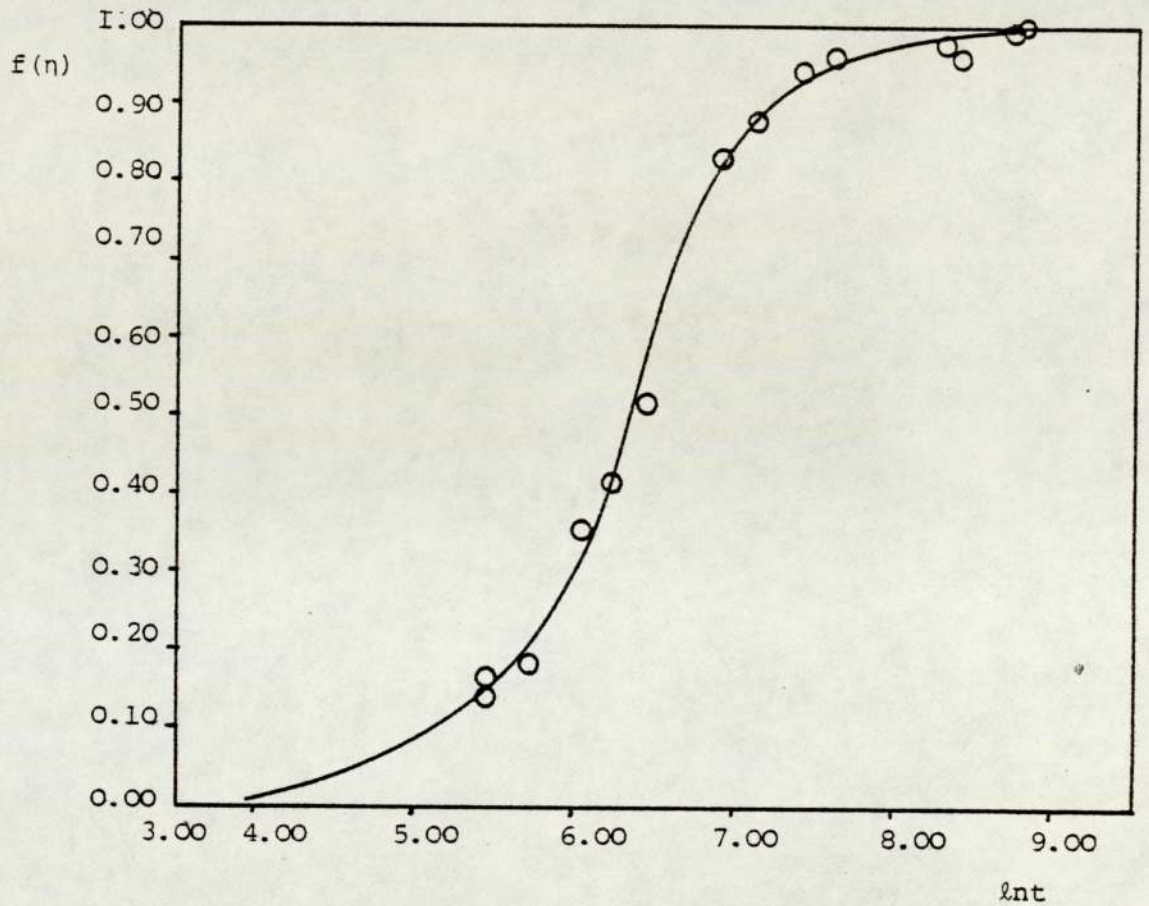

Fig.73

Fraction transformation of η phase in alloy AlZn60Cu3Si2 aged at 100°C deduced from η (0002) peak.

for $\alpha'_s \rightarrow \alpha'_T + \varepsilon + \eta$

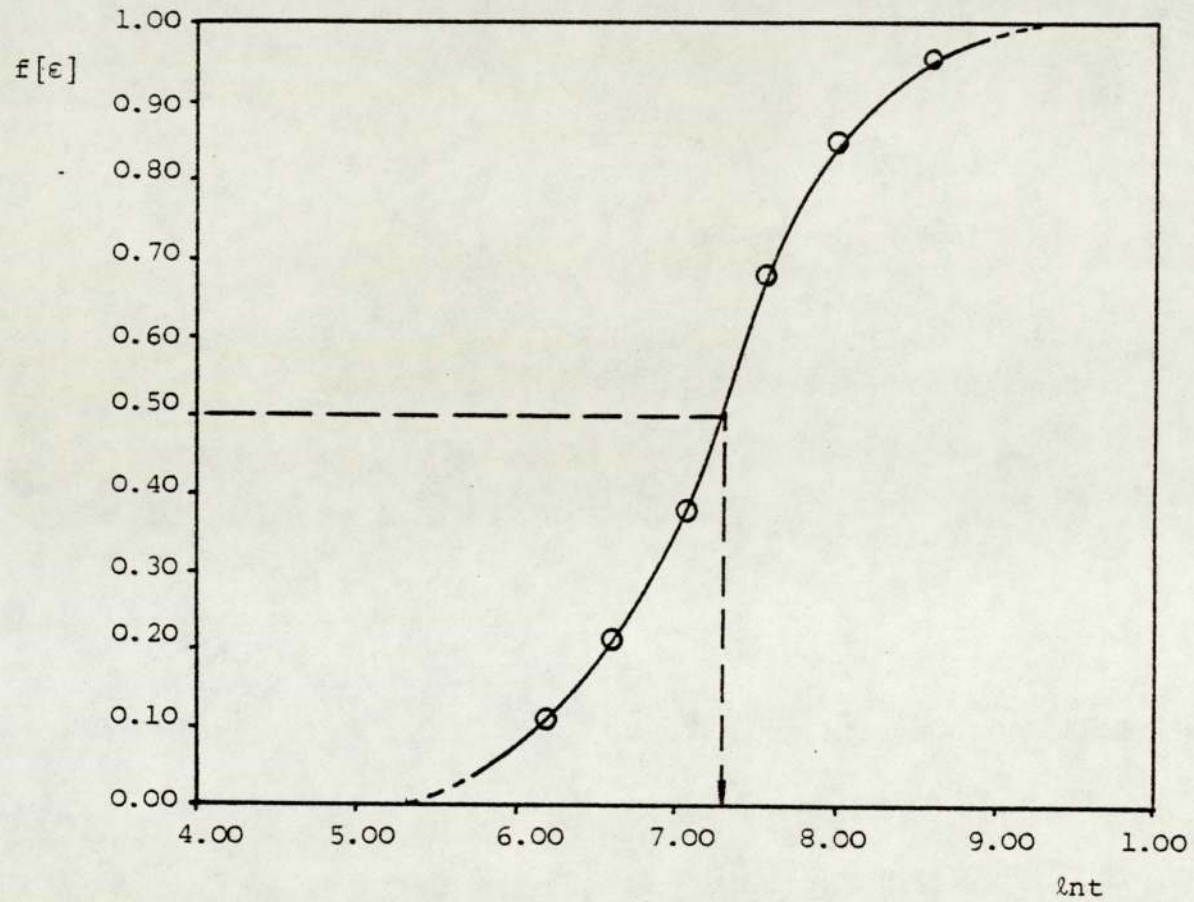

Fig. 74

Fraction transformation of ε phase in alloy AlZn30Cu3Si2, deduced from ε $(10\bar{1}1)$ peak, aged at 170°C

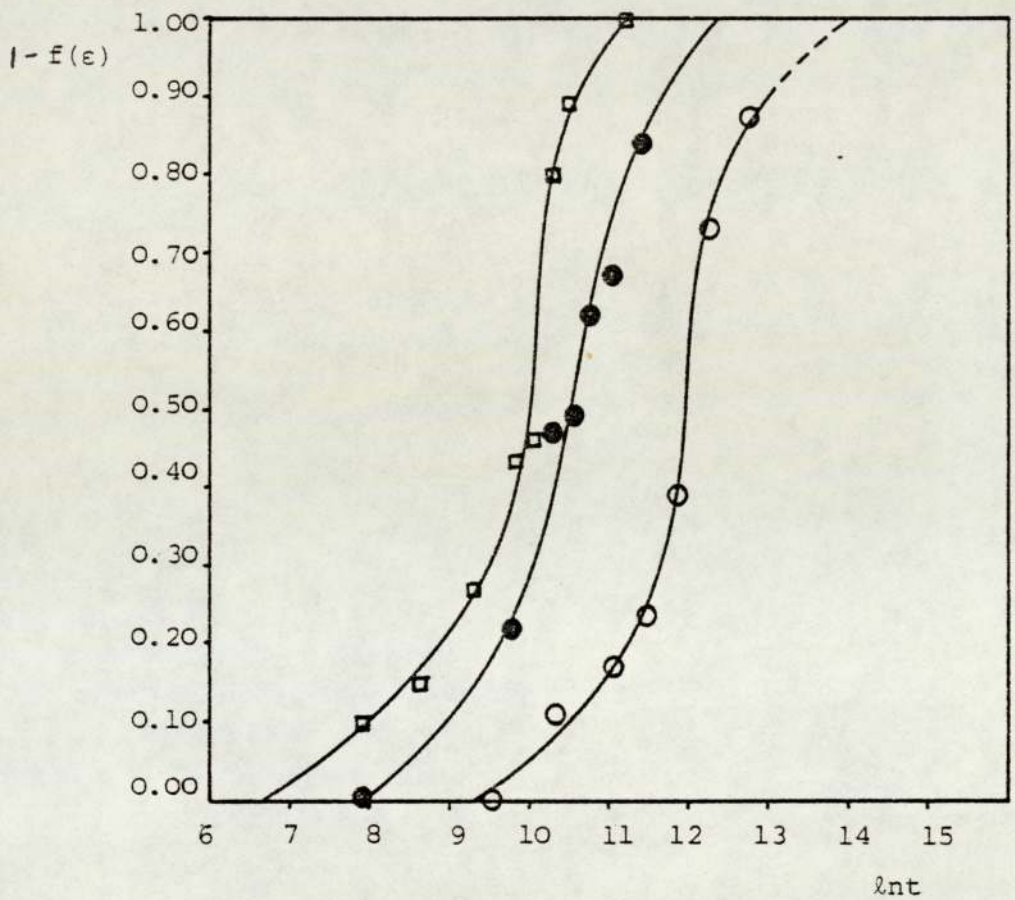

Fig.75

Fraction transformation of ε phase in alloy AlZn75Cu3Si2 aged at 170°C, 150°C, 100°C, for $\alpha_f + \varepsilon \rightarrow T' + \eta$

Table 20

DATA FOR TRANSFORMATION CURVE OF η PHASE IN ALLOY AlZn60Cu3Si2 AGED AT 100°C

t (s)	ℓnt	f	$\ell n \ell n \frac{1}{1-f}$	$\ell n \frac{f}{1-f}$
20	3.00	0.03	-3.49	-3.48
90	4.5	0.11	-2.15	-2.09
120	4.8	0.14	-1.89	-1.82
165	5.1	0.28	-1.11	-0.94
210	5.3	0.33	-0.92	-0.71
240	5.5	0.40	-0.67	-0.41
360	5.9	0.64	0.02	0.57
450	6.1	0.68	0.13	0.75
600	6.4	0.73	0.27	0.99
720	6.6	0.74	0.30	1.05
1440	7.3	0.76	0.36	1.15
1620	7.4	0.74	0.30	1.05
2340	7.8	0.77	0.39	1.21
2520	7.8	0.77	0.39	1.21
3960	8.3	0.79	0.45	1.32
5040	8.5	0.81	0.51	1.45
7200	8.9	0.81	0.51	1.45
18000	9.8	0.92	0.93	2.44
28800	10.27	0.93	0.98	2.59
72000	11.18	4.99	1.53	4.59
11600	11.6	0.94	1.03	2.75
154800	11.9	1.00	∞	∞

Table 21

DATA FOR TRANSFORMATION CURVE OF η PHASE IN REACTION $\alpha' \rightarrow \alpha_T' + \varepsilon + \eta$ FOR ALLOY Al Zn60 Cu3 Si2 AGED AT 100°C

t (s)	ℓnt	f	$\ell n \ell n \frac{1}{1-f}$	$\ell n \frac{f}{1-f}$
20	3.0	0.03	-3.49	-3.48
90	4.5	0.14	-1.89	-1.82
120	4.8	0.18	-1.67	-1.52
165	5.1	0.37	-0.77	-0.53
210	5.3	0.42	-0.61	-0.32
240	5.5	0.52	-0.31	0.08
360	5.9	4.83	0.57	1.59
450	6.1	0.87	0.71	1.90
600	6.4	0.94	1.03	2.75
720	6.6	0.96	1.17	3.18
1440	7.3	0.98	1.36	3.89
1620	7.4	0.96	1.17	3.18
2340	7.7	0.95	1.53	4.60
2520	7.8	1.00	∞	∞

Table 22

DATA FOR TRANSFORMATION CURVE OF ε PHASE IN ALLOY Al Zn60 Cu3 Si2 AGED AT 100°C

t (s)	ℓnt	f	$\ell n \ell n \frac{1}{1-f}$	$\ell n \frac{f}{1-f}$
120	4.8	0.27	-1.16	-0.99
165	5.1	0.30	-1.03	-0.85
210	5.7	0.28	-1.11	-0.94

Table 22 (contd.)

DATA FOR TRANSFORMATION CURVE OF ε PHASE IN ALLOY Al Zn60 Cu3 Si2 AGED AT 100°C				
t (s)	ℓnt	f	$\ell n \ell n \frac{1}{1-f}$	$\ell n \frac{f}{1-f}$
240	5.5	0.61	-0.06	0.45
360	5.9	0.85	0.64	1.73
840	6.7	0.90	0.83	2.20
2520	7.8	0.92	0.93	2,44
3960	8.3	0.83	0.57	1.59
5040	8.5	0.93	0.98	2.59
18000	9.8	0.91	1.25	3.48
28800	10.3	0.91	1.25	3.48
72000	11.2	0.97	1.25	3.48
111600	11.6	0.98	1.17	3.18
129600	11.8	0.98	1.36	3.89
154800	11.9	1.00	∞	∞

Table 23

DATA FOR TRANSFORMATION CURVE OF η PHASE IN ALLOY Al Zn30 Cu3 Si2 AGED AT 170°C				
t (s)	ℓnt	f	$\ell n \ell n \frac{1}{1-f}$	$\ell n \frac{f}{1-f}$
480	6.2	0.11	-2.15	-2.09
780	6.7	0.21	-1.45	-1.32
1200	7.1	0.38	-0.74	-0.49
1920	7.6	0.68	0.13	0.75
3000	8.0	0.85	0.64	1.77
5400	8.6	0.96	1.17	3.18

Table 24

DATA FOR TRANSFORMATION CURVE OF η PHASE IN ALLOY AlZn60Cu3Si2 AGED AT 150°C

t (s)	ℓnt	f	$\ell n \ell n \frac{1}{1-f}$	$\ell n \frac{f}{1-f}$
30	3.40	0.14	-1.89	-1.82
60	4.09	0.40	-4.47	-0.41
90	4.50	0.65	0.05	0.62
150	5.01	0.66	0.08	0.66
720	6.58	0.78	0.41	1.27
1080	6.98	0.79	4.45	1.32
1800	7.50	0.86	0.68	1.82
5400	8.59	0.88	4.75	1.oo
16200	9.69	0.90	0.83	2.19
28800	10.27	0,94	1.03	2.75
79200	11.28	0.95	1.10	2.94
198000	11.20	1.00	∞	∞

Table 25

DATA FOR TRANSFORMATION CURVE OF ε PHASE IN ALLOY AlZn60Cu3Si2 AGED AT 150°C

t (s)	ℓnt	f	$\ell n \ell n \frac{1}{1-f}$	$\ell n \frac{f}{1-f}$
30	3.40	0.22	-1.39	-1.27
60	4.09	0.78	0.41	1.27
90	4.50	0.77	0.39	1.21
150	5.01	0.93	0.98	2.59
720	6.58	0.57	1.25	3.48
1800	7.50	0.98	1.36	3.89
28800	10.27	1.00	∞	

Table 25 (contd.)

DATA FOR TRANSFORMATION CURVE OF ε PHASE IN ALLOY A1Zn60Cu3Si2 AGED AT 150°C

t (s)	ℓnt	f	$\ell n \ell n \frac{1}{1-f}$	$\ell n \frac{f}{1-f}$
79200	11.27	0.99	4.61	4.59
108000	11.59	0.92	0.93	2.44
158400	11.97	0.56	-0.20	0.24
198000	12.20	0.43	-0.58	-0.28
32400	12.69	0.36	-0.81	-0.58

Table 26

DATA FOR TRANSFORMATION CURVE OF T' PHASE IN ALLOY A1Zn60Cu3Si2 AGED AT 150°C

t (s)	ℓnt	f	$\ell n \ell n \frac{1}{1-f}$	$\ell n \frac{f}{1-f}$
28800	10.27	0		
79200	11.27	0.12	-2.06	-1.99
108000	11.59	0.12	-2.06	-1.99
158400	11.97	0.21	-1.44	-1.32
198000	12.20	0.37	-0.77	-0.53
388800	12.87	1.00	∞	∞

Table 27

DATA FOR TRANSFORMATION CURVE OF ε PHASE IN ALLOY AlZn75Cu3Si2 AGED AT 150°C

t (s)	ℓnt	f	$\ell n \ell n \frac{1}{1-f}$	$\ell n \frac{f}{1-f}$
0		0.61	-0.06	0.45
9	2.20	0.78	0.41	1.27
17	2.83	0.82	0.54	1.52
720	6.58	1.00	∞	∞
2880	7.98	1.00	∞	∞
18000	9.79	0.91	0.88	10.11
32400	10.39	0.53	-0.28	0.12
39600	10.59	0.51	-0.34	0.04
50400	10.83	0.38	-0.74	-0.48
64800	11.08	0.33	-0.92	-0.71
86400	11.37	0.16	-1.75	-1.66
223200	12.32	0	-	-

Table 28

DATA FOR TRANSFORMATION CURVE OF η PHASE IN ALLOY AlZn75Cu3Si2 AGED AT 150°C

t (s)	ℓnt	f	$\ell n \ell n \frac{1}{1-f}$	$\ell n \frac{f}{1-f}$
0		0.04	-3.20	-3.18
7	1.9	0.51	-0.34	0.04
10	2.3	0.65	0.05	0.62
30	3.40	0.83	0.57	1.58
120	4.79	0.89	0.79	2.09
2880	7.97	0.94	1.03	15.67
18000	9.80	0.94	1.03	15.67

Table 28

DATA FOR TRANSFORMATION CURVE OF η PHASE IN ALLOY AlZn75Cu3Si2 AGED AT 150°C

t (s)	ℓnt	f	$\ell n \ell n \frac{1}{1-f}$	$\ell n \frac{f}{1-f}$
32400	10.39	1.00	∞	∞
39600	10.59	0.96	1.17	3.18
64800	11.08	0.98	1.36	3.89
86400	11.37	0.95	1.10	2.94
219600	12.30	0.95	1.10	2.94

Table 29

DATA FOR TRANSFORMATION CURVE OF T' PHASE IN ALLOY AlZn75Cu3Si2 AGED AT 150°C

t (s)	ℓnt	f	$\ell n \ell n \frac{1}{1-f}$	$\ell n \frac{f}{1-f}$
32400	10.38	0.52	-0.31	0.08
39600	10.59	0.73	0.27	0.99
64800	11.08	0.87	0.71	1.90
86400	11.37	1.00	∞	∞

Table 30

DATA FOR TRANSFORMATION CURVE OF PHASE ε IN ALLOY AlZn75Cu3Si2 AGED AT 170°C

t (s)	ℓnt	f	$\ell n \ell n \frac{1}{1-f}$	$\ell n \frac{f}{1-f}$
as quenched		0.08	-2.48	-2.44
2	0.69	0.34	-0.88	-0.66
5	1.61	0.65	0.05	0.62
7	1.95	0.69	0.16	0.80
15	2.71	0.73	0.27	0.99
20	2.99	0.77	0.39	1.21
30	3.40	0.91	0.88	2.31
55	4.01	0.94	1.03	2.75
80	4.38	0.97	1.25	3.47
360	5.89	0.99	1.53	4.59
900	6.80	1.00	∞	∞
2700	7.90	0.96	1.17	3.18
10800	9.29	0.98	1.36	3.89
25200	10.13	0.99	1.53	4.59
28800	10.27	0.96	1.17	3.18

Table 31

DATA FOR TRANSFORMATION CURVE OF PHASE T' IN ALLOY AlZn75Cu3Si2 AGED AT 170°C

t (s)	ℓnt	f	$\ell n \ell n \frac{1}{1-f}$	$\ell n \frac{f}{1-f}$
2700	7.9	0.13	-1.97	-1.90
5400	8.59	0.25	-1.25	-1.10
10800	9.29	0.50	-0.37	0
25200	10.13	0.83	0.57	1.58
36000	10.49	0.85	0.64	1.73
158400	11.97	0.10	∞	∞

Table 32

DATA FOR TRANSFORMATION CURVES OF ε PHASE IN ALLOY AlZn75Cu3Si2 AGED AT 170°C

t (s)	ℓnt	f	$\ell n \ell n \frac{1}{1-f}$	$\ell n \frac{f}{1-f}$
as quenched		0.61	-0.06	0.44
5	1.61	0.76	0.36	1.15
7	1.95	0.80	0.48	1.78
15	2.71	0.81	0.51	1.45
20	2.99	0.92	0.93	2.44
30	1.40	0.92	0.93	2.44
40	3.69	0.93	0.98	2.59
80	4.38	1.00	-	∞
900	4.80	1.00	-	∞
2700	7.90	1.01	-	∞
5400	8.59	0.80	0.48	1.38
10800	9.29	0.68	0.13	0.75
25200	10.13	0.17	-1.68	-1.58
28800	10.27	0.21	-1.45	-1.32
36000	10.49	0.12	-2.06	-1.99

Table 33

DATA FOR TRANSFORMATION CURVE OF ε PHASE IN ALLOY AlZn75Cu3Si2 AGED AT 100°C

t (s)	ℓnt	f	$\ell n \ell n \frac{1}{1-f}$	$\ell n \frac{f}{1-f}$
60	4.09	0.61	-0.06	0.44
90	4.50	0.62	-0.03	0.49
150	5.01	0.63		0.53
480	0.17	0.78	0.41	1.26
900	0.80	0.79	0.45	1.32

Table 33 (contd.)

DATA FOR TRANSFORMATION CURVE OF ε PHASE IN ALLOY A1Zn75Cu3Si2 AGED AT 100°C

t (s)	ℓnt	f	$\ell n \ell n \frac{1}{1-f}$	$\ell n \frac{f}{1-f}$
1800	7.50	0.95	1.10	2.94
14400	9.57	1.00	∞	∞
32400	10.39	0.89	0.79	2.09
68400	11.13	0.83	0.57	1.58
104400	11.56	0.77	0.39	1.21
154800	11.95	0.61	-0.06	0.44
234000	12.36	0.27	-1.16	-0.99
352800	12.77	0.13	-1.97	-2.03

Table 34

DATA FOR TRANSFORMATION CURVE OF η PHASE IN ALLOY A1Zn75Cu3Si2 AGED AT 100°C

t (s)	ℓnt	f	$\ell n \ell n \frac{1}{1-f}$	$\ell n \frac{f}{1-f}$
as quenched		0.06	-2.78	-2.75
20	2.99	0.27	-1.16	-0.99
25	3.20	0.27	-1.16	-0.99
35	3.50	0.51	-0.34	0.04
45	3.80	0.57	-0.17	0.28
60	4.09	0.66	0.08	0.66
90	4.49	0.71	0.21	0.89
150	5.01	0.73	0.27	0.99
480	6.17	0.85	0.64	1.73
900	6.80	0.91	0.88	2.31

Table 34 (contd.)

DATA FOR TRANSFORMATION CURVE OF η PHASE IN ALLOY AlZn75Cu3Si2 AGED AT 100°C

t (s)	ℓnt	f	$\ell n \ell n \frac{1}{1-f}$	$\ell n \frac{f}{1-f}$
1800	7.50	0.94	1.03	2.75
5400	8.59	0.97	1.25	3.48
32400	10.39	0.98	1.36	3.89
104400	11.56	1.00	∞	∞
154800	11.95	0.90	0.83	1.59
23400	12.36	0.92	0.93	2.44
352800	12.77	0.91	0.88	2.31
568800	13.25	0.96	1.17	3.18
936000	13.75	0.96	1.17	3.18

Table 35

DATA FOR TRANSFORMATION CURVE OF T' PHASE IN ALLOY AlZn75Cu3Si2 AGED AT 100°C

t (s)	ℓnt	f	$\ell n \ell n \frac{1}{1-f}$	$\ell n \frac{f}{1-f}$
32400	10.39	0.10	-2.25	-2.19
68400	11.13	0.27	-1.16	-0.99
104400	11.56	0.26	-1.20	-1.05
154800	11.95	0.39	-0.70	-0.45
180000	12.10	0.47	-0.45	-0.12
234000	12.36	0.64	0.02	0.58

Obviously, the appearance of a set of new diffraction peaks means the formation of a new phase and the disappearance of a set of diffraction peaks means the vanishing of the phase which contributed that set of diffraction peaks. The changes in the peak heights or more accurately in the area of the diffraction peaks were used for tracing the phase transformation.

Eleven sets of short angular range X-ray diffractometer scans on alloys of Al-rich, monotectoid and eutectoid compositions were carried out during 70°C, 100°C, 150°C and 170°C ageing processes. The Cuk_{α} radiation applied within the angle range 2 θ from 35°C to 47°C produced the strongest lines of the phases assessed. The published diffractometer trace from an alloy ZnAl53Cu26[23] was used for the identification of T' lines.

4.4.1 Zn-Al-Cu-Si system

4.4.1.1 Alloys of monotectoid composition in Zn-Al-Cu-Si system

The X-ray diffractogram of alloy AlZn60Cu3Si2, aged at 100°C is shown in Figure 76. After 3.5 minutes ageing, the diffraction peak of the supersaturated phase α'_s had decreased accompanied by appearance of three sets of new diffraction peaks from α'_T, ε and η phases. Here α'_T was an Al-rich metastable phase, the diffraction peaks of which were located only 0.3°C to the low angle side of the original peaks of the supersaturated phase α'_s. After 12 minutes of ageing, the peaks of α'_s from both (200) and (111) positions, vanished and left the increased peaks of α'_T, ε and η phases clearly visible.

From the X-ray diffractogram in Figure 76, this transformation from α'_s to α'_T, ε and η was distinctly observed.

During subsequent ageing at 100°C, the α'_T (200) peak kept stable for about 12 minutes, while the intensities of peaks of ε and η phase increased very slowly. After 24 minutes ageing at 100°C, small peaks of the first transition phase α''_m appeared at higher angle side of the main peak and the Al-rich metastable phase became unstable. Three minutes later, the multiple peaks of α''_m had combined to a single peak α'_m and the (200) peak from the Al-rich metastable phase α'_T gradually shifted to the position of α" (200), the Al-rich matrix phase. At the same time, the peaks of ε and η phases developed further. After 5 hours ageing at 100°C, α'_m had disappeared and the α'_T (200) had changed to α_f (200). The fraction transformation of η phase in alloy AlZn60Cu3Si2 aged at 100°C deduced from η (0002) peak for $\alpha'_s \rightarrow \alpha'_T+\varepsilon+\eta$ is shown in Figure 73.

On prolonged ageing, the diffraction peak of T' phase (433) appeared after 66 hours and then developed with ageing time, accompanied by a decrease in the intensity of diffraction from phase. After 496 hours ageing at 100°C, the phase peak had greatly reduced and the T' phase peak had grown to the maximum. No further changing in diffraction peaks was observed with further ageing.

The X-ray diffractogram of this alloy aged at 70°C, in Figure 77, showed specifically the same kind of changes

in the diffraction peaks. After 1.5 hours ageing at 70°C, three new sets of diffraction peaks of α'_T, ε and η phase occurred and grew up while those of α'_s (200) and (111) dropped down quickly. After 8.45 hours, these newly formed peaks were well-developed and the α'_s peaks had vanished from the diffractogram. The whole process is shown clearly in the six diffractometer traces in Figure 77. Subsequent changes were the same as for 100°C ageing.

The X-ray diffractogram of this alloy AlZn60Cu3Si2 aged at 150°C, Figure 78, showed the same sequence of phase transformation as observed at 70°C and 100°C. During the first 2 minutes of ageing, the first stage of decomposition of the supersaturated alloy was the transformation from α'_s phase to α'_T, ε and η phases. The transition phases α''_m and α'_m and their related Al-rich matrix phase were observed on subsequent ageing. The appearance of the T' phase in the alloy after 8 hours ageing and the disappearance of the ε phase after 158 hours were both observed in the alloy.

The integrated peak areas of different phases were used to show quantitatively how the different phases developed or disappeared with time. The transformation was the same for alloys aged at 100°C or 150°C and Figure 69 shows the result for 150°C ageing.

4.4.1.2 Alloy of eutectoid composition in Zn-Al-Cu-Si system

Alloy AlZn75Cu3Si2 was investigated on ageing at 100°C, 150°C and 170°C. The supersaturated alloy was found to

decompose quickly. Even in the as-quenched condition, part of the supersaturated phase β was decomposed into α'_T, ε and η phases as shown in the X-ray diffractograms of Figures 79,80,83. Duplicated examinations on 100°C ageing are shown in Figures 79, 80.

Optical micrograph of this as-quenched alloy showed the discontinuous precipitates along the grain boundary as in Figure 81. After 0.5 minutes ageing at 100°C, it was observed that the discontinuous precipitates along the grain boundary developed in the optical micrograph, Figure 82.

Careful examinations were carried out at very short ageing time to show the decomposition of supersaturated β phase, as seen in Figure 80. The first four X-ray diffraction traces in Figure 73, revealed the first stage of ageing. The supersaturated β phase had transformed into α'_T, ε and η phases after 1.5 minutes ageing at 100°C. Then the α'_T phase line was observed to shift to the position of the line of the aluminium-rich α' phase after 2.5 minutes. The transition phase and α' phase were well developed after 8 minutes, as shown in both Figures 79 and 80. The ε phase started to reduce and T' phase appeared after 3 days ageing at 100°C.

The 150°C ageing process of this alloy involved the same stages of phase transformation, shown in Figure 83, but as expected each stage came earlier than in 100°C ageing. The first stage, the decomposition of supersaturated β phase into α'_T, ε and η phases was completed in only

10 seconds. The final stage ended after 61 hours ageing. The activation energy of the final stage was calculated using the Arrhenius plot, shown in Figure 66. The data is listed in Table 32.

The fraction transition curves, in Figures 70-72, present the phase change quantitatively. It was found that the same kind of phase transformation occurred in all 100°C, 150°C and 170°C ageing processes.

When the integrated intensities from the ε (0002) line were used to plot out the curves of fraction transformed versus ℓnt, the curves of Figure 75 were obtained for the temperatures 100°C, 150°C and 170°C.

Using the times to f = 0.5, an Arrhenius plot was made which allowed the activation energy for ε phase formation to be calculated as 37.4 KJ/mol.

4.4.1.3 Al-rich alloy in the Zn-Al-Cu-Si system

Compared with the monotectoid and the eutectoid alloy, a different mechanism of ageing was observed in alloy AlZn30Cu3Si2. Instead of the decomposition of supersaturated α'_s or β phase into α'_T, ε and η phases, first the transition phase α''_m was observed on X-ray examination e.g. after 2 minutes ageing at 170°C. A sudden reduction in the intensity of α'_s phase was observed accompanied by the appearance of ε phase after 5 minutes ageing at 170°C, while the α''_m phase peak was still growing up. During ageing for 5 to 30 minutes at 170°C, the peaks of α' were found to shift gradually to lower Bragg angle positions and the phase peaks η $(10\bar{1}1)$ and

ε $(10\bar{1}0)$ increased rapidly after 24 minutes, as shown in Figure 84.

From the fraction transformation curve of alloy A1Zn30Cu3Si2 in Figure 74, it was found that the fraction of ε phase increased to about 50% of maximum just after 24 minutes ageing at 170°C.

In the 100°C ageing process, the same stages occurred, as shown in Figure 85. After 45 hours ageing the transition phase was well developed. Accompanying the transformation of α''_m to α'_m changes in the matrix phase and η phase were observed from 10 hours till 63 hours of ageing at 100°C. These changes may explain the appearance of the two hardness peaks after the maximum hardness peak shown in Figure 62.

4.4.2 Zn-A1-Si system

4.4.2.1 Alloy of monotectoid composition in Zn-A1-Si systems. X-ray diffraction examination of alloy A1Zn60Si5 was carried out on 100°C and 170°C ageing. In both cases, the rapid decomposition of supersaturated α'_s phase was observed and the transition phases α''_m and α'_m occurred in both ageing processes, as shown in Figures 86 and 87.

On ageing at 100°C, α'_T and η phase were observed to coexist with α'_s phase in the as-quenched state, but the decomposition of the supersaturated α'_s phase had not been completed, as shown in Figure 86. During the first 1 minute's ageing, the intensities of phases involved were re-distributed, diminishing for the supersaturated α'_s phase, and increasing for the α'_T and η phase.

LIST OF FIGURES

FIGURE	TITLE	PAGE
1	Phase diagram of Al-Zn system[11]	9
2	Lattice-parameter/temperature curves[12]	10
3	Lattice-parameter/isotherms[12]	10
4	Phase diagram of Al-Zn system : a,b metastable diagrams according to[14]	10
5	Phase diagram of Al-Si system[15]	11
6	Phase diagram of Si-Zn system[15]	11
7	Phase diagram of Al-Cu system[16]	18
8	Phase diagram of Cu-Zn system[17]	12
9	Isothermal section of Zn-Al-Cu ternary system at 350°C[1]	17
10	Liquidus surface of the Zn-Al-Cu system[19]	17
11	Isothermal section of Zn-Al-Cu system at 350°C[23]	18
12	Isothermal section of Zn-Al-Cu system at 290°C[23]	19
13	Isothermal section of Zn-Al-Cu system at 280°C[23]	19
14	Isothermal section of Zn-Al-Cu system at 270°C[23]	20

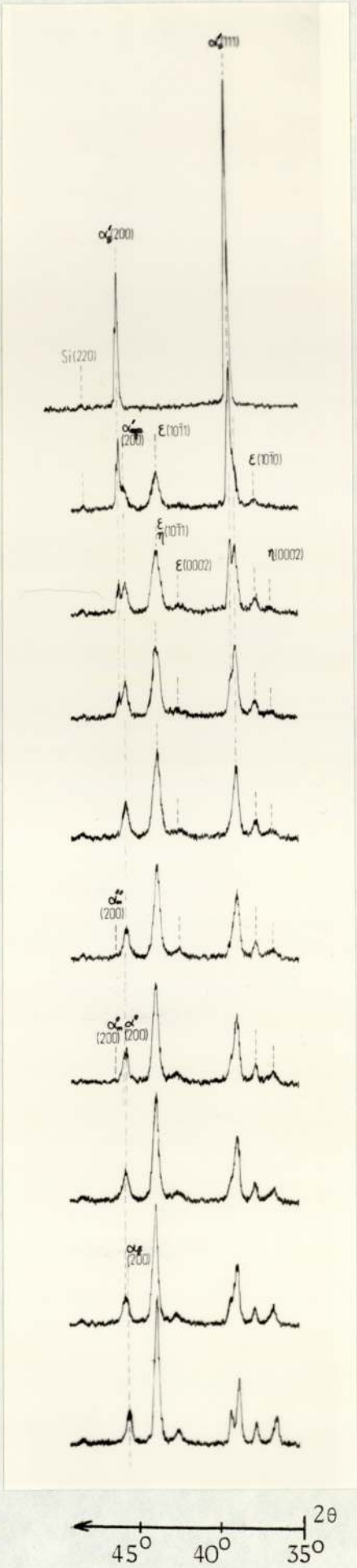

Figure 76

Set of X-ray diffractograms of alloy Al Zn60 Cu3 Si2 aged at 100 °C

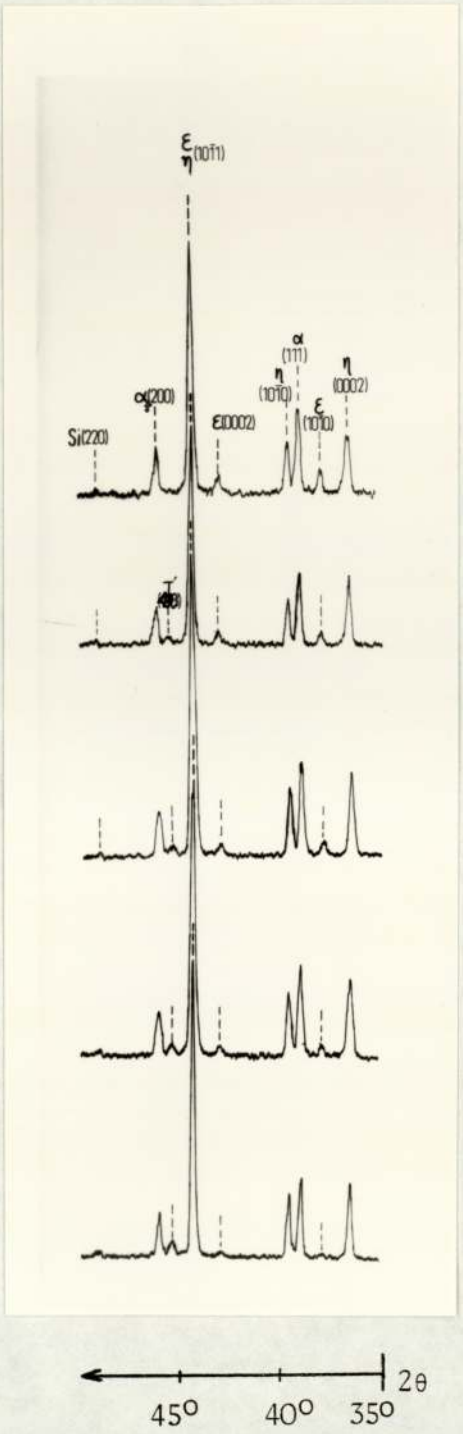

Fig.76 (contd)

Set of X-ray diffractograms of alloy AlZn60Cu3Si2 aged at 100°C

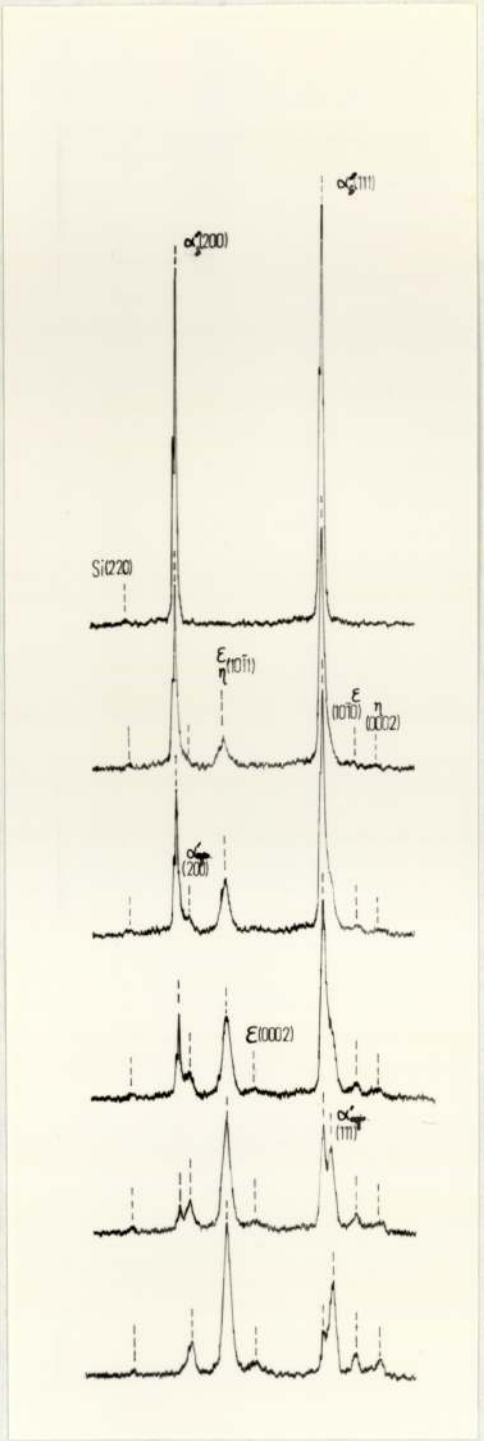

Figure 77

Set of X-ray diffractograms of alloy AlZn60Cu3Si2 aged at 70°C, showing the cellular reaction before G.P. zones

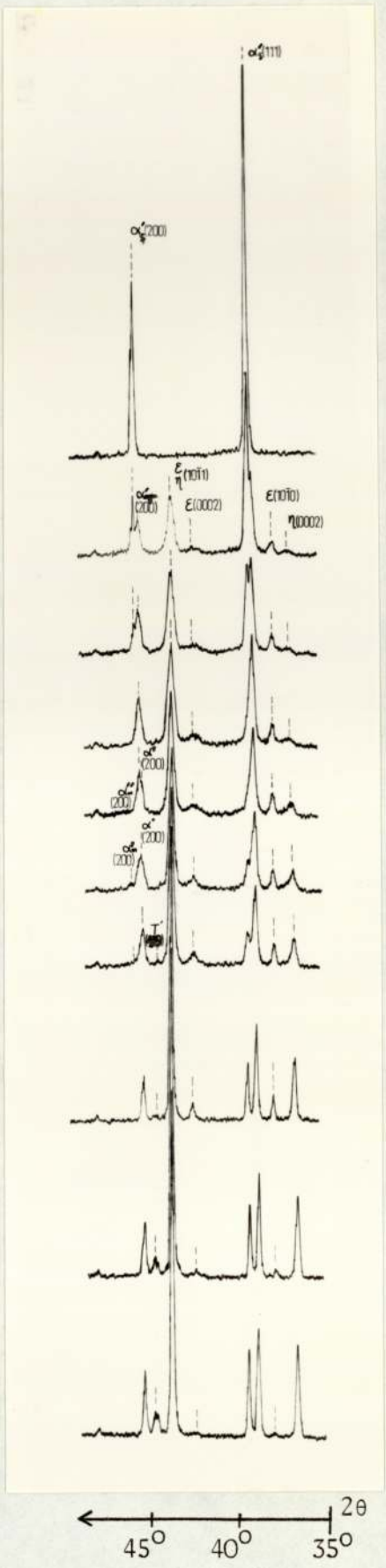

Figure 78

Set of X-ray diffractograms of alloy AlZn60Cu3Si2 aged at 150°C

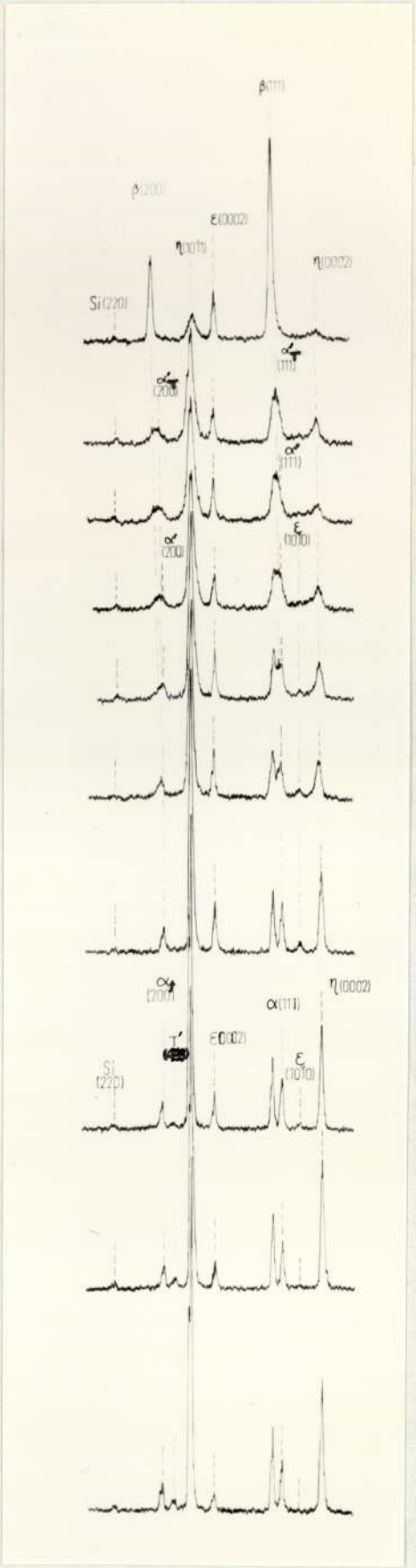

Figure 79

Set of X-ray diffractograms of alloy AlZn75Cu3Si2 aged at 100°C

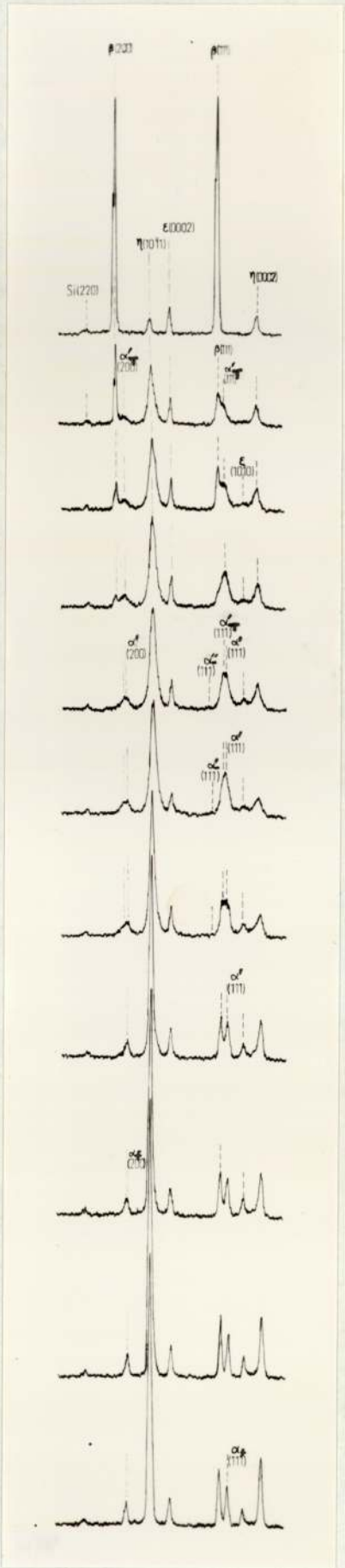

Figure 80
Set of X-ray diffractograms of alloy AlZn75Cu3Si2 aged at 100°C, showing the cellular reaction before G.P.zone

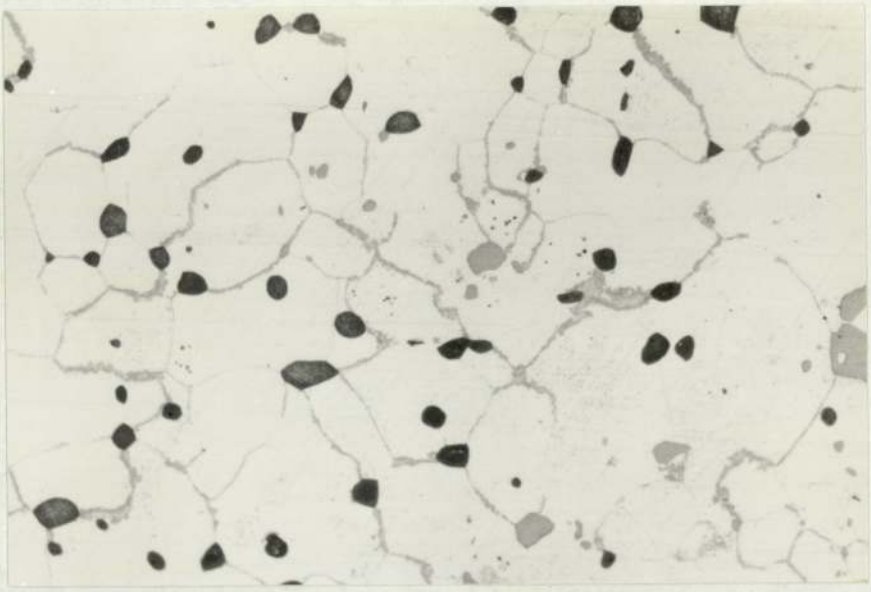

Fig.81 Optical micrograph of as-quenched alloy AlZn75Cu3Si2 showing the discontinuous precipitates along the grain boundary. x420.

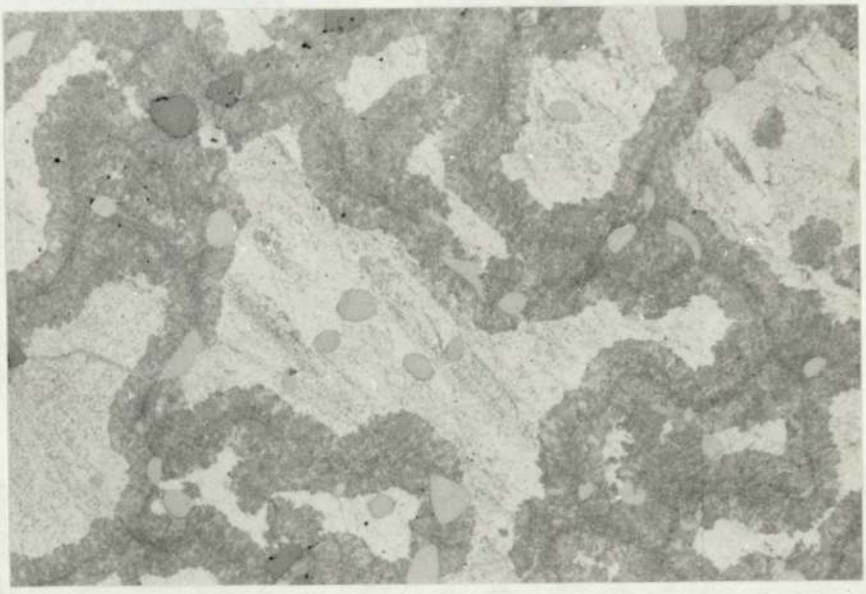

Fig.82 Optical micrograph of alloy AlZn75Cu3Si2 showing the developed discontinuous precipitates along the boundary after 25 minutes ageing at 100°C. x420.

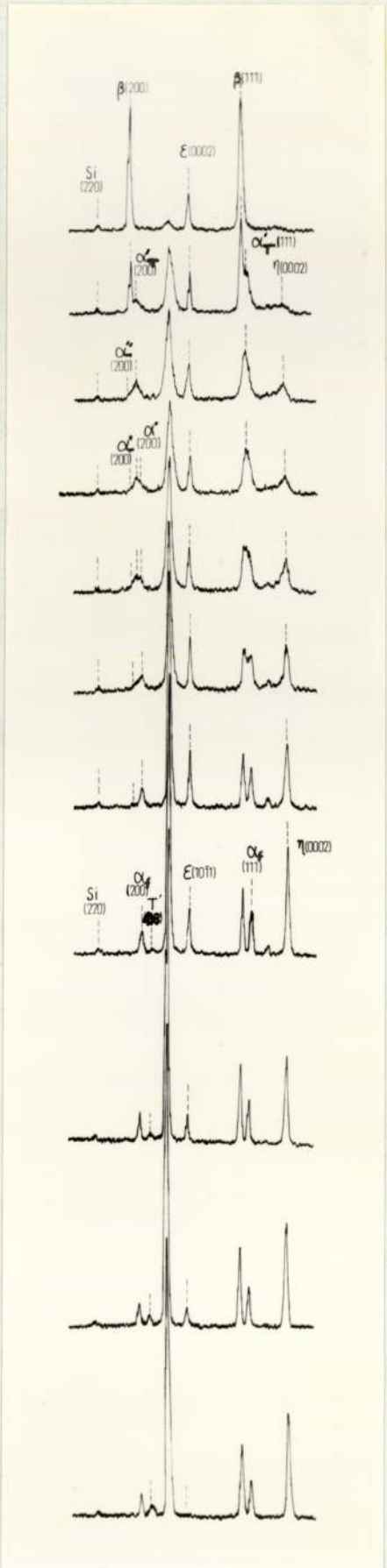

Figure 83

Set of X-ray diffractograms of alloy AlZn75Cu3Si2 aged at 150°C

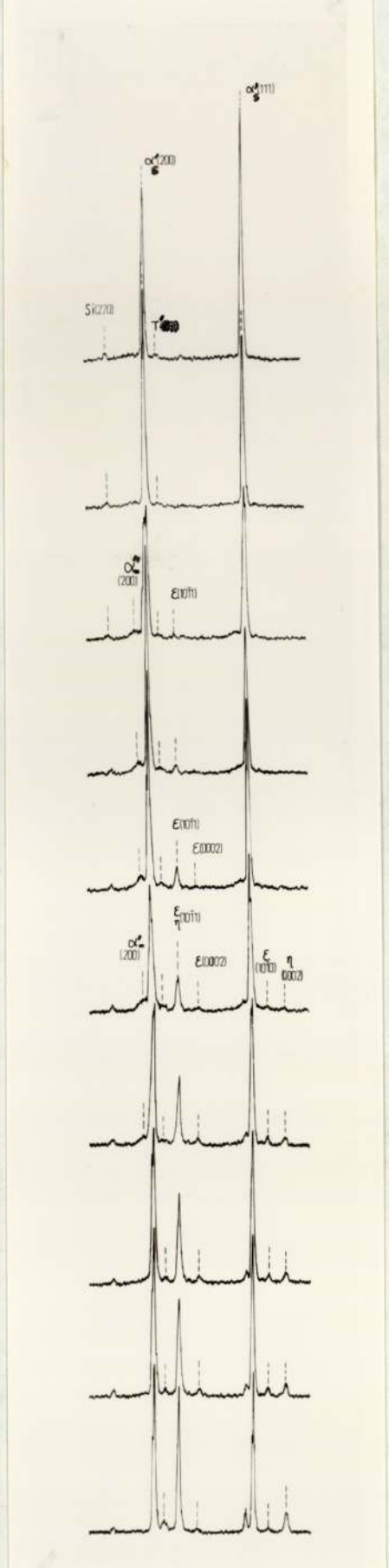

Figure 84
Set of X-ray diffractograms of alloy AlZn30Cu3Si2 aged at 170°C

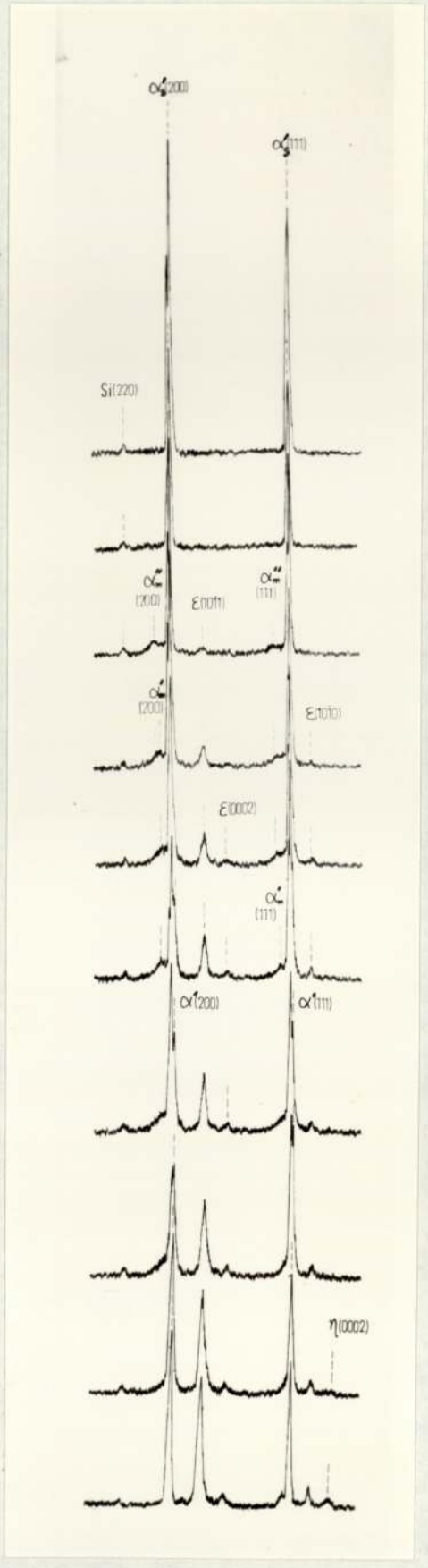

Figure 85

Set of X-ray diffractograms of alloy AlZn30Cu3Si2 aged at 100°C

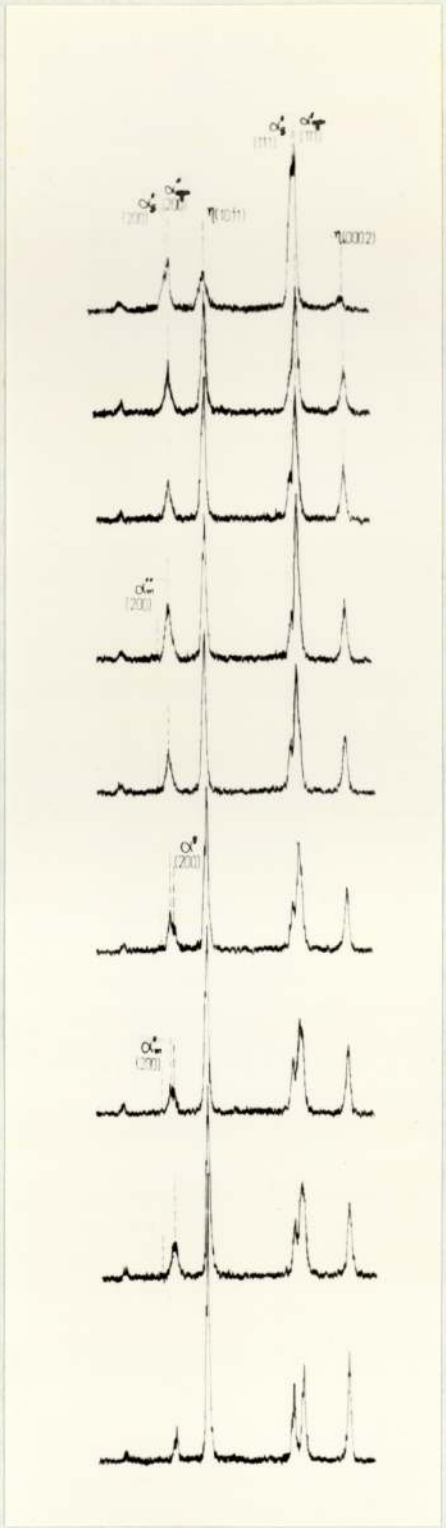

Figure 86

Set of X-ray diffractograms of alloy AlZn60Si5 aged at 100°C

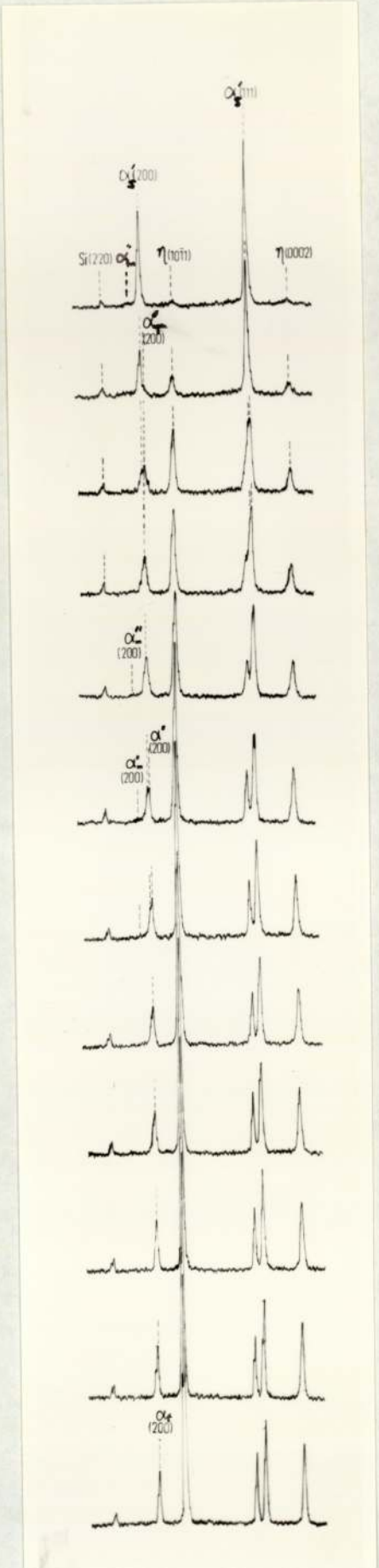

Figure 87

Set of X-ray diffractograms of alloy AlZn6OSi5 aged at 170°C

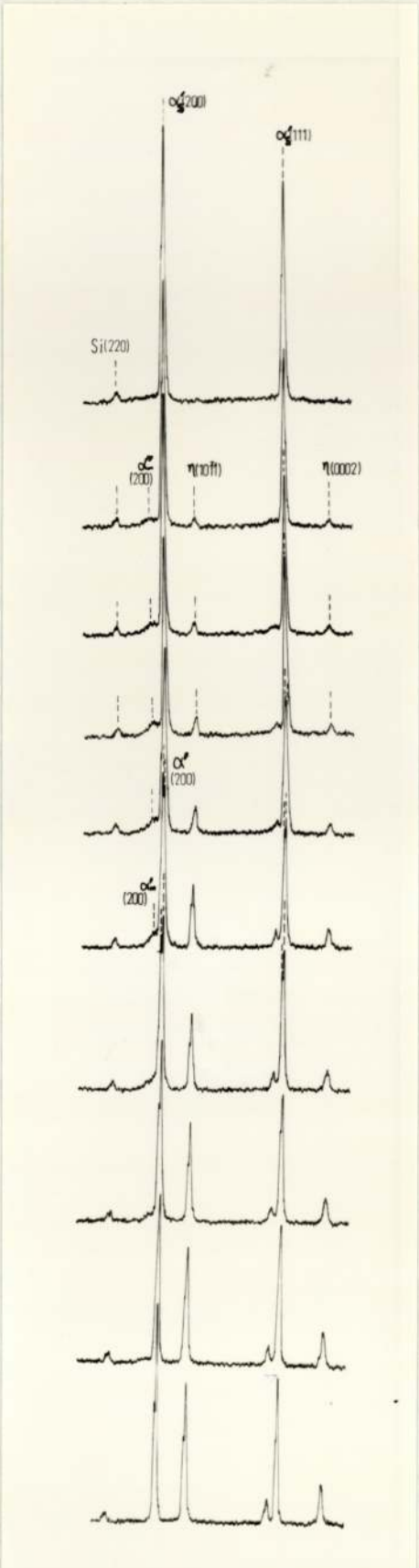

Figure 88

Set of diffractograms of alloy AlZn30Si5 aged at 170°C

4.4.2.2 Al-rich alloy in Zn-Al-Si system

Alloy AlZn30Si5 was examined on ageing at 170°C. The X-ray diffractogram is shown in Figure 88. In 170°C ageing process, it was found that the supersaturated α'_s phase had started to decompose to α''_m, α'' and η phases after 5 minutes ageing. The composition of α'' phase, which was in equilibrium with α''_m was so close to α'_s that it was hard to detect.

During the first 10 minutes, η phase increased slowly, while the transition phase α''_m grew rapidly to a maximum. On prolonged ageing, this transition phase α''_m changed gradually to the single peak α'_m phase with simultaneous shifting of Al-rich matrix phase to α'. After about 1 to 1.5 hours ageing at 170°C, a great increase in intensity of η phase was observed accompanied by a decrease of α'_m phase. All phase changes were completed after 67 hours ageing at 170°C.

In all X-ray diffraction examinations of both Zn-Al-Cu-Si and Zn-Al-Si systems, there was little change in Si-rich, σ, phase (220).

4.5 TEM Examination

4.5.1 Alloy AlZn30Si5

According to the hardness test and X-ray diffraction examination, the phase transformation of alloys AlZn30Si5 consisted of three typical stages of decomposition. In order to investigate the structural change during the ageing process, transmission electron microscopy studies were carried out on the corresponding stages.

General precipitation was observed within the greater part of the alloy AlZn22.4Si7.4 after ageing at room temperature for 2 months. Particles of average size 1200 Å diameter were shown in both bright and dark field images (Figure 89) and the contrast at a particle consisted of one or two dark lobes. It was concluded that the particles were probably coherent plates, made visible by strain field contract. The diffraction pattern from this area is shown in Figure 90. After 3 months ageing at room temperature, these particles were elongated parallel to a <110> direction in the $[\bar{1}12]$ orientated region seen in Figure 91. The diffraction pattern is shown in Figure 92. The average spacings between the five rod-shaped precipitates α''_m were about 2000 Å.

Very fine precipitates, about 100 Å in size and spaced about 200 Å were observed in alloy AlZn30Si5 aged at 100°C for 8.5 minutes, as shown in Figure 93. Since the spinodal wavelength is about 50 Å in Zn-Al alloys, these probably represent G.P.zones or small, coherent precipitates. Larger precipitates are also visible in the same area.

After 1.5 hours ageing at 100°C elongated precipitates of the first transition phase α''_m corresponding to the broad diffraction peak to the low angle side of the $(200)\alpha$ peak in the X-ray diffractogram of Figure 87 were well developed. Discontinuous precipitates adjoining a grain boundary are also evident in Figure 94.

According to the diffraction pattern of the matrix phase,

as shown in Figure 95, apparent growth directions of the precipitates were [001] and [11$\bar{1}$] in a <110> zone, as observed in Figure 92. At that stage of ageing, G.P.zones still existed as seen in the micrograph.

After ageing for 24 hours at the same temperature, the development of phase separation into α' and α'_m was well advanced. A rod or lath structure orientated in one distinct direction can be seen in Figure 96. The rods were found to be 0.1-0.15μm wide and were segmented into portions which had dark and light contrast alternatively. Generally each dark portion in a band was next to a light portion in the adjacent band (Figures 96-100).

The colonies apparently nucleated at a grain boundary and after growing with some slight curvature initially, adopted a preferred growth direction across the entire grain. The growth morphology was rarely precisely maintained and degenerated into rounded particles or short rods in some areas, (Figures 97,99,100). Branching was found to be entirely absent, and when the colonies were sectioned (e.g. lower L.H.corner of Figure 99) the α'_m rods seem to be isolated from each other in the α' matrix. No interconnection between lamellae were observed in the successive interfaces exposed as a cell was sectioned and in an overlapping case in Figure 100. Figures 98 and 102 indicated that the α'_m phase was parallel to [1$\bar{1}$1] in (112) oriented plane of matrix.

At this stage of ageing, diffraction patterns and its index (Figures 104,105) corresponding to the f.c.c. crystal

(a)

(b)

Fig. 89

Transmission electron micrographs showing particles precipitation in alloy AlZn225Si2.4 after 2 months ageing at room temperature x42.4K.

(a) bright field (b) dark field

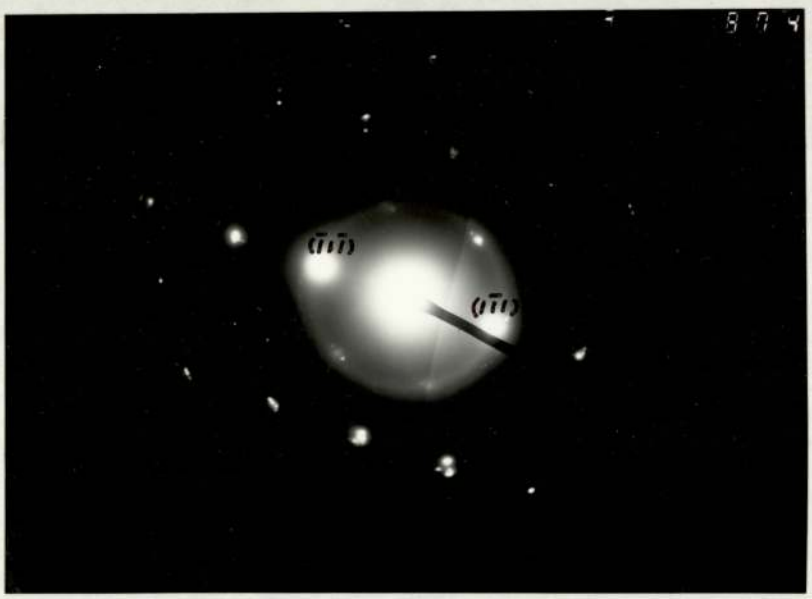

Fig. 90

The electron diffraction pattern from the matrix shown in Figure 89 (a)

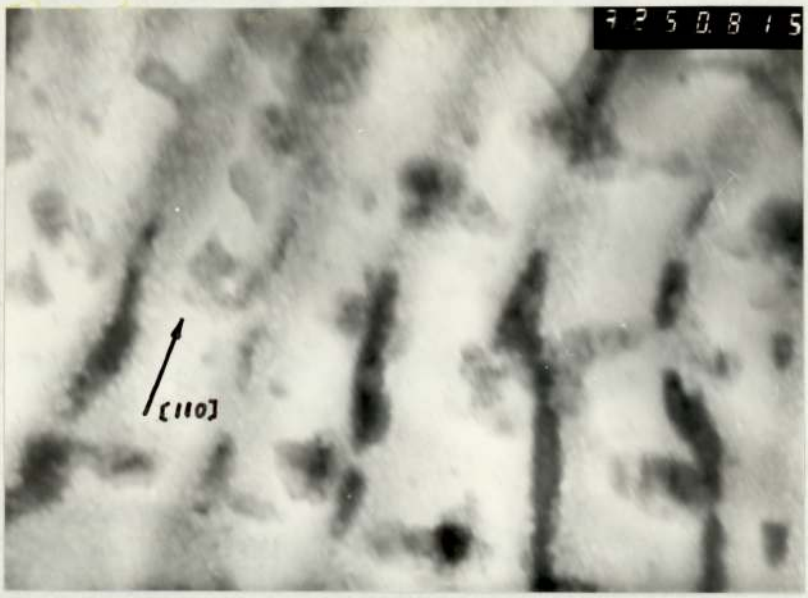

(a)

(b)

Fig. 91

Transmission electron micrographs showing rod shaped precipitates parallel to a [110] direction in the ($\bar{1}$12) oriented region. x108K

(a) bright field (b) dark field

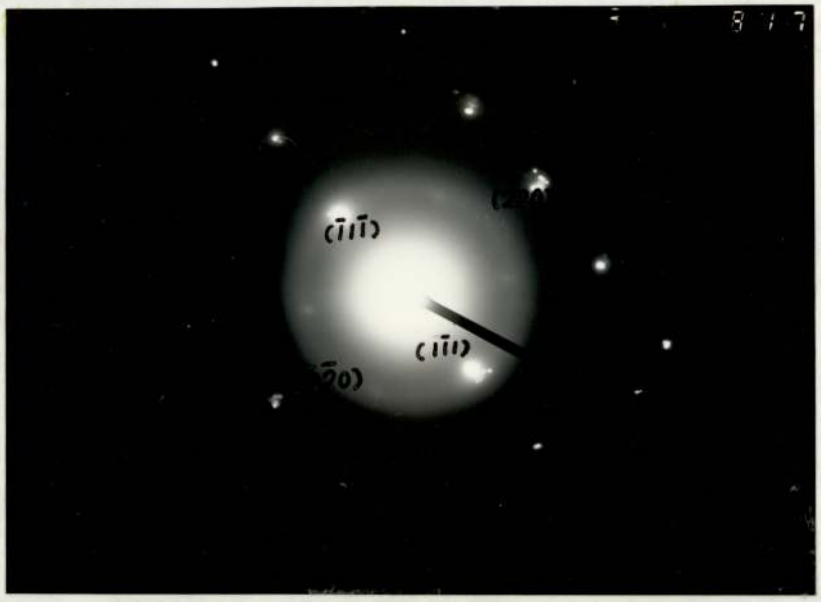

Fig. 92

The electron diffraction pattern from the matrix shown in Figure 91(a)

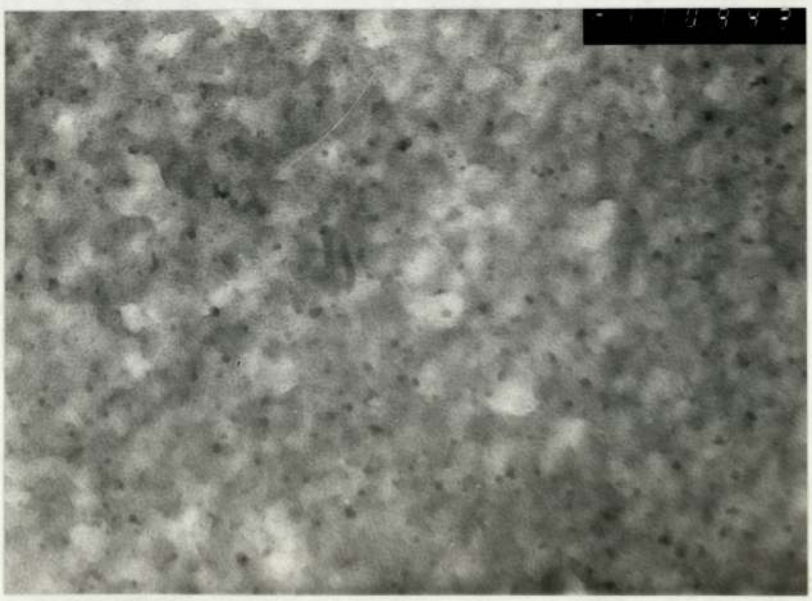

Fig. 93

Transmission electron micrographs showng G.P.zones in alloy AlZn30Si5 aged at 100°C. 8.5 minutes. x42.4K

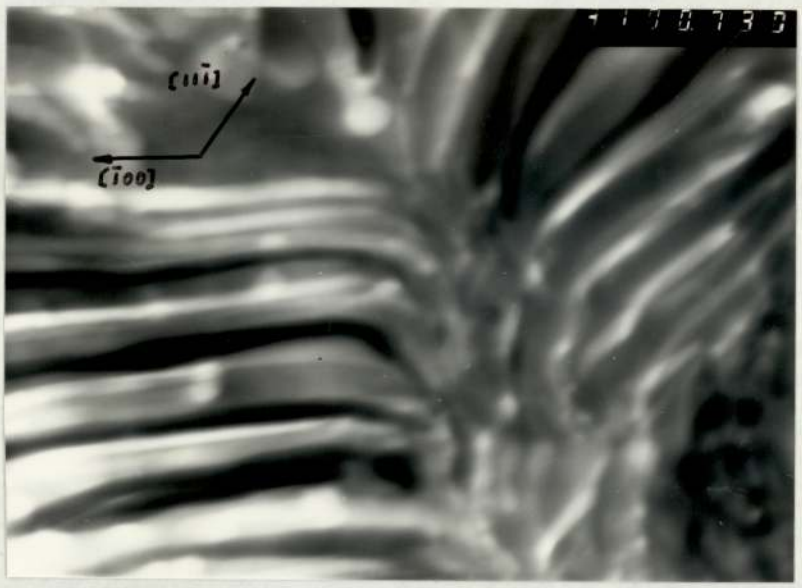

Fig. 94

Transmission electron micrograph of alloy AlZn30Si5 aged at 100°C for 1.5 hrs. x42.4K

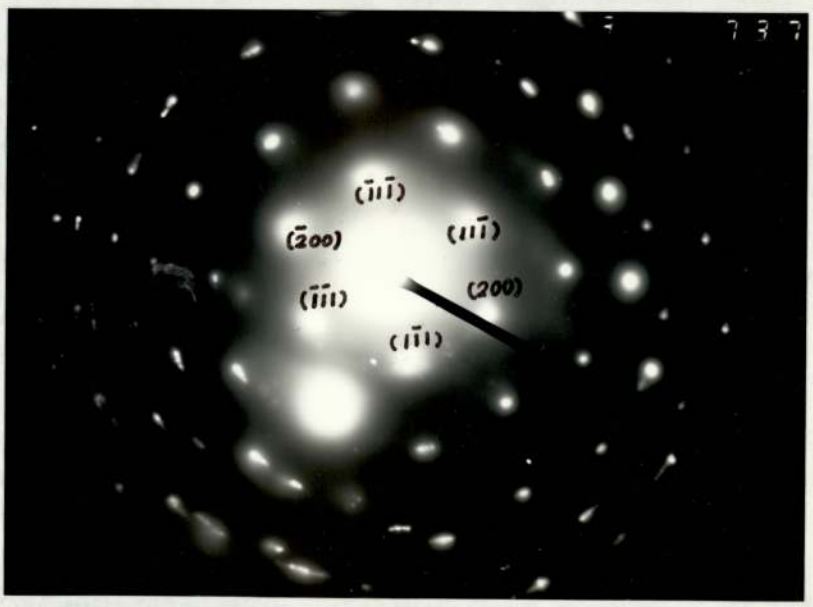

Fig. 95

The electron diffraction pattern from the matrix in Figure 94

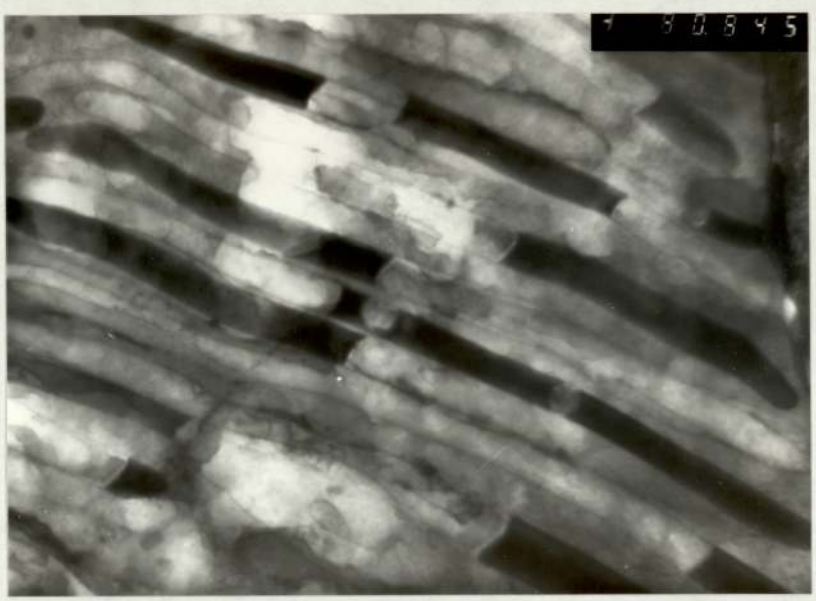

Fig. 96

Transmission electron micrograph of alloy AlZn30Si5 aged at 100°C for 24 hrs showing the segmentation of the zinc-rich precipitates. x34.5K

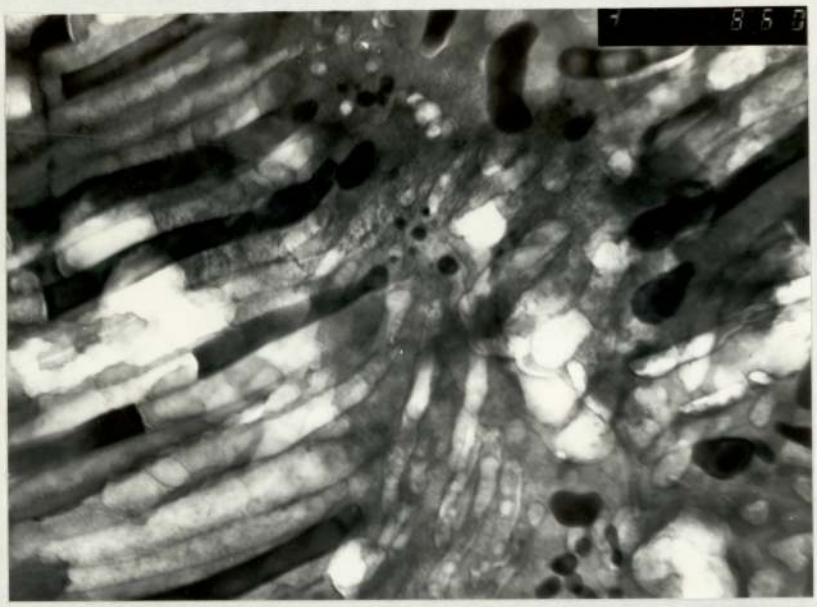

(a)

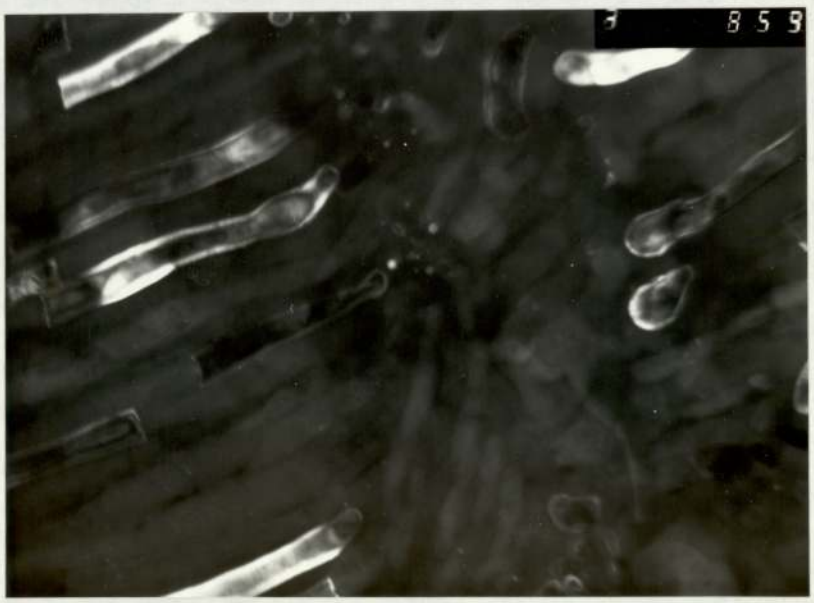

(b)

Fig. 97

Transmission electron micrograph of alloy AlZn30Si5 aged at 100°C for 24 hrs, showing the segmentation of the zinc-rich precipiates. x34.5K

(a) bright field (b) dark field

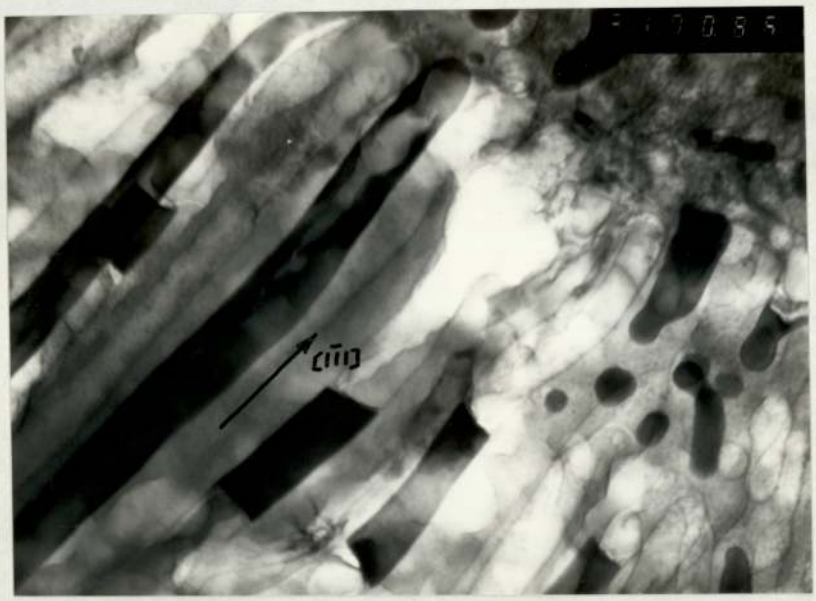

(a)

(b)

Fig. 98

Transmission electron micrograph of alloy AlZn30Si5 aged at 100°C for 24 hrs, showing the segementation of the zinc-rich precipitates. x42.4K

(a) bright field (b) dark field

Fig. 99

Transmission electron micrographs of alloy AlZn30Si5 aged at 100°C for 24 hrs, showing the segmentation of the zinc-rich precipitates

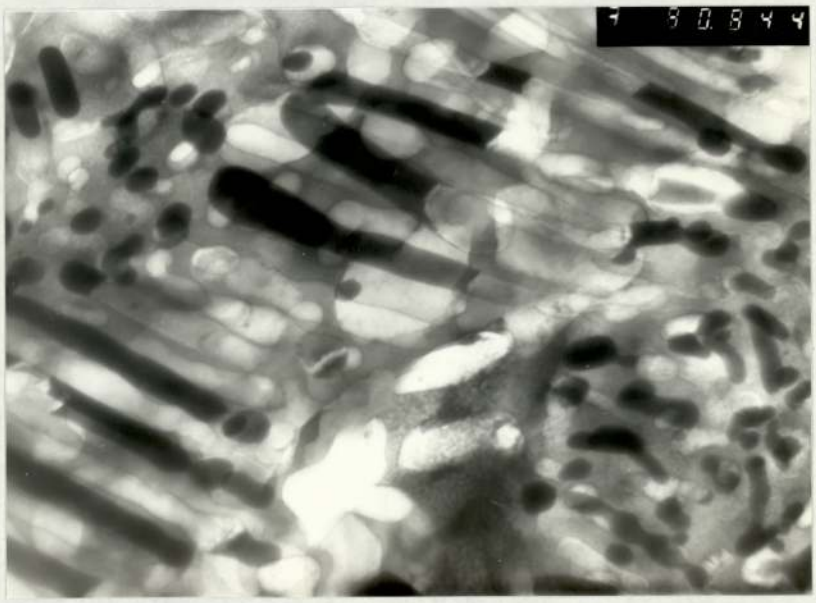

Fig. 100

Transmission electron micrographs of alloy AlZn30Si5 aged at 100°C for 24 hrs, showing the seg-mentation of the zinc-rich precipitates. x34.5K

Fig. 101

Transmission electron micrograph of alloy AlZn30Si5 aged at 100°C for 24 hrs, not showing the segmentation of the zinc-rich precipitates. x130K

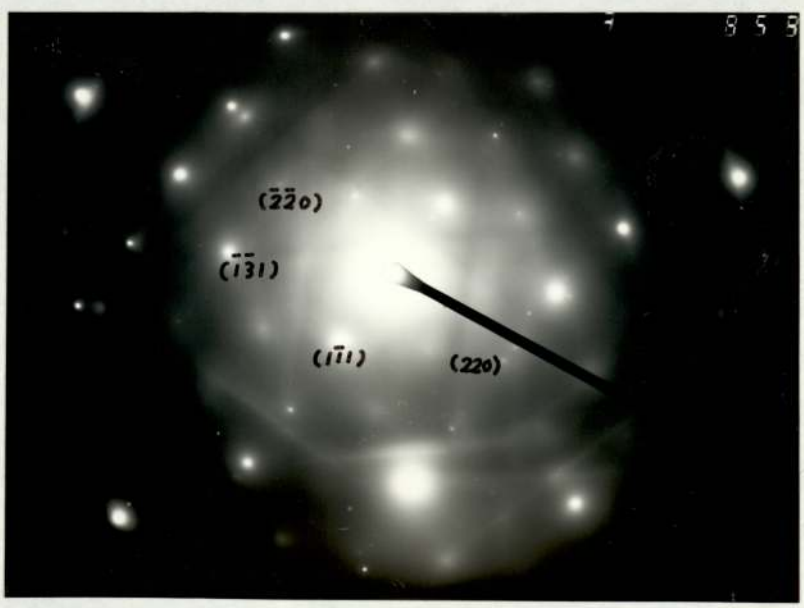

Fig. 102

The electron diffraction pattern from the matrix in Figure 97

(a)

(b)

Fig. 103

Transmission electron micrographs of alloy AlZn30Si5 aged at 100°C for 24 hrs. x86.5K.

(a) bright field (b) dark field

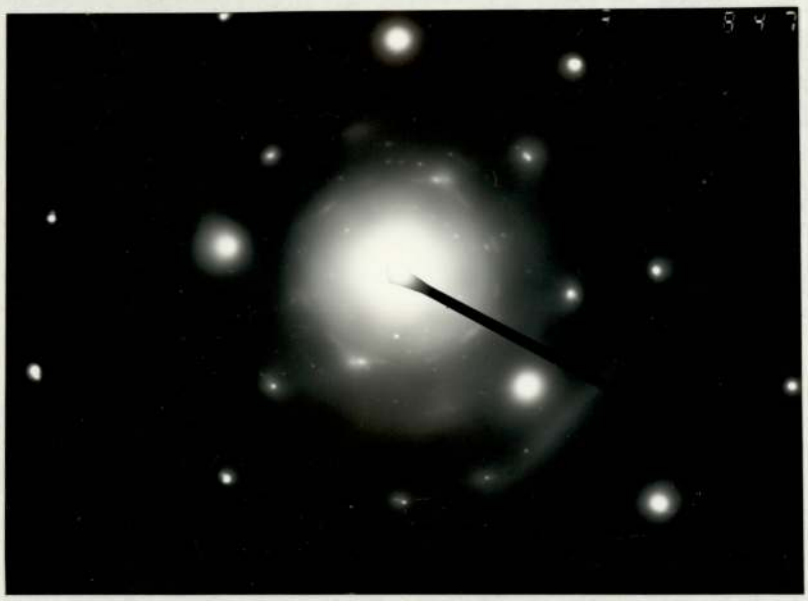

Fig. 104
The electron diffraction pattern from Figure 103 (a)

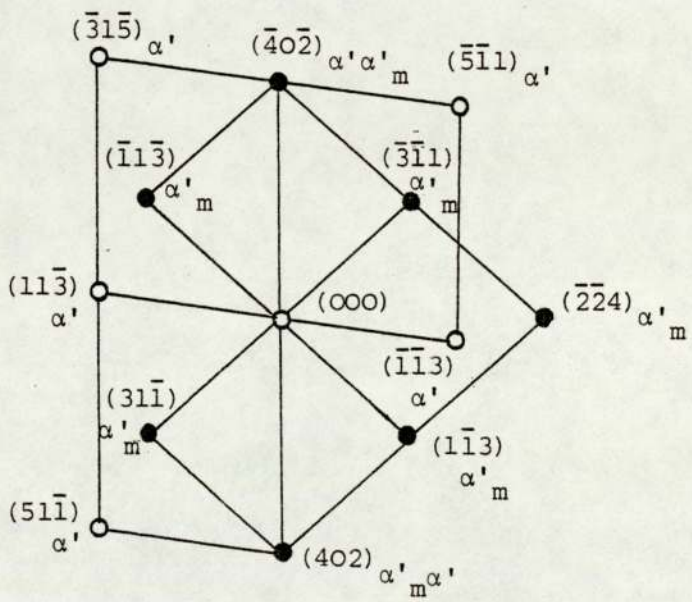

Fig. 105

The index of the electron diffraction pattern in Figure 104

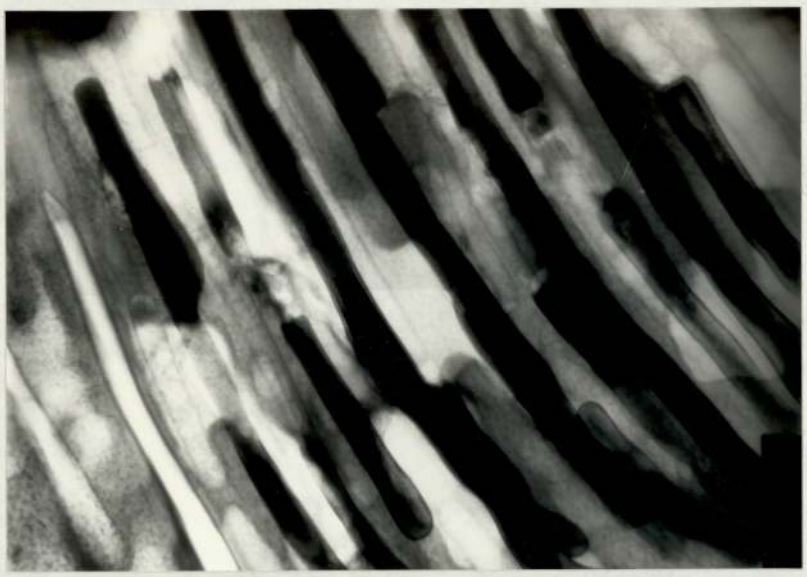

(a)

(b)

Fig. 106

Transmission electron micrographs of alloy AlZn30Si5 aged at 100°C for 24 hrs.

(a) bright field (b) dark field

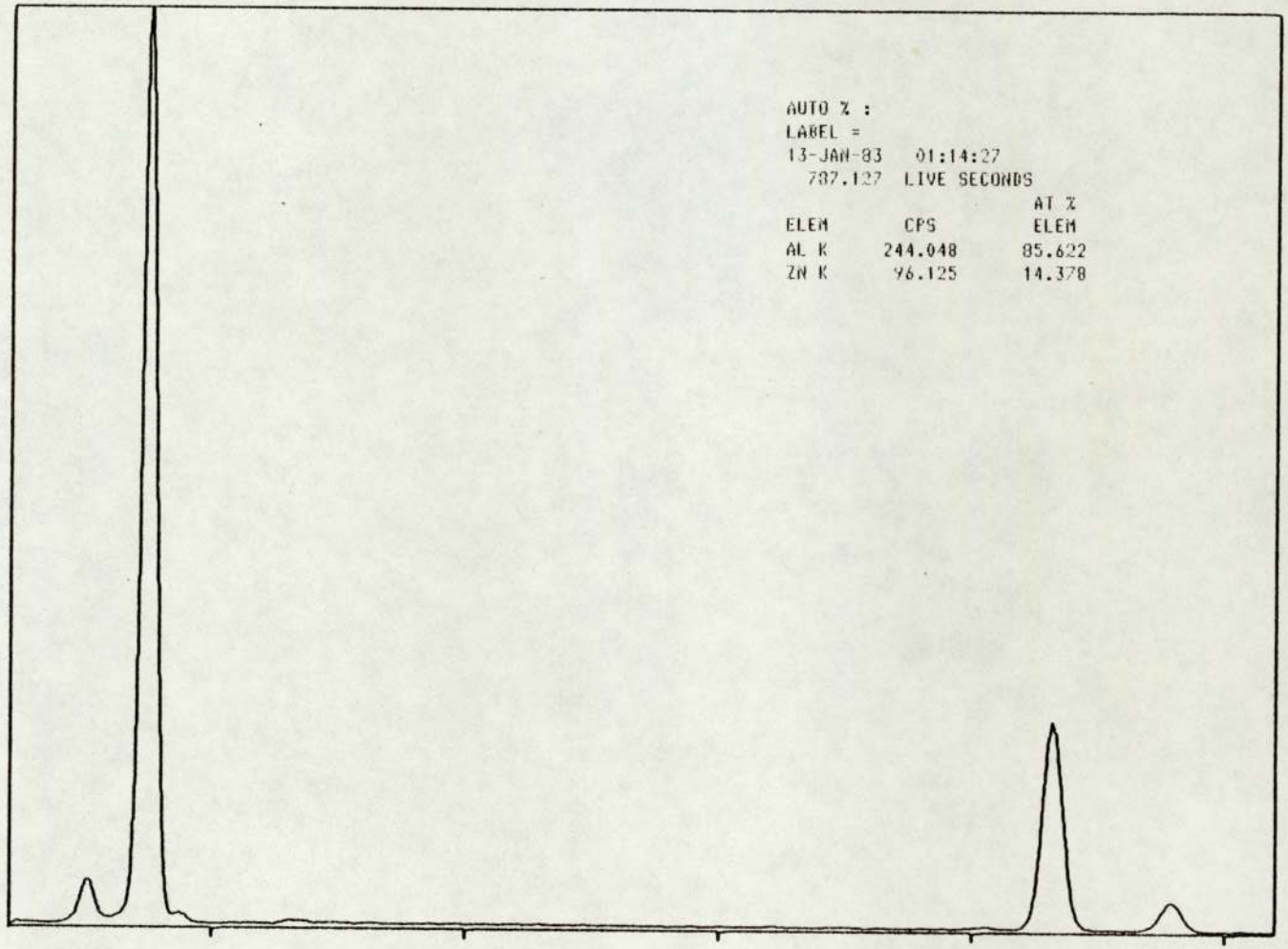

Fig. 107 The dispersive X-ray energy spectrum from the matrix in Figure 106 (a) obtained from STEM

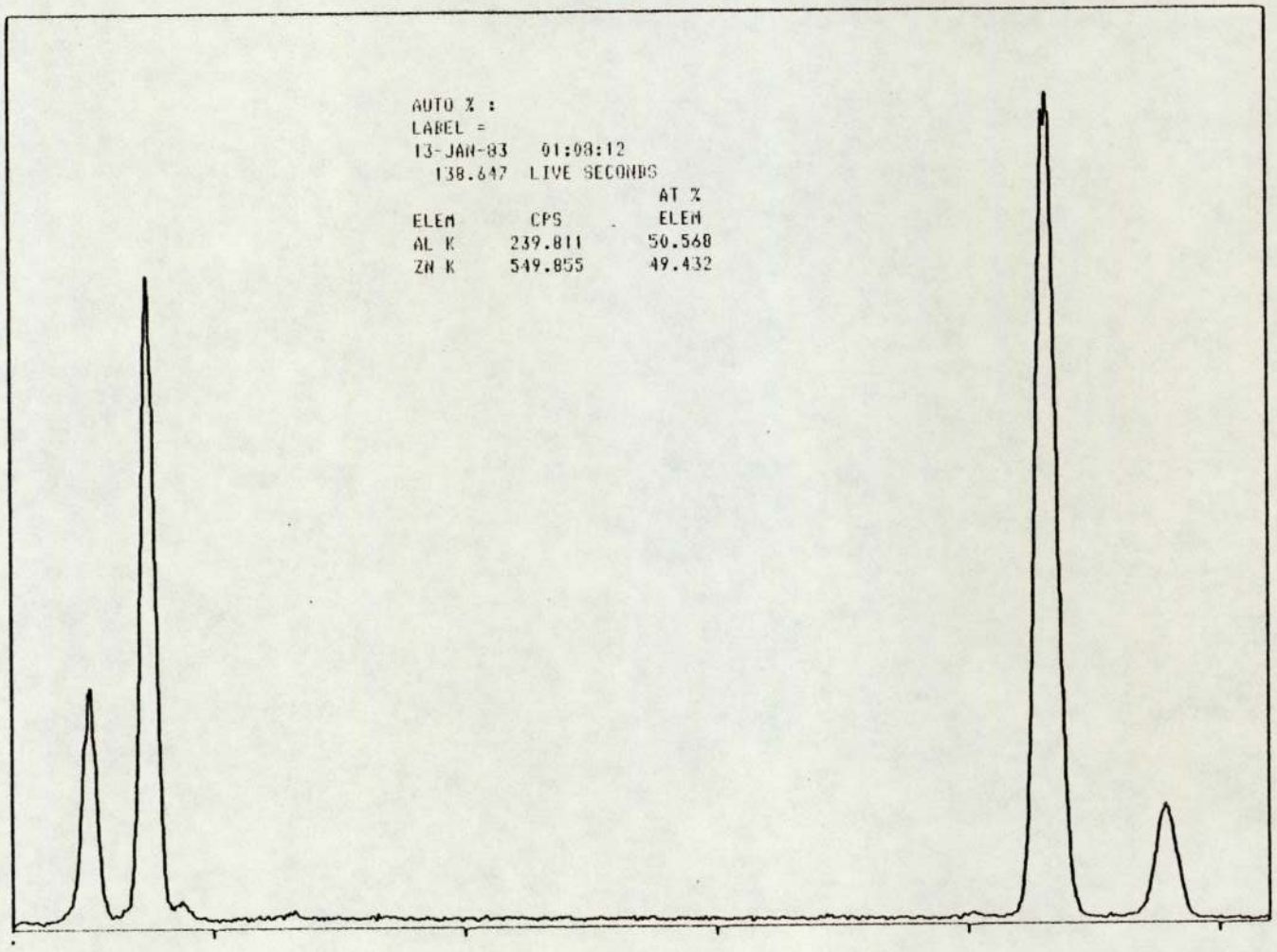

Fig. 108 The dispersive X-ray energy spectrum from the precipitate in Figure 106(a) obtained from STEM

structure only were found, even from areas with particulate morphology for the precipitates, e.g. Figure 103.

The chemical compositions of both the matrix phase and the oriented zinc-concentrated α'_m phase were determined using quantitative EDS analysis in STEM mode. Figure 106 shows the area where the chemical analyses were made. Figure 107 shows the spectrum and analysis of the matrix phase and Figure 108 that from the zinc-rich α'_m phase.

4.5.2 Alloy AlZn60Cu3Si2

Transmission electron microscopy investigations were carried out during the 100°C ageing process for alloy AlZn60Cu3Si2. Special care was taken in the first 5 minutes ageing at 100°C. The lamellar structure was not detected before 1.45 minutes. After 2 minutes, the lamellar structure and a two-phase equiaxed structure in the micrographs (Figures 109,110).

After ageing for 8.5 minutes at 100°C, two different modes of precipitation were observed, as seen in Figures 111,113 General precipitation was typically shown on one side of boundary and discontinuous precipitation on the other. The diffraction pattern from the matrix is shown in Figure 112.

According to the hardness and X-ray diffraction results, the alloy was at G.P.zone stage after 8.5 minutes ageing at 100°C. In the continuous precipitation region, the bigger particles were about 300 Å in size, the composition fluctuation in G.P.zones was clearly observed in Figures 111 and 113. On the other side, the lamellar grew parallel to the $[1\bar{1}1]$ direction in a $\langle 011 \rangle$ zone of matrix phase. The average

interlamellar spacing was 150 Å from the three micrographs of Figures 111,113,114.

The small precipitate particles grew on further ageing, and after 15 minutes were about 650 Å diameter. More lamellae had formed from the matrix phase (Figure 115). The increase in particle size indicated that they were going to lose their coherency with the matrix phase, while the phase was forming according to the X-ray diffraction results, shown in Figures 76 and 78.

After 24 minutes ageing at 100°C, the lamellar structure was well developed in most parts of the specimen both on grain boundaries and inside the matrix. The lamellae were found growing in two apparent directions $[1\bar{1}1]$ and [200] in a <011> zone of the matrix. The micrograph and the diffraction pattern from the matrix are shown in Figures 116 and 117. This result is consistent with <111> growth.

Considerable coalescence and some spheroidization of the precipitate rows had occurred after ageing for 18 hours at 100°C. The formation of the second transitional phase α'_m was observed as f.c.c. zinc-concentrated dark lamellae in matrix phase. The mechanism of the formation of α'_m phase was similar to that in Zn-Al-Si system presented before. In Zn-Al-Cu-Si system after 18 hours ageing at 100°C, the oriented shiftings of Zn atoms inside the α''_m lamellae lead to the formation of the α'_m phase of f.c.c. structure. The shifting traces were observed in the lamellae, but there was no distinct boundary at the

end of the lamellae with the shifting of Zn atoms, no segmentations were observed, as shown in Figure 118.

Also seen in Figure 118 were very wide lamellae structure of 5μm width with spacing of the lamellae about 2μm. It was observed that the lamellae in a single family formed from a single initial lamella by a branching mechanism.

Precipitates of ε phase were detected after 18 hours ageing at 100^{o}C. Bright and dark field electron micrographs are shown in Figure 119. The diffraction pattern of the area is shown in Figure 120, where the encircled diffraction spot gave the centred dark-field image. It was found that the precipitate of phase was rod shaped with long edges parallel to the $[01\bar{1}]$ direction in a $<\bar{1}22>$ zone. The chemical composition was determined, using quantitative EDS system in the Scanning Electron Microscopy.

The energy dispersive X-ray spectrum, and the composition are shown in Figure 121. This composition lies in the ε phase field in the Zn-Al-Cu-Si quartenary phase diagram with 0.1% Si, as seen in Figures 51 to 56.

The electron micrograph of this alloy after 48 hours ageing at 100^{o}C are shown in Figures 122 and 123. The spacing of the lamellae had increased to 4μm. The volume fraction of the wide lamellae in the specimen was found increased considerably. This coarsening gave rise to a further decrease in hardness.

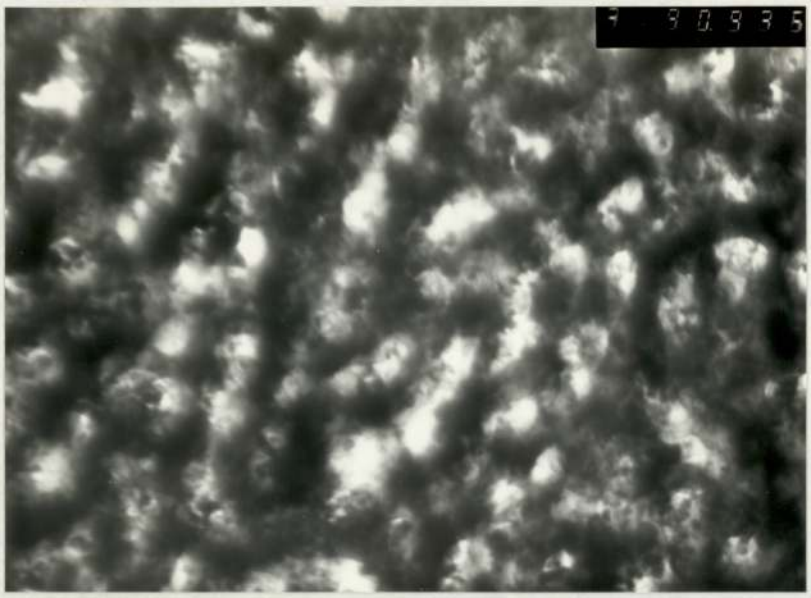

Fig. 109

Transmission electron micrograph of alloy AlZn6OCu3Si2 aged at 100°C for 2 minutes, showing a two-phase equiaxed structure. x39K.

Fig. 110

Transmission electron micrograph of alloy AlZn6OCu3Si2 aged at 100°C for 2 minutes showing the lamellae structure. x86.5K.

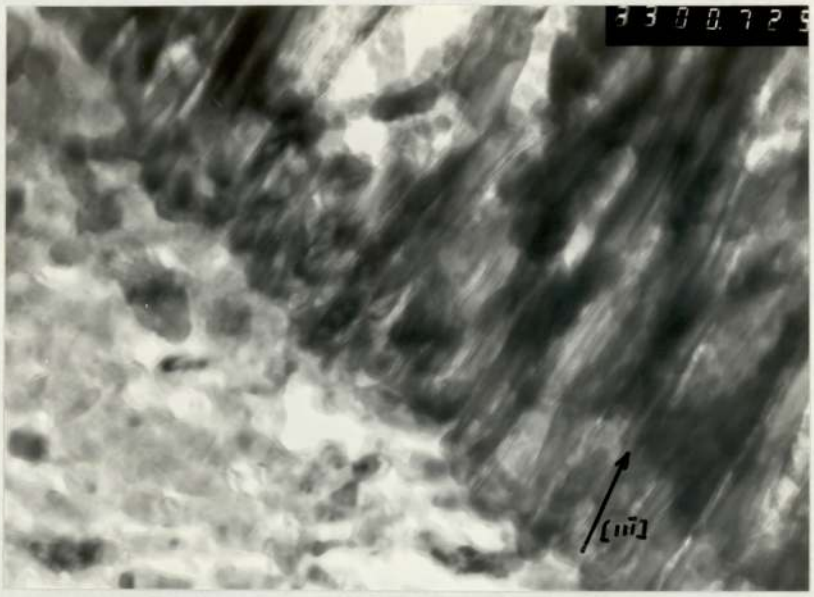

Fig. 111

Transmission electron micrograph of alloy AlZn60Cu3Si2 aged at 110°C for 8.5 minutes. x130K.

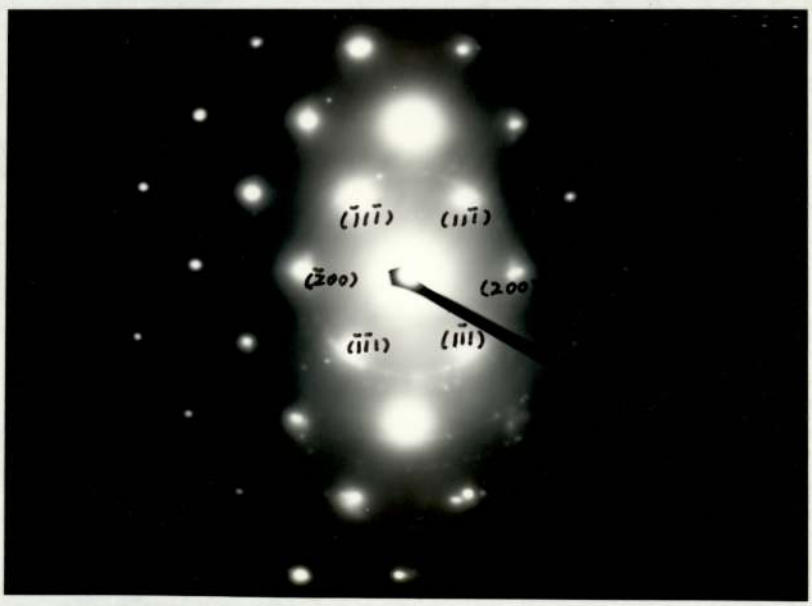

Fig. 112

The electron diffraction pattern from the matrix in Figure 111

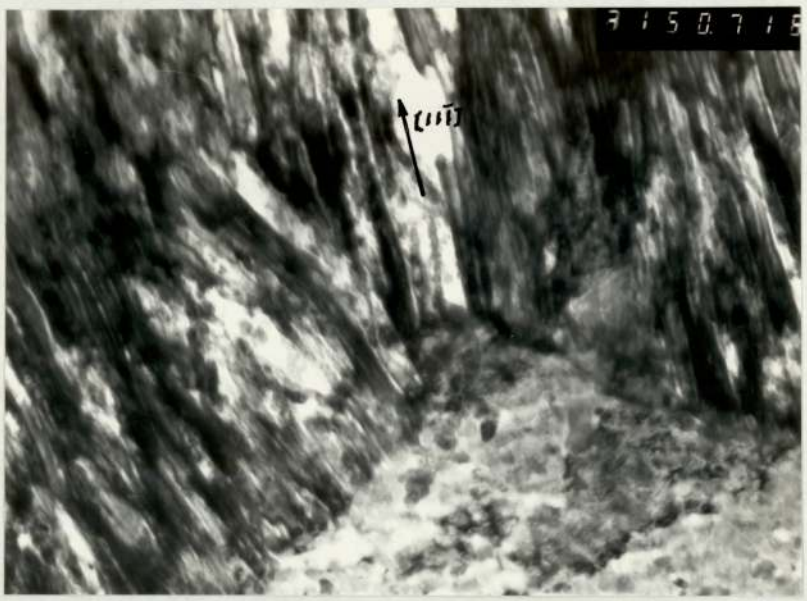

Fig. 113

Transmission electron micrograph of alloy AlZn6OCu3Si2 aged at 110°C for 8.5 minutes. x64.8K

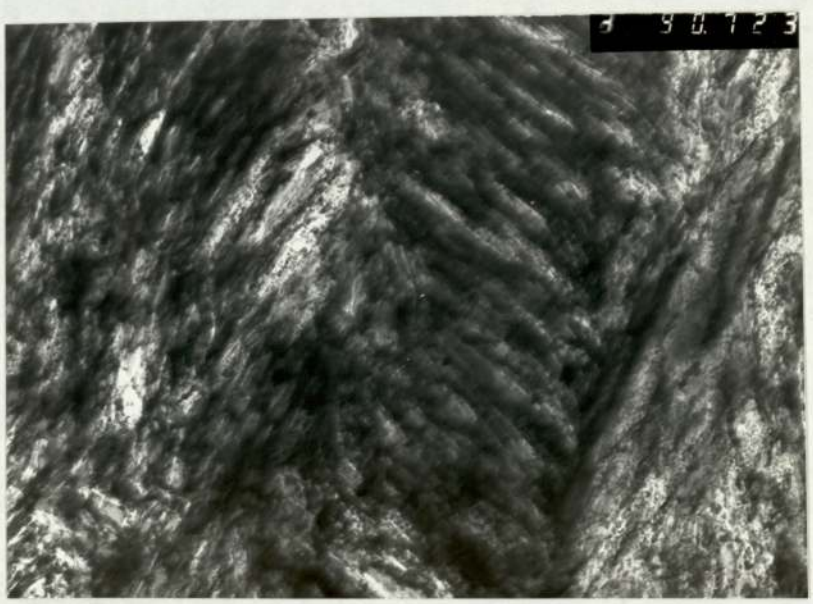

Fig. 114

Transmission electron micrograph of alloy AlZn6OCu3Si2 aged at 100°C for 8.5 minutes. x78.9K

Fig. 115

Transmission electron micrograph of alloy AlZn60Cu3Si2 aged at 100°C for 15 minutes. x108K.

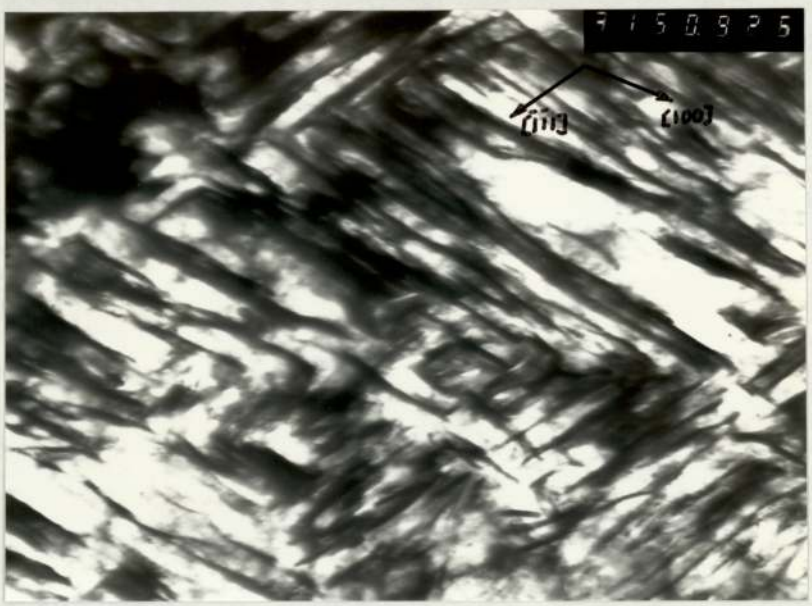

Fig. 116

Transmission electron micrograph of alloy AlZn60Cu3Si2 aged at 100°C for 24 minutes. x64.8K

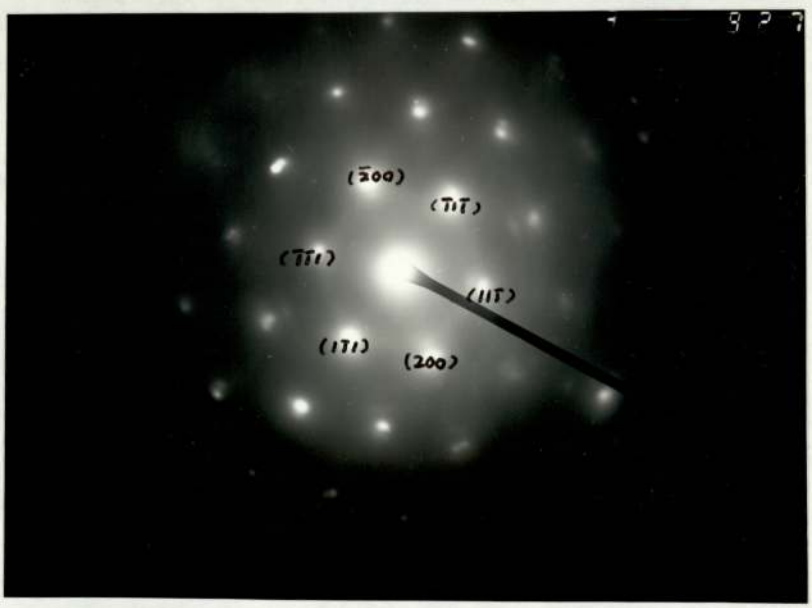

Fig. 117

The electron diffraction pattern from the matrix in Figure 116

Fig. 118

Transmission electron micrographs of alloy AlZn60Cu3Si2 aged at 100°C for 18 hours

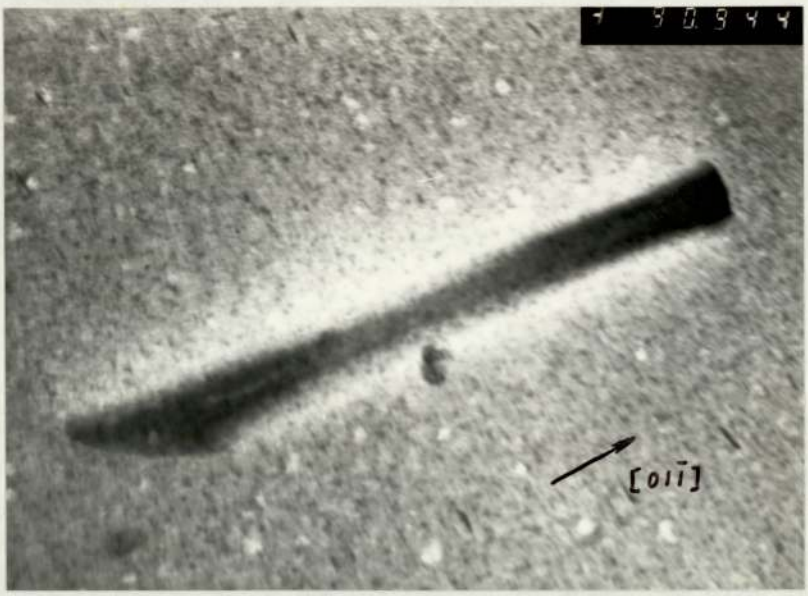

(a)

(b)

Fig. 119

Transmission electron micrographs of alloy AlZn60Cu3Si2 aged at 100°C for 18 hrs, showing the ε precipitate.

(a) bright field (b) dark field

Fig. 120
The electron diffraction pattern from Figure 119(a)

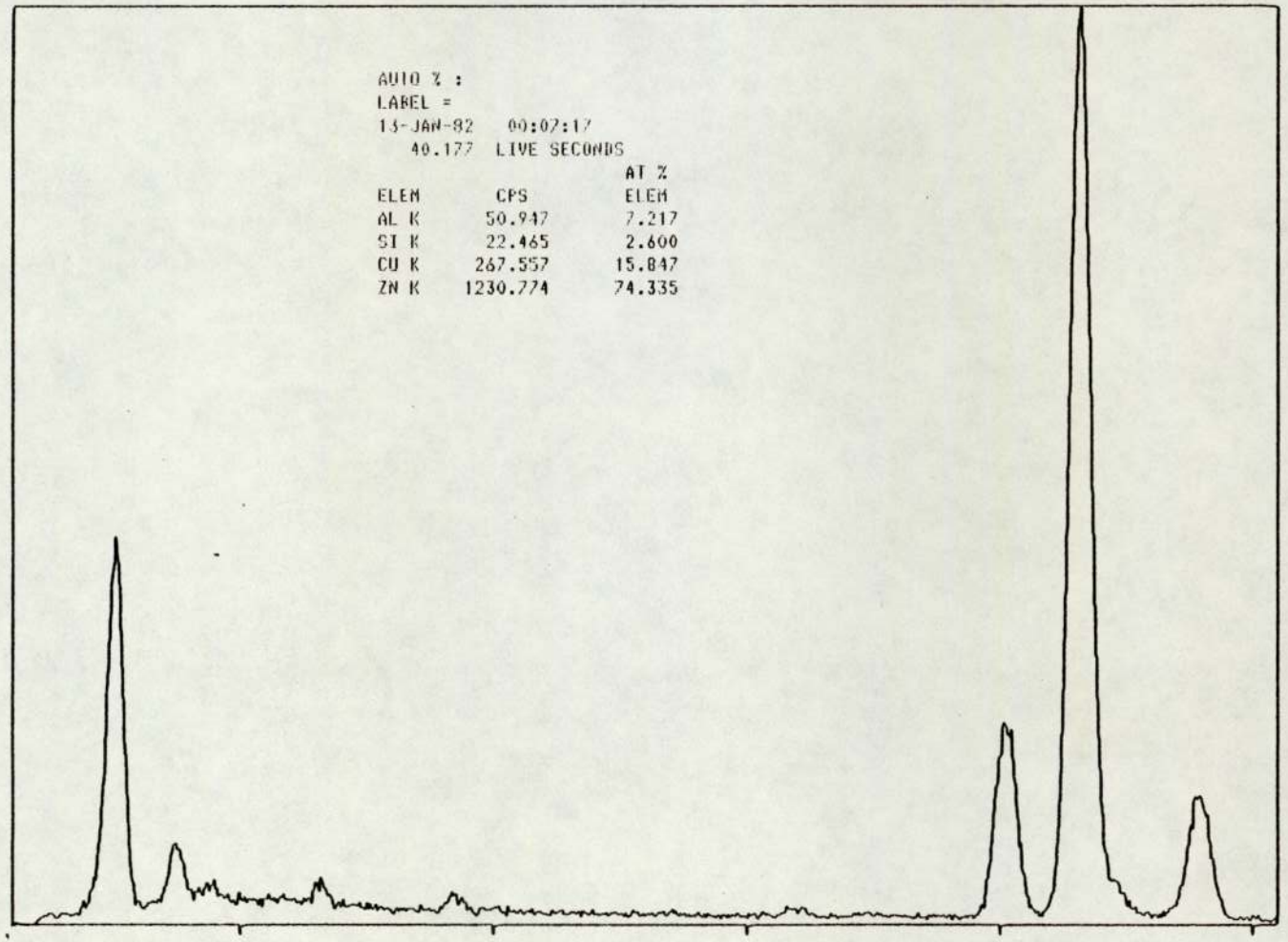

Fig. 121 The dispersive X-ray energy spectrum from ε precipitate in Figure 119(a)

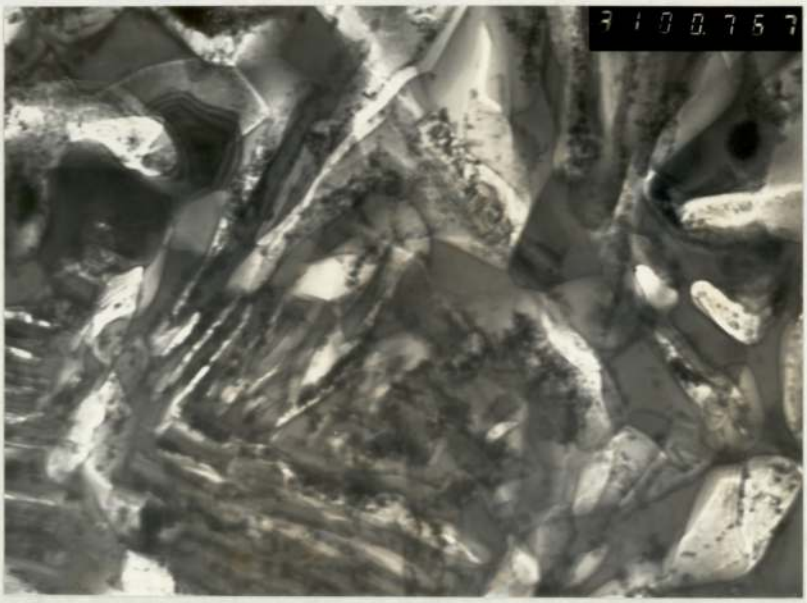

Fig. 122

Transmission electron micrograph of alloy AlZn6OCu3Si2 aged at 100°C for 48 hrs. x42.4K

Fig. 123

Transmission electron micrograph of alloy AlZn6OCu3Si2 aged at 100°C for 48 hrs. x42.4K

It was found that the spacing of the lamellae decreased in the early stage of ageing and then increased in the over-ageing state, and therefore caused the increase and then decrease in hardness of the alloy.

4.6 Physical and Mechanical Properties

4.6.1 Dimensional stability

From the measurement of the initial length (as-quenched condition) and the length change on ageing for Zn-Al-Si alloys, the linear expansion or contraction due to ageing was calculated. The results of the percent of the linear expansion versus logarithm of time of ageing are shown in Figure 124. With alloys AlZn10Si5, AlZn30Si5, AlZn60Si5 and AlZn95Si2, a contraction occurred during the first stages of ageing. Alloys AlZn10Si5 and AlZn75Si2 expanded on ageing, but the others continued to contract until stability was reached. All these alloys except alloy AlZn10Si5 became reasonably stable after 20 hours ageing at 150^{o}C, but the total changes were small in each case.

4.6.2 Impact and tensile strength

The ultimate tensile strengths (U.T.S.) and 0.2% yield strengths were determined from the stress curves and are listed in Table 37, together with the elongation and impact data measured under the same experimental condition, i.e. after 100 hours ageing at 100^{o}C.

Both alloy AlZn95Si2 and alloy AlZn90Cu3Si fractured in a brittle mode at 112 N/mm^2 and 164 N/mm^2 respectively and no 0.2% yield strengths were obtained.

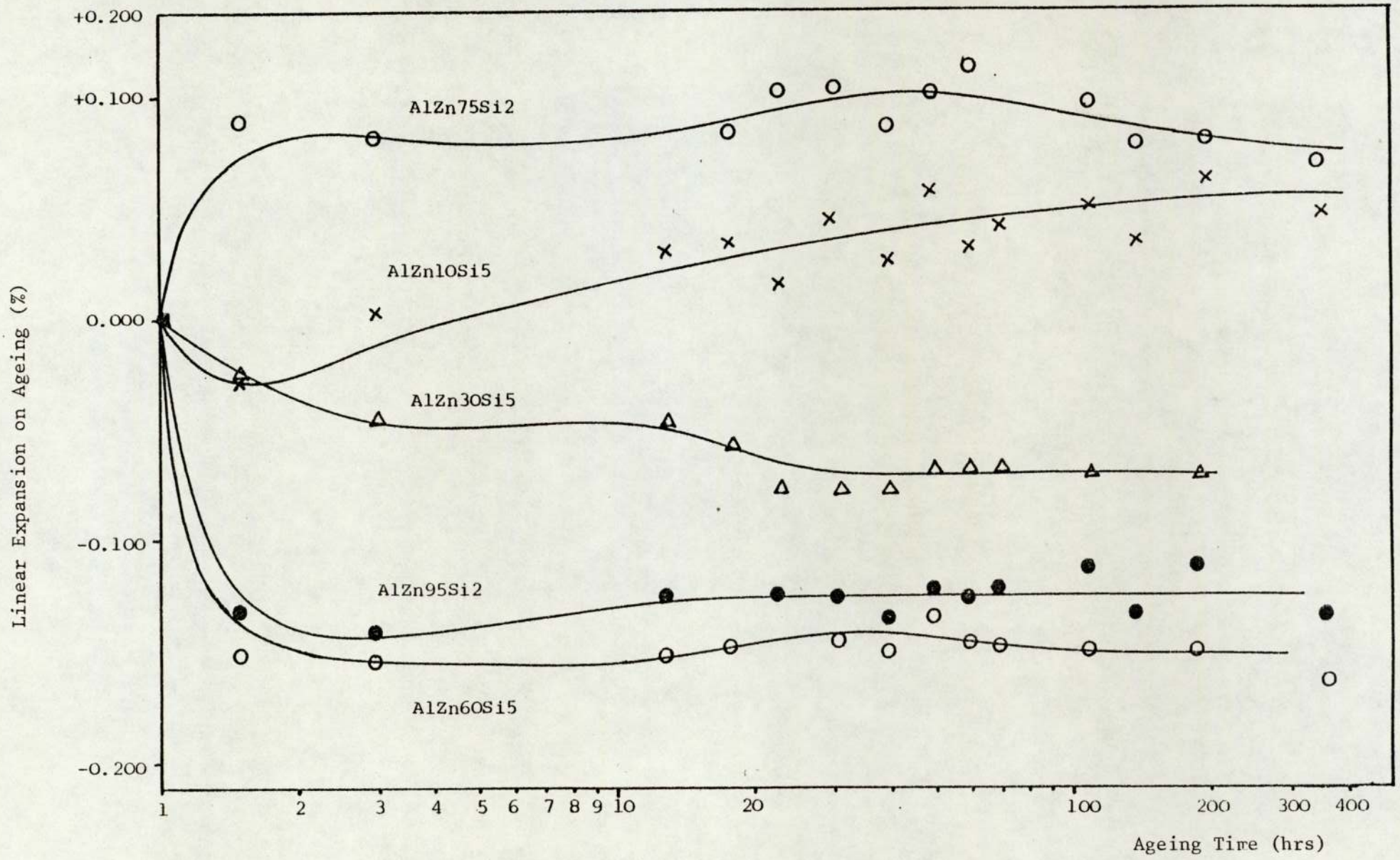

Fig. 124 Dimensional stability of alloy ZnAlSi after solution treatment, quench and ageing at 150°C.

Table 37

MECHANICAL PROPERTIES OF ALLOY Zn-Al-Si AND Zn-Al-Cu-Si

(AFTER 100 HRS AGED AT 100°C)

	Properties			
	Tensile Strength σ_{UTS} (N/mm^2)	0.2% Yield Strength (N/mm^2)	Elongation(%)	Energy Absorbed Impact (J)
AlZn10Si5	190	120	10.1	37
AlZn30Si5	296	262	6	6
AlZn60Si5	286	278	2.5	3
AlZn75Si5	119	109	7.3	3
AlZn95Si5	115	-	1.9	3
AlZn10Cu3Si2	218	77	9	8
AlZn30Cu3Si2	272	223	3.2	2
AlZn60Cu3Si2	321	267	2.3	2
AlZn75Cu3Si2	239	112	9.3	2
AlZn90Cu3Si2	164	-	1.2	2

4.6.3 Wear property

The wear rates of alloys of both systems in both as-cast and heat treated condition were listed in Tables 38,39.

The pins of AlZn60Si5 and AlZn75Si5 melted during the testing under so called 'severe wear'conditions, and it was not possible to obtain the wear rates of these two alloys.

It was found that the wear resistance of alloys in the Zn-Al-Cu-Si system were higher than those of the Zn-Al-Si system. In both systems, heat treatment improved the wear resistance of the alloys tested. In each system, the alloys of monotectoid composition were found to have lower wear rate, viz. about 0.4 x $10^{-8} cm^3/cm$ compared with the Al-rich and eutectoid alloys or cast iron. Little change in wear rate was observed when the load increased from 1 kgf to 3 kgf, as shown in Table 40.

Table 38

The Wear Rate ($x10^{-8}cm^3/cm$) for Zn-Al-Cu-Si System and Cast Iron with 2kgf Load and 0.84 m/s.

	As-Cast	Heat Treated
AlZn10Cu3Si2	2.4	2.2
AlZn30Cu3Si2	3.3	1.9
AlZn60Cu3Si2	1.9	1.7
AlZn75Cu3Si2	2.4	2.2
AlZn95Cu2Si2	4.8	4.5
Cast Iron	2.6	-

Table 39

The Wear Rate ($x10^{-8}cm^3/cm$) for Zn-Al-Si System with 2kgf Load and 0.84 m/s.

	As-Cast	Heat Treated
AlZn10Si5	3.2	3.3
AlZn30Si5	3.8	1.8
AlZn60Si5	-	-
AlZn75Si2	-	3.0
AlZn95Si2	6.7	6.1

Table 40

The Wear Rate of Alloy AlZn60Cu3Si2 with Different Loads

Load (kg_f)	Wear Rate ($x10^{-8}cm^3/cm$)
1	1.8
2	1.7
3	1.8

5 DISCUSSION

5.1 Phase diagram of Zn-Al-Si

The isothermal section in Figures 51-56 show the simplicity of this ternary system compared with that of Zn-Al-Cu. There are intermetallic phases introduced by adding silicon to the Zn-Al system. The silicon exists as a terminal solid solution with limited solid solubility of aluminium and zinc, and this phase, shown as σ in isothermal section, is in equilibrium with the phases introduced by the Zn-Al binary.

The isothermal sections are characterised by two enlarging three-phase fields of $\alpha+\beta+\sigma$, and $\beta+\eta+\sigma$ with decreasing temperature. When the temperature fell to 266°C, the phase transformation $\beta \rightarrow \alpha+\eta$ occurred. Below this temperature, β-phase disappeared, and the three phase $\alpha+\eta+\sigma$ formed. Only the Zn-rich η phase was found to change very little in composition.

A vertical section through the Zn-Al-Si diagram at 0.2% Si was constructed, and is shown superimposed on the binary Zn-Al diagram in Figure 125. Silicon appears to have a minor effect on the phase boundaries, but stabilizes the β phase to lower temperature. At temperatures below 266°C and 275°C, the isothermal section of the phase diagram must have the form of a typical ternary phase diagram, as shown in Figure 126. There must exist a single phase field β, three binary phase fields $\alpha+\beta$, $\beta+\eta$ and $\alpha+\eta$ and one ternary phase field $\alpha+\beta+\eta$. All these phase fields contain 0% to 2% of Silicon only, but

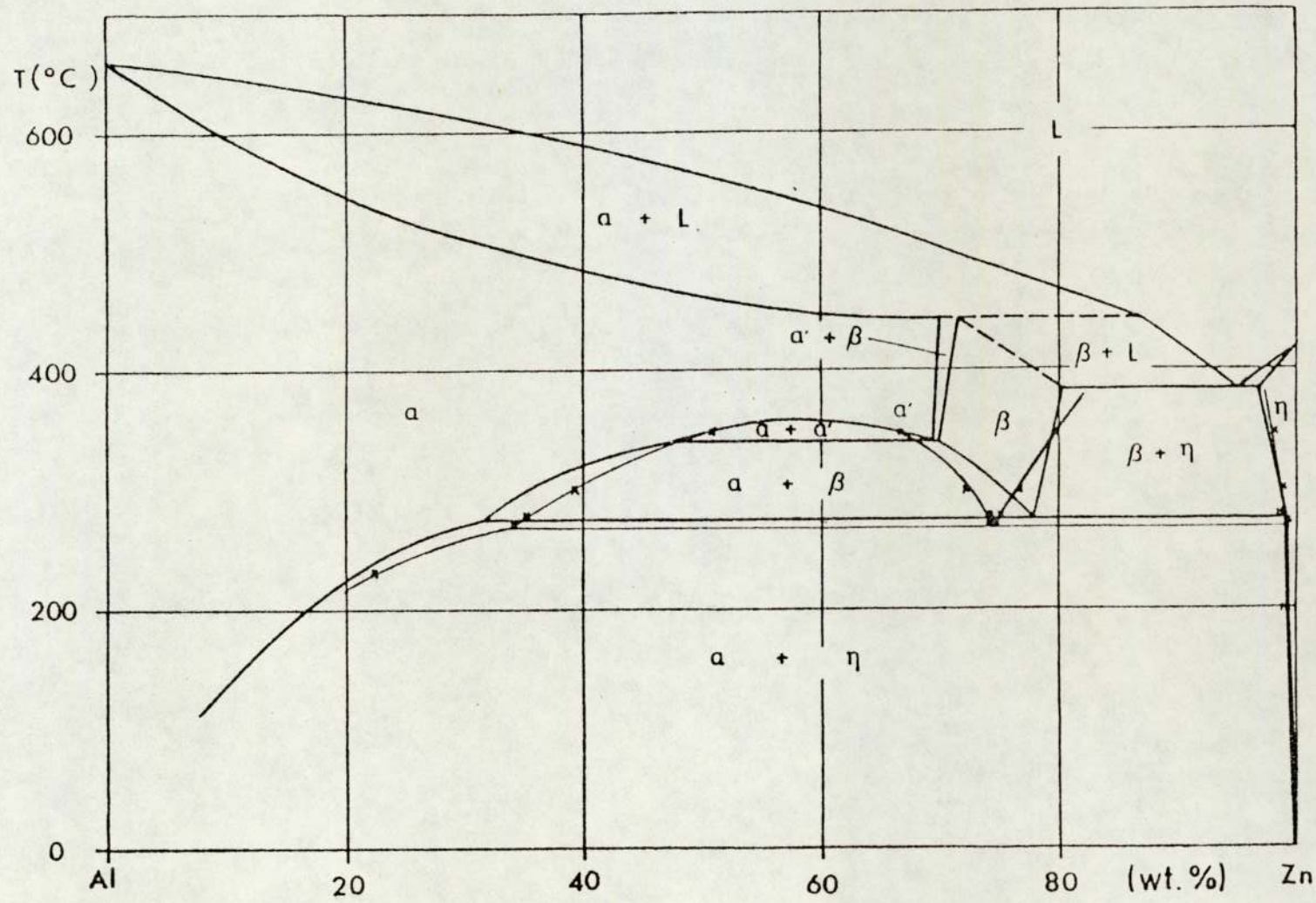

Fig.125 Vertical section through the Zn-Al-Si diagram at 0.2% Si

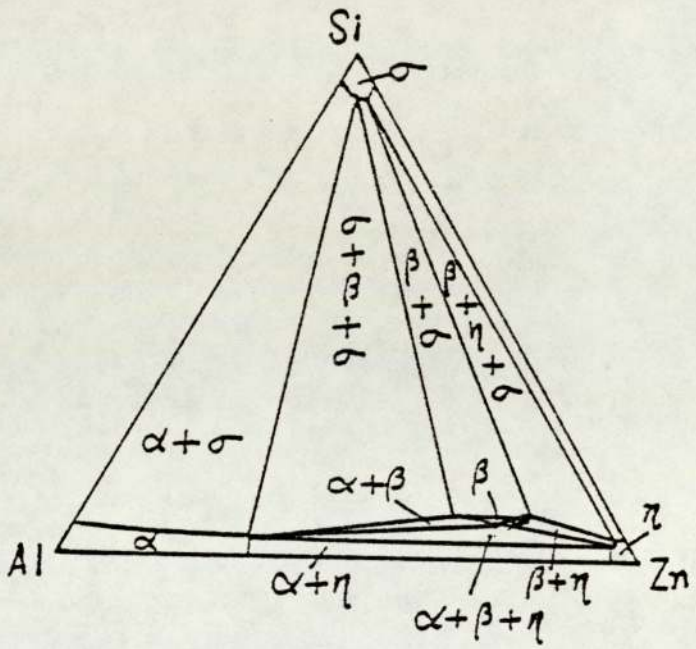

Fig. 126
The typical ternary phase diagram in temperatures in range 266°C - 275°C

due to this low solubility of Si in α, β and η, the $\alpha+\beta+\eta$ is extremely narrow and would be very difficult to detect experimentally.

The isothermal sections have shown that the compositions of the Si-rich corners of both $\alpha+\beta+\sigma$ and $\beta+\eta+\sigma$ three phase fields changed slightly with temperature. They were of composition about 96% Si. This result contradicts early work[15] which considered that aluminium and zincwere insoluble in silicon, but repeated determinations gave the same result. It is interesting that the solubility of Zn in σ exceeded that of Al, whereas it would be expected that the higher valency solute would be accommodated more easily in the covalent silicon structure. This effect may be due to zinc dissolving interstitially in the σ phase.

The lattice parameter of the diamond cubic structure was measured as 5.437 Å in alloys containing 69.7%$^{Zn}_{equilibrium}$ at 272°C. This is substantially higher than the figure for pure silicon (5.430 Å) and supports the hypothesis of interstitutial zinc solution which, due to the larger diameter of the zinc atom than the interstitial volume, must expand the σ structure cell.

Sigma phase with higher concentrations of aluminium and low zinc, ZAS 1,ZAS 4, had lattice parameters (5.401 Å and 5.402 Å) smaller than that (5.430 Å) of pure silicon, Table 9, indicating that the aluminium is probably substituted for silicon$^{in}_{,}$ the diamond cubic structure.

Both the Al-Si and Zn-Si phase diagrams show no appreciable solubility of either of these components in silicon, which might imply that Al and Zn together are soluble but each separately is not. However the fact that an Al-Si alloy with 20% Si equilibrated at 350°C contained σ with 2.4% Al by EPMA, shows on the contrary that the presence of zinc decreases the solubility of aluminium in Figure 41.

The two binary phase diagrams which show negligible solubility of Al and Zn in silicon should be redetermined.

Low solubilities of Si were found in all three single phases α, βand η. The solubility of Si in β phase of different compositions is shown in Figure 41. Comparison of the isothermal sections shows that the low solubility of Si in these phases does not change drastically with temperature, so silicon precipition is unlikely to contribute significantly to the hardness of the alloys on quench-ageing.

In the aluminium-rich solid solution α, the lattice parameter decreased from 4.044 Å to 4.021 Å (or 4.024 Å) with increasing zinc up to about 33% Zn. This is to be expected since the atomic radius of zinc is substantially lower than that of aluminium.

Zinc-rich η phase has a close packed hexagonal structure with a_o = 2.675 Å, c_o = 4.961 Å and c_o/a_o = 1.855.

5.2 Zn-Al-Cu-Si phase diagram

The silicon contents of all the phases except σ are so small that the quarternary phase diagram can be adequately

represented by a pseudo ternary or a quaternary section at a nominal 0.1% Si. σ phase is present as an additional phase in all the phase fields but is omitted from this discussion for the sake of clarity.

When the quaternary diagram is represented in this way, there is a very close similarity between the isothermal section of the Zn-Al-Cu-Si system and those of the Zn-Al-Cu system.

The 350°C isothermal section is characterised by a broad two phase field α and β+T' and considerable solid solubilities of copper in α and β phase. The broad phase field α+β with a relatively high Cu content allows precipitation hardening on heat treatment of this Zn-Al based alloy.

At 300°C, two three-phase fields α+T'+β and β+T'+ε, are separated by a two-phase field T'+β. But with falling temperature, the two-phase field T'+β narrows while the copper content in β phase remains at about 2%. The phase relationships in the quaternary Zn-Al-Cu-Si system at 290°C are similar to those in isothermal section of the Zn-Al-Cu ternary phase diagram[71].

The four phase transformation was determined at 285°C as follows :

$$\beta + T \rightleftharpoons \alpha + \varepsilon$$

Five phases, α, β, ε, T and σ co-existed at 285°C, representing a pseudo four phase plane. The phase field T'+β contracted into a line, so that at temperatures

slightly higher than 285°C, T'+β exists, while the α+ε phase field appears just below 285°C. Comparing this phase diagram with that of the Zn-Al-Cu ternary system[71], the addition of small amounts of Si gave rise to only a 3°C decrease in the temperature of the four-phase transformation. No further influence was found.

At 280°C, the two three-phase fields, α+β+ε and β+ε+η were separated by a two-phase field β+ε, but this had disappeared at 275°C. That means a four-phase transformation occurred between 280°C and 275°C to remove the β phase. The Al content of α in equilibrium with ε had decreased. The increase of copper content in η with decreasing temperature should be noted as far as its effect on quench-ageing treatments is concerned. Another four-phase transformation must occur below 275°C in the quaternary Zn-Al-Cu-Si system to eliminate the ε phase in zinc-rich, low copper alloy. Based on the Zn-Al-Cu diagram this must be :

$$\alpha + \varepsilon \rightleftharpoons T' + \eta$$

However although an isothermal section at 230°C was not constructed, the ageing of low copper alloys showed that the episilon phase eventually was replaced by T' phase, so the system did follow closely the Zn-Al-Cu system.

Compared with the phase diagram of the Zn-Al-Cu ternary system, the quaternary phase diagram has a similar construction and nearly the same positions of the phase fields at various temperatures except for the contents of Cu in

the T' phase which are different at 280°C and 275°C. The isothermal sections below 290°C showed a similar sequence of changes to those in the Zn-Al system, i.e. the $\alpha+\beta$ field enlarged and the Al content of α phase increased with decreasing temperature. The movement of the α phase corner closer to the pure aluminium corner may possibly change the mechanism of phase transformations in quench-ageing processes.

The data listed in Tables 7 and 9 give more evidence of the solubility of Al and Zn in silicon. As in the Zn-Al-Si system, the composition of the Si-rich phases in nearly all the specimens at various temperatures was about 96% Si. It was noticed that the solubility of Si in the α phase was generally bigger than that in β, ε, T' and η phases.

The data at 290°C are as follows :

Solubilities of Si	
in β phase	0.08-0.09%
in α phase	0.10-0.32%
in ε phase	0.08-0.09%
in T'phase	0.04-0.07%
in η phase	0.10%

The lattice parameter data in Table 12 shows that the larger the Zn content in Al-rich phase, the smaller the lattice parameters of the Al-rich phase. It was also found that the lattice parameters of α and β phases were very close to each other in the $\alpha+\beta$ phase field which is in agreement with Golda 's result, shown in Figure 3[12].

5.3 Mechanism of Phase Transformations in Zn-Al-Si and Zn-Al-Cu-Si systems

Hardness testing on alloys of the whole composition range in both the Zn-Al-Si and Zn-Al-Cu-Si systems showed that in the Al-rich, monotectoidal and eutectoidal composition ranges, pronounced age-hardening occurred during the ageing processes at various temperatures. Five different mechanisms of age-hardening were revealed by the hardness/time curves, Figures 57-64.

Subsequently, X-ray diffraction examinations were carried out in detail for the five alloys with pronounced age-hardening responses. Eleven sets of X-ray diffractograms and seven fraction transformation curves revealed the distinct mechanisms of phase transformations in both the systems.

Two typical structural changes occurring as a result of quench ageing processes were observed on the transmission electron microscopic studies.

Based on the X-ray diffraction examination, correlating with the results of hardness testing and TEM studies, the mechanisms of phase transformations were deduced as follows.

5.3.1 Zu-Al-Cu-Si system

5.3.1.1 Alloys of Monotectoid and eutectoid compositions

The ageing process in supersaturated solid solutions of both Al$_{60}$Zn$_{3}$Cu$_{2}$Si and Al$_{75}$Zn$_{3}$Cu$_{2}$Si involved three stages, on ageing at various temperatures. In the first stage, the Al-rich terminal eutectoid α_T' phase is formed by a cellular reaction:-

$$\beta\ (+\sigma) \rightarrow \alpha'_T + \varepsilon + \eta\ (+\sigma) \quad \text{for eutectoid alloy}$$

or: $\alpha'_S\ (+\sigma) \rightarrow \alpha_T + \varepsilon + \eta\ (+\sigma)$ for monotectoid alloy

The occurrence of a cellular reaction in a discontinuous formation mode was verified by the electron microscopic investigation. The lamellae were observed after 2 minutes ageing at 100°C in alloy AlZn60Cu3Si2. Discontinuous precipitates were observed at grain boundaries in the as-quenched alloy AlZn75Cu3Si2, as shown in Fig. 81. After 30 minutes ageing at 100°C, the discontinuous precipitates had grown larger, and are shown in Fig. 82. For alloys of monotectoid composition, this kind of discontinuous precipitation was reported to form along the grain boundaries on ageing at room temperature for 4 hours [97].

The X-ray diffraction peaks of the supersaturated β or α'_S phases reduced with ageing time, while the peaks of α'_T phase of lower zinc content appeared separately from the peaks of β and α'_S at lower Bragg angles on the X-ray diffractograms, accompanied with the development of peaks from the ε and η phases.

This first stage of phase transformation was observed in all X-ray diffractograms of alloys AlZn60Cu3Si2 and AlZn75Cu3Si2 at various temperatures, shown as Figures 76, 80, 83. Among these, Figures 76, 77 and 80 especially showed the first two stages of phase transformation on 70°C and 100°C ageing of alloy AlZn60Cu3Si2 and on 100°C ageing of alloy AlZn75Cu3Si2. The hardness/time curve of alloy AlZn60Cu3Si2, aged at 100°C showed a peak corresponding to this first stage (Fig. 68).

The second stage of the phase transformation, i.e. the spinodal decomposition of the Al-rich terminal eutectoid α_T' phase, occurred in both alloys after the first four-phase transformation, i.e. the cellular reaction, as the following sequence:

$$\alpha_T' \longrightarrow \text{G.P. zones} \begin{cases} \nearrow \alpha_m''^{Rh} \rightarrow \alpha_m'^{f.c.c.} \rightarrow \eta \\ \searrow \alpha'' \rightarrow \alpha' \longrightarrow \alpha_f \end{cases}$$

In the metastable phase α_T', small fluctuations in composition that produced the first transitional phase α_m'' in equilibrium with the matrix α'' phase, caused the total free energy to decrease. So call 'up-hill' diffusion leading to spinodal decomposition took place. A fine-scale clustering of zinc atoms to form G.P. zones then developed. Contrast changes similar to that expected from G.P. zones were observed after the cellular reactions by TEM examination, as shown in Figure 111. The hardness/time curve showed an increase in hardness at 8.5 minutes (Figure 61), while the X-ray diffraction peak of the α_T' phase did not change detectably in size or position during that period of ageing.

The formation of the G.P. zones was followed by the precipitation of the transitional phase α_m'' and α_m'. The first transitional phase α_m'' was found to form homogeneously from the G.P. zones after 24 minutes ageing at 100°C, as shown in electron micrograph Figure 116. On the X-ray diffractogram, the peak from the α_m'' phase occurred separately from the peak of α_T' phase, because the concentration of smaller zinc atoms within the coherent precipitates caused a lattice contraction. The reported rhombohedral distortion

of the structure cell was manifested by an elongation of precipitates parallel to {111} direction in the <011> zone of the diffraction pattern of Figure 116. Coherency between the {111} planes in α_m'' and the matrix is possible due to the relative ease with which the f.c.c. cell can be distorted in that direction [30,92], but such a distortion reduces the symmetry of the structure cell to rhombohedral and destroys coherency in directions away from the {111}. The matrix phase α'' peak in equilibrium with α_m'' was too close to the peak of α_T' phase to be detected on the X-ray diffractograms.

On prolonged ageing, the second transitional phase α_m' formed by a discontinuous mode by the oriented concentration of zinc atoms inside the α_m''. The zinc-concentrated lamellae were found to have the f.c.c. crystal structure. From the X-ray study the multiple peaks of the α_m'' were replaced by a single peak from α_m', and the Zn content in the matrix phase decreased further, so that the diffraction peaks of the f.c.c. matrix phase moved to the low angle side of the X-ray diffractogram. On further ageing the α_m' and α' phases changed into η and α phases respectively by continuous precipitation. The diffraction peak of the α_m' phase, i.e. a transitional phase, disappeared while the peak of α' shifted to a lower Bragg angle. Side bands on the X-ray diffractograms of both alloys were observed at various ageing temperatures, as shown in Figures 76 and 78.

The decomposition of the metastable phase α_T' was followed by a four-phase transformation:

$$\alpha_f + \varepsilon\ (+\sigma) \rightarrow T' + \eta\ (+\sigma)$$

This third stage of ageing in both AlZn60Cu3Si2 and AlZn75Cu3Si2 was shown by the appearance of a diffraction peak from the T' phase at $2\theta = 44.4^{o}$. This development is shown quite clearly in the sequence of diffractograms of Figures 78 and 83. The final stable phases were α_f, η and T'.

The above results show that the decomposition of supersaturated solid solutions in alloys AlZn60Cu3Si2 and AlZn75Cu3Si2 involved the formation of phases in the following sequence:

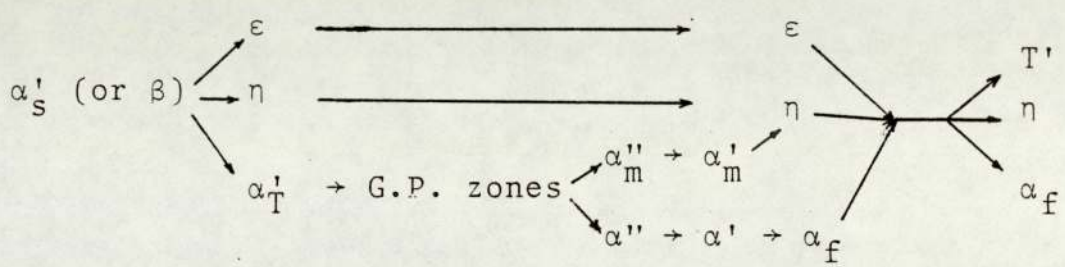

The Si-rich phase, σ, was found to change little during the phase transformation. As a result, the above mentioned sequence should also apply to the Zn-Al-Cu system.

5.3.1.2 Al-rich alloy

The X-ray diffraction results demonstrated a different mechanism of phase transformation in alloy AlZn30Cu3Si2. As-quenched, supersaturated α'_s phase probably decomposed spinodally in the early stage of ageing. Having passed through G.P. zone formation, it was found that the rhombohedral transitional phase α''_m occurred first, then ε and T' phases came before the full development of α''_m.

The appearance of ε and T' indicated a cellular mode of decomposition:

$$\alpha'_s \rightarrow \alpha'_T + \varepsilon + T'$$

Following the cellular reaction, the phase transformations were carried out in two ways simultaneously. The ε and T' phases increased while α'_T started to decompose spinodally. The fractional transformation curve Figure 74 showed that ε phase increased to a maximum after 24 minutes ageing at 170°C. The five-phase coexistence of α_f, ε, T', η and σ phases was observed on the X-ray diffractogram after the spinodal decomposition. This means that another four-phase transformation occurred, i.e.

$$\alpha_f + \varepsilon\ (+\sigma) \rightarrow T' + \eta\ (+\sigma)$$

Since the ε phase was a metastable phase, the final stable phases were α_f, η, σ and T' phases, the same as those in the alloys AlZn60Cu3Si2 and AlZn75Cu3Si2.

Therefore the sequence of phase transformations is outlined as:

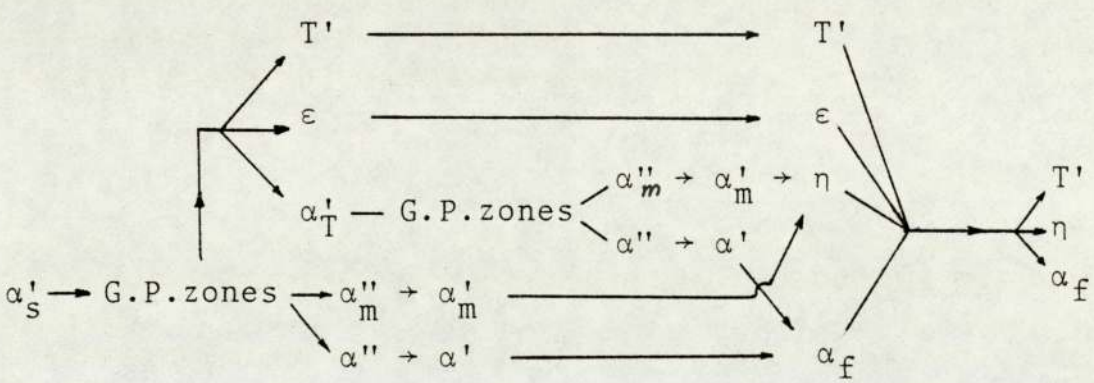

5.3.2 Zn-Al-Si system

5.3.2.1 Alloys of monotectoid and eutectoid compositions

The phase transformation of ageing in alloy AlZn60Si5 started with a cellular reaction:

$$\alpha_s' \ (+\sigma) \rightarrow \alpha_T' + \eta \ (+\sigma)$$

Four phases were detected at the as-quenched stage. The supersaturated α_s' phase had started to decompose into the metastable phase α_T' and zinc-rich η phase. After the cellular reactions were completed, the alloy entered into the G.P. zone stage and then decomposed into the first transitional phase α_m'' in equilibrium with the matrix phase α''. On prolonged ageing, the α'' phase and the first transitional phase α_m'' transformed to α' and the second transitional phase α_m'. Finally α_f and η formed by continuous precipitation from α' and α_m' phases.

Because the transformation occurred rapidly, the contribution of the cellular reaction and the formation of G.P. zones to the increase in hardness combined to give rise to a hardness peak in the hardness/time curve at an early stage of ageing, shown in Figure 57.

The sequence of the phase transformation is as follows:

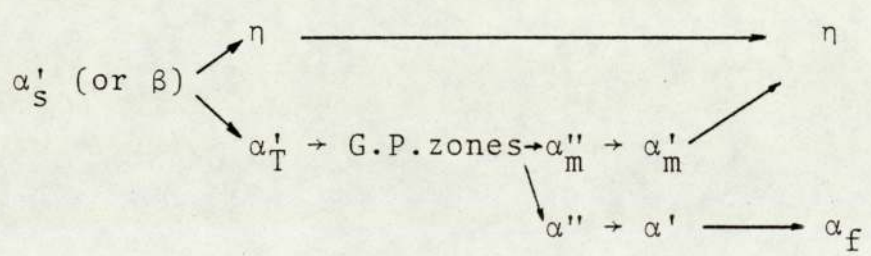

5.3.2.2 Al-rich alloy

According to the results of hardness testing, X-ray diffraction and TEM investigation, the three hardness peaks of the hardness/time curve, Figure 58, were related to the phase and/or structural changes. The phase transformation consisted of four typical steps:

1) formation of G.P. zones
2) the first transitional phase α_m'' in equilibrium with the matrix phase α''
3) the second transitional phase α_m' in equilibrium with the matrix phase α'
4) final stable α_f and η phases.

The sequence is described as:

$$\alpha_s' \longrightarrow \text{G.P. zones} \begin{cases} \longrightarrow \alpha_m'' \rightarrow \alpha_m' \rightarrow \eta \\ \searrow \alpha'' \rightarrow \alpha' \rightarrow \alpha_f \end{cases}$$

According to the observation on the TEM, particles with f.c.c. structure and discontinuous striated precipitates of α_m' phase formed adjoining a grain boundary after the formation of G.P. zones in alloy AlZn30Si5. These are shown in Fig. 94.

In all the alloys involved in the present investigation, the Si-rich σ phase had only a minor influence in phase transformations.

5.3.3 Fraction transformation curves

The fraction transformation curve is often used for describing schematically the sequence of phase transformation.

5.3.3.1 The cellular reaction

Seven fraction transformation curves were constructed with distinct sequences for alloys AlZn30Cu3Si2, AlZn60Cu3Si2 and AlZn75Cu3Si2 aged at various temperatures.

The first stage of phase transformation in alloy AlZn60Cu3Si2 and AlZn75Cu3Si2, i.e. the cellular reaction, was clearly presented by the fraction transformation curves of ε and η phases. From Figures 68 to 72 it was found that over 70% of the incoherent precipitates of η formed by the cellular reaction. Only 30% came from spinodal decomposition. The optical and transmission electron microscopic observation on both the alloys provided evidence. The lamellae structure occurred after 2 minutes ageing at 100°C, as shown in Fig. 110, and was well developed after 8.5 minutes ageing. Figures 81 and 82 show the cellular reaction in this early stage of ageing. Therefore it is reasonable to assume that cell nucleation and growth is one of the most important modes of formation of incoherent precipitates, which is in agreement with Turnbull's observation [48].

In his recent investigation, Toldin et al [67] found that the decomposition of the supersaturated solid solution in alloy AlZn60 and AlZn73 and AlZnMg alloys consisted of two stages, both in natural ageing and in treatment at higher temperature. In the first, the zinc-enriched α_1' phase of f.c.c. structure was formed by a cellular reaction after the formation of G.P. zones. It was suggested that this cellular reaction was in accordance with the horizontal eutectoid at T = 340°C [67] in the binary system.

The present investigation has ascertained that the cellular reaction: (see section 5.3.1)

$$\alpha_s' \text{ (or } \beta) \rightarrow \alpha_T' + \varepsilon + \eta$$

or $$\alpha_s' \text{ (or } \beta) \rightarrow \alpha_T' + \eta$$

is in accordance to the horizontal eutectoid at about $T = 276^{o}C$ and occurs before the formation of G.P. zones. Because a small addition of copper totally changes the phase relationship, new metastable phase ε takes part in the phase transformation, the difference between two horizontal eutectoids can be distinctly determined. A more detailed discussion of this is in section 5.4.

Extrapolation of the solvus line from $(\alpha_1^T + \alpha_2^T)$ two-phase monotectoidal region in the metastable diagram as shown in Figure 4 according to (67) was formed close to the coherent spinodal curves. The composition of the α_m', on determined by EDS (4.5.1.) was: Zn 49.4 at%, Al 50.6 at % and that of the corresponding matrix phase α' was Zn 14.4 at %, Al 85.6 at %. Therefore one must be careful to distinguish these two stages of ageing. Actually it would be very difficult to maintain the metastable phase at a temperature higher than $200^{o}C$, because according to the metastable solvus curves for G.P. zones and α_m'' in Al-Zn system, Figure 17, there would be only the transitional phase α_m'' or α_m' existing at higher temperature.

As discussed in Section 5.3.2.2, the cellular reaction mentioned by Toldin naturally is a part of the spinodal decomposition. The zinc-enriched α_1' phase of f.c.c. structure formed by this cellular reaction actually is the second transitional phase involved in the present investigation. This cellular reaction (by Toldin) has nothing to do with the horizontal eutectoid at 340°C or 276°C.

Based on the observation of discontinuous precipitation at an early stage of ageing in Al-38 at % Zn alloy by opteical and TEM, Vijayalkshmi et al [97] suggested this microstructure formed probably as a result of the monotectoid reaction $\alpha_I \rightarrow \alpha_I + \alpha_{II}$ (ZnAl), but according to the present investigation this discontinuous precipitation along the grain boundary at the early stage (before the formation of G.P. zones) is due to the above-mentioned cellular reactions at about 278°C or 276°C for Zn-Al, Zn-Al-Si, Zn-Al-Cu and Zn-Al-Cu-Si systems.

5.3.3.2 The fraction transformation curves of α_s' and β phases

In the literature, much effort has been devoted to describing the decomposition of the supersaturated phases α_s' and β by fraction transformation curves and calculating their activation energy. But the results seem not to be correct. As seen in Figures 69 and 72 the whole process of the decomposition of α_s' and β phases consists of several steps, such as:

$$\alpha'_s \text{ (or } \beta) \rightarrow \alpha'_T + \varepsilon + \eta$$

$$\alpha'_T \rightarrow \text{G.P. zones} \rightarrow \alpha''_m + \alpha''$$

$$\alpha''_m + \alpha'' \rightarrow \alpha'_m + \alpha'$$

$$\alpha'_m + \alpha' \rightarrow \eta + \alpha_f$$

It is impossible to describe all these steps in one single fraction transformation curve of the matrix phase. Because there is only $0.1 \sim 0.3^{\circ}$ 2θ difference showing on X-ray diffractograms corresponding to these steps in the decomposition, overlapping of diffraction peaks of these matrix phases makes it impossible to calculate the fraction transformations separately. The steps in the decomposition can only be described qualitatively as a series of overlapping curves, shown as dashed lines in Figures 69, 71 and 72. The activation energies of these steps, except for the cellular reaction, could not be calculated from X-ray diffraction data. Even using the plot for activation energy of hardening of these alloys, the results represent mainly a part of the transformation, i.e.

$$\text{G.P. zones} \rightarrow \alpha''_m + \alpha''$$

because the maximum hardness peak is contributed mainly by the formation of the first transitional phase α''_m according to the X-ray diffraction examination.

However, by combining hardness testing and X-ray diffraction examination, the detailed decomposition can be qualitatively represented using a dashed line. The sequences are presented schematically in the fraction transformation curves of Figures 69, 71 and 72.

So one of the two phase transformation patterns attributed to the Zn-Al-Cu system [58], $\beta \rightarrow \alpha + \eta$, should be corrected as follows:

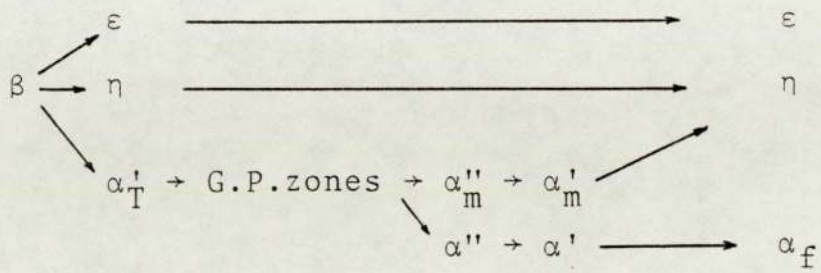

5.3.3.3 The activation energy of the four-phase transformation

The fraction transformation curves are usually used for calculating the activation energy of a four-phase transformation. As an example (described in Section 4.4), the activation energy of the final four-phase transformation,

$$\alpha_f + \varepsilon \rightarrow T' + \eta$$

is calculated as 37.4 KJ/mol which is close to 33.7 KJ/mol deduced from hardness testing.

5.3.4 The segmentation of the precipitation

Of special interest was the phenomenon of the segmentation of the elongated phase at a subsequent stage, as shown in the electron micrographs of Figures 96-100 taken after 24 hours ageing at 100°C. The oriented concentration of zinc atoms within the phase gave rise to a further increase in the lattice parameter difference between the transitional phase and the matrix phase, and therefore to growth of the local strain nearby the interface between the precipitates and matrix. The strain increase due to the increased difference of lattice parameters destroyed the orientation relationship between the phases and raised the interfacial

free energy. This process might move the interface away from a 'cusp' orientation with its stabilizing 'tongue' term and cause fracture of the lamelle [94].

A gradual change in zinc-content at one of the zinc concentrated lamelle was observed in the same specimen, as shown in Figure 101. According to Zener and Cahn :

$$R\Delta G = \frac{2\sigma_1 V}{S}$$

where V is the molar volume, which is assumed to be the same for the solution and the precipitate, and R is the fraction of ΔG that goes into the interfacial tension, S is the interlam ellar spacing, the interfacial tension is partly dependent on the interlamellar spacing values.

From Turnbull's conclusions [48], the precipitation rate was determined by three parameters:

D_B - the diffusion coefficient of atoms in the cell boundary

ℓ - the spacing between precipitate lamellae in the cell

N - the number of cell/volume nucleated

and was inversely proportional to the specific free energy that drove precipitation. That result was quantitatively in agreement with Zener's formula. It was found that S value of 0.3 μm in Figure 101 was about 3.7 times bigger than S = 0.08 μm in Figure 96 showed broken-shot lamellae.

Therefore it is concluded that the segmentation of the second transitional phase shape of lamellae is caused by the oriented concentration of zinc atoms within the lamellae with small interlamellae spacing.

In the Zn-Al-Cu-Si alloy, it is presumed that due to the different effect of atoms of various size on strain field, copper atom in matrix phase decreased the lattice parameter of the matrix phase and reduced the strong strain field between the lamellae and the matrix phase which causes lamellae and the matrix phase, which causes lamellae to suddenly break, therefore the segmentation does not occur.

5.4 The general rule of phase transformations of supersaturated solid solution of alloys

5.4.1 Relationships between the equilibrium phase diagram and the phase transformation of ageing

The phase relationships in the equilibrium state are a basis for investigation of phase transformations occurring during quench-ageing. Alloys of different composition which occupy different phase fields at high temperature, will transform to their final stable state in different ways. It depends on which phase fields the alloy passes through and what kind of phase transformation occurs. If the high temperature alloy cools down to room temperature very slowly, and remains in close approach to equilibrium all the time, the rule of lowest free energy is always obeyed. Whatever phase transformations take place, they must keep the alloy at the lowest free energy.

In non-equilibrium processes, the alloy may miss out some phase transformations and arrive at the final stable state directly from some phase field at high temperature. During

quench-ageing processes, a high temperature phase is retained at room temperature as an unstable supersaturated phase, and will eventually transform to a final stable state. Though the driving force at the ageing temperature is larger than at a high transformation temperature, the possible phase transformations may be the same, i.e. the value of free energy must be at the lowest value allowed by the kinetics of the changes involved, while the mechanism of these transformations could be or must be different.

Phase transformation starts in quenched alloys with decomposition of the unstable supersaturated phase. It is because the driving force of the phase transformation consists of two parts, one, the main part (if ageing temperature is not high) is from the unstable supersaturated phase itself, which depends on the quench temperature and the composition, while the other is from the ageing temperature, i.e. the thermal conditions.

Based on the well determined equilibrium phase diagram, the high temperature equilibria which correspond to decomposition of the supersaturated phase in alloy Al$Zn_{60}Cu_3Si_2$ and Al$Zn_{75}Cu_3Si_2$ are

$$\beta + \varepsilon \rightleftharpoons \alpha + \eta \quad \text{at } 276^{\circ}C$$

Therefore, in both the alloys, the phase transformation, which occurred at a temperature higher than 276°C, (at which the equilibrium, $\beta + \varepsilon \rightleftharpoons \alpha + \eta$ exists), could not occur at ageing temperature, because it needs only a smaller

driving force to pass over the energy barrier. However, this may not always be true, if the driving force of the quench-ageing can be decreased, e.g. by decreasing pressure [98] or by addition of some of the third elements which may totally change the phase relationships.

The phase transformations corresponding to all the equilibria below the above mentioned equilibrium are possible, while what kind of phase transformation will happen depends on which phase field the alloy was located in at the solution treatment temperature. For example, alloys AlZn75Cu3Si2 and AlZn60Cu3Si2 are in the ($\beta + \varepsilon$) and (α) phase fields respectively, according to the equilibrium phase diagram, both alloys are located in a five-phase field $(\alpha + \varepsilon + \eta + \beta + \sigma)_{\wedge}^{at\ 276°C}$, and enter another five-phase field ($\alpha + \varepsilon + \eta + T' + \sigma$) below the equilibrium reaction $\beta + \varepsilon \quad \alpha + \eta$. There must be another equilibrium reaction, $\alpha + \varepsilon \rightleftharpoons T' + \eta$, going to occur, if they cool down very slowly. Therefore, the phase transformations of these two quenched alloys, start with the decomposition of α_s' or β, i.e. the so-called cellular reaction,

$$\alpha_s' \text{ (or } \beta)(+ \sigma) \rightarrow \alpha_T' + \varepsilon + \eta \ (+ \sigma)$$

and the cellular reaction must eventually be followed by the other four-phase transformation, $\alpha_f + \varepsilon \rightarrow T' + \eta$.

In the equilibrium state, the solubility of zinc and copper in aluminium decreases gradually as equilibrium temperature decreases below the temperature for the transformation

$\beta + \varepsilon \rightleftharpoons \alpha + \eta$, at 276°C. The content of Al in the α phase increases and the composition position on the phase diagram moves closer to the pure Al corner.

Because the driving force of these alloys after the cellular reaction is not so high that they have to pass through steps of transformation, i.e. the spinodal decomposition to finish the composition modulation above mentioned and start to occur the other four-phase transformation $\alpha_f + \varepsilon \rightarrow T' + \eta$. The ε phase, as a metastable phase, will disappear finally in both alloys during the ageing processes. The α_f, T' and η phases are the final stable phases. According to the same consideration, this final phase transformation, $\alpha_f + \varepsilon \rightarrow T' + \eta$, will eventually occur for all the alloys of composition within the phase fields $(\alpha + T' + \eta)$ at about 268°C.

The well determined sequences of phase transformation in both alloys

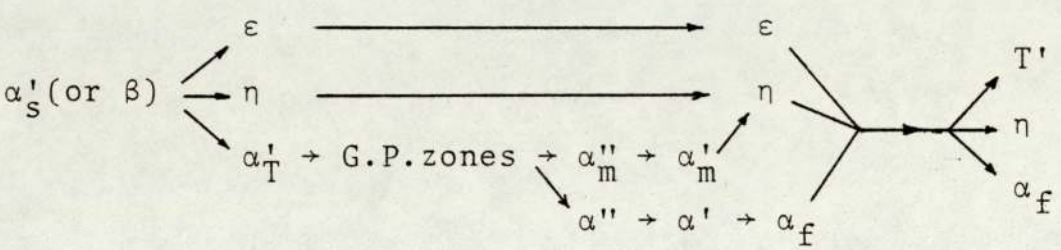

is in good agreement with the principle. According to this principle, the cellular reaction must be in accordance with the horizontal eutectoid at about T = 276°C thermodynamically.

Based on the phase relationships in the equilibrium state, all alloys of compositions such that the alloys pass through the ($\alpha + \beta + \varepsilon + \eta$) phase field of the phase diagram during cooling from high temperature to room temperature, will obey this sequence of phase transformation during the quench-ageing processes.

For alloy Al$Zn_{30}Cu_3Si_2$, because it is out of the ($\alpha + \beta + \varepsilon + T'$) phase field, a different mechanism should be obeyed.

The decomposition of the supersaturated solid phase in alloy Al$Zn_{30}Cu_3Si_2$ starts with the transformation as follows:

$$\alpha'_s \rightarrow \text{G.P. zones} \rightarrow \alpha''_m \rightarrow \alpha''_m$$
$$\searrow \alpha'' \rightarrow \alpha'$$

The α'_s phase begins to decompose after 1 minute ageing at 170°C as shown in the X-ray diffractograms of Figure 84.

From the equilibrium phase diagram of Zn-Al-Cu-Si and Zn-Al-Cu systems in Figures 51-56 and Figures 11-15 it has been found that the same phenomenon occurred in both alloy Al$Zn_{60}Cu_3Si_2$ and Al$Zn_{75}Cu_3Si_2$, none of these equilibria such as

$$\beta + T' \rightleftharpoons \alpha + \varepsilon$$

can occur, because β phase does not decompose at temperatures higher than 275°C. This is also seen in the phase diagram. The

aluminium content in α phase increases from 65% at 275°C to 70% at 268°C. The positions of the α phase corner in both (α + T' + ε) and (α + ε + η) three phase fields migrate towards the pure aluminium corner when the alloys slowly cools down from 275°C.

During the ageing process, the migration of the corner of α_T' phase field happends in the same way as in equilibrium transformation. So long as the alloy enters the three phase field (α_T' + T' + ε), the four phase transformation,

$$\alpha_s' \rightarrow \alpha_T' + T' + \varepsilon$$

occurs, accompanying the spinodal decomposition of α_s'.

By then the alloy is located well inside the three phase field (α + T' + η) at about T = 268°C. The final four phase transformation takes place as

$$\alpha_f + \varepsilon \rightarrow T' + \eta$$

The sequence observed on X-ray diffraction examination was in agreement with this explanation.

Therefore, for Al-rich alloys (Al content up to 86%) the sequence of the phase transformation is summarised as follows:

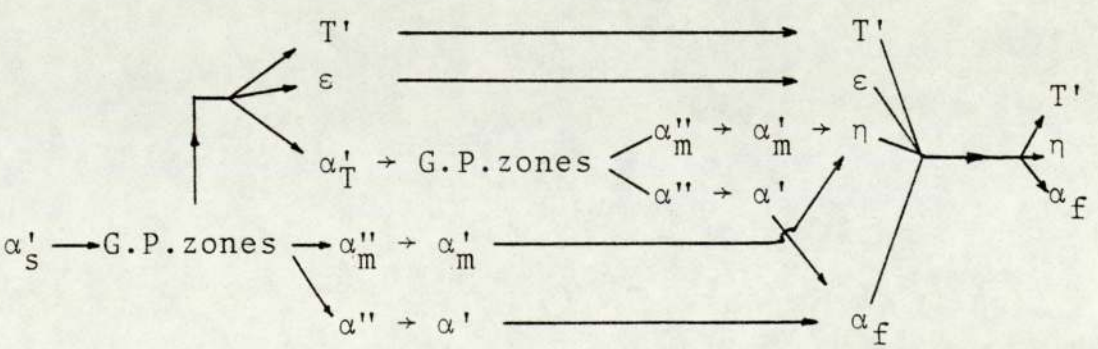

For the Zn-Al-Si and Zn-Al systems, the mechanisms of phase transformation in alloy AlZn60Si5 and AlZn75Si5 are similar to those in alloy AlZn60Cu3Si2 and AlZn75Cu3Si2, as have been shown on the X-ray diffraction examination. The phase transformation starts with the cellular reaction:

$$\alpha_s' \rightarrow \alpha_T' + \eta$$

Then α_T' phase decomposes spinodally into transition phases α_m'' and α_m' in equilibrium with the matrix phase α'' and α' respectively. G.P. zones form before the formation of α_m'' and α_m'. The final stable phases are α_f and η.

This is the same as in the Zn-Al-Cu-Si and Zn-Al-Cu systems, it is reasonable to conclude that all alloys of composition within the zinc range of the eutectoidal line at 278°C, have the same mechanism of phase transformation in quench-ageing processes. No matter where the alloys are quenched from either ($\beta + \eta$), β, or α' (beyond the monotectoid curve in equilibrium phase diagram) phase fields, the cellular reaction, $\alpha_s' \rightarrow \alpha_T' + \eta$, should always occur first, followed by the spinodal decomposition. The α_f and η phases are the final phases.

The sequence of phase transformation in monotectoidal and eutectoidal alloys is outlined as follows:

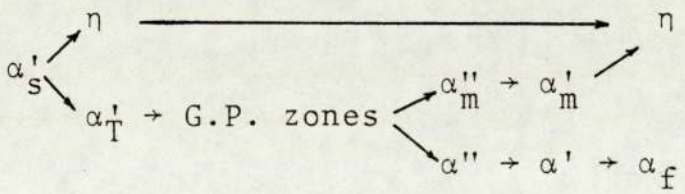

It has been found that the β phase decomposed into α'_T and η phases during or immediately after quenching just as observed in the determination of the phase diagram of Zn-Al-Si and Zn-Al-Cu-Si systems, seen in Section 4.1 and 4.2. This is because as-quenched β is located in the so-called 'coupled region'[99], i.e. the shadow area in the metastable phase diagram Figure 128. Within the 'coupled region', α'_T, β and η coexisted. From the point of view of thermodynamics, β in this region is unstable. In alloys of the eutectoidal composition, the G.P. zones become unstable at a high ageing temperature [40], from the point of view of kinetics which will be discussed in more detail in Section 5.4.4.Therefore the cellular reaction and the G.P. zones are very difficult to detect.

Previous work dealt with it as a different mechanism of transformation.

According to the equilibrium phase diagrams of the Zn-Al-Si and Zn-Al systems, the Al-rich alloys cross only one phase boundary, $\alpha/\alpha + \eta$, when slowly cooled down from high temperature to room temperature. But the supersaturated solid phase in the as-quenched Al-rich alloys cannot transform into α_f and η in one step. G.P. zones are fully coherent with the matrix and therefore have a very low interfacial energy. Transition phases are intermediate between those of the supersaturated phases and the equilibrium, and therefore can achieve a high degree of coherence and a low interfacial energy. The

equilibrium phases on the other hand usually have a complex crystal structure which can only form with high-energy incoherent interfaces. Therefore the activation energy barrier to the formation of G.P. zones and each transition phase is very small in comparison to the barrier against the direct precipitation of the equilibrium phase. As-quenched alloys will be easy to transform into final stable phases by passing through G.P. zones and transitional phases.

For Al-rich alloys in Zn-Al-Si and Zn-Al systems, the sequence of transformation should be as follows:

$$\alpha_s' \rightarrow \text{G.P. zones} \rightarrow \begin{cases} \alpha_m'' \rightarrow \alpha_m' \rightarrow \eta \\ \alpha'' \rightarrow \alpha' \rightarrow \alpha_f \end{cases}$$

which is in agreement with Ciach's sequence for low zinc alloys (up to 30% Zn) [55]. Strictly speaking, all alloys of composition between α_T' (i.e. the Al-rich end of the eutectoid line) and the composition of G.P. zone solvus line, shown in Figure 17, at ageing temperature have the same sequence.

5.4.2 The general rule of phase transformation

Correlating all the mechanisms of phase transformation with the equilibrium phase relationships, the general rule of phase transformation of supersaturated solid solution of alloys is summarised as follows:

"Phase transformation of a supersaturated solid solution of an alloy begins with decomposition of the supersaturated phase, which is associated with some phase equilibrium at high temperature. Then it is followed

by one (or more) phase transformation(s) which agrees with all these phase equilibria with the alloy after the first associated phase equilibrium at the high temperature. Steps of intermediate transformation with a low activation energy barrier, such as the formation of G.P. zones or other transitional phases, etc., could always be involved in the whole process of phase transformations. The higher the degree of supersaturation, the more transitional phases may occur. The final products of ageing must be the stable phases, if the kinetics allow this to be reached."

From the view of thermodynamics, the rule reveals the relationship between equilibrium and non-equilibrium states. According to the rule, it becomes possible to predict what kind of phase transformation will occur in non-equilibrium processes based on the understanding of the phase relationships in equilibrium.

With the same chemical composition, the way to approach the final equilibrium state for alloys both at high quench temperatures and supercooled temperature would, thermodynamically, be the same, if the driving forces for the phase transformation were the same. Apparently the driving force in the quench-ageing alloy is bigger than in alloy at high quench temperature. The process of moving towards the equilibrium state can start with some lower level equilibrium, i.e. the phase transformation associated with the decomposition of supersaturated phase (the main part of the driving force). This starting level

is dependent on the degree of supersaturation and ageing temperature.

On the other hand, for alloys with low temperature eutectoid equilibrium, the cellular reaction corresponding to the eutectoid equilibrium is more likely to occur prior to G.P. zones during the quench-ageing process. Whether the cellular reaction occurs prior to the formation of the G.P. zones depends also on the competition of the activation energy barrier between the cellular reaction and the G.P. zones. If the activation energy barrier of the cellular reaction, which corresponds to the equilibrium associated with the decomposition of the supersaturated phase, is higher than that which the driving force of the supersaturated phase can jump over, the phase transformation starts with the formation of G.P. zones. But the phase transformations, the activation energy barriers of which are lower than those of the formation of G.P. zones,will occur followed by the G.P. zones. Because the circumstances are different from that at high temperature, at low-ageing temperature diffusion of solute atoms in the supersaturated phase becomes very difficult, the same phase transformation is carried out, in a different way from high temperature equilibrium. Steps of transformation with low activation energy barriers, such as G.P. zones and some transition phases, etc., could always be necessary to the whole process of phase transformations. As supersaturation decreases, the number of intermediate transformation steps decreases. The multi-stage precipitation process

will continue until the most stable state is produced, i.e. the formation of a more stable product resulting in the re-solution of less stable phases formed in the earlier stages.

Most papers concerning the phase transformation in Zn-Al and Zn-Al-Cu systems dealt with the decomposition of α_s' and β phase simply as a spinodal decomposition [54,55,57]. It is correct only for those alloys, the composition of which are within the range between α_T' and the G.P. zones solvus curve or surface at the ageing temperature in Zn-Al, Zn-Al-Si, Zn-Al-Cu and Zn-Al-Cu-Si systems. The mechanisms of alloys of monotectoid and eutectoid composition become more complicated because of the cellular reactions:

α_s' (or β) $\rightarrow \alpha_T' + \eta$	in Zn-Al and Zn-Al-Si systems
α_s' (or β) $\rightarrow \alpha_T' + \varepsilon + \eta$	in Zn-Al-Cu and Zn-Al-Cu-Si systems

and the phase relationship changes due to the addition of the third or fourth component element.

The mechanisms of the decomposition of supersaturated phase in Zn-Al binary and Zn-Al-Cu, Zn-Al-Mg ternary system have been a topic for discussion for many years. Most investigations provided only the mechanism for single compositions or limited composition ranges which were selected by investigators.

According to the general rule, the mechanism of phase transformation in an alloy represents not the alloy itself but a general pattern of phase transformation for some phase field. Correlating the determination of the transformation mechanism of one or two alloys with the well-established phase diagram actually provides the mechanism of alloys within one phase field in a phase diagram, as described in Section 5.4.1. Based on a detailed investigation of the mechanisms of the successive phase transformations, the mechanisms for the whole composition range in Zn-Al binary and Zn-Al alloys containing copper and/or silicon have been provided in the present investigation, as described in Section 5.3.1 and 5.3.2, using the general rule. Vice-versa, the phase equilibrium at relatively low temperatures can be established by tracing the phase transformation on the quench-ageing, i.e. the non-equilibrium processes.

5.4.3 Free energy curve and surface

The general condition of equilibrium is defined by the four fundamental equations of thermodynamics :

$$dE = TdS - PdV \qquad (1)$$

$$dH = TdS + VdP \qquad (2)$$

$$dF = - SdT - PdV \qquad (3)$$

$$dG = - SdT + VdP \qquad (4)$$

Equation (1) relates the change in energy to the change in entropy and volume. Equation (2) relates the change in entropy and pressure. Equation (3) relates the change in work function to changes in temperature and volume. Equation (4) relates the free energy to changes in temperature and pressure.

For phase transformations that occur at constant temperature and pressure the relative stability of a system is determined by its Gibbs free energy. This Gibbs free energy is particularly interesting because equilibrium is then characterised by a minimum in this quantity and the decrease in Gibbs free energy during a spontaneous transformation can be regarded as the driving force. The free energy curve is used for describing the change in free energy with the change in composition. The common tangent is basic to the interpretation of all free energy curves. In order to demonstrate the relationships between the equilibrium and non-equilibrium states, the free energy curve (for binary alloys) or free-energy surface (for multi-component systems) with the common tangent construction are presented for comparison.

Figures 127 a and b, show the free energy vs composition surfaces in equilibrium and quench-ageing processes respectively.

For the equilibrium state in Zn-Al-Cu and Zn-Al-Cu-Si systems there is a four-phase transformation :

$$\beta + T' \rightleftharpoons \alpha + \varepsilon \quad \text{at about } 285^{o}C$$

The four free energy surfaces of T', α, β and ε phases at $285^{o}C$ have a common tangent plane. The free energy surfaces of β and ε phases have in addition a common tangent plane with the free energy surface of η phase at different positions on their surfaces, as shown in Figure 127 a. The free energies of α and ε phases increase more slowly with the decrease in temperature

cooling. In comparison, Figure 127 b presents the movement of free energy surfaces correlating with phase transformations during the quench-ageing processes, based on the results of the X-ray diffraction examination.

The free energies of the system decrease and approach their final equilibrium value during the whole process of ageing. As a result of the competition of the increase in free energies of phases, common tangent planes of phases form and change their shape and position in space.

The phase transformation during ageing starts with the decomposition of supersaturated α_S' or β phases. The free energy surface of α_S' (or β) phases is well within the common tangent plane of α_T', ε and η phases. After the cellular reaction

$$\alpha_S' \text{ (or } \beta) \longrightarrow \alpha_T' + \varepsilon + \eta$$

the phase relationships is similar to that below 276°C in equilibrium state, as shown in Figure 127 a. The common tangent planes of α_T', η and ε occurs. Because the phase transformation taking place at low temperature, the driving force is not big enough to migrate the α_T' phase free energy surface towards the pure Al corner in one step. A typical spinodal decomposition is described in Figure 127 b. The free energy surfaces of the two transition phases α_m'' and α_m' form and bring about two common tangent planes of α'', α_m'', ε and η; α', α_m', ε and η. The composition of the matrix phase is moderated from α_T' to α_f by the formation of these two common tangent

than those of T' and β phase, and two phase field (α+ε) occurs. The free energy of η phase increases more slowly than those of α,β and ε phases, and at about 276°C the common tangent plane of α, β, ε and η phases occur while the two-phase field (β+ε) disappears. That means that the other four-phase equilibrium :

$$\beta + \varepsilon \rightleftharpoons \alpha + \eta$$

exists at about 276°C. This four-phase co-existence of α, β, ε and η phases corresponds to the decomposition of the supersaturated phase in quenched-aged alloys. As the temperature is lowered just below 276°C the β phase becomes unstable, the free energy surface of which migrates up from the common tangent plane of α, ε and η phases, and disappears in the alloy. When the alloy is cooling from 276°C to 268°C, the T' and η phases become more stable and their free energy surfaces migrate down faster than those of α and ε phases. Both common tangent plane beside the free energy surfaces of α and ε phases : (α+ε+T') and (α+ε+η) are getting closer and closer, meanwhile the α phase free energy surface migrates towards the pure Al corner. At 268°C the two phase field (α+ε) disappears from the phase diagram while the final four-phase co-existence (α+ε+η+T') occurs. On prolonged cooling, the ε phase becomes unstable and its free energy surface moves up from the common tangent plane of α, η and T' phases. By then there are only three phases α, η and T' stable in the alloy.

Figure 127a shows the free energy surfaces movement correlating with the phase equilibrium on very slow

planes in sequence, as arrow points in Figure 127 b. Meanwhile the free energy surfaces of η phases is lowered more quickly than that of ε phase. On prolonged ageing, a four-phase co-existence of α_f, ε, η and T' comes into being. That implies the existence of a common tangent plane of free energy surfaces of α_f, ε, η and T' phases, which is correlating the equilibrium : $\alpha + \varepsilon \rightleftharpoons T' + \eta$ at $268^{o}C$. After the four-phase reaction :

$$\alpha + \varepsilon \longrightarrow T' + \eta$$

the free energy surfaces of ε phase separates from the common tangent plane and the common tangent plane of α_f, η and T' phases below, while the X-ray diffractogram shows three stable phases α_f, η and T' as the final products of ageing in the alloy.

From figures 127 a and b, it is found that both β and ε phases are unstable at low temperature and decompose before the formation of the final stable phases during ageing. Under equilibrium conditions the β phase disappears at a higher temperature than ε phase, and on ageing after quenching, it decomposes at an earlier stage.

It is clearly seen that the phase transformations which take place during the ageing process are in agreement with phase equilibria occurring in equilibrium states in their general sequences. The free energy surface appears to be one of the ways of interpreting graphically the relationship between equilibrium and non-equilibrium phase transformations.

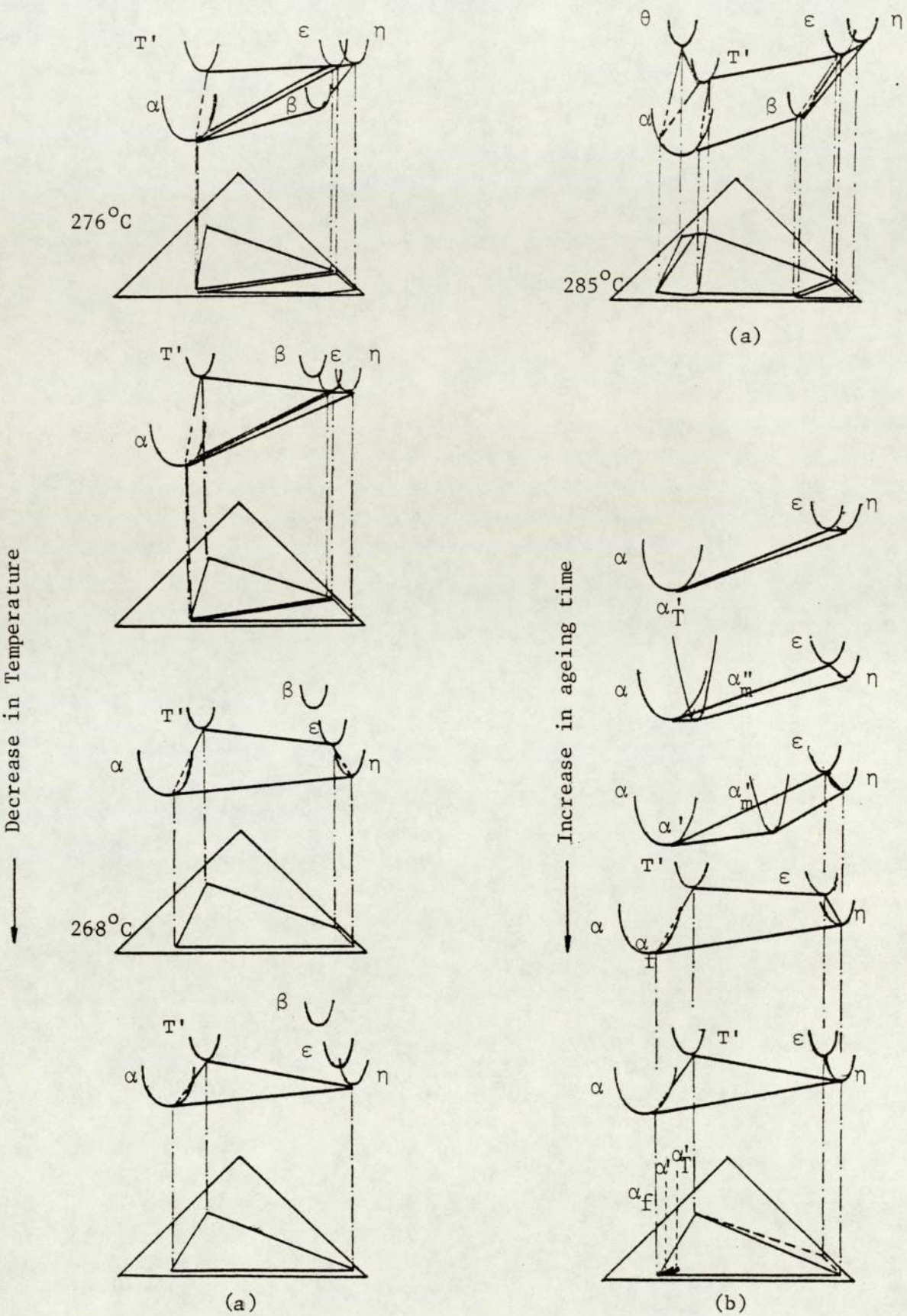

Fig.127 Free energy surfaces of phases in alloys Zn-Al-Cu and Zn-Al-Cu-Si at various temperatures (a) and at various stages of ageing (b).

5.4.4 Kinetic considerations

According to the general rule, phase transformations which agree with all the phase equilibrium in the phase diagrams after the first phase equilibrium associated with the decomposition of supersaturated solid solution, will occur. From this point of view of thermodynamics, it predicts what kind of phase transformation could occur during the quench-ageing process. But the ageing process is actually taking place in certain kinetic circumstances where the alloy is involved.

At as-quenched state, the kinetic condition is apparently different from that at high quench temperature. Solutes in supersaturated solid solution tend to precipitate out and lead the system to the equilibrium state. But at low temperatures this thermodynamically possible process could not be completed due to the very low diffusion rates.

For spinodal decomposition which is often involved in ageing processes, its sequence could be different at different temperatures of ageing. For example, in Zn-Al and Zn-Al-Si systems, all alloys of composition within the eutectoid reaction line or plane at about T = 278°C have the same mechanism thermodynamically, that is :

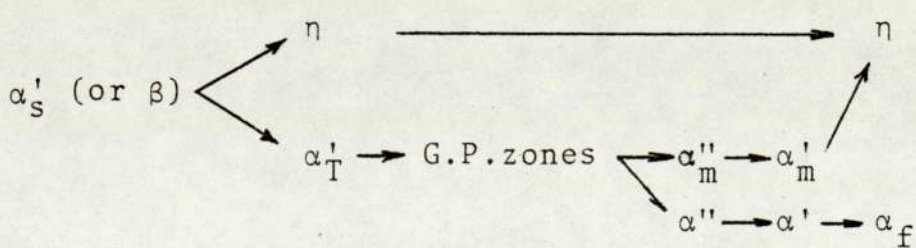

But G.P.zones could be missed for alloy of composition 80% Zn aged at 100°C. Instead of the above mentioned

sequence, the transformation occurs in the following sequence :

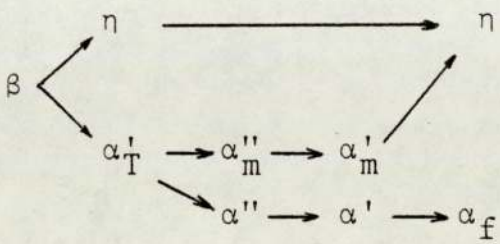

It is because the alloy is beyond the metastable solvus for G.P.zones that the G.P.zones have dissolved at 100°C, as seen in Figure 7.

Therefore the kinetic condition could practically change the sequence of transformation and some phase transformation would 'never' complete. For example, in alloy AlZn75Cu3Si2 aged at 100°C, all the phase transformations are completed in only about 100 hours, according to the X-ray diffraction examination shown in Figure 70, while the final four-phase transformation, $\alpha_f+\varepsilon \rightarrow T'+\eta$ in alloy AlZn60Cu3Si2 lasts more than 500 hours due to the low diffusion rate of zinc in aluminium matrix, shown in Figure 23. If the ageing temperature is decreased, the time to complete the final four-phase transformation will be much longer, and practically can be considered never to be complete.

In order to understand the phase transformation better, combination of considerations of both thermodynamics and kinetics is necessary.

As far as the Zn-Al based alloys are concerned, the well determined G.P.zones and R phase (i.e. α''_m or α'_m phase) solvus in Figure 17 should be especially considered when the general rule is used for investigating the phase

transformation during quench-ageing processes. These two solvus curves imply the sequence of the spinodal decomposition which could always be an important part of an age-hardening.

According to these two solvus lines the Arrhenius plots for determining the activation energies of age-hardening in alloys AlZn30Si5, AlZn60Si5, AlZn30Cu3Si and AlZn60Cu3Si2 can not be extrapolated indefinitely in the direction of increasing temperature, shown in Figures 65 and 67. The broken lines represent the ageing temperature above G.P.zones, and the mechanisms of hardening are different from those at temperatures within the solid straight line where α''_m or combinations of α''_m and α'_m contribute to the maximum peak hardnesses.

5.5 The response of properties to phase transformation

5.5.1 Hardness

Physical and mechanical properties of alloys Zn-Al-Cu-Si and Zn-Al-Si, such as hardness, impact, tensile strength and dimensional stability have been measured in quench-ageing processes. Correlating with the mechanisms of the phase transformation deduced from hardness tests, X-ray diffraction and transmission microscopy investigations, the relationships between the properties and phase transformation are simply displayed in Figure 68 as an example.

The phase transformation occurring in alloy AlZn60Cu3Si2 aged at 100°C consisted of three stages, which were as follows :

1. The decomposition of α_s' phase, i.e. cellular reaction, into α_T', ε and η phases and led the first peak,

$$\alpha_s' \longrightarrow \alpha_T' + \varepsilon + \eta$$

where α_T' was still an unstable phase and was going to further decompose spinodally.

2. The spinodal decomposition of α_T' phase,

$$\alpha_T' \longrightarrow \text{G.P.zones} \begin{cases} \nearrow \alpha_m'' \longrightarrow \alpha_m' \longrightarrow \eta \\ \searrow \alpha'' \longrightarrow \alpha' \longrightarrow \alpha_f \end{cases}$$

3. The four-phase transformation,

$$\alpha_f + \varepsilon \longrightarrow T' + \eta$$

With respect to all these phase transformations, the hardness curves of alloy A1Zn60Cu3Si2 aged at 100°C showed five hardness peaks. In the ageing processes of most specimens of A1Zn60Cu3Si2 and A1Zn75Cu3Si2 at various temperatures, the first peak occurred in the first stage of ageing, because the precipitates of Zn and Cu formed η and ε phases.

Then α_T' metastable phase started to decompose spinodally as small fluctuations in composition, that produced later on Al-rich α'' phase and Zn-rich α_m'' phase. G.P.zones appeared to be homogeneously nucleated on a fine scale throughout the matrix crystal and fully coherent with the matrix phase. The hardness increased due to the extra stress required to force dislocations through the coherent zones [30] shown as the second hardness peak.

The hardness continued to increase to maximum with the formation of the coherent α'' and α''_m because the dislocations then must also be forced through the highly strained matrix phase. The third hardness peak occurred. After partial formation of α''_m phase homogeneously throughout the crystal by growth of some G.P.zones at the expense of others, the second transition phase α'_m started to form heterogeneously on dislocations, grain-boundaries, etc., as happened in AlZn30Si5, shown in Figure 100. Combination of the formation of α''_m and α'_m phases (α''_m mainly) contributed to the maximum hardness peak.

The hardness then decreased due to transformation of α''_m into α'_m, in other words, due to the coarsening of α''_m. At the same time, the zinc atoms continuously diffused into α'_m phase, which gradually gave rise to a great change in the lattice parameters of the transition phase and the matrix phase. The elastic strain due to the increased difference of lattice parameters and loss of coherency was responsible for structural change from rhombohedral to f.c.c. and for the hardness increase. Therefore, the formation of α'_m phase contributed the fourth hardness peak, which appeared as a plateau because coarsening of all precipitates had already commenced.

Prolonged ageing increased the distances between the precipitates making dislocation bowing easier and the hardness decreased. The matrix phase α' in equilibrium with α'_m changed into α_f and as a transitional phase, α'_m transformed into η phase and disappeared by the end of the second stage.

The fifth peak of hardness was associated with the four-phase transformation :

$$\alpha_f + \varepsilon \longrightarrow T' + \eta$$

The ε phase was converted into Cu-rich T' phase of high hardness, so the hardness of alloys increased.

Thus, Zn-rich phase η, Al-rich phase α_f and T' phase were formed as the final stable phases.

A lower peak hardness formed on ageing at higher temperature. This was because at high temperature the α_m'' nucleated under the influence of a smaller driving force than at lower temperature[100] and resultant precipitate dispersion was therefore coarser[99]. Also the maximum volume fraction of α_m'' was reduced. From the metastable monotectoid curve in Figure 128 for the Zn-Al binary system, the higher the ageing temperature, the smaller the fraction of α_m'' phase responsible for the maximum hardness peak, according to the Lever Rule. The position of the hardness peaks were shifted to shorter times by increasing the temperature of ageing, as the diffusion rate was faster at higher temperatures.

Figure 68 shows the response of hardness to the phase transformations deduced from X-ray diffraction for alloy Al$Zn_{60}Cu_3Si_2$ aged at 100°C. A good agreement was found between hardness testing and X-ray diffraction examination.

The mechanism of phase transformation of alloy Al$Zn_{30}Cu_3Si_2$ in the ageing process is quite different from that of alloy Al$Zn_{60}Cu_3Si_2$. It is because alloy Al$Zn_{30}Cu_3Si_2$ is located outside the phase field ($\alpha+\beta+\varepsilon+\eta$) at about 276°C.

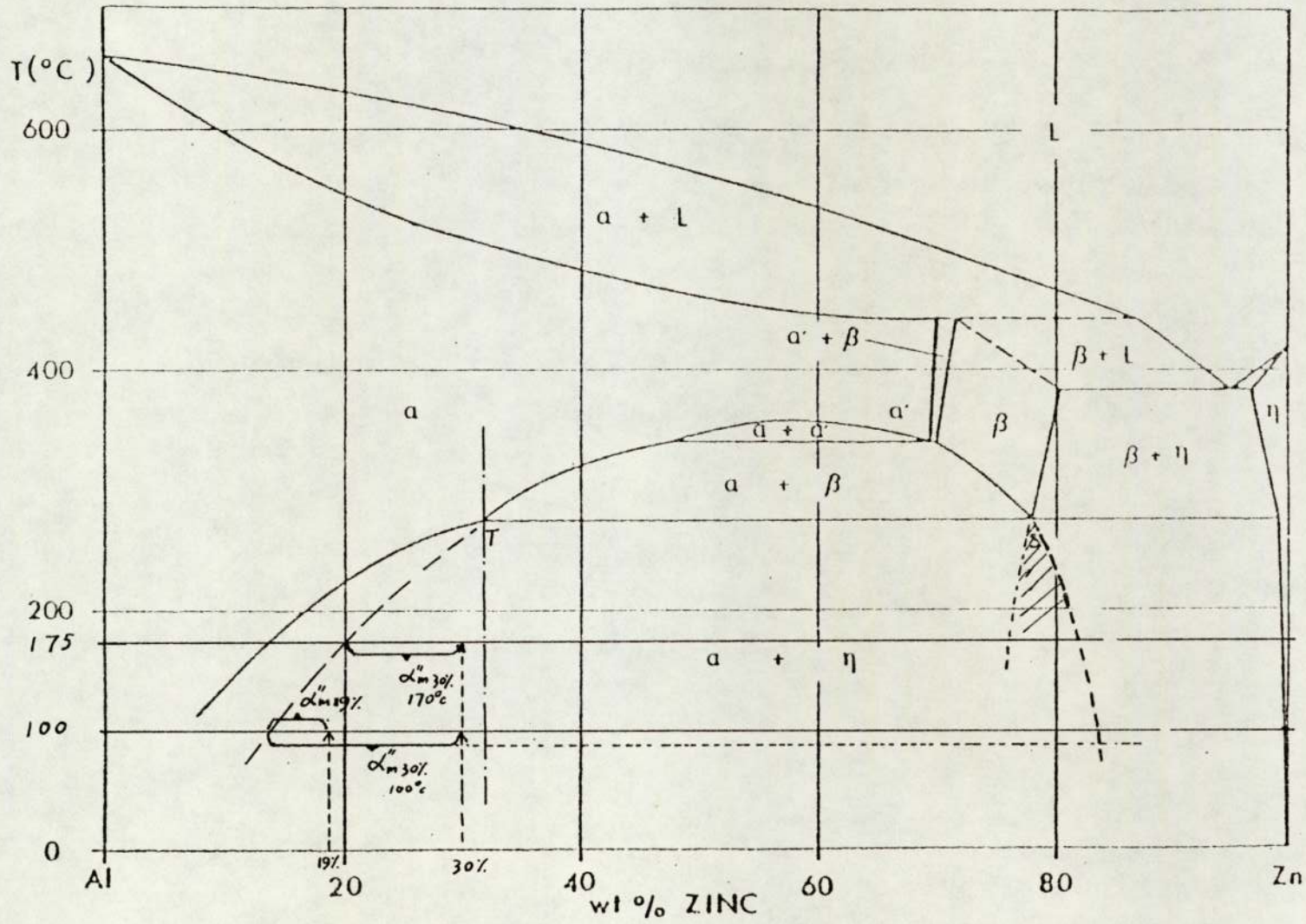

Fig.128 The Zn-Al binary phase diagram, showing the lever rule.

The supersaturated phase α'_s began to decompose spinodally after quenching and entered the phase field ($T'+\alpha'_T+\varepsilon$). The first stage was :

$$\alpha'_s \longrightarrow \text{G.P.zones} \longrightarrow \alpha''_m + \alpha''$$

The second stage was :

$$\alpha'_s \longrightarrow \alpha'_T + \varepsilon + T'$$
$$\alpha'_T \longrightarrow \text{G.P.zones} \longrightarrow \alpha''_m + \alpha'' \quad \ldots$$

In these two stages, the hardness of alloy A1Zn30Cu3Si2 aged at 170°C climbed over a small peak, which was contributed by G.P.zones, and then quickly increased up to the maximum value. The X-ray diffractogram showed that the α'_T decomposed into α''_m and the α''_m phase diffraction peak developed to the maximum height after about 8 minutes at 170°C in Figure 62. The hardness curve showed a maximum hardness peak at nearly the same time as the α''_m diffraction peak arrived at the highest level. Then α''_m changed to α'_m and finally to η phase, and hardness decreased with ageing time. The matrix phase changed gradually from α'_T to α'', α' and finally to α_f, while the precipitates were developing.

The rate of precipitation of ε increased sharply to the maximum after 24 minutes ageing at 170°C, showing in the fractional transformation curve of ε phase as $f[\varepsilon](10\bar{1}1) = 0.5$ in Figure 74. The increase of hardness due to α'_m phase formation and precipitation of zinc balanced the decrease caused by over-aged coarsening, a hardness peak appeared just after 24 minutes aged at the temperature. The result from X-ray diffraction was in a good agreement with that from hardness testing. So the next hardness peak after the maximum hardness peak was contributed by both the

cellular reaction $\alpha'_s \longrightarrow \alpha'_T + \varepsilon + T$ and $\alpha''_m \longrightarrow \alpha'_m$.

Comparing the hardness curve and X-ray diffractogram of alloy AlZn30Cu3Si2 aged at 100°C, the maximum hardness peak occurred after 4.5 hours ageing and was due to the formation of α''_m phase. The first hardness increase after the maximum hardness peak was caused by the rapid formation of ε phase and the changing $\alpha''_m \rightarrow \alpha'_m$. After a long period of ageing, e.g. 270 hours, T' phase formed, as $\alpha+\varepsilon \rightarrow T'+\eta$, and the rate of softening slowed down.

Because the spinodal decomposition happened simultaneously with decomposition of the supersaturated phase α'_s into α'_T, ε and T' phases, the hardness curve showed a changeable wave shape and on the X-ray diffractogram a sudden change in height of the characteristic diffraction peak α'_s {200} occurred after 5 minutes ageing at 170°C, shown in Figure 62. During the sharp increase in hardness, a small hardness peak occurred due to the competition between the two decompositions, and the G.P.zones gave rise to the first hardness peak, as shown in hardness curves at 100°C in Figure 62.

All alloys of compositions within the phase field $\alpha+T'+\varepsilon+\eta$ of high temperature equilibrium phase diagram will have the final phases α, T' and η after ageing. The four-phase transformation will definitely occur during ageing processes according to the general rule of phase transformation. This four-phase transformation always gives rise to an increase in hardness. The results of hardness testing and X-ray diffraction examination showed a good agreement in the activation energy of the phase transformation, shown

in the Arrhenius plot in Figure 59. They were 33 KJ/mol for hardness testing and 37.3 KJ/mol for X-ray diffraction examination on alloy AlZn75Cu3Si2.

For the Zn-Al-Si system, good agreement of mechanical properties and transformation has also been found.

In alloy AlZn30Si5, there existed three hardness peaks in the hardness/time curves for various ageing temperatures. As discussed in the section on hardness results in the Zn-Al-Cu-Si system, G.P.zones contributed the first peak hardness. The other two hardness peaks were due to the formation of the two transitional phases α''_m and α'_m respectively. On the X-ray diffractogram of Figure 88, the first transitional phase α''_m came after 8-10 minutes ageing at 170°C, and gave rise to a maximum hardness peak shown in Figure 58. After 15 minutes ageing the multi-peaks of the α''_m reduced on X-ray diffractogram, while the hardness dropped down sharply. The third hardness peak occurred after 1-1.5 hours, while the simple peak of the second transitional phase α'_m was well developed and the matrix phase peak shifted to α' position on X-ray diffractogram.

For alloy AlZn60Si5, the response of mechanical properties to the phase transformation was similar to alloy AlZn60Cu3Si. The first stage was found to be the cellular reaction, i.e.

$$\alpha'_S \longrightarrow \alpha'_T + \eta$$

It was found that the supersaturated α'_S phase decomposed during or immediately after quenching, and the α'_T phase was observed in the as-quenched state. As a result of

the cellular reaction followed by the formation of G.P. zones, the hardness of the alloy increased a great deal. Because both the precipitation of formed in the cellular reaction and also the formation of G.P.zones contributed to the hardness in only 1 or two minutes ageing at 100°C, the hardness testing was not able to separate these first two hardness peaks from each other.

After 3 minutes ageing at 100°C, the well-developed α''_m phase brought the hardness up to a maximum. As in all cases, the matrix α' phase was observed to develop, accompanied by the changing of the multi-peaks of α''_m phase to a single peak of the α'_m phase. Thereby the hardness curve right after the maximum hardness peak flattened out as a plateau, and this is shown in the hardness curve of Figure 57.

On prolonged ageing, α'_m disappeared and the η both from the cellular reaction and decomposition of the second transition phase α'_m coarsened. This growth made it easier for dislocations to bow through between the precipitates, and the alloy softened further.

Based on all these investigations of the mechanism of age-hardening, it became quite clear that phase transformations cause the change in mechanical and physical properties of alloys during quench-ageing processes, and therefore the change in properties can be used for tracing phase transformations. Any fluctuation observed on hardness/time curves should be associated with a phase transformation and/or crystal structural change. But

X-ray diffraction is a much more sensitive technique for the investigation because it is based on the structural change that occurs during the phase transformation.

The response of hardness to the phase transformations are summarised as follows :

1. Precipitation caused increase in hardness of alloys
2. G.P.zones always increase alloy hardness
3. The subsequent transitional phase formations contributed a great deal to the hardness increases, usually coinciding with the maximum hardness peak. In other words, a sharp decrease in hardness always occurs when these transition phases transform to final stable phases
4. The second transition phase, e.g. α'_m often gives rise to a distinct hardness peak on hardness/time curves (i.e. inner strain hardening due to lattice parameters of phase changing[81]).
5. The formation of new phases of high hardness, e.g. T' phase bring about an increase in the hardness value of the alloy.

The mechanism of phase transformations in the Al-Cu system has been well investigated, and the principles of age-hardening have been established. The present investigation gives strong support to these principles. The responses of the properties to the phase transformations were investigated in more detail in this study by using X-ray diffraction and electron microscopy techniques.

According to the phase relationships and the mechanism of

phase transformation in Zn-Al based alloys which have been well established, the effect of Zn content on the extending of age hardening should be considered in several different cases.

Within the composition range where the eutectoidal reaction occurs at about 276°C, the extent of age-hardening increases with decrease in Zn content. It has been found that the maximum hardness peak is contributed mainly by the first transition phase α''_m. The α''_m is one of the intermediate precipitates formed from the metastable α'_T phase. Therefore the extent of age-hardening is mainly dependent on the volume fraction of α'_T phase in the quenched alloys. From the Zn-Al binary phase diagram, shown in Figure 128, the extrapolated lines of the monotectoidal curves, eutectoidal curve and terminal solid solution curve are considered as the metastable phase boundaries[2]. According to the Lever Rule, zinc content controls the volume fraction of α'_T; the less Zn in the alloys, the more α'_T phase exists after the cellular reaction :

$$\alpha'_s \longrightarrow \alpha'_T + \eta$$

and therefore, the more the first transition phase α''_m contributes to the age-hardening. In other words, the higher the Zn content the lower the maximum peak hardness will be.

As-quenched alloys of eutectoidal composition at s in Figure 128 are located within the so-called 'coupled region' which is shaded in that Figure 101. According to the Lever Rule the α'_T phase from the cellular reaction is less

than that in monotectoid alloys and contributes a lower maximum peak hardness.

However, when the alloy composition is close to the zinc-rich end of the 276°C eutectoid reaction line, as a result of little α'_T existing, the precipitates of η phase play the main part in causing hardening. The closer the composition to the zinc-rich end of the eutectoidal line, the greater the volume of zinc precipitates that will form and the maximum peak hardness increases again. Therefore the maximum hardness and over-aged hardness values of alloy AlZn95Si2 are both higher than that of alloy AlZn75Si2 aged at 100°C and shown in Table 18. As far as the initial decomposition is concerned, the full sequence of G.P.zones and transition precipitates is only possible when the alloy is aged at a temperature below the G.P.zone solvus. The temperature used for ageing alloy AlZn95Si2 is above the metastable solvus of G.P.zones in Figure 17. So the G.P.zones contained in alloy AlZn95Si2 aged at 100°C do not form at the higher ageing temperature and a 'different' mechanism of age hardening comes about. A large amount of Zn precipitates gave rise to a higher hardness than that in alloy AlZn75Si2.

For Al-rich alloys of the Zn-Al-Si system (Zn content less than 32wt% i.e. at point T in Figure 128), the more zinc the alloy contains, the more the volume fraction of α''_m and the less the volume fraction of matrix phase α'' will be present and therefore the higher the maximum peak hard-

ness will be, according to the Lever Rule within the metastable monotectoid curve, as shown in Figure 128.

Comparing the alloys A1Zn30Si5 and A1Zn60Si5 aged at the same temperature, the volume fraction of the transition phase α_m'' in alloy A1Zn60Si5 is higher than in alloy A1Zn30Si5, as shown in Figure 128. Meanwhile, the cellular reaction gives rise to an increase in hardness in alloy A1Zn60Si5. So the maximum peak hardness of alloy A1Zn30Si5 is lower than that of alloy A1Zn60Si5.

So, for Zn-Al binary and Zn-Al-Si ternary systems (as Si does not take part in the transformation), the composition near to the Al-rich terminal eutectoidal composition produces the greatest age hardening. The alloy of eutectoidal composition, S, in Figure 128 shows the property of superplasticity and being near to the Zn-rich terminal eutectoidal composition, a reasonable high hardness is also obtained.

For ternary Zn-Al-Cu and quarternary Zn-Al-Cu-Si systems, instead of the eutectoidal reaction line in the Zn-Al binary system, the eutectoidal plane where $\alpha, \beta, \varepsilon$ and η coexist at 276°C is dealt with. As discussed before, all alloys of composition located within the eutectoid plane (i.e. with 4 coexisting phases) at 276°C show the same sequence of phase transformations and in particular the first cellular reaction occurs before formation of G.P.zones. According to the same principle dealt with for the Zn-Al binary system, the closer the alloy com position to the α phase corner, the more α_T' phase will

form by the cellular reaction :

$$\alpha'_S \text{ (or } \beta) \longrightarrow \alpha'_T + \varepsilon + \eta$$

Therefore, the more volume fraction of α''_m will be obtained by the decomposition of α'_T phase. As a result the alloy shows a greater extent of age-hardening.

As in the Zn-Al binary system, a reasonable high hardness will be obtained during the ageing process for alloys of composition close to η phase corner within the eutectoid plane (i.e. with 5 coexisting phases) $(\alpha+\beta+\varepsilon+\eta+\sigma)$. Alloys near the β phase corner show superplastic properties.

For Al-rich alloys (Zn content up to α phase corner of the eutectoid plane, i.e. 4 coexistent phases), the extent of age-hardening is smaller than that of alloys which are close to the α corner within the coexistent plane. Again, according to the Lever Rule, the more zinc in the alloys, the more α''_m will form, therefore a greater extent of age-hardening will occur.

5.5.2 Tensile, impact strength, dimensional stability and wear property

The responses of mechanical and physical properties to the phase transformations are seen in Tables 37 and 38.

For Al-rich Zn-Al-Si alloys (Zn content up to 32wt%), increased zinc had a marked strengthening effect on the matrix phase. The tensile strength σ_{uTs} and 0.2% yield strength $\sigma_{0.2y}$ increased from 190 N/mm^2 and 120 N/mm^2 respectively for alloy AlZn10Si5 to 296 N/mm^2 and 262 N/mm^2 respectively for alloy AlZn30Si5. The elongation

and impact values decreased from 10.2% to 6.0% and 37.5 J to 6.0 J respectively. These changes came about because the volume fraction of α''_m phase increased.

Within the composition range where the eutectoid reaction occurred, the strength properties of alloys decreased with increase in zinc content. Alloy ZnA160Si5 had the highest tensile strength σ_{UTS} of 286 N/mm^2, $\sigma_{0.2y}$ = 278 N/mm^2 and lowest elongation, 2.5%, coinciding with the highest hardness, as shown in Table 18. As in Al-rich alloys, the greater volume fraction of α''_m phase was taken to be responsible for the increase in strength and the decrease in elongation value.

Superplastic behaviour was observed in alloy A1Zn75Si2. The elongation value was 73.0% and the hardness, tensile strength and 0.2% yield strength were relatively low. It was because the volume fractions of both α''_m and η precipitates were not high in the alloy and a fine, uniform equiaxed grain structure formed after rapid phase transformation[59][60].

The high volume fraction of α''_m in alloy A1Zn60Si5 and of η precipitates in alloy A1Zn96Si2 lead to low elongations of 2.5% and 1.9% respectively.

For the volume fraction of α''_m, alloy A1Zn60Si>alloy A1Zn30Si5>alloy A1Zn10Si5, and as a result, the elongation values of these three alloys were in an increasing series : 2.5% 6% 10.2%.

With the addition of copper to Zn-Al-Si alloys, the

hardness increased, but the elongation of all the alloys examined decreased a great deal accompanied by an increase in tensile strength. Especially for the superplastic alloy AlZn75Si2, the elongation value decreased from 73.1% to 9.3% with an increase in tensile strength from 119 to 239 N/mm^2. The impact property of the alloys decreased, especially for alloy AlZn10Si5, from 37.5 down to 8.0 J.

All these changes in properties came about because Cu-rich precipitates and T' phase of high hardness formed in alloys of the Zn-Al-Cu-Si system.

The decomposition of supersaturated phases α'_s and β was responsible for the length contraction and major heat evolution, observed in other work. Because the decomposition of β phase was so rapid, the dimensional stability testing on 150°C ageing did not show an initial length change. After about 50 hours ageing at 150°C, the phase transformations were completed in all these Zn-Al-Si alloys and therefore little change in dimensions was observed.

However, with copper additions to Zn-Al-Si alloys, the decomposition of the supersaturated phases was followed by a four phase transformation :

$$\alpha_f + \varepsilon \longrightarrow T' + \eta$$

By this means, the intermediate ε phase was replaced by a stable copper-rich intermetallic phase T' of high hardness, which gave rise to an increase in length and hardness in An-Al-Cu-Si alloys on prolonged ageing[58][83].

A very fine two-phase structure obtained during the spinodal decomposition is also responsible for the increase in wear resistance as seen in Tables 38 and 39. The similar explanation to the response of the hardness and tensile strength to the phase transformation is suited to the wear property. More transition phase α''_m forms for the Al-rich terminal eutectoid alloys giving rise to a lower value of wear rate and therefore to a better wear resistance and for the same reason by wear rate of the superplastic alloy AlZn75Cu3Si2 decreased from 0.64 to 0.46cm^3/cm. With copper additions, T' phase of high hardness forms in the alloy and adds to the effect of Si-rich (σ) phase. The dispersed hard T' phase particles bear the loads in softer matrix phases, and therefore improve the wear properties.

To summarize the relationship between the properties and phase transformation, it is found that different Zn-Al based alloys proved to be different structural materials which will be suitable for different commercial demands.

It is practically possible to use different types of heat treatment to improve the mechanical and physical properties. For example, the Al-rich terminal eutectoid alloys show high tensile strength, high hardness and good wear property due to a great deal of α''_m formed in the spinodal decomposition. However, as phase transformations last a long time, one may apply two steps of ageing to take the benefits of transition phases α''_m and α'_m in using this alloy with oil lubricant agent at low temperatures in which

condition the thermodynamically unstable transition phases α_m'' and α_m' are actually stable kinetically. For superplastic alloys, it is better to use the two steps of ageing to get the stable phases[54], and with small amounts of copper addition the hardness, tensile strength, and wear property of the alloys are apparently improved at the expense of the elongation and impact properties which are not important as far as the tribological and mechanical properties are concerned.

6. CONCLUSIONS

1. The Si-rich terminal solid solution was found in both Zn-Al-Si system and Zn-Al-Cu-Si system. The composition of Si in σ phase at various temperatures are about 96% Si. In Al-Si binary systems, the saturated solubility of aluminium in silicon at 350°C is 2.4% Al (97.8% Si).

2. The isothermal sections of Zn-Al-Si system at 350°C, 300°C, 280°C, 272°C and 230°C are constructed as in Figures 35, 39. In aluminium 'rich' solid solution α the lattice parameter a_o(f.c.c.) decreased from 4.044 Å to 4.021 Å with increasing zinc up to about 33% Zn. In Si-rich solid solution σ, the lattice parameter a_o(Diamond cubic) increases from 5.401 Å to 5.430 Å. Zinc-rich phase η has a close packed hexagonal structure with a_o = 2.675 Å, c_o = 4.691 Å and c_o/a_o = 1.855.

3. The isothermal sections of Zn-Al-Cu-Si systems at 350°C, 300°C, 290°C, 285°C, 280°C and 275°C are constructed as in Figures 51, 56. The four phase transformation was determined at T = 285°C as follows :

$$\beta + T' \rightleftharpoons \alpha + \varepsilon$$

4. Both β and ε in Zn-Al-Cu-Si system are unstable at low temperature. The β phase decomposes at about 276°C while ε at 268°C. The β phase is found to decompose during or immediately after quenching.

5. The lattice parameter of η and ε phases are as follows :

η phase a_o = 2.671 Å c_o = 4.946 Å c_o/a_o = 1.852

ε phase a_o = 2.767 Å c_o = 4.289 Å c_o/a_o = 1.550

6. Among Zn-Al based alloys with small amounts of silicon and silicon together with copper, those of compositions in five ranges, i.e. Al-rich, monotectoid, eutectoid in the Zn-Al-Cu-Si system and Al-rich, monotectoid in Zn-Al-Si system, show pronounced age-hardening responses, as shown in Figures 57,64.

7. Distinct increases in hardness occur at the different stages of phase transformation. The response of hardness to the phase transformations are summarised as follows :

   1. Precipitation causes increase in hardness of alloys.
   2. G.P.zones always increase alloy hardness.
   3. The subsequent transitional phase formations contributed a great deal to the hardness increases, usually coinciding with the maximum hardness peak.
   4. The second transition phase, e.g. α_m', often gives rise to a distinct hardness peak on hardness/time curve.
   5. The formation of new phases of high hardness, e.g. T' phase bring about an increase in the hardness value of the alloy.

8. The pronounced response to age-hardening on adding small quantities of copper to the ternary Zn-Al-Si system was evident, the maximum hardness peak increased about 50 VPN.

9. In both the Zn-Al-Si and Zn-Al-Cu-Si systems, the

positions of peak hardness in hardness/time curves moved to shorter times with increases in zinc in the Al-rich α phase (e.g. for alloys Al Zn10 Cu3 Si2, Al Zn10 Si5, Al Zn30 Cu3 Si2, Al Zn30 Si5, Al Zn60 Cu3 Si2 and Al Zn60 Si5), and the maximum hardness peaks decreased and was recorded at shorter time as the ageing temperature increased.

10. The activation energy of hardening of alloys in Zn-Al-Si system were calculated as 79KJ/mol for alloy Al Zn30 Si5 and 61KJ/mol for alloy Al Zn60 Si5.

11. The activation energy of hardening of alloys in Zn-Al-Cu-Si system were calculated as 69KJ/mol for alloy Al Zn30 Cu3 Si2 and 51KJ/mol for alloy Al Zn60 Cu3 Si2.

12. The cellular reactions were for the first time observed before the formation of the G.P.zones in alloys of monotectoid and eutectoid compositions in Zn-Al binary alloys and Zn-Al based alloys with small amounts of silicon and/or copper as follows :

α'_s (or β) → α'_T + η for Zn-Al and Zn-Al-Si alloys

α'_s (or β) → α'_T + ε + η for Zn-Al-Cu and Zn-Al-Cu-Si alloys

About 70% incoherent precipitate of ε or η phases formed in this cellular reaction. It was characteristic of the appearance of the distinct lamellar structure. The cell nucleation and growth is one of the most important modes of formation of incoherent precipitates. The cellular reactions were according to the horizontal eutectoid at about T = 276°C rather than T = 340°C.

13. For Zn-Al based alloys, the spinodal decomposition was one of the most important transformations which occurred in the quench-ageing process.

14. All alloys of compositions within (α+T'+η) phase field at about 270°C in both Zn-Al-Cu and Zn-Al-Cu-Si systems have the four phase transformation as the final stage of the ageing processes :

$$\alpha + \varepsilon \longrightarrow T' + \eta$$

The activation energy of the four phase transformation in alloy AlZn75Cu3Si2 is 33.7KJ/mol deduced from hardness testing, or 37.4KJ/mol calculated from the fraction transformation curves, shown in Figure 66.

15. For alloys of compositions in various ranges in Zn-Al, Zn-Al-Cu and Zn-Al-Cu-Si systems, the mechanisms of the phase transformations during quench-ageing are as follows :

1. For all alloys of compositions within the (α+β+ε+η) phase field in equilibrium phase diagram of both Zn-Al-Cu and Zn-Al-Cu-Si systems at about T = 276°C, the sequence of phase transformations during the ageing process is as follows :

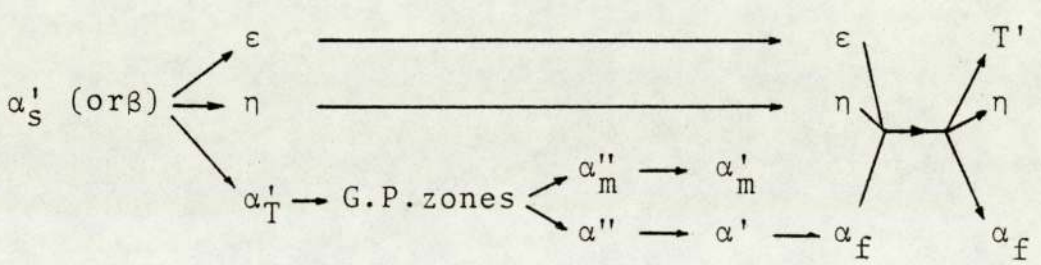

2. For alloys of compositions within the eutectoid horizontal of Zn-Al and Zn-Al-Si systems at about

T = 278°C, the sequence of phase transformation during ageing processes is as follows :

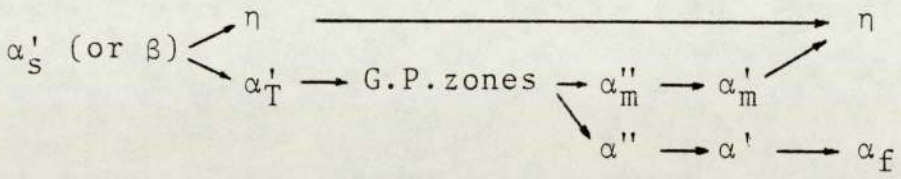

3. For alloys of compositions between α_T' (i.e. Al-rich terminal eutectoid) composition and the composition on the G.P.zone solvus surface shown in Figure 17 at ageing temperature in both Zn-Al-Cu and Zn-Al-Cu-Si systems, the sequence is as follows :

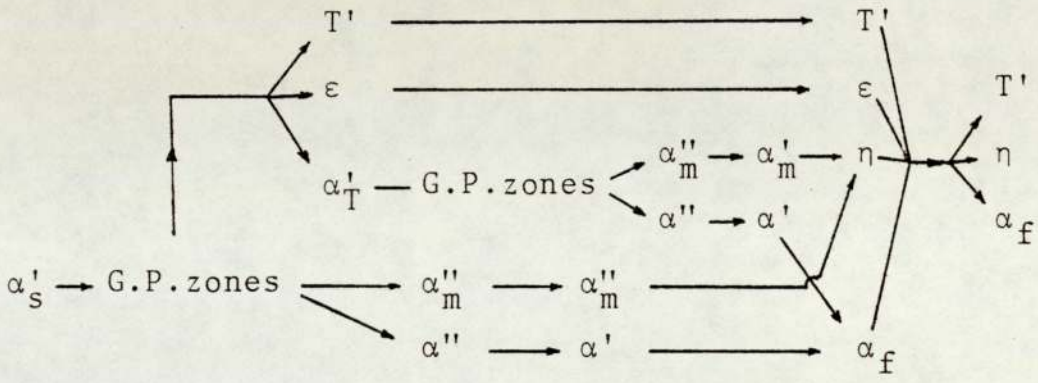

4. For alloys of composition between α_T' (i.e. Al-rich terminal eutectoid) composition and the composition on the G.P.zones solvus line for Zn-Al system, or the G.P.zones solvus surface for Zn-Al-Si systems, at ageing temperature the sequence is as follows :

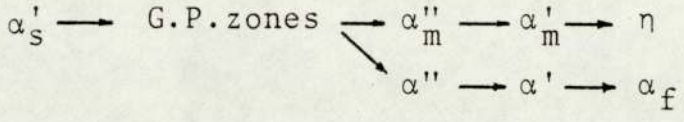

16. The addition of a small amount of copper retarded the ageing process in Zn-Al based alloys.

17. The sequence of phase transformation in quench ageing process depends on the quench rate and temperature

and the composition of alloy, i.e. the intrinsic phase relationship.

18. The mechanism of phase transformation in an alloy represents a general pattern of phase transformation for one phase field.

19. Correlating all these mechanisms of phase transformations with the equilibrium phase relationship, the general rule of phase transformations of supersaturated solid solution of alloys is summarised as follows : 'Phase transformation of a supersaturated solid solution of an alloy begins with decomposition of the supersaturated phase, which is associated with some phase equilibrium at high temperature. Then it is followed by one (or more) phase transformation(s) which agree with all these phase equilibria with the alloy after the first associated phase equilibrium at the high temperature. Steps of intermediate transformation with a low activation energy barrier, such as the formation of G.P.zones or other transitional phases etc. could always be involved in the whole process of phase transformations. The higher the degree of supersaturation, the more transitional phases may occur. The final product of ageing must be the stable phases, if the kinetics allow this to be reached'.

20. For alloys with low temperature eutectoid equilibrium, the cellular reaction corresponding to the eutectoid equilibrium is more likely to occur prior to the formation of G.P.zones.

21. The G.P.zones and R phase (i.e. α''_m or α'_m phase) solvus in Figure 17 imply the sequence of the spinodal decomposition which could always be an important part of age-hardening.

22. According to the general rule, it becomes possible to predict what kind of phase transformation will occur in non-equilibrium processes based on the understanding of the phase relationships in equilibrium.

23. The phase equilibrium at relatively low temperature can be established by tracing the phase transformation in quench ageing, i.e. the non-equilibrium processes.

24. Transmission electron microscopy investigation shows in alloy AlZn30Si5 the precipitates in G.P.zones are elongated parallel to a [110] direction in the ($\bar{1}12$) - oriented region, as shown in Figure 90. The average fringe spacing between rod-shaped precipitates is about 2000 Å.

25. When the first transition phase α''_m is developed, discontinuous precipitates (striated)adjoining a grain boundary was observed. The directions of growth of the precipitates are [100] and [$11\bar{1}$] in (011) - oriented plane, as shown in Figure 94.

26. In alloy AlZn30Si5, the segmentation of the second transitional phase α'_m (f.c.c.) shape of lamellae is caused by the oriented concentration of zinc atoms within the lamellae with small interlamellae spacing.

In alloy AlZn60Cu3Si2, because the lattice parameter of the matrix decreases due to the copper atoms existence, the strong strain field between lamellae and the matrix phase reduced and therefore the broken short phenomenon disappears. In both alloys, the shifting traces of zinc atoms were observed inside the lamellae.

27. The second transition phase α'_m had the f.c.c. structure. The chemical compositions of both oriented zinc concentrated and the matrix phase were determined as follows :

α'_m	50.57 at % Al	49.43 at % Zn
α'	85.62 at % Al	14.38 at % Zn

In both alloy AlZn30Si5 and AlZn60Cu3Si2, considerable coalescence of precipitates occur at over-ageing stage accompanying with decrease in hardness.

28. Within the composition range where the cellular reaction $\alpha'_s \rightarrow \alpha'_T + \eta$ or $\alpha'_s \rightarrow \alpha'_T + \varepsilon + \eta$ occurs the extent of age-hardening increases with the decrease in zinc content, while the rate of transformation in ageing increases with the increase in zinc content.

29. The decomposition of supersaturated phases α'_s and β was responsible for the length contraction and major heat evolution.

30 After shrinkage reduced by decomposition of super-

saturated solid solution in the early period of ageing, the Zn-Al based alloys with additions of small amounts of silicon show a good dimensional stability.

31. The formation of the transition phases α_m'' and α_m' appears to be responsible for the increases in hardness, tensile strength and wear resistance etc., properties. The alloys of compositions close to Al-rich terminal eutectoid, show the greatest increases in these properties, while the alloy of s, in Figure 128 show the property of superplascitiсy.

32. Zinc-aluminium based alloys, especially those with small amounts of copper together with silicon, proved to be a good bearing material. The addition of small amounts of copper changes phase relationships of zinc-aluminium alloy. The T' phase of high hardness increases the hardness, tensile strength and wear resistance of the alloys at expense of the elongation and impact properties. Combining the effect of T' phase and Si-rich (σ) phase on these properties, the alloys of monotectoid and eutectoid composition are supposed to be the superior bearing materials of high tribological and mechanical properties.

7. FUTURE WORK

1. The mechanisms of the Zn-Al binary alloys of composition in various ranges and the Zn-Al based alloys with additions of small amounts of silicon and/or copper have been well determined by hardness testing and X-ray diffraction examination and TEM observation. But more detailed TEM investigation on structural change of these alloys would be necessary to explain the change in physical and mechanical properties by alloying and heat treatment.

2. It has been suggested that the additions most likely to be useful would be Mg, Cu, Ag, Si, Fe, Mn, Ni and Li to improve the physical and mechanical properties and among these additions of magnesium showed the outstanding effect. Detailed investigation of the mechanism of Zn-Al based alloy with addition of small amounts of Mg, and Mg together with Cu and Si will be able to provide some of the best compositions of alloys with high tribological and mechanical properties.

3. Correlating the well-established equilibrium phase diagram and the detailed investigation of mechanism of phase transformation in the Zn-Al based with addition of small amounts of silicon or silicon and copper, the general rule of phase transformation of supersaturated solid solutions has been summarised based on the thermodynamical and the kinetic

consideration. This general rule is supposed to suit other alloy systems. In order to improve the correctness, one or more alloy systems should be investigated in the same way as that presented in this work.

8. REFERENCES

1. W. Köster and K. Moeller, Z. Metallkde, 33 (1941) pp. 278-283.

2. R. J. Marczak and R. Clach, Proc. 1st European Tribology Conference, London (1973), Institute of Mechanical Engineers, pp. 223-227.

3. E. P. Daneliya, V. M. Rozenberg and M. D. Teplitskii, FIZ Met Metalloyed, March 1976, 41, (3), pp. 581-586.

4. T. Savaskan, Ph.D. Thesis, "The Structure and Properties of Zn-Al Based Bearing Alloys", (1980) University of Aston in Birmingham.

5. E. Garvaiz, A. Y. Kandeil, H. Levert, Die Casting Engineer, September-October 1981, 25, (5), pp. 44-49.

6. Kenneth J. Alterfer, Metal Progress November 1982, pp. 19-31.

7. E. Gervais, H. Levert, M. Bess, The 84 Casting Congress and Exposition of the American Foundryman's Society, St. Louis, Missouri U.S.A., April 21-25 1980.

8. E. Gervais, A. Y. Kandeil, H. Levert, The 11th S.D.C.E International Die Casting Congress, Cleveland, Ohio, U.S.A., June 1-4 1981.

9. E.C.Ellwood, Journal of the Institute of Metals, Vol.66, pp.87-96 (1940).

10. E.C.Ellwood, Ibid, Vol.80, pp.217-224 (1951-52).

11. A.A.Presnyakv, Y A Gotban and V V Cherpyakova, Russian Journal of Physical Chemistry, Vol.35, No. 6, pp.623-633 (1961).

12. G.R.Goldak and J.Gordon Parr, Journal of the Institute of Metals, Vol.92, pp.230-233 (1963-64).

13. M.Hansen, "Structure of Binary Alloys".

14. A.Krupowski, R.Ciach and I.Krol, J.Bull.Acad,polon, Sci.cl.XV.11, 25-29 (1967).

15. M.Hansen, "Constitution of Binary Alloys", McGraw-Hill Book Company, Published 1958, pp.134 and 1205.

16. Metals Handbook, 8th Edition, 1973, Vol.8, p.259, by American Society for Metals.

17. Giles F.Carter, "Principles of Physical and miscibility Chemical Metallurgy", 1979, American Society for Metals.

18. W.Köster and K.Moeller, Z.Metallkde, 33, pp.284-288

19. W.Köster and K.Moeller, Ibid, pp.206-207 + p.289

20. A.J.Bradley and H.Lippon, Proc.Roy.Soc., (A), Vol.167, pp.421-438 (1938).

21. M.G.Brown, Acta Crystallographica, Vol.9, pp.70-74, (1956).

22. S.S.Lu and T.Chong, Reported by W.B.Pearton in "Handbook of Lattice Spacings and Structures of Metals and Alloys", Vol.2, p.552 (1957). London (Pergama Press).

23. S.Murphy, Metal Science, Vol.9, pp.163-168, (1975)

24. A.Gurnier, Solid State Physics, Vol.9, Academic Press, New York,p.294, (1959).

25. G.Borelins, J.Metals, 3 (1951) pp.477-484.

26. K.Hirans and H.Hori, J.Japan Inst.Metals, 36, (1972), p.97, 37,(1973) p.175.

27. W.Merz, T.R.Anantharaman and V.Gerold, Phys. Status Solid 8(1965), K5.

28. W.Merz and V.Gerold, Z.Metallk, 57, (1966).

29. R.P.Wahi and T R Anantharaman, Corr.Sci, 38, (1969), 1.

30. M.Simerska and Y.Synecek, Acta Metallurgical 15, (1967), pp.223-230.

31. G.J.C.Carpenter and R D Grawood, Met.Sci,J. 1, (1967), p.202.

32. P.P.Wahi, V.V.P.K.Ros and T.R.Anantharaman Trans.Ind.Metals, 23, (1970), 20.

33. K.Krishna Ras, L.E. Katz and H.Herman, Met.Sci, and Eng., 1, (1966), p.262

34. B.G.Strongiss, Phys.Met.Metallog, 23, (1967), p.55.

35. T.Niklewiski, P.Speigelberg and K.Sumbulli, Mat.Sci.J., 3, (1969), p.23.

36. T.R.Anantharaman, V.Ramas and E.P.Butler, J.Matls.Sci, 9, (1974), p.240.

37. K.Krishan Ras, H.Herman and E.Parthe, Matls.Sci, and Eng., 1, (1966-67), p.162.

38. G.V.Kleschev and A.J.Sheynkman, Phys.Met.Metallog, 23, (1961), pp.56 and 173.

39. T.R.Anantharaman and K.G.Satyanarayana, Scripta Met., 7, (1973), pp.189-192.

40. S.Yoshikawa, Y.Nakayama, N.Hosokawa and K.Nakaw, Japan Light Metals, 19, (1969), p.28.

41. G.J.C.Carpenter and R.D.Garwood, Metals Science Journal, Vol.1, pp.202-210 (1967).

42. A.Kelly and R.B.Nicholson, Progress in Materials Science, Vol.10, Pergamon Press, New York, (1963), p.153.

43. Y.Umakoshi, M.Yamaguchi and G.Mima, Trans., J.I.M., 12, (1971), p.7.

44. M.Kirtain and S.Neissmann, J.Appl.Phys., 42, (1971), pp.2603-2611.

45. G.T.Grider and H.P.Leighley, Phil.Mag., 28, (1973), p.465.

46. R.D.Garwood and A.L.Davies, Journal of the Inst. of Metals, Vol.88, pp.311-317, (1959-60).

47. M.H.Jacobs, Metals Science Journal, Vol.6, pp.143-148, (1971).

48. D.Turnbull, Acta Metallurgica, Vol.3, pp.55-63, (1955).

49. M.H.Jacobs, Met.Sci.J., 6, (1972), p.143.

50. K.G.Satyanarayana and Ken-ichi Mirano, Transaction Japan Ins.of Met., Vol.18, pp.403-411, (1977).

51. R.D.Garwood and A.D.Hopkins, Journal of the Inst, of Metals, Vol.81, pp.407-415, (1952-53).

52. C.Panseri and T.Federighi, Acta.Met., 1960, 8, p.217.

53. L.Huston, J.W.Oahi and J.E.Hillard, Acta.Met., 1960, 14, p.1053.

54. R.Ciach, B.Dukiet-Zawadzka and J.Dutkiewicz, Proc.16th International Heat Treatment Conference, Startford-upon-Avon, 1976. The Metals Society, pp.111-115.

55. R.Ciach, B.Dukiet-Zawedzka, T.D.Ciach, Journal of Materials Science, 13, (1978), pp.2676-2686.

56. K.Krishna Ras and H.Herman, Journal of the Institute of Metals, Vol.94, 1966, pp.420-424.

57. Jan Dutkiewicz, Poldeepolska akad Nank Prace Kom Metal Odlaw, 1973, (Met.), Vol.18, pp.53-64.

58. R.Ciach, J.Król and K.Wegrzyn, Bulletin de Lacademie Polonaise Des Sciences Serie des Sciences techniques Vol.XVII, 1963.

59. A.J.Ardell, K.Nuttal and R.B.Nicholson, Proc. International Conference, University of Manchester 1966, The Metallurgy Committee of the Institute of Metal, pp.22-26.

60. K.Nuttal and R.B.Nicholson, Phil.Mag, Vol.17, pp.1089-1091, (1969).

61. V.A.Toldin, G.V.Kleschev, D.V.Shumilov and A.I.Sheynkman, Fiz Metal, Metalloved, 40 No. 6, pp.1224-1226 (1975).

62. A.E.W.Smith and G.A.Hare, Journal of Inst. of Metals, Vol.101, pp.320-328 (1973).

63. M.L.Fuller and R.L.Wilcox, (Tech.Publ.572), A.I.M.M.E. Tech.Publ. 575, Metals Technology, (1974), September, p.1.

64. H.Naziri and R.Pearce, Internat.I.Mech.Sci, 1970, p.513.

65. R D Garwood and A D Hopkins, J.Inst.Metals,1952-53,81,407

66. R.Ciach, J.Salawa, O.Kabisch and G.Wendrock, ARCHINUM HUTNICTWA Tom 23, 1978, Zeszyt2, pp.233-255.

67. V.A.Toldin, A.A.Burykin and G.V.Kleschev, Phys. Met.Metall, Vol.51, No. 1, pp.116-124, 1981,

68. V.A.Toldin, A.A.Burykin and G.V.Kleshchev, Fiz.Metal.Metalloved, 45, 342-346 (1978).

69. A.Krupkowski, R.Ciach and I.Krul, J.Bull.Acad. polon. Sci.cl.XVII, pp.25-29, (1967).

70. A.Krupkowski, Bull.Acad.Polon.Sci.Tech. 1970, 18, (I), p.15.

71. S.Murphy, Zeitschrif and Metallkunde, Vol.71, pp.96-102, (1980).

72. W.Köster, Ibid, 33, (1941), p.299.

73. E.Gebhardt, Ibid, 33, (1941), p.297.

74. E.Gebhardt, Ibid, 34, (1942), p.208.

75. W.Truszkowski and J.Dutkiewicz, Bulletin de Lacedemie Polonaise des Sciences Serie des Sciences Techniques, Vol.XIX, No. 11-12, 1971.

76. J. Kröl, K.Wegrzyn-Tasior, ARCHIWUM HUTNICTWA, Tom XVI, 1971, pp.119-218.

77. G.V.Klwshchev, A.M.Yelistrator, A.I.Seynkman et al, Fiz. tverd tel, 9, pp.2811-2819, (1967).

78. G.V.Kleschev, V.A.Toldius, A.ISheynkman, D.V.Shumuluv, Yu G.Raspopov and V.N.Panov, Izv.Vuzov, Fizika, 2, pp.30-35, (1971).

79. G.V.Kleshchev, Author's abstract of dissertation, Moscow, JSN, IICHM (1972).

80. I.J.Polmear, Journal of the Institute of Metals, Vol.86, (1957-58), pp.113-121.

81. I.J.Polmear, Ibid, Vol.86, (1957-58), pp.535-538.

82. G.V.Kleschev, Yu G.Raspopov, V.A.Toldin and A I Sheynkman, Fiz.Metal.Metalloved, 33, pp.653-656, (1972).

83. S.Murphy, T.Savaskan and J.K.Wheeldon, Int.Congress on Metals Engineering, University of Aston,Birmingham 1981

84. K.Nuttall, Journal of the Institute of Metals, Vol.101, 1973, pp.329-332.

85. R.D.Jones, Iron and Steel Inst., June 1978, 51, (3), pp.149-152.

86. S.roy, V.Sivan, V.Balesubramayan and B.A.Shenoi, Surface Techn., November 1978, 7 (5), pp.361-365.

87. M. Hiroshashi, E. Kawai et al, J.Jpn.Inst.Met. May 1977, 41, (5), pp.487-492.

88. S. N. Ananin, P. T. Efremov, Teckhnol. Legh,kg, Splavov, Nanchu Teckhn, Byal Vilsa, 1973, (3), pp.21-26.

89. H. Suznki, I. Araki, M.Kanno et al, J.Jpn.Inst.of Light Met, May 1977, 27, (5), pp.239-245.

90. P Duncumb and E M Jones, T.I.Tech.Rep. No. 260 (1969).

91. Welsh Phil.Trans.Roy.Soc., 1965, pp.31-70.

92. R.Ciach, Proc.International Conference, University of Manchester 1966, The Metallurgy Committee of the Institute of Metal, pp.86-88.

93. B. Sontiere and A.W. Kerr, Trans.Met.Sci, A.I.M.E., (1969), pp.245 and 2595.

94. C. Zener, Trans.Amer.Inst.Min.Met.Eng., 1946, pp.167 and 550.

95. J. W. Cahn, Acta Met., 1959, pp.7-8.

96. M. Hillert, "Decomposition of Austenite by Diffusional Processes", p.197, 1962, New York and London (Interscience Publishers).

97. M. Vijayalakshani, V. Seetharaman and V. S. Raghunathan, Materials Science and Engineering, Vol.52-No. 1, January 1982, pp.249-256.

98. L. Terziev and Karaivanor, Metallurgiya, 1979, (11), pp.8-11.

99. Lawrence H.Van Vlack, Elements of Materials Science, Sixth Print, Addison-Wesley Publishing Company, Inc. 1969.

100. D.A.Porter, K E Easterling, "Phase Transformation in Metals and Alloys", 1981, Van Nostrand Reinhold Co. Ltd.

101. K N Tu and D Turnbull, Proc.International 1966, The Metallurgy Committee of the Institute of Metals, pp.32-35.

9. ACKNOWLEDGEMENTS

I would like to thank the Chinese Government for having provided me with adequate financial support.

I am greatly indebted to Dr S Murphy for his continual encouragement and expert guidance throughout the research work.

I wish to express my gratitude to Dr J L Aston for his ceaseless enthusiasm and helpful discussions.

I also wish to thank Professor J T Barnby for his great support.

My thanks are also due to all the technicians in the Metallurgy Department, especially Mr Z Ahmed and Mr P Dent, who have always been helpful and willing to assist me in the laboratories.

I am thankful to Dr M Loretto in the Department of Physical Metallurgy at Birmingham University for his help on STEM work.

Many thanks are given to Miss C M Kelly for her immense co-operation and excellent typing.

Last, but not least, I am grateful to my wife, L.Q. Qu, for her support and encouragement throughout the project and especially for looking after the family during my long period of absence from home.